Calcium, Strontium and Barium Complexes in Organic Synthesis

Yann Sarazin, Peter M. Chapple

Comprehensive Organometallic Chemistry IV

CALCIUM, STRONTIUM AND BARIUM COMPLEXES IN ORGANIC SYNTHESIS

Author and Co-author Contact Information
Yann Sarazin* and Peter Chapple
Institut des Sciences Chimiques de Rennes – UMR 6226 CNRS – Université de Rennes 1
Campus de Beaulieu, Bâtiment 10C
263 avenue du Général Leclerc 35042 RENNES Cedex FRANCE
yann.sarazin@univ-rennes1.fr
(+33) (0)2 23 23 30 19

Abstract
In the space of twenty years, molecular complexes of the large alkaline earths calcium, strontium and barium have gone from being mere oddities to some of the most exciting catalysts in the landscape of homogenous metal-mediated catalysis. This chapter reviews the main achievements in the area of organic transformations catalyzed by alkaline-earth complexes. It encompasses a broad range of hydrofunctionalization reactions (e.g. hydroamination, hydrophosphination and hydrogenation) and dehydrocouplings, as well as a range of other reactions that do not fit into any specific category. A survey of the sophisticated processes catalyzed by alkaline-earth Lewis acids is included.

Keywords
Alkaline-earth metal
Barium
Calcium
Catalyst
Dehydrocoupling
Homogeneous catalysis
Hydroamination
Hydrofunctionalization
Hydrogenation
Hydrophosphination
Lewis acid
Strontium

Table of contents

List of abbreviations and acronyms

Ad	adamantyl
Ae	alkaline earth
AN	acceptor number
BDE	bond dissociation energy
BDI	β-diketiminato
BDI^{DiPP}	$CH\{C(Me)N\text{-}DiPP\}_2^-$
BINOL	1,1′-bi-2-naphthol
Bn	benzyl
Boc	*tert*-butoxycarbonyl
Box	bis(oxazoline)
CN	coordination number
Cy	cyclohexyl
dabco	1,4-diazabicyclo[2.2.2]octane
DiPeP	2,6-diisopentylphenyl
DiPP	2,6-diisopropyl-phenyl
dme	dimethoxyethane
DPE	1,1-diphenylethylene
dr	diastereomeric ratio
DXE	dixylylethylene
E_a	activation energy
ee	enantiomeric excess
eq	equivalent
Et	ethyl
FIA	fluoride ion affinity
FLP	frustrated Lewis pair
Fmoc	fluorenylmethyloxycarbonyl
GEI	global electrophilicity index
HBCat	catecholborane
HBPin	pinacolborane
Hex	hexyl
hfip	hexafluoroisopropanol
HIE	hydrogen isotope exchange
hmpa	hexamethylphosphoramide
HOMO	highest occupied molecular orbital
^{i}Pr	*iso*-propyl
KIE	kinetic isotope effect
L	monoanionic ligand
LA	Lewis acid
LUMO	lowest occupied molecular orbital
Me	methyl
Mes	mesityl
MS	molecular sieves
Naph	naphtyl
^{n}Bu	butyl
NHC	N-heterocyclic carbene
NTf	triflimidate
OS	oxidation state
OTf	triflate
Ph	phenyl
PyBox	pyridine-based bi(oxazoline)
S	solvent molecule
r_{ionic}	effective ionic radius
^{t}Bu	*tert*-butyl
thf	tetrahydrofuran
thp	tetrahydropyran
TM	transition metal
TON	turnover number
TOF	turnover frequency
tmeda	tetramethylethylenediamine
Tf_2NH	triflimide
TfOH	triflic acid
Ts	tosyl
X_P	Pauling electronegativity
XRD	X-ray diffraction
1,4-CHD	1,4-cyclohexadiene
9-BBN	9-borabicyclo[3.3.1]nonane

1 Alkaline-earth metal catalysis: an introduction

The present chapter is a survey of the recent accounts of alkaline-earth mediated homogeneous catalysis applied to organic transformations relevant to small molecules. The literature for Ae-promoted polymerization catalysis, reviewed elsewhere in this volume, is not discussed here.

Nota bene: unless otherwise stated, hereafter Ae stands for the three large alkaline-earth metals Ca, Sr and Ba.

1.1 General background

Catalysis is a key contributor to the chemical industry. It is estimated that about 90% of all chemical processes are catalyzed, and catalysis is thought to contribute to 30-40% of the world's GDP. By far and large, industrial homogeneous catalysis has, until recently, revolved around the utilization of precious transition metals such as rhodium, palladium, iridium and platinum. However, these metals are both scarce and expensive (costs in USD per ozt as of April 2021: Rh, 28500; Pd, 2650; Ir, 6250; Pt, 1200); market prices can also be unstable and fluctuate with worldwide availability. Since the beginning of this century, main group metal catalysis has begun to appear as a viable response to these limitations. Molecular, soluble catalysts built around the abundant and cheap metals of the s- and p-blocks of the Periodic Table are now involved in a myriad of transformations. Group 13 metals (Al, Ga, In and Tl)[1] and, to a lesser extent, tin[2,3] and other group 14 metals,[4] have long been known to generate useful reagents and catalytic systems for organic chemistry; a detailed survey can be found in this volume. Early main group metals, that is, alkali and alkaline-earths metals, are a comparatively recent addition to the set of tools applied in molecular catalysis.[5] The input of alkali metals and magnesium, the smallest of the synthetically relevant alkaline earths, is comprehensively surveyed in relevant chapters of the present volume; this includes the synergic multimetallic systems. The applications of the heavier alkaline earths -calcium, strontium and barium- in organic chemistry are covered in this chapter; it encompasses the literature of the past 15 years. For the interested reader, the first reviews on homogeneous catalysis mediated by calcium[6] and, more generally, large alkaline-earth metals,[7] were released only in 2010; the initial insight into the area was covered in more detail in book chapters published in the following years.[8-10]

The large alkaline earths (= Ae) calcium, strontium and barium are both abundant (calcium, the 5th most common element, accounts for 3.39 wt% of the Earth crust) and affordable. Their toxicity is limited, although barium can even in small doses induce hypokalemia by blocking transmembrane potassium channels; yet, it is not carcinogenic and does not bioaccumulate.[11,12] These metals are characterized by their large ionic radii (effective r_{ionic} for a coordination number of 6: Ca^{2+}, 1.00 Å: Sr^{2+}, 1.18 Å: Ba^{2+}, 1.35 Å)[13] and high electropositivity (Pauling electronegativity X_P: Ca, 1.00; Sr, 0.95; Ba, 0.89; see Figure 1). They are highly polarizable, and generate ionic complexes with ns^2 $(n-1)d^0$ outer electronic configurations where non-directional bonding is dictated by electrostatic considerations. Except for two notable examples of Ca(I) compounds,[14,15] Ca, Sr and Ba generate redox-inert complexes with the metal in the +II oxidation state. They do not undergo oxidative addition – reductive elimination processes that are more typical of middle to late transition metals, which, as detailed below, bears implications on the mechanisms of Ae-mediated chemical processes. These features are similar to those of the lanthanide elements, and the analogy between Ae and lanthanide elements has

indeed been drawn on multiple occasions.[10,16] In particular, it is this analogy which prompted the seminal investigations in the potential reactivity and catalytic behavior of molecular Ae complexes. Yet, the two families of elements display substantial differences that go beyond the presence of core *f*-electrons for the lanthanides: whereas the 4*f*-elements are characterized by a small reduction of their size upon increasing atomic number due to the lanthanide contraction (r_{ionic} for CN = 6: Ce^{3+}, 1.01 Å; Lu, 0.86 Å), the ionic radius of alkaline earths increases dramatically upon descending group 2 from Mg^{2+} (0.72 Å) to Ba^{2+} (1.35 Å). Similarly, the electronegativity of the element increases substantially from Ba to Mg (X_P = 0.89 and 1.31, respectively) whereas the fluctuation is more modest for the lanthanides, with X_P confined between 1.10 (La) and 1.27 (Lu). The comparatively high electronegativity of magnesium confers a certain covalent character to the bonding in Mg complexes, which makes this metal stand apart from the other Ae elements. Beyond this peculiarity, the large variations of size and electronegativity across the other large metals entails much more diverse and less predictable reactivity patterns than for the lanthanide counterparts. For example, ligand exchange in solution, a significant issue for the alkaline earths, is relatively innocuous for the lanthanides, and constitutes another difference between the two families of these hard and oxophilic elements.

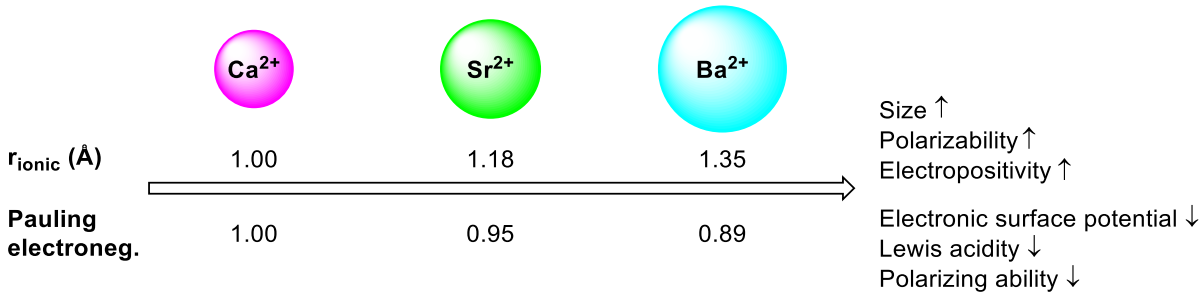

Figure 1. Main physical properties of the large alkaline earths calcium, strontium and barium.

1.2 The Schlenk equilibrium: problems and solutions

Ligand redistribution in solution, also named Schlenk equilibrium after the dynamic ligand exchange that characterizes Grignard reagents RMgX and lead to the formation of homoleptic species MgR_2 and MgX_2,[17] affects all alkaline earths. The properties of the metal, in particular the increasing ionic bonding and metal size, make it a much greater problem upon descending group 2, as metal-to-ligand bonds become weaker and ligand lability is amplified accordingly. Hence, for heteroleptic complexes LAeX, ligand exchange often leads to the formation of new AeL_2 and AeX_2 species (Figure 2) in proportions that vary both with the nature of the monoanionic ligands L^- and X^-, and with the reaction conditions (temperature, concentration, nature of the solvent). It can result in the formation of polymeric aggregates or cluster compounds with low solubility. Although ill-defined mixtures may still be able to mediate catalytic transformations, control over the reaction will be altered or even entirely suppressed. Beyond catalyst speciation, such mixtures effectively prohibit accurate mechanistic and kinetic analysis of the operating systems. This is particularly irksome for enantioselective reactions and for living polymerizations, where control of the reaction parameters by a carefully designed coordination sphere around the metal is critical.

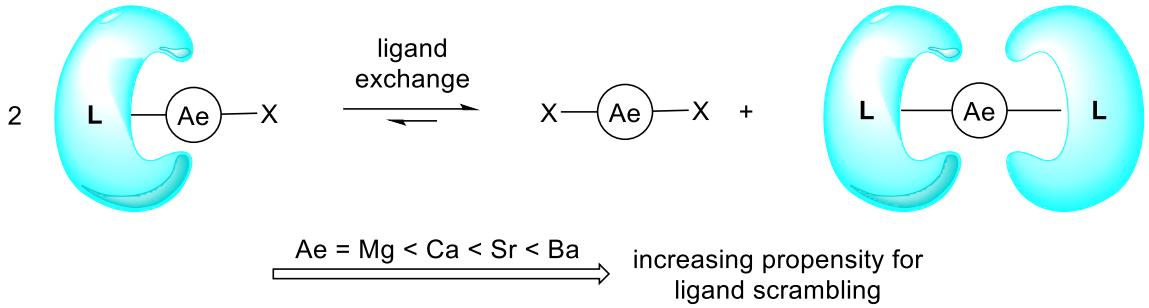

Figure 2. General ligand exchange ("Schlenk equilibrium") in alkaline-earth complexes.

The difficulty associated to ligand scrambling is perhaps best exemplified with the archetypal nitrogen-based β-diketiminate ligand $CH\{C(Me)N\text{-}DiPP\}_2^-$ (DiPP = 2,6-di-isopropylphenyl), hereafter abbreviated as BDI^{DiPP}. This ligand has been used with great effect to suppress ligand redistribution for calcium (and magnesium) chemistry, allowing access to many unprecedented and exciting compounds.[18-21] Nonetheless, it is unable to stabilize heteroleptic strontium or barium complexes, as they have been shown to redistribute to equilibrium mixtures with the corresponding homoleptic species (Figure 3).[22] The use of a specifically designed bulky, monoanionic and multidentate ancillary ligand L^- in heteroleptic complexes $LAeX\cdot(S)_n$, where X^- is a reactive coligand and S is a coordinated solvent molecule (e.g. thf, Et_2O, tmeda, etc.), has overall proved a successful strategy to overcome ligand reshuffling in Ae chemistry.[23-26] Such ligands kinetically stabilize the heteroleptic complexes by taking advantage of steric and/or electronic factors and, in some cases, structural rigidity.[27] The use of a judicious ancillary ligand enables control of the first coordination sphere around the metal; it enhances catalyst properties and lifetime, and generally improves the solubility of the relevant metal species in a given catalytic manifold. The chemistry of barium is particularly representative of the benefits gained through sophisticated ligand design; ligands with tailored properties have allowed access to a plethora of heteroleptic complexes that feature unique bonds to a negatively charged reactive group such as $(Me_3Si)_2N^-$, $(Me_3Si)_2CH^-$, Ph_2P^- or H^-.[28] Beyond the construction of sterically shielding and electronically stabilizing ligands, intramolecular secondary interactions are also a valuable synthetic tool that help obtain Ae complexes.[29] A number of stable heteroleptic complexes, some of them devoid of bulky multidentate ligands, were for instance generated thanks to the presence of intramolecular Ae···H–Si,[27,30-32] Ae···F[33,34] or Ae···C(π)[35,36] interactions.

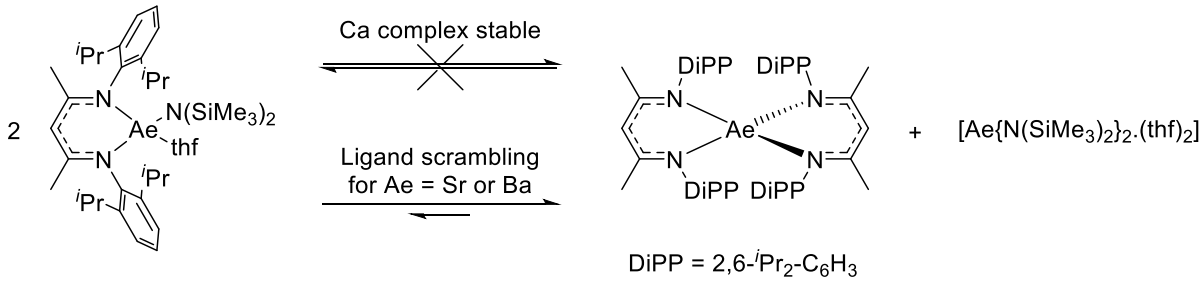

Figure 3. Schlenk equilibria with BDI-ligated Ae complexes for Ae = Ca, Sr and Ba.

1.3 Historical developments

For a long time, development of the molecular chemistry of the alkaline earths was impeded by the high air-sensitivity and reactivity of Ae complexes, and was therefore lagging well behind the

chemistry of their lighter congener magnesium. However, the synthetic organometallic chemistry of Ca, Sr and Ba took a decisive turn in the 1990s when the stable σ-bonded amide and alkyl precursors $[Ae\{E(SiMe_3)_2\}_2\cdot(thf)_2]$ became available (Ae = Ca, Sr, Ba; E = N, CH).[37-39] A range of amide and cyclopentadienyl Ae complexes were also synthesized and were reviewed on several occasions,[40-44] but reactivity features were seldom explored until the mid-2000s. One of the reasons behind this is that heteroleptic Ae complexes bearing a single cyclopentadienyl-type ligand were often found to be prone to ligand scrambling.

Although simple amido complexes of the type $[Ae\{N(SiMe_3)_2\}_2]_2$ and the related thf adducts $[Ae\{N(SiMe_3)_2\}_2\cdot(thf)_2]$ are very conveniently synthesized[37-38] and are sometimes seen to act as competent precatalysts, but on the whole, simple AeX_2 species are often polymeric and insoluble in hydrocarbons; this is typically the case for Ae alkoxides. Heteroleptic complexes LAeX (often found as solvated species) bearing two different monoanionic ligands, a bulky and commonly multidentate ancillary ligand L^- and a reactive (nucleophilic or basic) group X^-, have become the quintessential examples of Ae molecular precatalyst. The bulky ligand L^- is installed onto the metal to provide stability to the complex and to improve its solubility in non-polar solvents. The efforts paid into the development of increasingly sophisticated ancillary ligands have with time allowed for the synthesis of stable and soluble Ae-amides, alkyls, alkoxides and even hydrides, with all of these species being relevant to Ae-mediated catalysis. The seminal breakthrough came from the group of M. Chisholm, when they reported in 2003 that heteroleptic β-diketiminate (**1**) and (pyrazolyl)borate calcium complexes were very efficient precatalysts for the stereocontrolled ring-opening polymerization of lactide (Figure 4).[45-46] Shortly afterwards, Hill and co-workers demonstrated that **1** could also be used very effectively to catalyze the intramolecular hydroamination of aminoalkenes.[47] Although interesting results had been obtained earlier in Ae-mediated catalysis, notably for polymerization reactions, these results convincingly showed the advantages of using a bulky ancillary to stabilize the catalytically active species in a given reaction manifold.

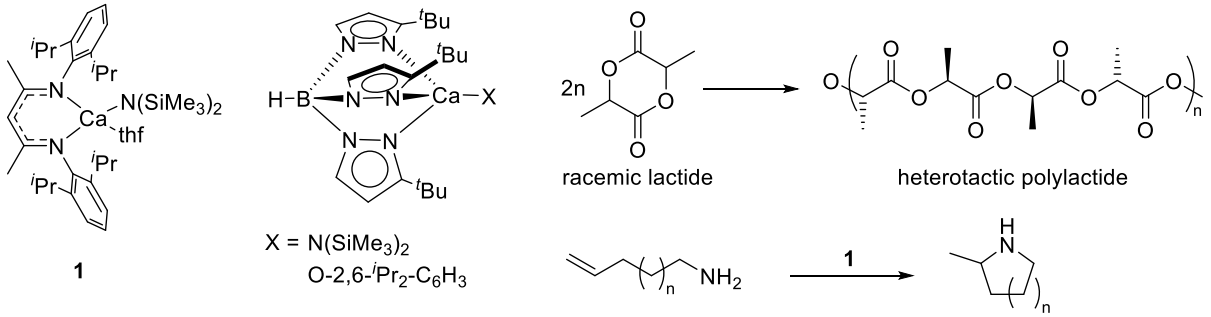

Figure 4. Alkaline-earth ring-opening polymerization[45-46] and hydroamination[47] precatalysts.

1.4 Principles of Ae-mediated catalysis

In the past 20 years, the bulky of newly prepared Ae complexes were designed to be catalysts or precatalysts in reactions as varied as olefin hydrofunctionalization, E-H/E'-H heterodehydrocouplings, and polymerizations. The reactivity of alkaline-earth metals being restricted to redox-neutral pathways, an Ae complex that contains a polarized $Ae^{\delta+}$-$X^{\delta-}$ bond where X is a reactive group, can only engage in two fundamental elementary steps (Figure 5), that is: (1) the [2σ-2σ] exchange of electronic density during σ-bond metathesis with a polarized $^{\delta-}Y$-$Z^{\delta+}$ bond, which advances through a highly organized and polarized 4-membered transition state to return the newly-formed Ae-Y and X-Z bonds,

and (2) the insertion of a polarized, unsaturated $^{\delta-}Y{=}Z^{\delta+}$ bond into the $Ae^{\delta+}\text{-}X^{\delta-}$ bond to yield the Ae-Y-Z-X sequence.

The catalytic manifolds of Ae-catalyzed reactions can typically be deconvoluted in a succession of these two key elementary processes, as simply depicted in Figures 6 and 7. In a preliminary off-cycle step, the precatalyst LAeX reacts with a polarized substrate to generate the catalytically active species LAeY. The reactivity of the Ae-Y bond is rationalized by the electronegativity difference between the Ae metal and the more electronegative Y atom(s) (where Y = H or a p-block element, e.g. C, N, O or P), in a way that the $^{\delta+}Ae\text{-}Y^{\delta-}$ σ bond is always polarized negatively towards the Y atom. Although the charge distribution within the Ae-Y bond is always relative and depends on the identity of the Y substituent, the reactivity with another σ-bonded, polarized substrate $^{\delta-}H\text{-}Z^{\delta+}$ is limited by the polarized nature of this interaction to a σ-bond metathesis (Figure 6).[48,49] The outcome of the reaction is imposed by the polarization of the $^{\delta+}Ae\text{-}Y^{\delta-}$ bond, as the more electronegative hydride in the polarized $^{\delta-}H\text{-}Z^{\delta+}$ substrate will take the position α to barium in the pertaining 4-membered transition state. In heterodehydrocoupling catalysis, the combination of both 'protic' and 'hydridic' σ-bond metathesis steps for the dehydrocoupling of $^{\delta+}H\text{-}Y^{\delta-}$ and $^{\delta-}H\text{-}Z^{\delta+}$ pre-polarized substrates (e.g. $HNEt_2$ and $HSiPh_3$, respectively) has been used to build various types of Y-Z bonds between p-block heteroelements upon release of dihydrogen. Except for the specific example of hydrogenation reactions where the ability of Ae metal to trigger polarization of H_2 will be critical, this type of reactivity is, for now, essentially limited to pre-polarized protic or hydridic element-to-hydrogen bonds. Depending on the identity and intrinsic reactivity of the pair of substrates H-Y and H-Z, the catalytic cycle for dehydrocoupling catalysis can be accessed via two different ways from the precatalyst LAeX.

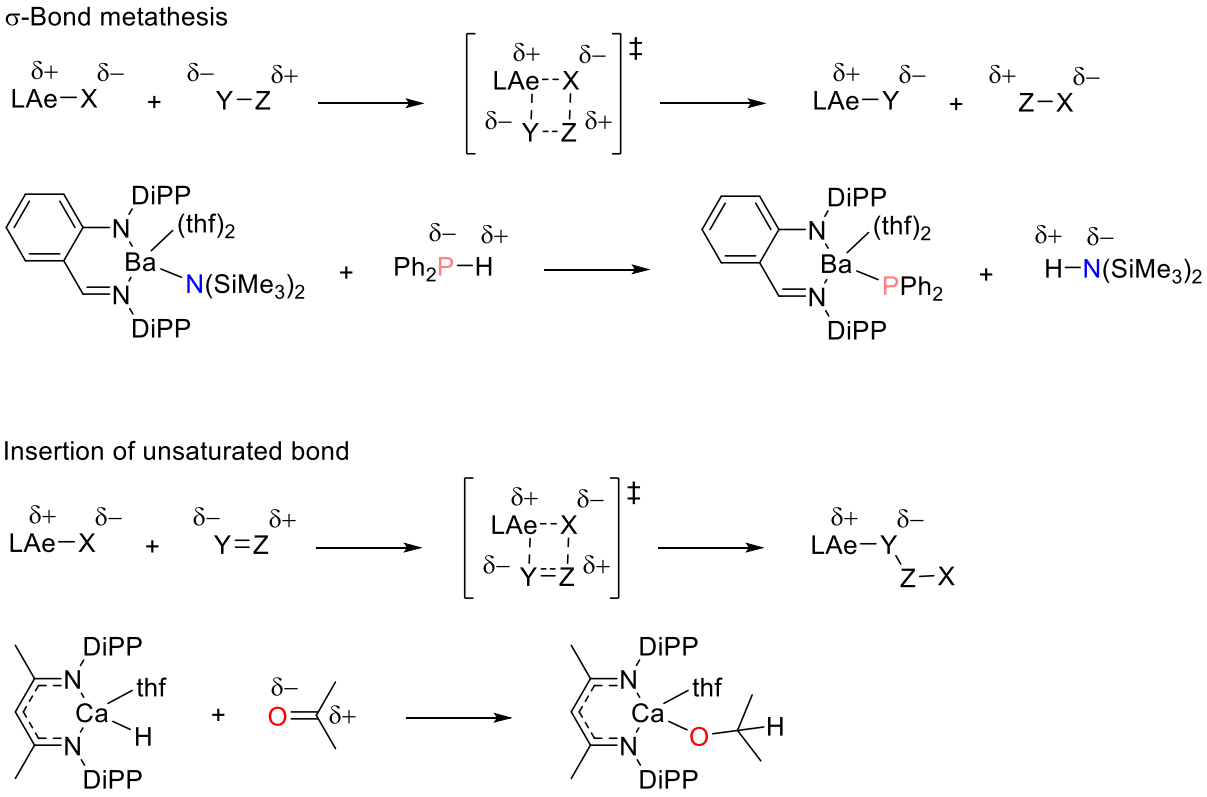

Figure 5. The two elementary steps (with illustrative examples) in the reactivity of alkaline-earth metals: σ-bond metathesis and insertion of unsaturated bond. DiPP = 2,6-$^{i}Pr_2$-C_6H_3.

The $^{\delta+}$Ae-Y$^{\delta-}$ bond of the catalytically active species can also induce polarized insertion into multiply bonded substrates, such as ketones, imines, alkenes and alkynes (Figure 7), as for instance in hydrofunctionalization reactions. Whether the reaction occurs is influenced by the thermodynamics of the relative energy of all broken and formed bonds. However, the kinetic feasibility of any given transformation relies on the substrates ability to stabilize the charge separation induced in the 4-membered transition state. Again, an element of directionality is conferred from the metal: in pre-polarized substrates, e.g. ketones or imines, the more electronegative heteroatom will pre-coordinate to the alkaline earth and will as a result occupy the position α to the metal in the four-membered transition state. This sequence will control the regiochemistry of the whole insertive process. In contrast, for non-polar unsaturated bonds such as alkenes and alkynes, polarization of the π-electrons is induced by the $^{\delta+}$Ae-Y$^{\delta-}$ unit itself; one often speaks in this case of "metal-induced polarization", a key step in the hydrofunctionalization of unsaturated C=C and C≡C bonds.[50] The precise operating manifold will be dictated by the polarization of the H-Y between the hydrogen atom and the heteroelement within the substrate. With a $^{\delta-}$H-Y$^{\delta+}$ bond negatively polarized towards hydrogen, as for instance, with hydrosilanes in hydrosilylation reactions, the species responsible for catalytic turnovers is a metal-hydride (Figure 7, bottom). In the opposite scenario of a $^{\delta+}$H-Y$^{\delta-}$ bond negatively polarized towards the heteroatom Y, as in the hydroamination or hydrophosphination of olefins, the catalytically active species will feature a $^{+}$Ae-Y$^{\delta-}$ polarized bond (Figure 7, top). Beyond the hydrofunctionalization of alkenes and alkynes, the chain-growth polymerizations of unsaturated monomers such as olefins and cyclic esters catalyzed by Ae metals may also advance through iterative insertive pathways. Conceptually, the specificity of these metal-promoted polymerizations resides in the fact that the product of each insertion step, i.e. the growing polymer chain, uniquely remains bound to the metal for the entire duration of the chain extension.

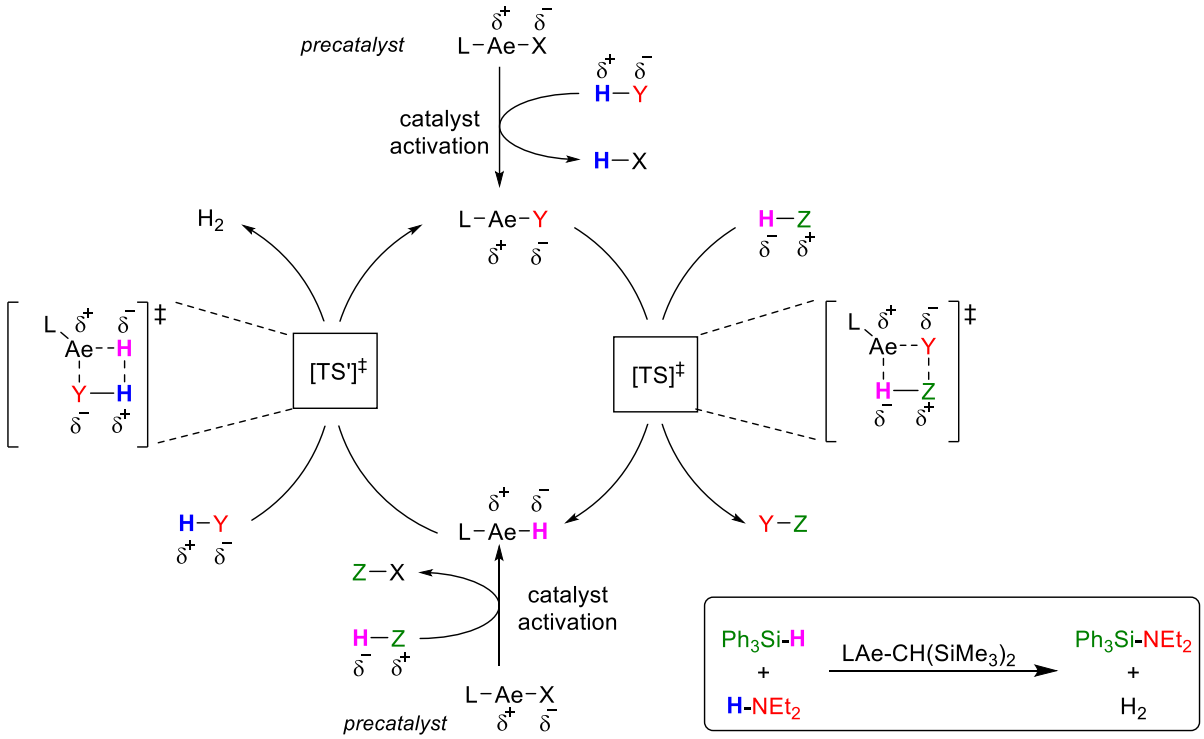

Figure 6. Common mechanism for Ae-catalyzed heterodehydrocouplings, illustrated with the coupling of Ph_3SiH and $HNEt_2$. L = ligand.

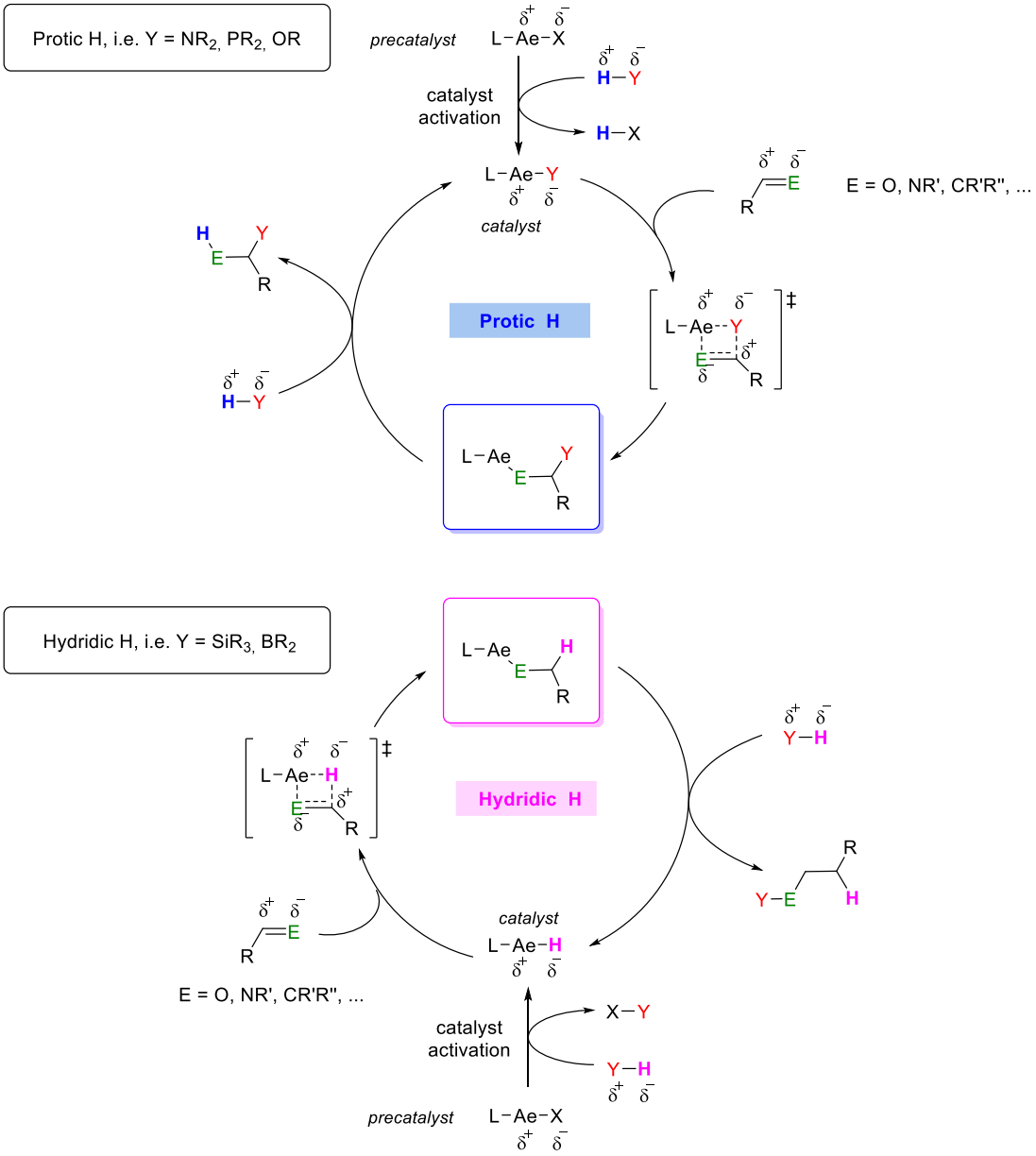

Figure 7. Classical stepwise insertive mechanisms for Ae-catalyzed hydrofunctionalizations for substrates containing protic (top) or hydridic (bottom) H atoms.

2 Hydroamination of unsaturated carbon-carbon bonds

The majority of Ae-promoted homogeneous catalysis since 2005 has focused on the hydrofunctionalization of unsaturated bonds. The intramolecular hydroamination of aminoalkenes (also referred to as cyclohydroamination) and its intermolecular version between a primary/secondary amine and an alkene have in particular attracted the largest share of the attention in the years following the initial communication by Hill and co-workers.[47] The hydroamination of alkenes is essentially thermoneutral, but it is entropically disfavored, while the electrostatic repulsion between a nitrogen atom and an electron-rich alkene renders the direct nucleophilic attack difficult. The utilization of well-defined molecular catalysts allows for more facile reactions, and has opened access to a range of amine products with original regio- and, in some cases, enantioselectivity. Alkaline-earth complexes are a small contribution to the extensive toolbox of metal-based hydroamination

(pre)catalysts, but they can be singled out for their remarkable combination of selectivity and high reaction rates.

2.1 Intramolecular hydroamination reactions

The first example of Ae-mediated intramolecular hydroamination of aminoalkenes was reported in 2005 by Hill and co-workers,[47] who showed that the heteroleptic [{BDI^{DiPP}}CaN(SiMe$_3$)$_2$·(thf)] calcium complex (**1**) promoted the ring-closure of aminoalkenes to yield a range of substituted pyrrolidines and piperidines (Figure 8, n = 1 and 2). The formation of azepanes (n = 3) could not be achieved with calcium complexes and was only observed with magnesium analogues. Their initial study was complemented by a set of stoichiometric reactions and the preparation of model compounds aimed at delineating the nature of the operative mechanism,[51-53] and by a more comprehensive survey that explored both substrate scope and kinetic and mechanistic aspects of the catalyzed process.[50,54] Beyond **1**, the investigations were also extended to the utilization of the bis(amide) and bis(alkyl) complexes [Ca{N(SiMe$_3$)$_2$}$_2$·(thf)$_2$], [Ca{N(SiMe$_3$)$_2$}$_2$(thf)$_2$]$_2$ and [Ca{CH(SiMe$_3$)$_2$}$_2$·(thf)$_2$], and to their heavier Sr and Ba congeners.

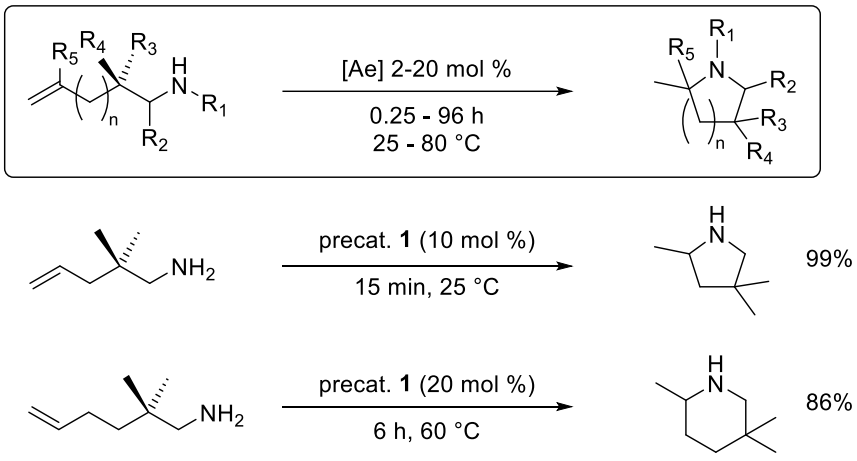

heteroleptic precatalyst **1** > precatalysts [Ca{N(SiMe$_3$)$_2$}$_2$.(thf)$_x$]

metal: Ca > Sr > Ba

reactive group: CH(SiMe$_3$)$_2$ > N(SiMe$_3$)$_2$

solvent: aromatic hydrocarbons >> ethers (e.g. thf)

ring size: n = 1 >> n = 2 ; no reaction for n = 3

substitution patterns on substrate

R_1: H > $CH_2CH{=}CH_2$ > Ph

R_2: H > Me

R_3, R_4: Ph, Ph > Cy > Me, Me >> H, H

R_5: H >> Me

Figure 8. Observed trends in the intramolecular hydroamination of aminoalkenes catalyzed by [{BDI^{DiPP}}CaN(SiMe$_3$)$_2$·(thf)] (**1**) and [Ae{E(SiMe$_3$)$_2$}$_2$·(thf)$_2$] complexes (Ae = Ca, Sr, Ba; E = CH, N).

Catalysis proceeded under mild conditions, with relatively low catalyst loading and short reaction times except for the most reluctant substrates. Reaction rates were found to be at least competitive with those reported earlier by Marks and co-workers with benchmark lanthanide precatalysts in the 1990s.[55] Ring closure followed Baldwin's guidelines (cyclisation rates: 5 > 6 > 7-membered rings), with the formation of pyrrolidines (near-complete conversion within minutes with a catalyst loading of 2-10 mol % at room temperature) being substantially faster than that of

piperidines. Positive Thorpe-Ingold effects were very noticeable, with the presence of geminal alkyl/aryl substituents in β position to the amine facilitating alkene coordination onto the metal center through the formation of favorable conformations in the transition state; this effect was particularly notable for Ph substituents. The inclusion of substituents onto the nitrogen atom or the C=C double were shown to severely reduce reaction rates for N-substitution (R_1) or internal C-atom (R_5) of the C=C double bond, whereas cyclization was entirely prohibited with internal alkenes. The catalyzed cyclization of 1-amino-1-phenyl-4-pentene and 2-amino-5-hexene, that is, substrates with substituents in α to the nitrogen atom (R_2), proceeded with good diastereoselectivity, affording the *trans*-pyrrolidines with diastereoisomeric excesses of 90 and 78%, respectively. However, reactions with prochirality in the β position (R_3 and R_4) did not exhibit any diastereoselectivity. For all its merits, precatalyst **1** was still somewhat hampered by its propensity to decompose through Schlenk equilibrium at high temperatures, and its inability to mediate the formation of seven-member azepanes or the cyclization of internal alkenes. Comparison of the reaction rates and observed yields indicated that for identical ligand environments, calcium precatalysts outclassed their strontium analogues, while barium was the least efficient of the three metals.

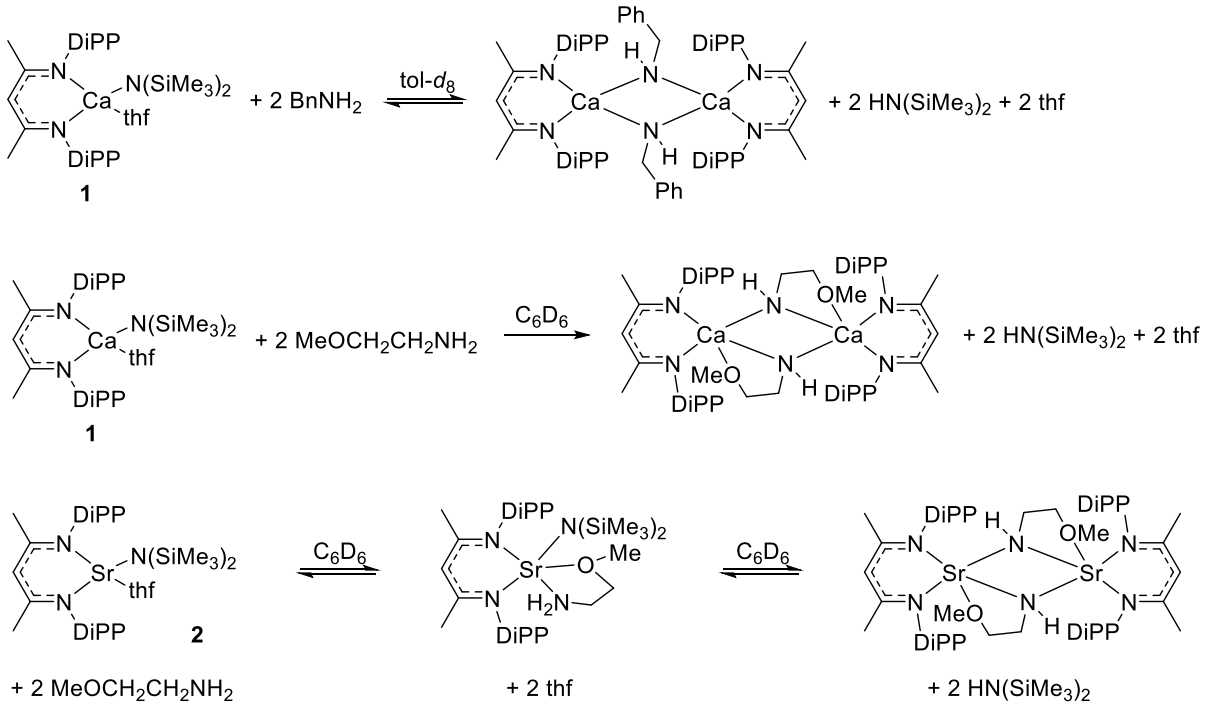

Figure 9. Transaminative protonolysis with [{BDI^{DiPP}}AeN(SiMe$_3$)$_2$·(thf)] precatalysts (Ae = Ca, **1**; Sr, **2**).

Stoichiometric studies (Figure 9) showed that although fast, the reaction between **1** and the benzylamine is equilibrated (ΔH° = –12.3 kcal mol^{-1}, ΔS° = –32.1 cal mol^{-1}, ΔG°_{298} = –2.7 kcal mol^{-1}).[52] With other, comparatively less acidic amines such as ^{t}BuNH$_2$ and CyNH$_2$, transamination did not occur. Instead, these amines were found to displace thf from the metal center and generate an amine adduct. This finding was consistent with the necessity for amine coordination onto the metal during catalysis, and was also consistent with the observed catalyst inhibition by both substrate and product during catalysis. In a similar study, the reaction of the strontium complex [{BDI^{DiPP}}SrN(SiMe$_3$)$_2$·(thf)] (**2**) in benzene-d_6 with the model substrate 2-methoxyethylamine corroborated these results.[54] It led to the

formation of an equilibrated mixture between the starting materials, the intermediate adduct [{BDI^{DiPP}}SrN(SiMe$_3$)$_2$·(MeOCH$_2$CH$_2$NH$_2$)] (which could be isolated by crystallization), and the dimeric product of transamination [{BDI^{DiPP}}SrN(H)CH$_2$CH$_2$OMe]$_2$. By contrast, the equimolar reaction of **1** with 2-methoxyethylamine was found to quantitatively generate [{BDI^{DiPP}}CaN(H)CH$_2$CH$_2$OMe]$_2$,[51] which was consistent with the superiority of the calcium precatalyst **1** over its strontium derivative **2** for catalysis. Catalyst activation with much more basic Ae-alkyl precursors was found to be irreversible and to provide overall more effective catalytic systems.

Kinetic analysis pointed to a rate law that showed first order dependence upon catalyst concentration consistent with a monometallic active species, and first order dependence upon [substrate]. It also highlighted catalyst inhibition by the product and by the substrate, in particular with an inverse dependence in the initial substrate concentration [substrate]$_0$. Unsurprisingly, the presence of thf was also found to considerably reduce reaction rates, due to competitive coordination onto the metal center. Deuterium labelling experiments highlighted the existence of a short-lived metal-alkyl intermediate within the catalytic manifold, produced upon insertion of the unsaturated C=C double bond into the Ca-N bond and then irreversibly cleaved upon reaction with an incoming substrate molecule that releases the final product and regenerates the catalytically active metal-amide species. Overall, reaction rates and catalytic turnover were found to be impeded by the coordination of Lewis bases (substrate, product, thf), dimerization of the complex to form a catalytically inactive species, and gradual decomposition through ligand scrambling at elevated temperatures. Based on these observations, the stepwise mechanism is depicted in Figure 10 as initially proposed by Hill and co-workers.

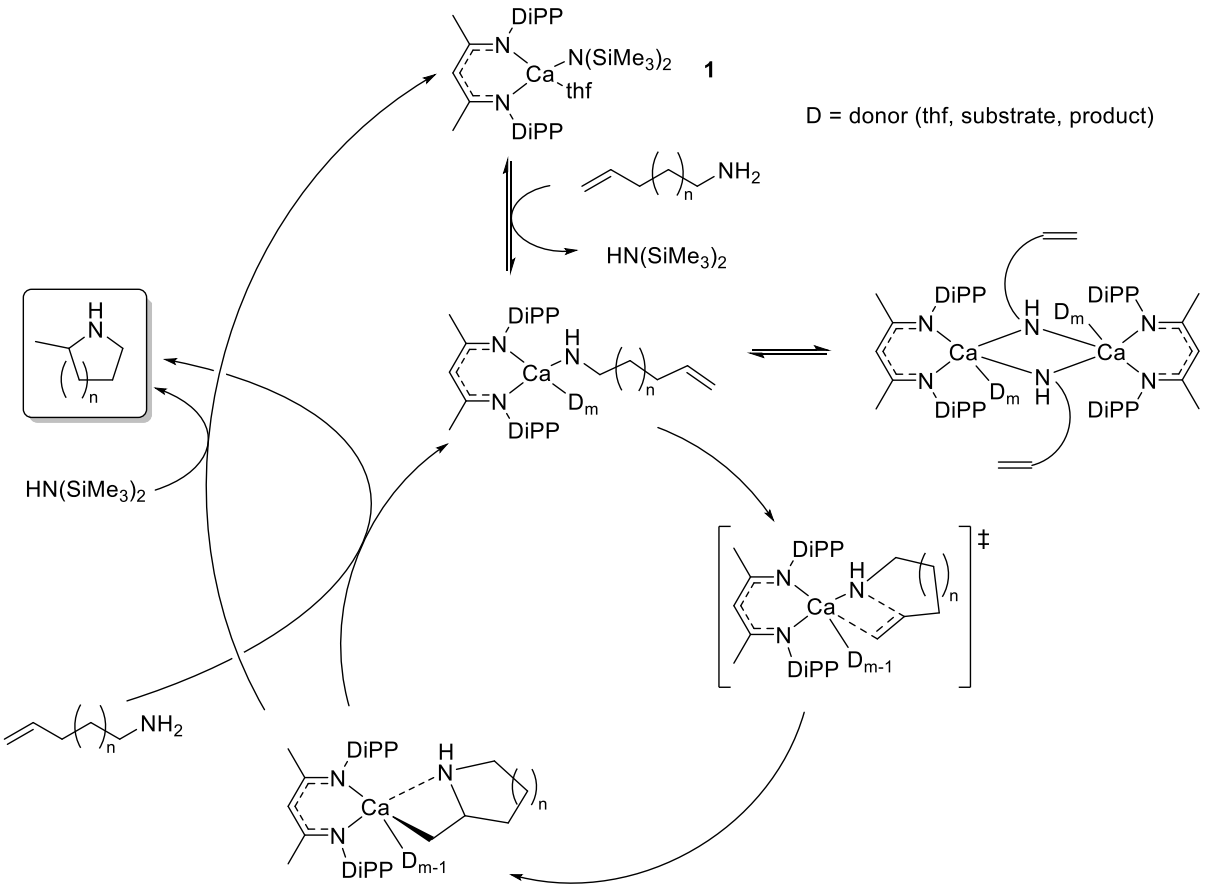

Figure 10. Proposed stepwise mechanism for the hydroamination of aminoalkenes catalyzed by **1**.

Further kinetic studies of the cyclization of the benchmark (1-allylcyclohexyl)methanamine (that is, n = 1, R_1 = R_2 = R_5 = H and R_3, R_4 = Cy in Figure 8) catalyzed by the unsolvated $[Ae\{N(SiMe_3)_2\}_2]_2$ for Ae = Ca and Sr confirmed that reactions rates decreased with increasing $[substrate]_0$. Eyring analysis provided the activation parameters, which showed that the observed increase of activation enthalpies as metal size increased was compensated by a favorable entropy of activation, the latter being a result of a decrease of the charge-to-size ratio and a less constrained geometry in the transition state. A substantial kinetic isotope effect detected when deuterated amines were used (k_H/k_D = 3.4-3.5). This KIE appeared to be unreconcilable with the initially proposed stepwise mechanistic pathway. Instead, it was suggested to reflect a rate-limiting step consisting of a non-insertive concerted proton transfer leading to ring-closure in a single step (Figure 11). Such concerted mechanism involving a six-centered transition state was consistent with a similar proposal made by Sadow and co-workers for their magnesium-mediated intramolecular hydroamination reactions, where the precatalyst was a tris(oxazolinyl)phenylborate magnesium methyl.[56]

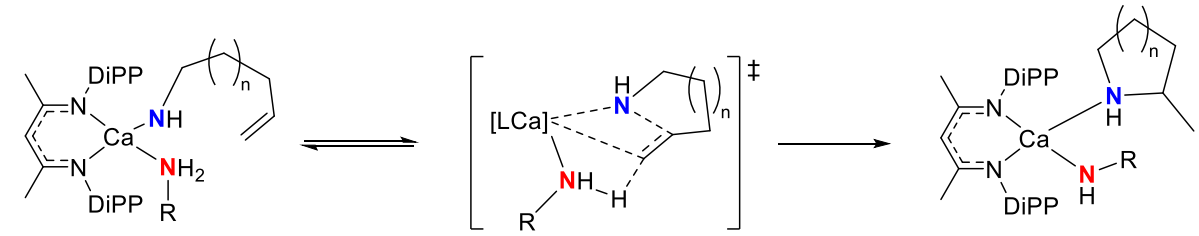

R = $CH_2(CH_2)_nCH_2CH{=}CH_2$ L = ligand

Figure 11. Refined non-insertive six-centered concerted transition state for intramolecular hydroaminations catalyzed by **1**.

A subsequent detailed DFT investigation of the mechanism of Sadow's magnesium-catalyzed hydroaminations, carried out by Tobisch, is relevant to the discussion on calcium-promoted catalysis.[57] Both the regular σ-insertive and the six-centered non-insertive pathways were found to be kinetically viable, and fully agreed with the experimental data. However, the transition state for the rate-limiting step for the insertive manifold (consisting of the aminolysis of the transient Mg-C bond) was calculated to be 5.0 kcal mol^{-1} lower in energy than that for the concerted mechanism, and hence for this case of magnesium-catalyzed hydroamination, the classical mechanism seems to be clearly prevailing. This study was not extended to reactions catalyzed by **1**, and therefore the question as to the exact nature of the operating mechanism with this calcium precatalyst is still unresolved.

Following the landmark studies by Hill and co-workers, a number of other calcium and strontium precatalysts were disclosed for the intramolecular hydroamination of aminoalkenes (Figure 12). They were most commonly stabilized by nitrogen-ligands, e.g. the bulky triazenides **3**-**4**,[58] the aminotromoniminates **5**-**6**,[59-60] the iminoanilides Ae-amides (**7**-**9**) and alkyls (**10**-**12**).[27,61-62] and the bis(imino)pyrrolides **7**-**8**.[63] The attempt to utilize bis(imino)napthene to generate Ae-alkyls precatalysts resulted in the formation of **15** and **16** through dearomatization of the ligand backbone; these precatalysts proved remarkably robust against Schlenk redistribution.[64] Some systems also incorporated oxygen-based ligands, such as the Ae-phenoxides **17**-**19**.[61] The zwitterionic bis(imisazolin-2-ylidene)borate **20**-**21** displayed excellent reaction rates, outperforming **1** by some margin in the case of **21**; interestingly, this strontium precatalyst was more efficient than its calcium counterpart, and both enabled the cyclisation of 2-methyl-6,6-diphenylazepane.[65] Overall, the

observed catalyst behaviors and reaction rates were similar to those observed with **1** and **2**. With some exceptions, for the same supporting ligand framework, cyclization rates were generally found to decrease upon descending group 2, with calcium often giving the best results: Ca > Sr > Ba. The amido precatalysts **7** and **8** supported by the rigid a comparatively rigid iminoanilide ligand proved superior to their β-diketiminato analogues **1** and **2**.[62] This trend was rationalized by the observation that no decomposition of **7** and **8** via ligand redistribution was detected under the chosen experimental conditions, in contrast to **1** and **2**.

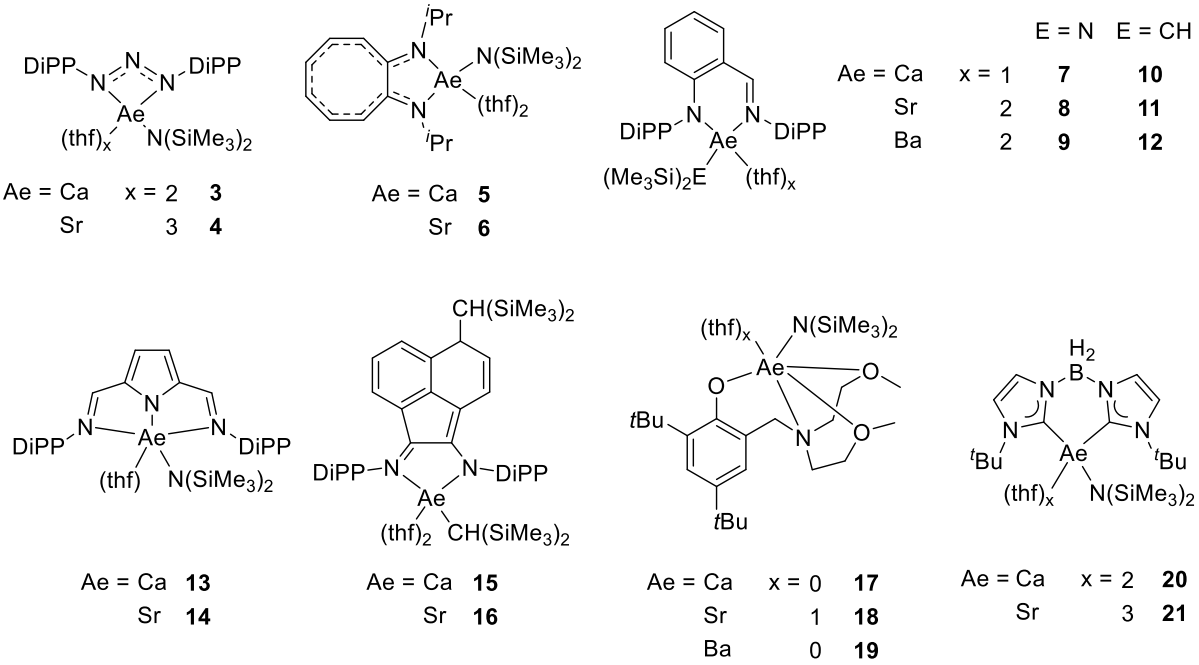

		E = N	E = CH
Ae = Ca	x = 1	**7**	**10**
Sr	2	**8**	**11**
Ba	2	**9**	**12**

Ae = Ca x = 2 **3**; Sr 3 **4**

Ae = Ca **5**; Sr **6**

Ae = Ca **13**; Sr **14**

Ae = Ca **15**; Sr **16**

Ae = Ca x = 0 **17**; Sr 1 **18**; Ba 0 **19**

Ae = Ca x = 2 **20**; Sr 3 **21**

Figure 12. Selected precatalysts for intramolecular hydroamination of aminoalkenes.

The alkyl precatalysts (**10-12**) provided much greater reactions rates than their amido counterparts (**7**-**9**) in the cyclization of 1-amino-2,2-dimethyl-pent-4-ene,[62] due to their greater basicity and ability to produce irreversibly the catalytically active Ae-amidoalkene species. Accordingly, the Gibbs energy of activation determined by Eyring analysis for the barium-alkyl **12** was lower than that for **9** ($\Delta G^{\ddagger}$ = 21.1(2) and 23.8(3) kcal mol^{-1}, respectively). A moderate kinetic isotope effect was measured when N-deuterated aminoalkene was used (k_H/k_D = 2.6(4)), and the kinetic rate law showed a first-order dependence upon both [catalyst] and [aminoalkene]. Based on these data, Sarazin and co-workers proposed a six-centered non-insertive concerted mechanism as the prevailing pathway for intramolecular hydroamination catalyzed by the barium complexes **9** and **12**, in agreement with the mechanism previously proposed by Hill for his calcium catalysts (see Figure 11).[54,62]

A thorough computational assessment of the two possible alternative mechanisms (stepwise σ-insertive vs concerted proton-assisted) for the intramolecular hydroamination of aminoalkenes catalyzed by **7**-**9** was performed.[66] This DFT study supported a prevalent mechanistic pathway consisting of (i) a stepwise insertive route, with a catalytically active Ae-amidoalkene that undergoes reversible σ-insertive N-C bond-forming ring-closure, followed by (ii) a rate-limiting, irreversible σ-bond aminolysis between the newly formed Ae-C bond in the Ae-alkyl intermediate and an incoming aminoalkene (Figure 13). The DFT-derived mechanism was compatible with the experimental data.

Rate-determining aminolysis was consistent with the observed kinetic isotope effect, and the DFT-computed energy barrier also agreed with the data obtained from kinetic analysis.[62] The reactivity trend Ca < Sr < Ba observed in intramolecular hydroaminations catalyzed by **7**-**9** was rationalized as being the outcome of increasingly favorable metal-aminoalkene interactions when the metal was more compact, since regardless of its size (Ca < Sr < Ba), the metal center was found to be equally accessible and the approach of the substrate was not sterically hindered.

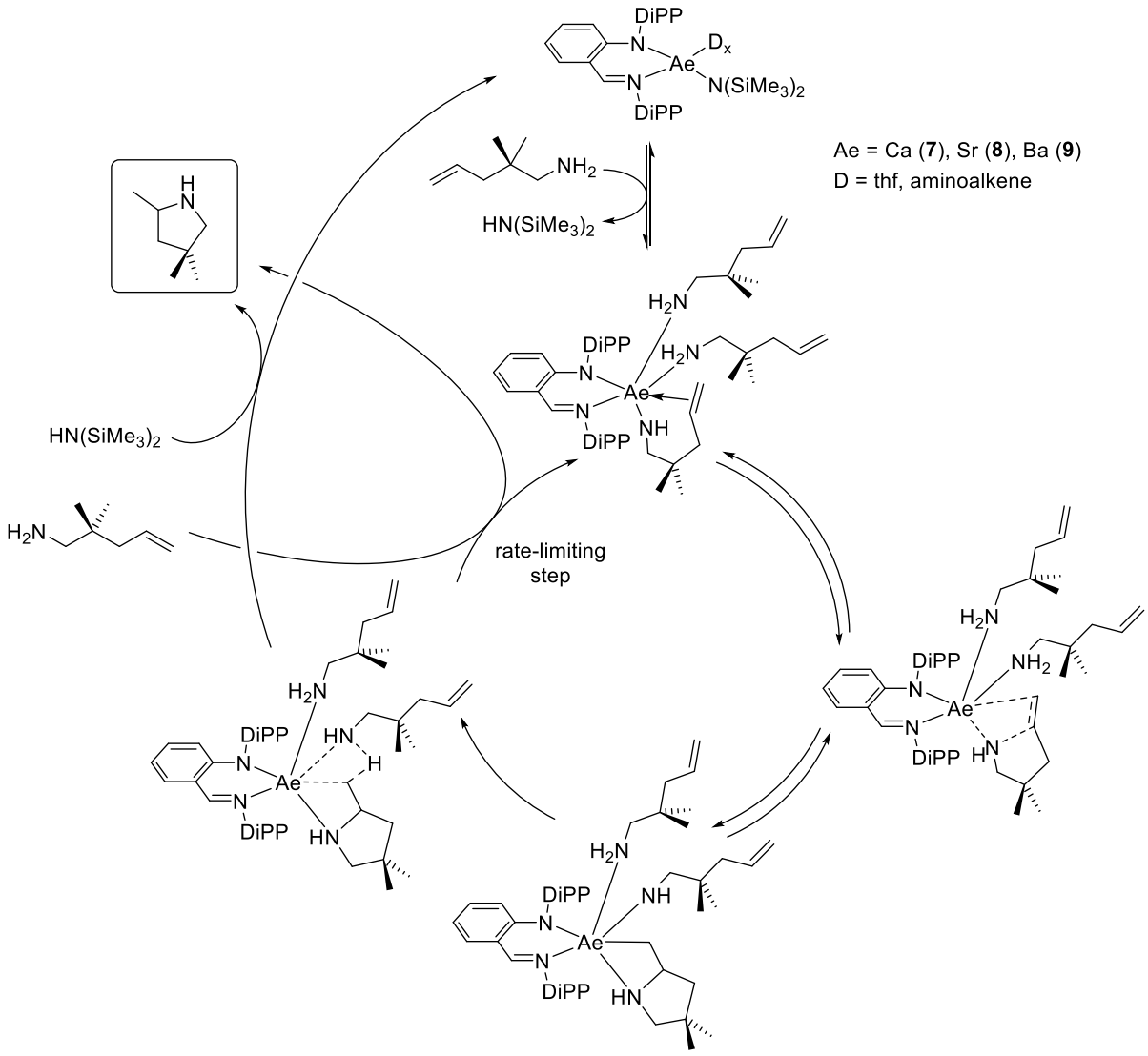

Figure 13. Prevailing stepwise σ-insertive pathway for the hydroamination of aminoalkenes catalyzed by **7**-**9** derived from experimental and DFT investigations.

2.2 Asymmetric intramolecular hydroamination reactions

Because complexes of the large alkaline earths are easily prone to ligand scrambling, Ae-based precatalysts for asymmetric hydroaminations are rare, and the overall performances of such complexes have been unimpressive. By contrast, a small number of very selective (ees up to 92%) magnesium precatalysts have been described, where the metal is encapsulated by a rigid aminophenolate.[67-68]

The first attempt to achieve the asymmetric intramolecular hydroamination reactions came from the group of Harder, who used the enantiopure calcium bis(oxazoline)-amide [{(*S*)-Ph-BOX}CaN(SiMe$_3$)$_2$·(thf)$_2$] (**22**, Figure 14) but despite achieving high substrate conversions, they only observed low ees (5-10%).[69] The diamido calcium precatalyst **23** gave slightly higher ees (up to 26%), but the reactions required several days to partly convert 10 equivalents of 1-amino-2,2-R$_2$-pent-4-ene (R = Me or Ph).[70] The utilization of chiral calcium-bis(imidazoline) complexes did not provide any improvement,[71] but tangibly better results (ees up to 50%, reaction time 24 h) were achieved by using bis(oxazolinylphenyl) ligands (**24**).[72] High reaction rates (full conversion in 5 min) but low ees (16%) were observed when the tris(oxazolinyl)borato calcium complex **25** was used.[73] Generally, all attempts to obtain ees in the upper ranges were thwarted by the participation of the calcium complexes in ligand-redistribution processes; to alleviate this issue, the attempt to use a calcium complex supported by axially chiral dianionic (*R*)-(+)-2,2'-diamino-1,1'-binaphthyls only led to similar ees, up to 57%.[74] No asymmetric cyclohydroamination was reported for Sr or Ba precatalysts.

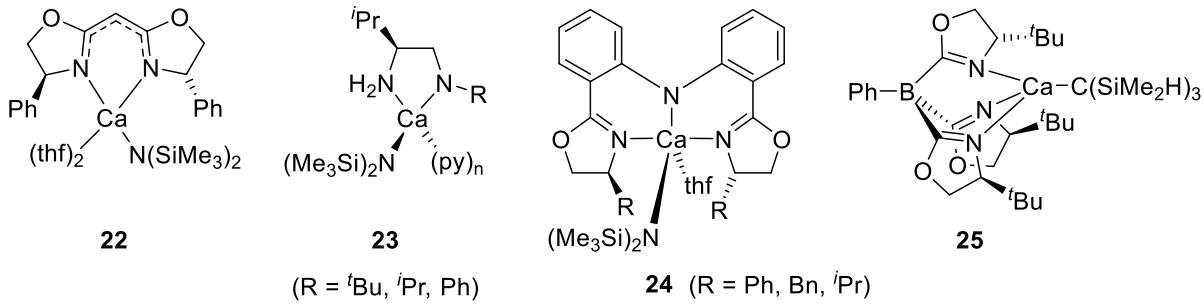

22 **23** **24** (R = Ph, Bn, ^{i}Pr) **25**

(R = ^{t}Bu, ^{i}Pr, Ph)

Figure 14. Calcium precatalysts for the asymmetric intramolecular hydroamination of aminoalkenes.

2.3 Intermolecular hydroamination reactions

The intermolecular hydroamination of unsaturated C-C bonds is entropically more demanding than its intramolecular version. The observed reactions rates are considerably slower, and, with Ae catalysts, it is, for now, restricted to activated alkenes (i.e., styrene derivatives and conjugated double bonds) and alkynes. Accordingly, fewer investigations have been led in the area of intermolecular Ae-mediated hydroamination. It is likely to remain so until the current deadlock concerning the elusive functionalization of non-activated alkenes, necessary to expand the scope and utility of this catalysis, is broken.

2.3.1 Intermolecular hydroamination of alkenes

Hill and co-workers first showed that the bis(amido) and bis(alkyl) complexes [Ae{N(SiMe$_3$)$_2$}$_2$]$_2$ and [Ae{CH(SiMe$_3$)$_2$}$_2$·(thf)$_2$] (Ae = Ca, Sr, Ba) efficiently catalyzed the hydroamination of vinylarenes and conjugated dienes with a wide range of cyclic or acyclic amines such as pyrrolidine, piperidine, benzylamine and tert-butylamine.[75-76] Later, the iminoanilide complexes **7**-**12** also emerged as highly competent catalysts, providing the highest reactions rates measured for these reactions.[27,62] The reactions proceeded under mild conditions (room temperature to 60 °C, low catalyst loading) with excellent regiospecificity, affording exclusively the *anti*-Markovnikov addition products (Figure 15).

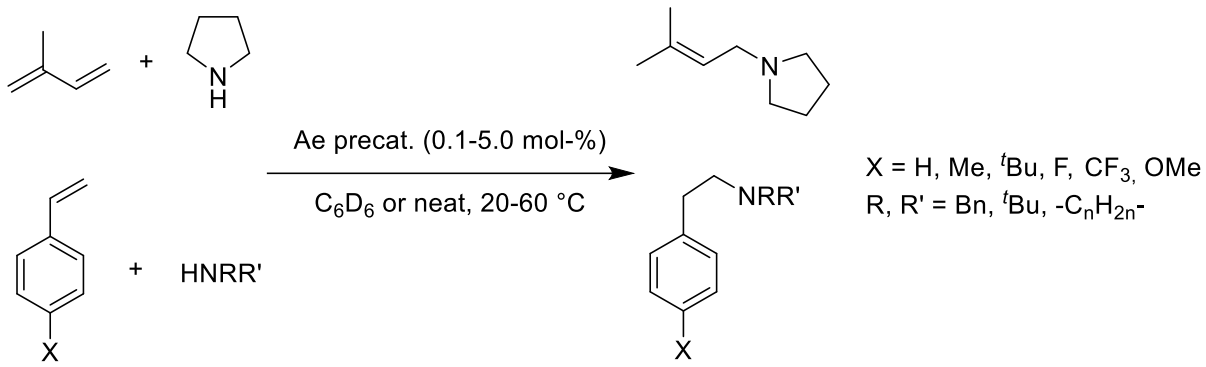

Figure 15. Ae-catalyzed intermolecular hydroamination of activated alkenes. Only the formation of *anti*-Markovnikov products is observed.

The general mechanism is presumed to follow the main guidelines displayed in Figure 7 for substrates with a protic hydrogen atom. The entry into the catalytic cycle is achieved through quantitative and irreversible (for Ae-alkyl) or equilibrated (for Ae-amide) protonolysis between the precatalyst and the reactive amine substrate. The regioselective outcome of the catalytic event is dictated by the relative distribution of charges along the Ae-N and C=C bonds, as the positioning of the unsaturated substrate with respect to the metal is governed by the intrinsic polarity of these two bonds. In the case of vinylarenes, the aromatic ring will stabilize the incipient negative charge on the C atom in the position α to the ring, hence promoting the exclusive formation of the *anti*-Markovnikov addition product. Accordingly, reaction rates were substantially enhanced when electron-withdrawing groups (F, CF_3) were introduced in *para* position to the vinylic moiety as a result of transition state lower in energy compared to benchmark styrene (R = H), whereas inversely, the kinetics were much slower when electron-donating groups (OMe < ^{t}Bu < Me) were added instead. In all cases, Ae-alkyl precatalysts that irreversibly entered the reaction manifold displayed much greater efficacy than their amido analogues, for which activation was reversible.

Kinetic analysis of the $[Ae\{N(SiMe_3)_2\}_2]_2$ precatalysts showed that hydroamination rates were in the order Ba << Ca < Sr.[75-76] The low performance of this barium system to catalyze the reaction was attributed to its large and diffuse nature, and its resulting inability to sufficiently polarize the incoming C=C unsaturated bond in order to enable its insertion into the prepolarized Ba-N_{amide} bond. The kinetic rate law that was established and given is equation (1) shows a second-order dependence in [catalyst] that was hypothesized to be the consequence of the dimeric nature of the catalyst.

$$\text{Rate} = k\,[\text{catalyst}]^2\,[\text{amine}]^1\,[\text{alkene}]^1 \qquad (1)$$

A strong kinetic isotope effect was detected when *N*-deuterated amines were utilized, which led the authors to propose a catalytic manifold consisting of a six-centered transition state with concerted H-assisted bond-breaking and bond-forming processes, reminiscent of that suggested for intramolecular hydroaminations (see Figure 11).

Kinetic investigations of the intermolecular hydroamination of vinylarenes and pyrrolidine catalyzed by **7**-**9** provided different conclusions.[27,62] The barium precatalyst provided by far the highest reactions rates, and rate dependence varied with Ca < Sr < Ba. A very strong kinetic isotope effect was measured for *N*-deuterated pyrrolidine (k_H/k_D = 6.8 at 40 °C and 7.3 at 60 °C), whereas the kinetic rate late given in equation (2) showed a partial first-order dependence in the concentrations of each of the components in the system.

Rate = k [catalyst]^1 [amine]^1 [alkene]^1 (2)

The activation parameters obtained by Eyring analysis ($\Delta H^{\ddagger}$ = 18.3 kcal mol^{-1}, $\Delta S^{\ddagger}$ = –13.1 cal mol^{-1}, $\Delta G^{\ddagger}_{298}$ = 22.2 kcal mol^{-1}) showed the reaction to be kinetically affordable in the chosen temperature range (25-60 °C). Again, a non-insertive proton-assisted mechanism consistent with the experimental and kinetic data was proposed as being the prevailing mechanism (Figure 16).

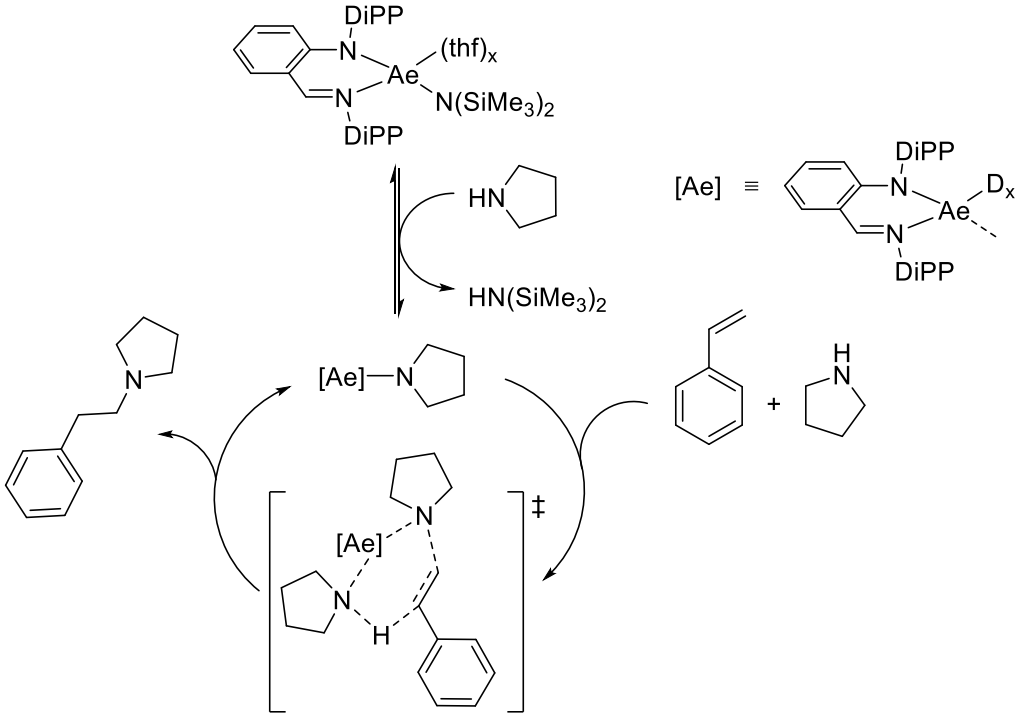

Figure 16. Transition state in the initially proposed non-insertive mechanism for the hydroamination of vinylarenes and amines catalyzed by iminoanilide precatalysts **7**-**9**.

Yet, a comprehensive computational analysis of the two plausible mechanisms for the hydroamination of vinylarene catalyzed by **7**-**9** showed that the kinetically prevailing mechanism most likely consisted of a stepwise σ-insertive pathway (with a corresponding transition state 4.2 kcal mol^{-1} lower than for the proton-assisted mechanism, Figure 17), with fast and reversible migratory C=C bond insertion into the suitably polarized Ae-$N_{pyrrolide}$ σ bond.[77] This insertion was found to occur with 2,1-regiospecificity through a highly polarized four-center transition state, followed by irreversible intramolecular aminolysis of the Ae-C bond in the alkaline-earth alkyl intermediate. The experimentally observed Ca < Sr < Ba trend was rationalized as being the outcome of weaker Ae-$N_{pyrolide}$ bonds along with decreased steric protection of the metal center by the iminoanilide ligand as group 2 is descended.

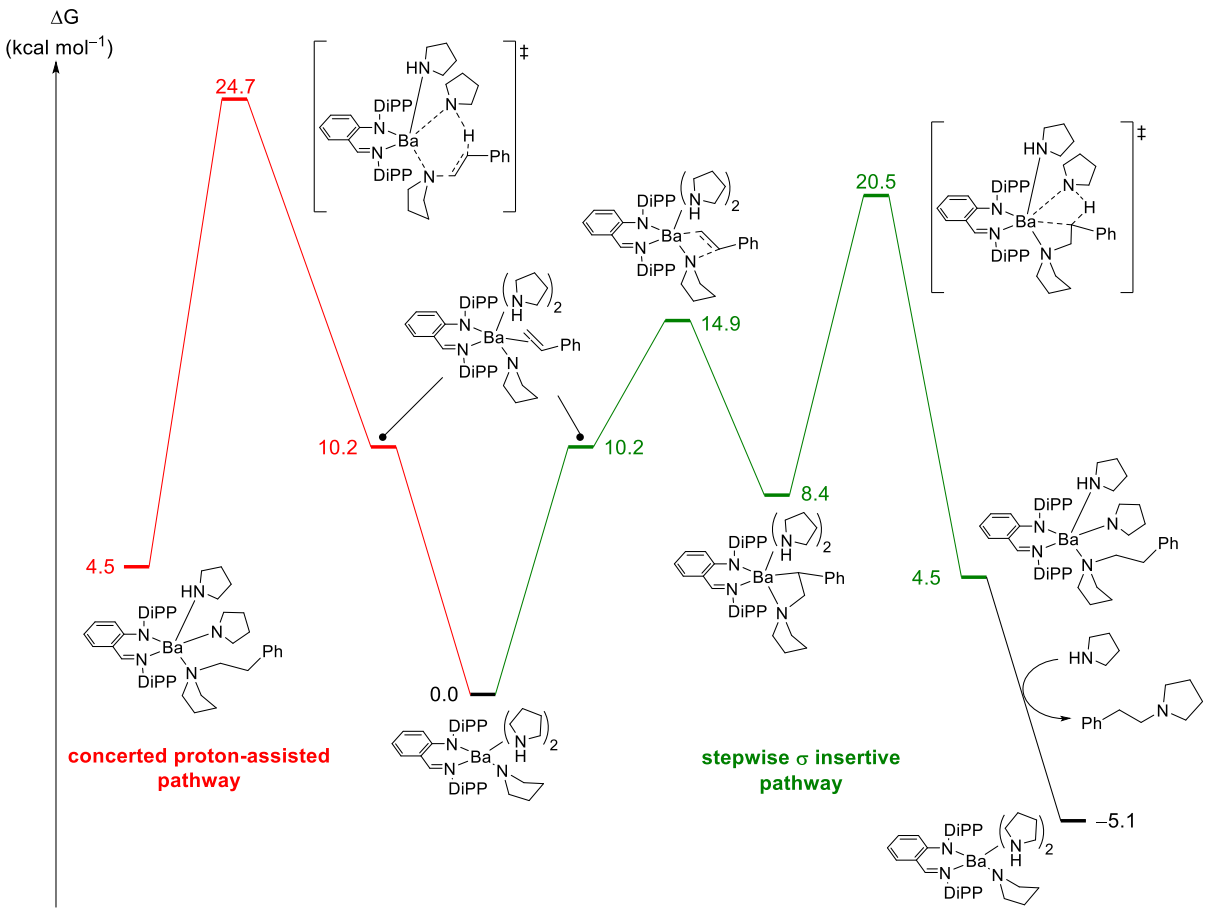

Figure 17. DFT analysis of the rival mechanistic pathways for the hydroamination of styrene with pyrrolidine catalyzed by **9**, showing the σ-stepwise insertive route (green) to be kinetically favored over the more energetically demanding concerted route (red).

Intermolecular hydroamination reactions are more sluggish than their intramolecular version, generally requiring more forceful conditions (higher temperature, longer reaction times and greater metal loading). This was illustrated by the one-pot domino intramolecular and intermolecular hydroamination that combined styrene and 1-amino-2,2-dimethyl-pent-4-ene to selectively yield 2-(2,4,4-trimethylcyclopentyl)ethyl)benzene when catalyzed by the barium precatalyst **9** (Figure 18). Because the observed rate dependence on metal identity are opposite for the intramolecular (Ba < Sr < Ca) and intermolecular (Ca < Sr < Ba) hydroaminations, careful examination of the performances for each precatalyst is a requisite to obtain chemospecific reactions.[62]

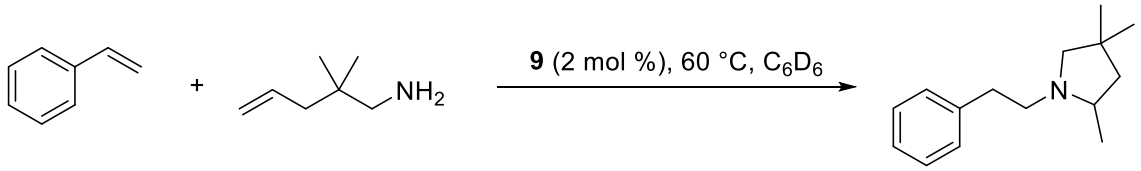

Figure 18. Domino intra- and intermolecular hydroamination of styrene with aminoalkenes.

2.3.2 Intermolecular hydroamination of carbodiimides and isocyanates

Heterocumulenes such as carbodiimides[78] and isocyanates[79] were found to be suitable substrates for intermolecular hydroaminations with aromatic amines, yielding respectively guanidines and ureas in controlled fashion (Figure 19). With 2-6 mol% catalyst loading and in the temperature range 25-80 °C, the reaction catalyzed by **1** or the amido precatalysts [Ae{N(SiMe$_3$)$_2$}$_2$·(thf)$_n$] (Ae = Ca, Sr, Ba; *n* = 0, 2) proceeded with rates greater than those observed with alkenes. The rates were heavily influenced by the nature of the metal (Ba < Sr < Ca), with the barium systems being poorly efficient, likely as a result of the formation of insoluble and inactive polynuclear species. Product formation was greatly affected by substitution on both the amine and the carbodiimide (^{t}Bu < ^{i}Pr < Cy). Although high yields could be achieved (reaching sometimes over 90%), the reactions were never quantitative.

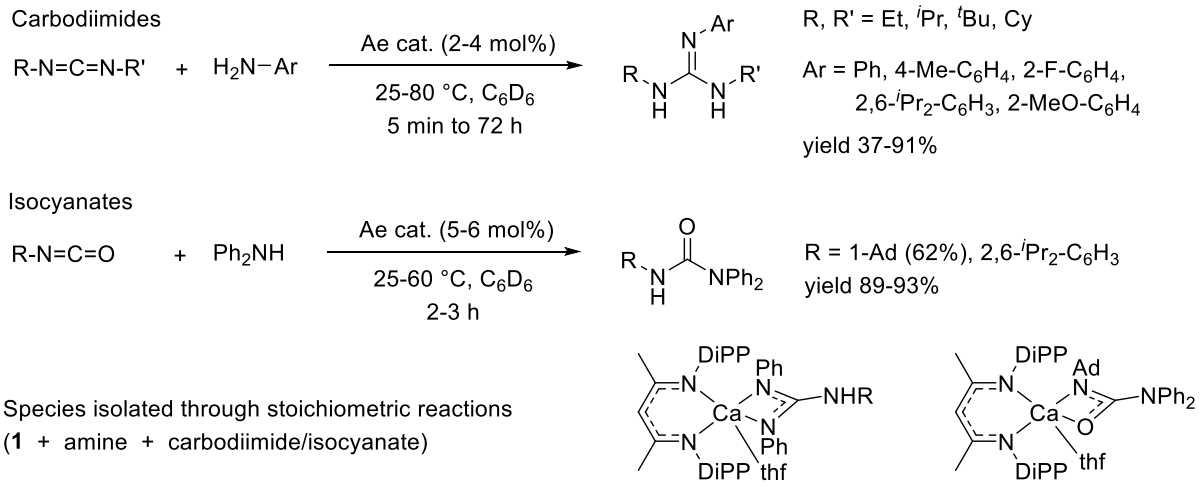

Figure 19. Hydroamination of carbodiimides and isocyanates catalyzed by **1** or [Ae{N(SiMe$_3$)$_2$}$_2$·(thf)$_n$].

The formation of stable guanidinate or ureate resting states, in concentrations that increased as the substrates were gradually consumed, was presumed to inhibit full conversion to the products. Substrate scope was limited to aromatic amines. Aliphatic amines were insufficiently acidic to allow for the aminolysis re-activation of these resting states. The isolation of catalytically active homoleptic guanidinate and heteroleptic ureate complexes, achieved through stoichiometric reactions,[80] agreed with reaction manifolds advancing via σ-insertive pathways.

2.3.3 Intermolecular hydroamination of alkynes

The hydroamination of alkynes can be catalyzed by Ae precatalysts, often yielding alkenylamines as mixtures of *E* and *Z* isomers.[76] [Sr{CH(SiMe$_3$)$_2$·(thf)$_2$] mediated the quantitative hydroamination of diphenylacetylene (phenylacetylene could not be used on account of the acidity of the terminal C-*H* hydrogen) with piperidine in thf within 2 h at 60 °C (Figure 20). It outperformed its calcium analogue [Ca{CH(SiMe$_3$)$_2$·(thf)$_2$] and, even more so, the Sr-amide derivative [Sr{CH(SiMe$_3$)$_2$]$_2$.

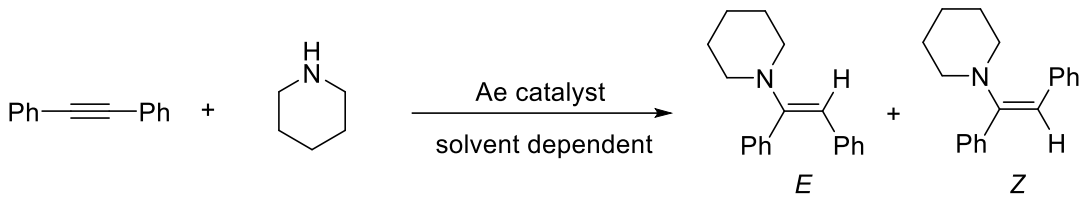

Figure 20. Hydroamination of alkynes.

The reaction was found to be very solvent dependent, with thf affording greater *E*/*Z* selectivity (91:9) than hydrocarbons (ca. 60:40). Other ethers (dioxane, 2-Me-thf, dme) did not afford any conversion.

2.3.4 Intermolecular hydroamination of diynes

Westerhausen and co-workers have explored the hydroamination of diynes with secondary amines. The reaction can be catalyzed by alkaline-earth complexes, often as ate salts obtained upon mixing with alkali species. For instance, neither $KNPh_2$ nor $Ca(NPh_2)_2$ catalyze the addition of $HNPh_2$ onto diphenylbutadiyne, but the reaction proceeds when the ate heterobimetallic $[K_2Ca(NPh_2)_4]$ is used instead.[81] Replacement of an aromatic group by an alkyl one in the amine results in increased reaction rates, due to the enhanced basicity of the resulting amide. Quantitative addition of $HNPh^iPr$ onto diphenylbutadiyne is catalyzed within 1 h by 5 mol% of $[K_2Ca(NPh_2)_4]$ at 65 °C in thf (Figure 21). Starting from the ubiquitous heterobimetallic $[K_2Ca\{N(H)DiPP\}_4]$, a typical catalytic manifold starting with a preliminary aminolysis and leading to the *E* and *Z* isomers is proposed in Figure 22; the exact identity of the active species remains unknown.

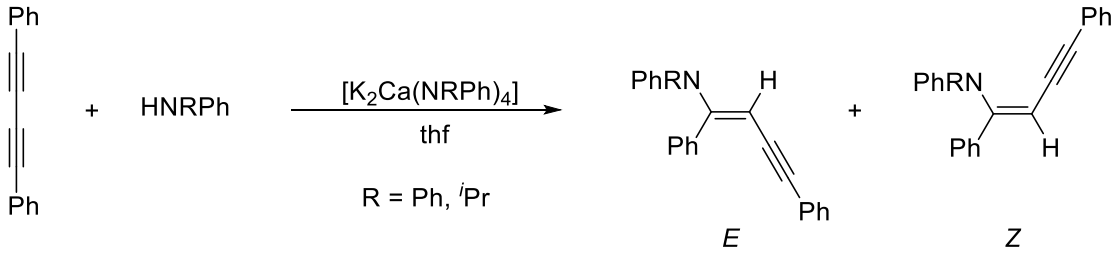

Figure 21. Hydroamination of diphenylbutadiyne with the calciates $[K_2Ca(NRPh)_4]$ in thf.

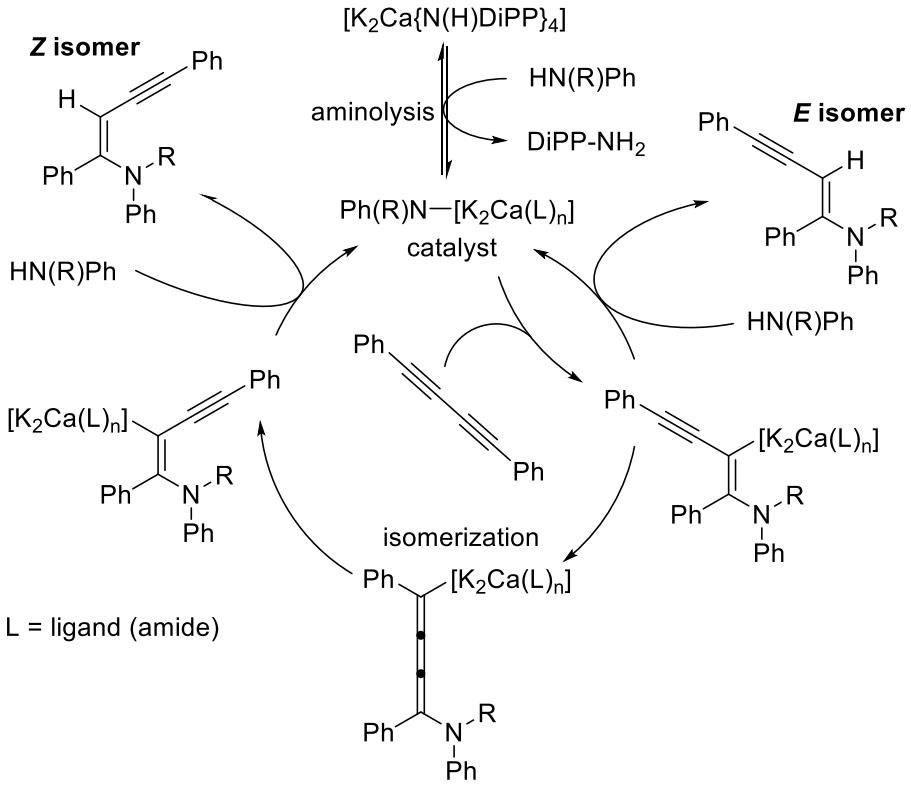

Figure 22. Proposed mechanistic pathway to the hydroamination of diphenylbutadiyne.

The second triple bond in diphenylbutadiyne is less reactive than the first one. Hence, the unsolvated and pre-isolated $[K_2Ca\{N(H)Dipp\}_4]$[82] readily catalyzed the hydroamination of diphenylbutadiyne with N-methyl-anilines in thf at room temperature, regioselectively yielding (N-methyl)-(N-aryl)-1,4-diphenylbut-1-ene-3-yne-1-ylamine within a few hours as a mixture of *E*/*Z* isomers. However, hydroamination of the second unsaturated bond required extended reaction times and could only be achieved with *N*-methyl-aniline and *N*-methyl-4-fluoroaniline; a mixture of *E*,*E*-, *E*,*Z*- and *Z*,*Z*-isomers was obtained (Figure 23).[83]

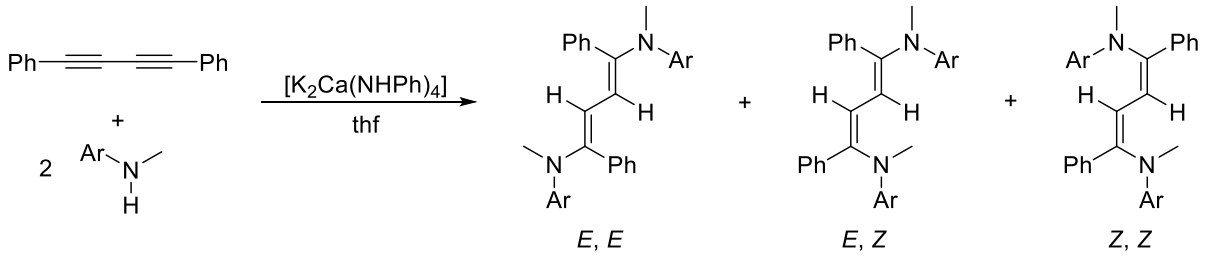

Figure 23. Hydroamination of diphenylbutadiyne with the isolated calciate $[K_2Ca(NRPh)_4]$.

The elegant attempt to exploit the difference in reactivity between the two triple bonds in diphenylbutadiyne using 1,2-dianilinoethane for the production of a cyclic butadiene through consecutive inter- and intramolecular hydroaminations led to the unexpected formation of acyclic enyne derivatives (Figure 24). A mixture of *E*,*E*-, *E*,*Z*- and *Z*,*Z*-isomers was again generated within a few hours using the combined action of $[K_2\{1,2\text{-}(PhN)_2\text{-}C_2H_4\}\cdot(thf)_3]$ and $[Ca_2\{1,2\text{-}(PhN)_2\text{-}C_2H_4\}_2\cdot(thf)_5]$ (with a K/Ca ratio of 2:1).[84] The formation of the entropically favored cyclic butadiene was never detected.

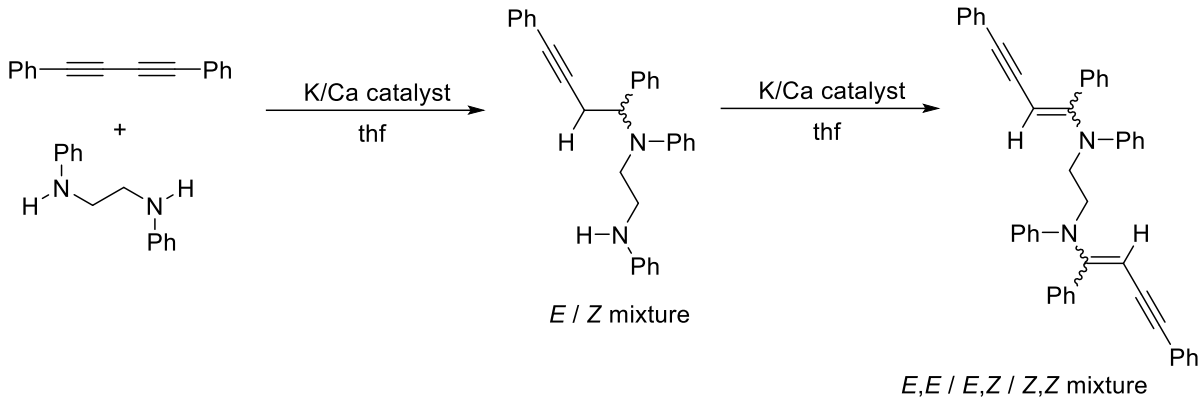

Figure 24. Double Hydroamination of 1,2-dianilinoethane and diphenylbutadiyne.

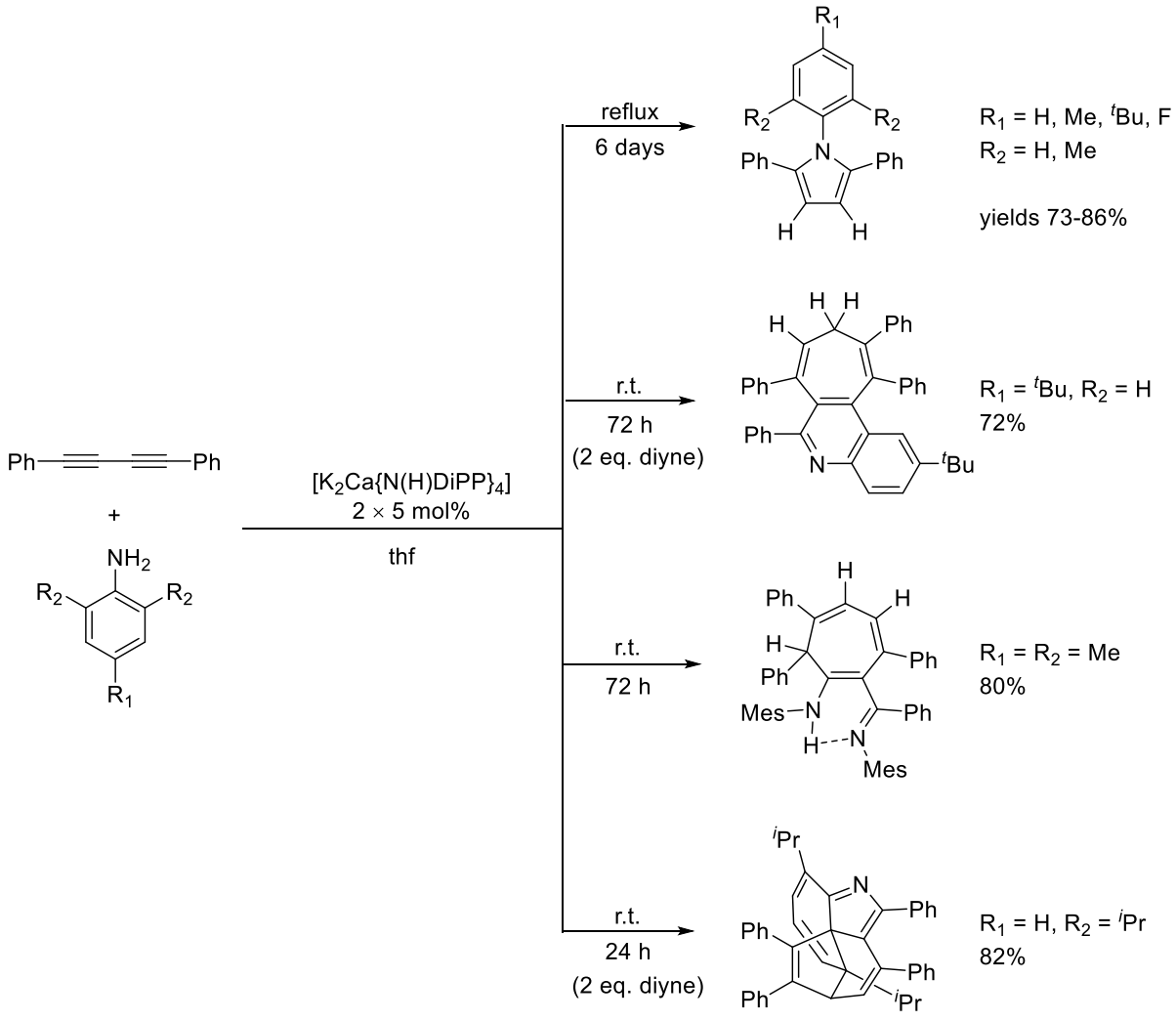

Figure 25. Hydroamination of diphenylbutadiyne with substituted anilines, showing the influence of substrate and reaction conditions.

By contrast, the use of primary amines for the double hydroamination of diynes allows for the formation of cyclic products. Hence, the addition of substituted aniline onto diphenylbutadiyne is efficiently catalyzed by $[K_2Ca\{N(H)DiPP\}_4]$.[85] With 10 mol% of catalyst in refluxing thf, the expected *N*-

aryl-2,5-diphenylpyrroles were obtained in high yields after 6 days, independently of the identity of the *N*-aryl group (Figure 25). However, entirely different products were formed if the reactions were performed at room temperature, due to the low reactivity of the second C-C triple bond and kinetically competitive C-H activation processes for *ortho*-C-H positions of the *N*-aryl moieties. Hence, quinolines with annelated cycloheptatriene rings were obtained with *p*-^{t}Bu-aniline. If the *ortho* positions on the *N*-aryl substrate were blocked by methyl substituents (e.g. with mesityl), a substituted cycloheptatriene formed instead. Utilization of the bulkier 2,6-diisopropylaniline led to the formation of a very unusual, strained tetracyclic product.[86] Several plausible mechanisms were proposed to explain the formation of the different observed products; that leading to the substituted pyrroles is depicted in Figure 26, but accurate catalyst speciation could not be accomplished. On the whole, the reactivity of the amines in the hydroamination of diynes increased with diphenylamine < *N*-alkylaniline < dialkylamine < aniline. It is also clear that the synergistic effect of the combined potassium and calcium anilido salts to generate a heterobimetallic active species was necessary to achieve high turnovers and acceptable reactions rates, as each component taken on its own failed to deliver equally satisfactory results.

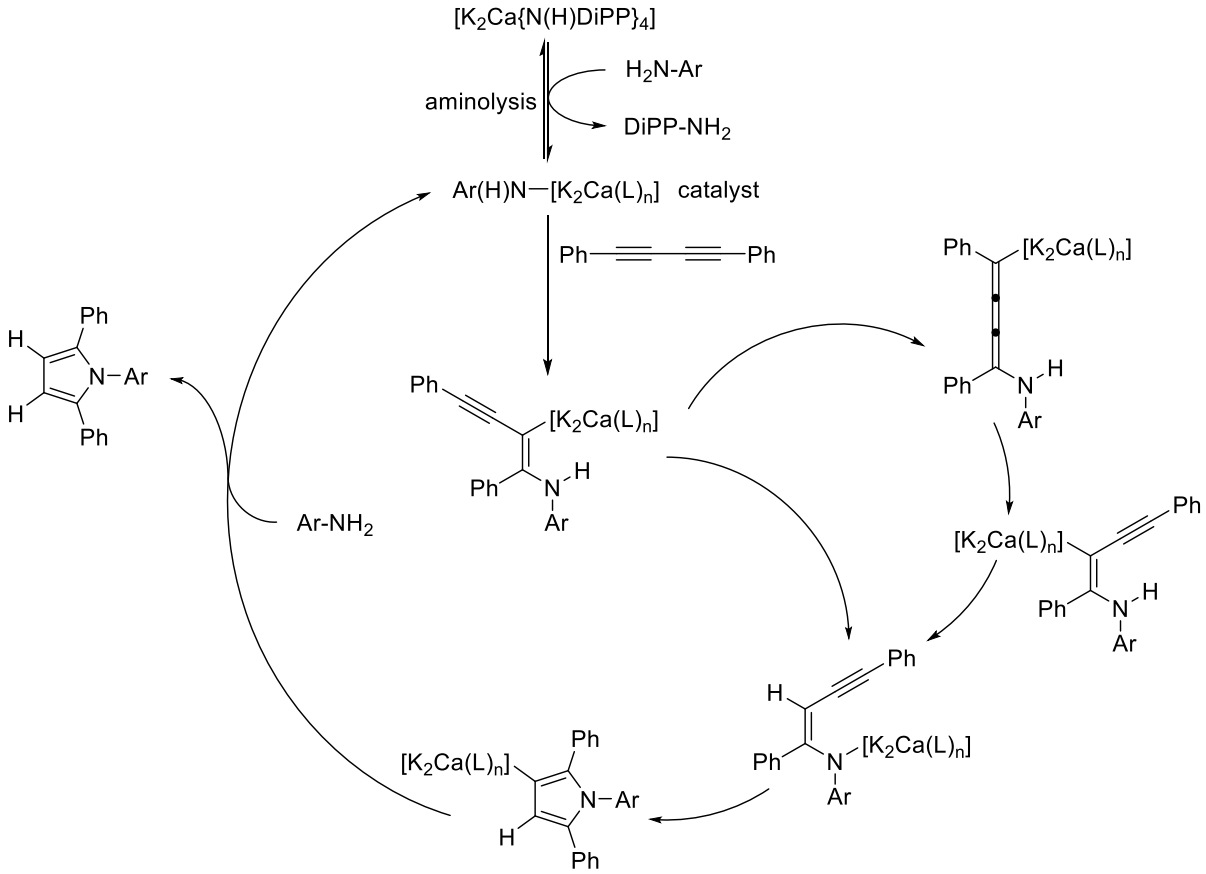

Figure 26. Proposed operative mechanism for the formation of substituted formation of 2,5-diphenyl-pyrroles catalyzed by K/Ca heterobimetallic precatalysts.

3 Hydrophosphination and related catalysis

The creation of C-P bonds through metal-mediated catalysis has been attracting interest for over 30 years because it allows for the convenient formation of valuable phosphines and related P-containing

molecules. *P*-hydroelementations are split into three categories that are defined by the number of oxygen atoms contained in the *P*-substrate that is going to be added to the C≡C, C=C, C=O or C=N unsaturated bonds. Hydrophosphination (also called hydrophosphanylation) involves a phosphine HPR_2. Hydrophosphinylation (for $HP(O)(R)_2$ and HP(O)(OR)R', one and two oxygen atoms, respectively; the name hydrophosphorylation is also often used for $HP(O)(R)_2$) and hydrophosphonylation (for $HP(O)(OR)_2$, three oxygen atoms) are the two other sets of reactions. On the whole, the attention has mostly focused of hydrophosphination reactions. Although lanthanidocenes built on trivalent rare earths are known to catalyze the intramolecular hydrophosphination of phosphinoalkenes and phosphinoalkynes to yield cyclic phosphines, they have failed to promote the equivalent intermolecular reactions.[87-88] However, in 2003 a ytterbium(II) system was shown to enable the addition of diphenylphosphine onto alkynes.[89] The analogy between Yb(II) and Ca, combined to the fact that calcium and larger Ae complexes competently catalyzed intermolecular hydroamination reactions, naturally prompted exploration in the area of Ae-mediated intermolecular hydrophosphinations. The seminal report of a discrete Ae catalyst by Hill and co-workers dates back to 2007.[90] It was followed by a series of contributions from the group of Westerhausen for the alkaline-earth promoted hydrophosphination of alkynes and diynes, and by other studies dealing with the hydrophosphination of activated alkenes and heterocumulenes catalyzed by Ae complexes. A handful of other contributions disclosed Ca, Sr and Ba precatalysts to promote the hydrophosphonylation of non-activated alkenes, aldehydes and ketones.

3.1 Intermolecular hydrophosphination of alkenes

A number of alkaline-earth complexes have been disclosed for the hydrophosphination of activated arenes, such as vinylarenes and conjugated dienes. To date, there is no example of successful catalysis with non-activated alkenes, e.g. 1-hexene. The *P*-substrates that are employed are mostly limited to benchmark secondary phosphines ($HPPh_2$ and, to a lesser extent, $HPCy_2$) and, in some cases, the primary phosphine $PhPH_2$. The reactions afford the products of *anti*-Markovnikov addition with excellent regioselectivity (Figure 27). Intermolecular hydrophosphinations are more sluggish than the hydroamination version, and require more forcing conditions. Depending on its identity and overall efficiency, precatalyst loading typically range between 2-10 mol%, with temperatures generally between 25-80 °C. Reactions can be run in C_6D_6 or, to improve reaction rates, in neat substrates. A selection of alkaline-earth precatalysts that have been used for the hydrophosphination of alkenes is listed in Figure 28. Some of the different ligands that have been implemented with mitigated success include β-diketiminates,[90] variously substituted iminoanilides[27,62,91,92] and amidinates,[93-95] NHC-stabilized amides,[96] benhydryls,[97] phenolates[27,62,98] and fluoroalkoxides.[99] By and large, most of the effective precatalysts to date are hence supported by sterically shielding nitrogen-based ligands. The majority of systems have been built around calcium, although there is now abundant evidence that reaction rates increase from calcium to strontium and, even more so, to barium.

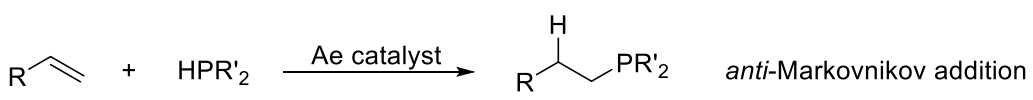

Figure 27. Ae-catalyzed intermolecular hydrophosphination of alkenes.

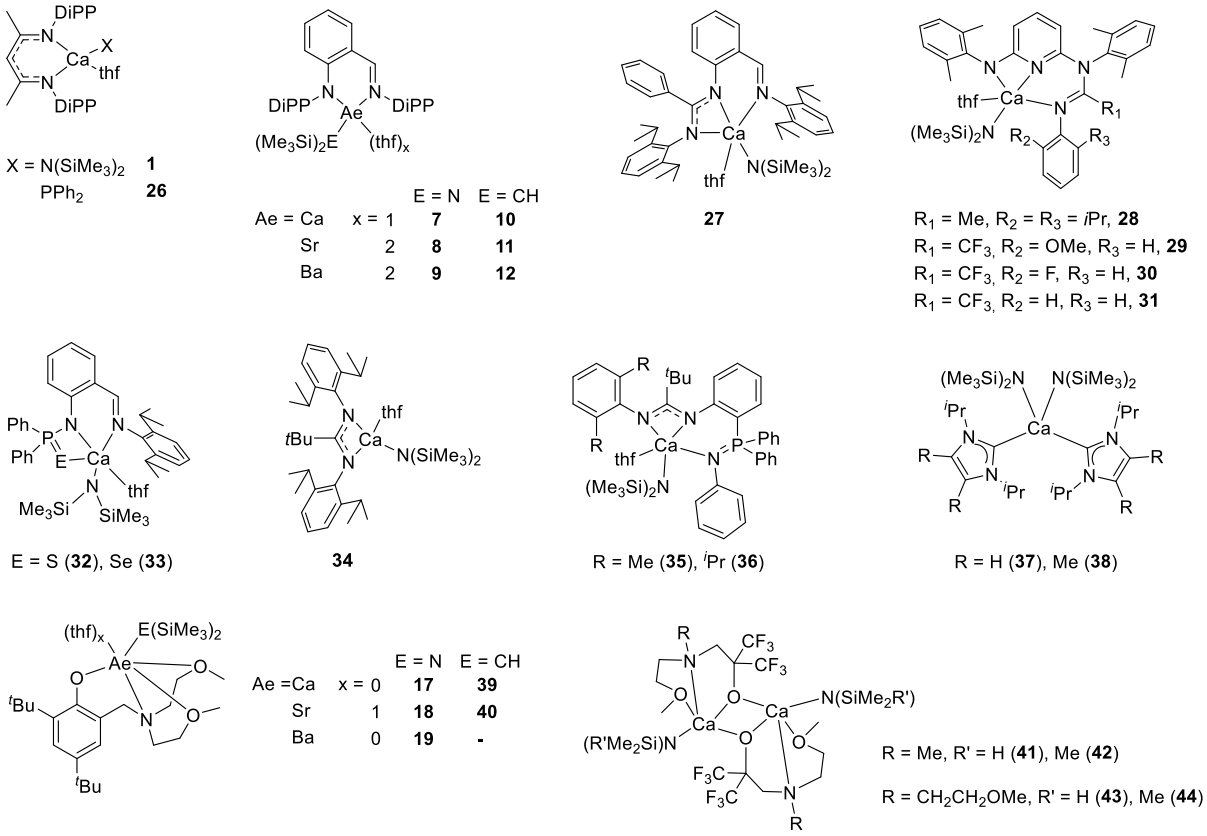

Figure 28. Selected alkaline-earth precatalysts for the intermolecular hydrophosphination of alkenes.

In 2007, Hill and co-workers first reported on the intermolecular hydrophosphination of activated alkenes with $HPPh_2$, catalyzed by the β-diketiminate calcium precursor **1** or by its phosphido analogue, [{BDI^{DiPP}}CaPPh$_2$·(thf)] (**26**) under relatively mild conditions (10 mol%, 25-75 °C, 13-24 h in C_6D_6).[90] Compound **26** was obtained by slow protonolysis between **1** and $HPPh_2$. The role of the supporting ligand in this catalysis is crucial. For instance, [Ca{N(SiMe$_3$)$_2$}$_2$·(thf)$_2$]$_2$ (10 mol%) was a poor precatalyst in comparison with **1**, needing 36 h at 75 °C to achieve near-quantitative conversion of the substrates. It was found to be plagued by the formation of the bis(phosphido) complex [Ca(PPh$_2$)$_2$·(thf)$_4$], a yellow solid very poorly soluble in hydrocarbons. Compound **26**, shown to be the likely active catalyst, slowly degraded in solution to generate a mixture of [{BDI^{DiPP}}$_2$Ca] and [Ca(PPh$_2$)$_2$·(thf)$_4$], thereby limiting the catalytic efficiency of the system. Precatalyst **1** also catalyzed the addition of diphenylphosphine onto isoprene and 1,3-cyclohexadiene, but not on more hindered alkenes such as 1,1-diphenylethene or α-methylstyrene. With the more electrophilic 2-vinylpyridine, **1** and **26** did not give hydrophosphination products, but instead catalyzed the formation of phosphine-capped poly(2-vinylpyridine). The hydrophosphination of alkenes catalyzed by **1** and **26** was assumed to proceed via a σ-insertive pathway, with coordination and regiospecific 2,1-insertion of the polarized C=C bond into the Ca-P bond, followed by protonolysis of the resulting Ca-alkyl intermediate by an incoming $HPPh_2$ molecule. The observed 2,1-regiospecificity was thought to lower the energy of the transition state traversed in the insertion step, presumed to be rate-limiting, by better stabilization of the developing negative charge on the carbon atom in α position to the aromatic ring (Figure 29). Potential stabilizing interactions between the π cloud of the aromatic ring and the electron-deficient metal center may also be a favorable factor encouraging the observed 2,1-insertion.

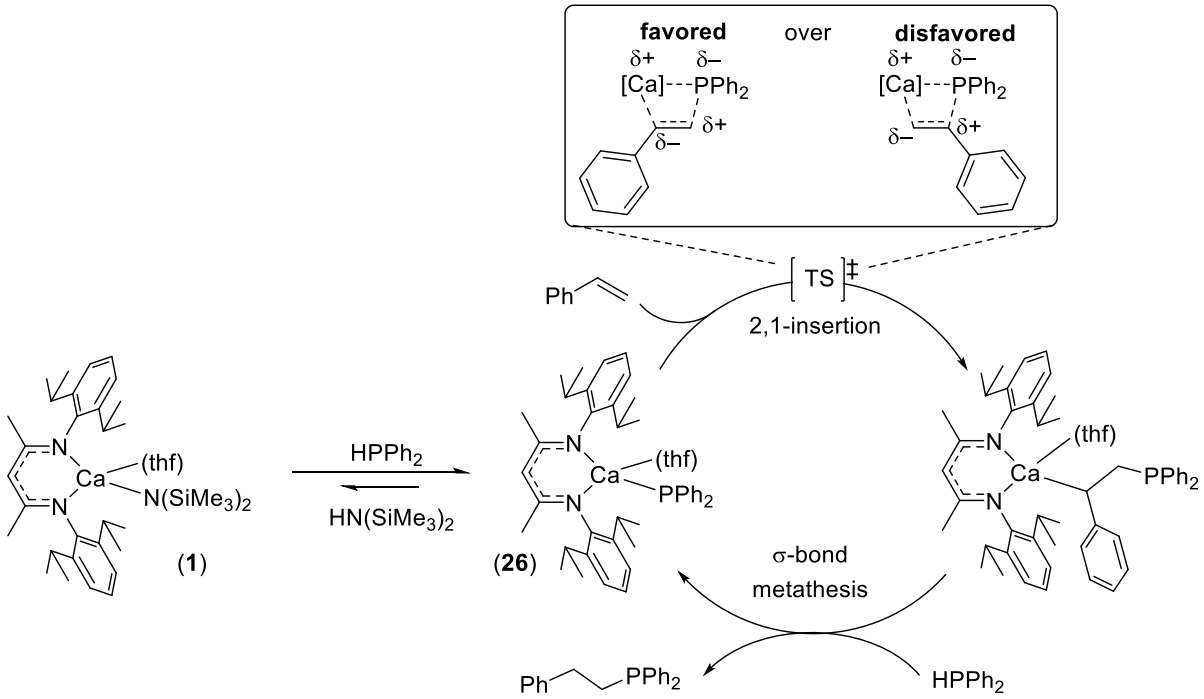

Figure 29. Proposed mechanism for the hydrophosphination of alkenes catalyzed by **1** and **26**.

Some years later, the family of homologous heteroleptic precursors **7**-**12** were also shown to catalyze the hydrophosphination of vinylarenes and dienes, with reaction rates and substrate conversions that increased very substantially with metal size (Ca < Sr < Ba); the barium catalysts **9** and **12** still range among the most active systems for these reactions.[27,62] At about the same time, the calcium precursor [{2-NC(Ph)-NArC_6H_4CHNAr}CaN($SiMe_3$)$_2$·(thf)] (**27**) supported by an imino-amidinate catalyzed the *anti*-Markovnikov addition of $HPPh_2$ onto styrene and *p*-Me-styrene.[91] It also catalyzed the regioselective 1,4-addition of $HPPh_2$ to isoprene, 2,3-Me_2-1,3-butadiene and myrcene. The 1,4-regioselectivity of the addition catalyzed by **27** is different from that observed with **1**, which, with conjugated dienes, mostly generated the products of 1,2-addition. Besides, in contrast with **1**, precatalyst **27** was also reported to convert hindered substrates such as α-methylstyrene and *cis*-stilbene. However, in these cases, the reactions required more forcing conditions than for styrene and *p*-Me-styrene. The suite of phenolato precatalysts **17**-**19** and **39**-**40** were globally less efficient than precursors bearing nitrogen-based ligands, although again, rate dependence increased according to Ca < Sr < Ba.

Despite substantial efforts paid into the design of sophisticated ancillary ligand aimed at improving catalyst lifetime and solubility, on the whole few breakthroughs in the area of Ae-catalyzed alkene hydrophosphination were disclosed following the initial reports. In typical reactions, 2-10 mol% of the precatalyst was required to achieve complete conversion, at temperature that were often in the range 60-75 °C. Reactions required hours or days in C_6D_6, although in the best cases they could be shortened to 3-15 min when performed in neat substrates.[27,62] The TONs remained limited to a few hundred at best, with corresponding TOF values between a few dozens to a few hundred turnovers per hour. The utilization of chiral benzamidinato ligands did not bring any added value, as the addition of diphenylphosphine onto styrene was still found to ensue via 2,1-insertion, forming the *anti*-Markovnikov product devoid of chiral carbon atom; yet, it further confirmed the Ca < Sr < Ba trend in hydrophosphination catalysis.[100]

The question of the mechanisms at work in alkaline-earth catalyzed alkene hydrophosphination was probed experimentally by Sarazin and co-workers with their suite of Ae iminoanilides **7**-**12**.[27,62] The amido barium precatalyst **9** (2 mol%) quantitatively converted styrene and diphenylphosphine to the *anti*-Markovnikov product $PhCH_2CH_2PPh_2$ within 15 min at 60 °C in neat substrates, with a corresponding TOF value of 192 mol_{subst} $(mol_{Ba}\ h)^{-1}$. The reaction with $HPCy_2$ was slower (42% conversion under the same conditions). The more basic alkyl precursors **10**-**12** were tangibly more active than their amido counterparts **7**-**9**, as full conversion with **12** was achieved within 3 min (TOF > 1000 mol_{subst} $(mol_{Ba}\ h)^{-1}$), presumably as the result of irreversible vs reversible formation of the catalytically competent species. Kinetic analysis was performed with the amido systems **7**-**9** for the benchmark addition of $HPPh_2$ onto styrene. Electron-withdrawing substituents in *para* position of the aromatic ring in *p*-X-C_6H_4-$CH{=}CH_2$ vinylarenes led to sizably higher reaction rates, whereas electron-donating groups lowered the reaction kinetics (OMe < ^{t}Bu < Me < H < Cl < CF_3). The kinetic rate law (equation 3) showed first order dependence in both [catalyst] and [styrene], while it was independent from $[HPPh_2]$.

$$\text{Rate} = k\,[\text{catalyst}]^1\,[\text{styrene}]^1\,[\text{diphenylphosphine}]^0 \qquad (3)$$

Eyring analysis corroborated the rate trend Ca < Sr < Ba. Taken collectively, these experimental data were consistent a stepwise pathway progressing through a turnover-limiting insertion of the C=C double bond into the Ae-P bond, as proposed by Hill for catalysis mediated by **1** (see Figure 29); the two systems were assumed to follow a similar mechanistic pathway.

The mechanism of the hydrophosphination of styrene with diphenylphosphine catalyzed by $[\{HC(C(Me)NPh)_2\}CaPPh_2]$, i.e. a simplified version of **1**, was explored to a considerable length by DFT computations.[101] The investigations revealed that insertion of the C=C bond did not follow the traditional route, and the calculations hence contradicted the assumption of a stepwise, insertive reaction manifold suggested by the groups of Hill[90] and Sarazin.[62] By contrast with the intermolecular hydroamination mechanism, it was found that the prevailing mechanism implicated an unusual outer sphere, conjugative addition. The pertaining computed free energy profile displayed in Figure 30 shows the initial insertion of the alkene to constitute the rate-limiting step and, with $\Delta G^{\ddagger}$ = 18.2 kcal mol^{-1}, to be kinetically accessible. In this mechanistic scenario, there is no direct interaction between the metal center and the C=C double bond. The aromatic ring of the vinylarene moiety was identified to hold a key role. In this scenario, the multiple Ca···Cπ and CH···Cπ secondary interactions govern the modes of coordination of the substrates and products onto the metal. Moreover, the vinylarene aromatic ring counterbalances unfavorable charge localization in the transition state.

Beyond the initial discoveries and enthusiastic reports, the main achievements in recent years dealt with the broadening of the substrate scope, mostly with amidine-amidopyridinato calcium complexes. The very first report of the hydrophosphination of the non-activated 1-nonene with $PhPH_2$ or $HPPh_2$ catalyzed by complexes **30** and **31** was particularly exciting,[94] although the reaction remained very sluggish (2 mol% Ca, 40 h, 70 °C, ca. 25% conversion). Yet, despite the very small number of systems capable of catalyzing the hydrophosphination of non-activated alkenes,[102-105] no further work has capitalized on these promising initial results. The primary phenylphosphine $PhPH_2$ has been used in reactions with vinylarene in ratios that varied from 1:1 to 1:2. Because primary phosphines are more reactive than secondary ones, the reactions were generally chemoselective, and afforded accordingly the products of single of double hydrophosphinations, respectively $PhCH_2CH_2P(H)Ph$ and $PhP(CH_2CH_2Ph)_2$ in the case of styrene, with excellent selectivity.[94-98] Other phosphines that have been

used successfully include $MesPH_2$ and 2-PH_2-pyridine. However, the utilization of amidine-amidopyridinates has surprisingly been limited -for now- to calcium, and has not been extended to the more efficient metals strontium and barium.

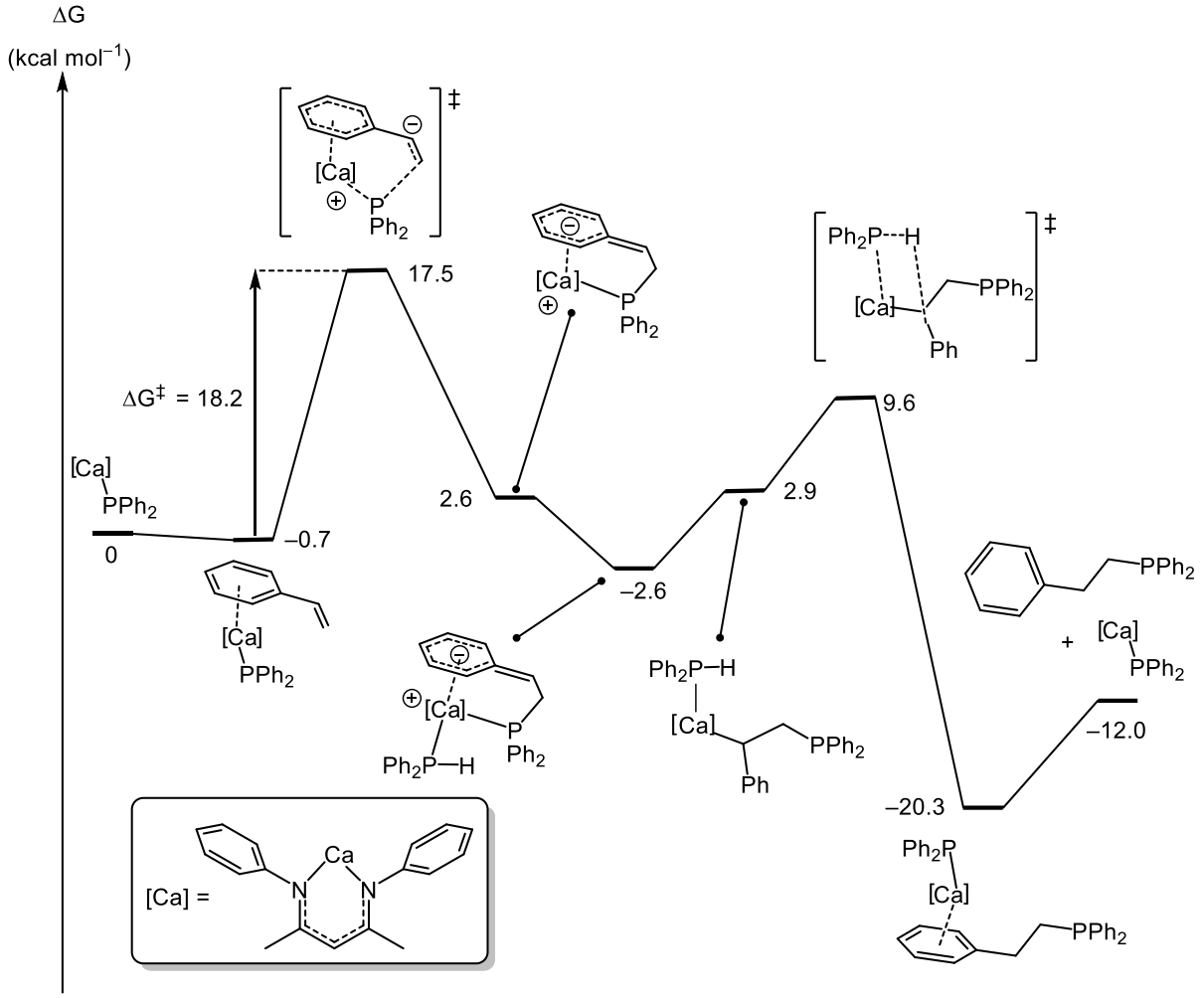

Figure 30. DFT-computed free energy profile for the prevailing mechanism in the hydrophosphination of styrene with diphenylphosphine catalyzed by [{HC(C(Me)NPh)$_2$}CaPPh$_2$]. All energies in kcal mol^{-1}.

3.2 Intermolecular hydrophosphination of alkynes

A number of calcium complexes have been reported to catalyze the addition of diphenylphosphine onto alkynes. Despite being insoluble in hydrocarbons, the calcium bis(phosphide) [Ca(PPh$_2$)$_2$·(thf)$_4$] dissolves in ethers. It was found to catalyze (Ca = 6 mol%) the hydrophosphination of diphenylethyne (25 °C) or 1-phenylpropyne (85 °C) with $HPPh_2$, providing selectively the *Z* isomer in the latter case (Figure 31).[106,107] Precatalysts **1** and **27** were also ale to allow for the hydrophosphination of diphenylacetylene, although unexpectedly, the distribution between *E* and *Z* isomers depended on the nature of the supporting ligand framework.[90,91] Under forcing conditions (2 mol%, 60 °C, 70 h; 84% conversion), the amidinato precursor **34** led to a 58:42 mixture of *E* and *Z* isomers after catalyzing the addition of phenylphosphine on diphenylacetylene.[93]

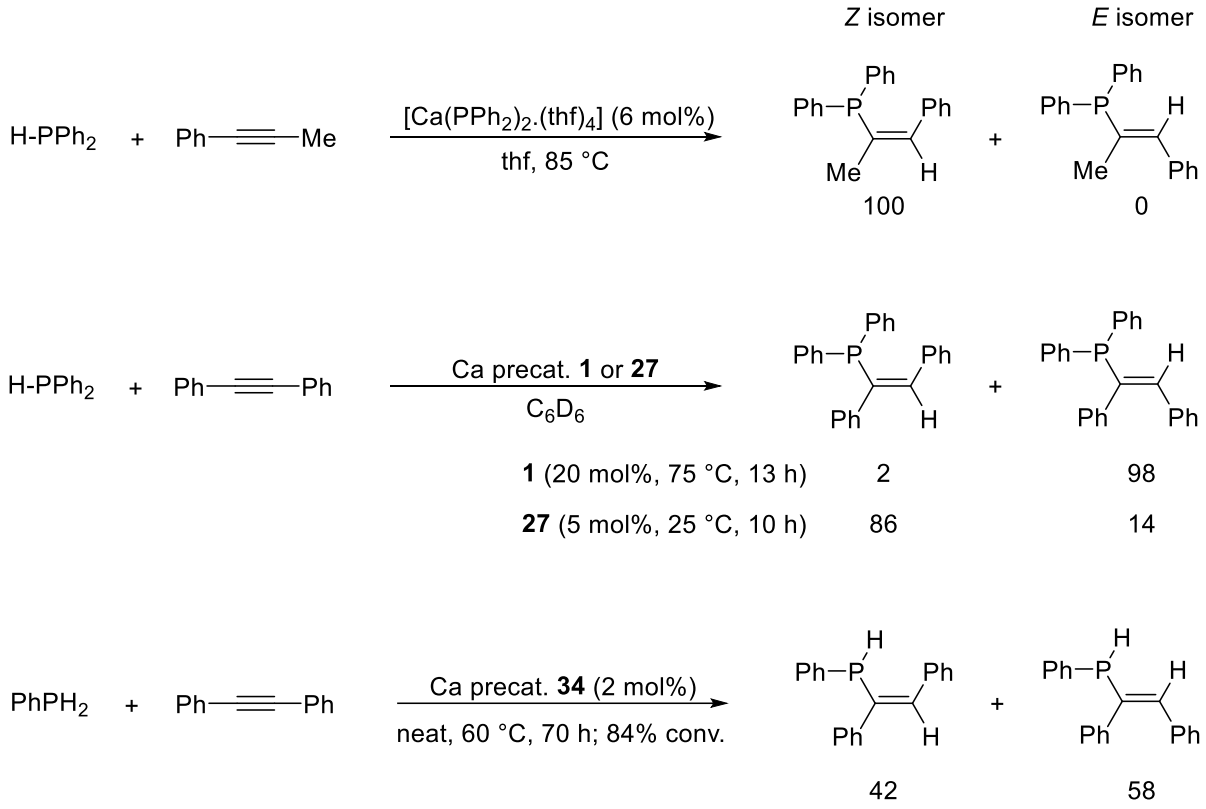

Figure 31. Alkaline-earth catalyzed hydrophosphination of alkynes.

The calcium bis(phosphide) $[Ca(PPh_2)_2{\cdot}(thf)_4]$ also catalyzed the addition of diphenylphosphine onto substituted 1,3-diynes R-C≡C-C≡C-R (R = Me, Mes, ^{t}Bu, Ph and $SiMe_3$).[107] Double addition to 1,4-disubsituted dienes was systematically observed, but the distribution of regio and configuration isomers was found to be heavily dependent upon the identity of the substituents on the diyne. Product identification was ensured through X-ray diffraction analysis of the crystallized dienes. In the simplest cases for R = Me and Mes, 1,4-bis(diphenylphosphanyl)buta-1,3-dienes formed exclusively through consecutive *syn*-additions, but a mixture of *E*,*E*, *E*,*Z* and *Z*,*Z* stereoisomers was obtained(Figure 32).

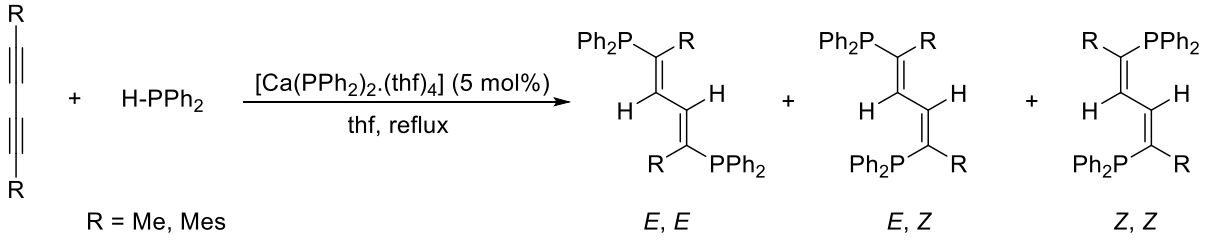

Figure 32. Alkaline-earth catalyzed hydrophosphination of substituted butadiynes.

3.3 Hydrophosphination of carbodiimides

The addition of diphenylphosphine onto carbodiimides, yielding phosphaguanidines, was catalyzed by the amido complexes $[Ae\{N(SiMe_3)_2{\cdot}(thf)_2]$ and the solvent-free $[Ca\{N(SiMe_3)_2]_2$, with activities which increased upon descending group 2 (Ae = Ca < Sr < Ba).[108] On the other hand, the heteroleptic precursor **1** was far less efficient. Catalysis with the bis(amide)s in C_6D_6 was facile, occurring at room temperature with typical precatalyst loading of 1.5-2.0 mol%. Reaction times ranged between 15 min

and, for the most reluctant substrates, 28 h. Substrate scope was explored, and the reaction was seen to proceed more slowly as sterically demanding *N*-substituents were introduced in the carbodiimide (Figure 33). The addition of $HPCy_2$ onto carbodiimides could not be achieved under the same experimental conditions, assumed to be the outcome of its low acidity compared to $HPPh_2$. $[Ca(PPh_2)_2{\cdot}(thf)_4]$ was elsewhere shown to react with diisopropyl- and dicyclohexylcarbodiimides, yielding $[(Ca\{RNC(PPh_2)NR\}_2{\cdot}(thf)_2]$ (R = ^{i}Pr, Cy).[109] However, both phosphaguanidinato complexes were only poorly active in the hydrophosphination of carbodiimides and diphenylphosphine.

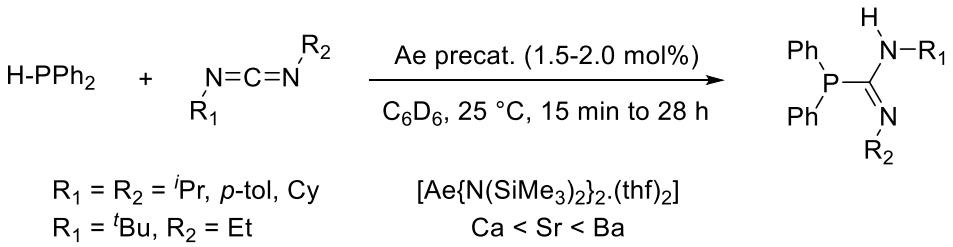

Figure 33. Alkaline-earth catalyzed hydrophosphination of carbodiimides.

3.4 Hydrophosphorylation and hydrophosphonylation catalysis

3.4.1 Hydrophosphorylation of alkynes

The amido precursors $[Ae\{N(SiMe_3)_2\}_2{\cdot}(thf)_2]$ were used to catalyze the hydrophosphorylation of phenylacetylene with phosphine oxides (Pudovik reaction, Figure 34).[110] Ae-di(aryl)phosphinites $[Ae(OPAr)_2{\cdot}(thf)_x]$ were presumed to be the catalytically active species. Catalytic activity increased drastically with metal size (Ca << Sr << Ba), with calcium being inactive under the chosen experimental conditions (5 mol% precatalyst, room temperature, 1 h in thf) and barium being both very fast and selective. For diarylphosphine oxides, $Ar_2P(O)H$ (Ar = Ph, Mes), the reactions yielded *E*/*Z* isomeric mixtures of phenylethenyl-di(aryl)phosphine oxides, with barium giving a 22:1 selectivity in favor of the *E* isomer. The operative mechanism was proposed to involve insertion of the C≡C bond into the Ae-P bond in the postulated $[Ae(OPAr)_2{\cdot}(thf)_x]$ active species. The hydrophosphorylation of diynes with diphenylphosphine oxide was also catalyzed by $[Ca(PPh_2)_2{\cdot}(thf)_4]$.[111] Products formation depended heavily on the substitution of 1,3-butadiyne (Figure 34), with diphenyl- and di(*tert*-butyl)butadiyne yielding respectively 1,4-diphenyl-1,3-butadiene-2,3-bis(diphenylphosphine oxide) and 2,2,7,7-tetramethyl-4-octyne-3,6-bis(diphenylphosphine oxide). $[Ca(PPh_2)_2{\cdot}(thf)_4]$ was also an effective precatalyst for the hydrophosphorylation of isocyanates and isothiocyanates (5 mol% precatalyst, thf, room temperature, 12-48 h), affording *N*-alkyl and *N*-aryl substituted diphenylphosphorylformamides and -thioformamides respectively, of the type $Ph_2P(=O)–C(=E)–N(H)R$ (E = O, R = ^{i}Pr, ^{t}Bu, Cy, Ph, 4-Br-C_6H_4, C_6H_2-2,4,6-Me_3 and Naph) (E = S, R = ^{i}Pr, Cy, Ph and 4-Me-C_6H_4).[112] Product isolation was ensured by recrystallisation, which enabled easy characterization but led to limited isolated yields.

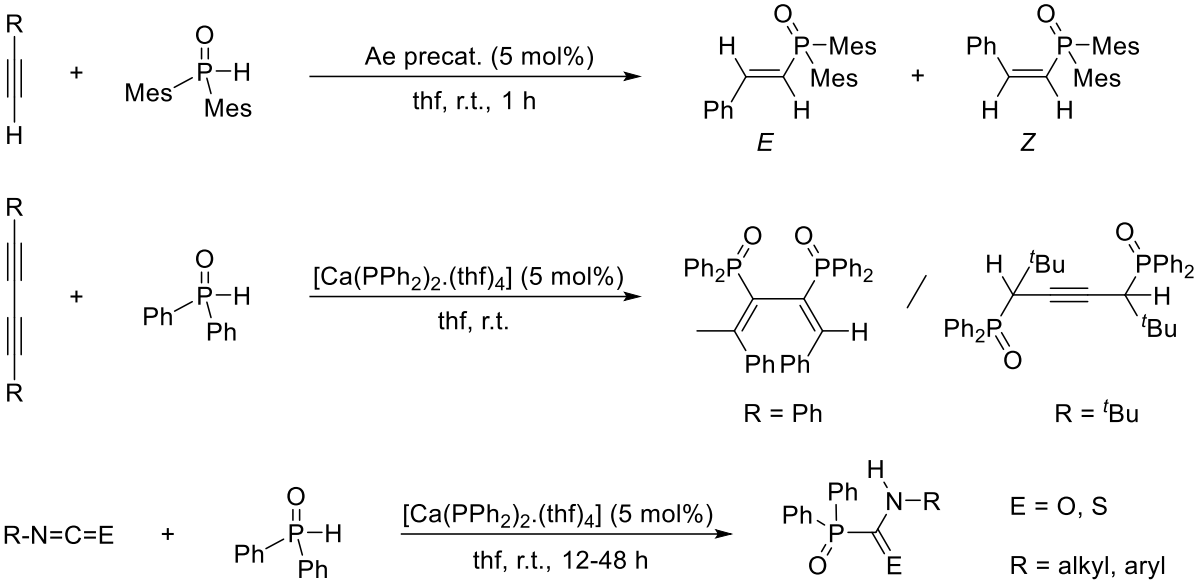

Figure 34. Alkaline-earth catalyzed hydrophosphorylation of alkynes, diynes and iso- and isothiocyanates.

3.4.2 Hydrophosphonylation of aldehydes and ketones

The bis(amides) $[Ae\{N(SiMe_3)_2\}_2\cdot(thf)_2]$ are extremely effective precatalysts for the addition of dialkylphosphites $HP(=O)(OR)_2$ onto aldehydes and ketones to produce tertiary or quaternary phosphonates, respectively (Figure 35).[113] No stereoselectivity was observed. The catalytic activity in neat substrates increased according to Ca < Sr < Ba. With aldehydes, full conversion was achieved within minutes at room temperature, using a precatalyst loading as small as 0.02 mol%. With the less electrophilic ketones, TOF values as high as 1,200-1,500 $mol_{subst}\ mol_{Ae}^{-1}\ min^{-1}$ were reached. The reaction was sensitive to steric demands on the substrates, e.g. the activity dropped upon introduction of large substituents in *ortho* position of the aromatic ring of arylketones. However, reaction rates were largely unaffected by the addition of electron-donating/withdrawing group on the substrates. No proposal was made as to a potential catalytic mechanism.

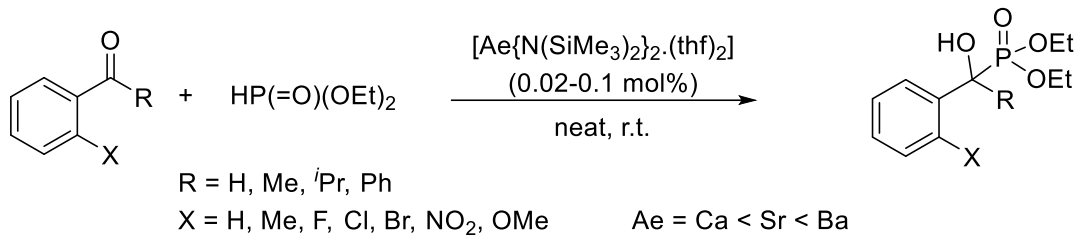

Figure 35. Alkaline-earth catalyzed hydrophosphonylation of ketones and aldehydes.

3.5 Hydroalkoxylation of alkynyl and allenyl alcohols

Some years after their investigations in alkaline-earth-mediated intramolecular hydroamination catalysis, Hill and co-workers revealed that homoleptic $[Ae\{N(SiMe_3)_2\}_2]_2$ amido complexes were also competent precatalysts for the regioselective intramolecular hydroalkoxylation of alkynyl and allenyl alcohols, yielding 5- and 6-membered enol ethers.[114] Typical reactions were carried out in C_6D_6 at 60-

120 °C with 5 mol% precatalyst. Substrate scope was probed to a great extent, and showed that in most cases, ring-closure for alkynylalcohols returned mixtures of the endo- and exocyclic enol ethers (Figure 36). This distribution of products was rationalized as the outcome of isomerization of the alkynylalkoxide (initially formed upon alcoholysis of the Ae-amide bond) into the pertaining allenylalkoxide. Cyclization rates were much greater for allenylalcohols than for their alkynyl counterparts, while terminal alkynylalcohols were found to lead to ring-closure much more rapidly than internal alkynes. Ring-closure proceeded following Baldwin's guidelines, with a pronounced Thorpe-Ingold effect. The established kinetic rate law indicated catalyst inhibition upon increasing [substrate], suggesting that rate-limiting insertion of the unsaturated C-C bond into the Ae-O bond required the dissociation of coordinated substrate molecules away from the metal center.

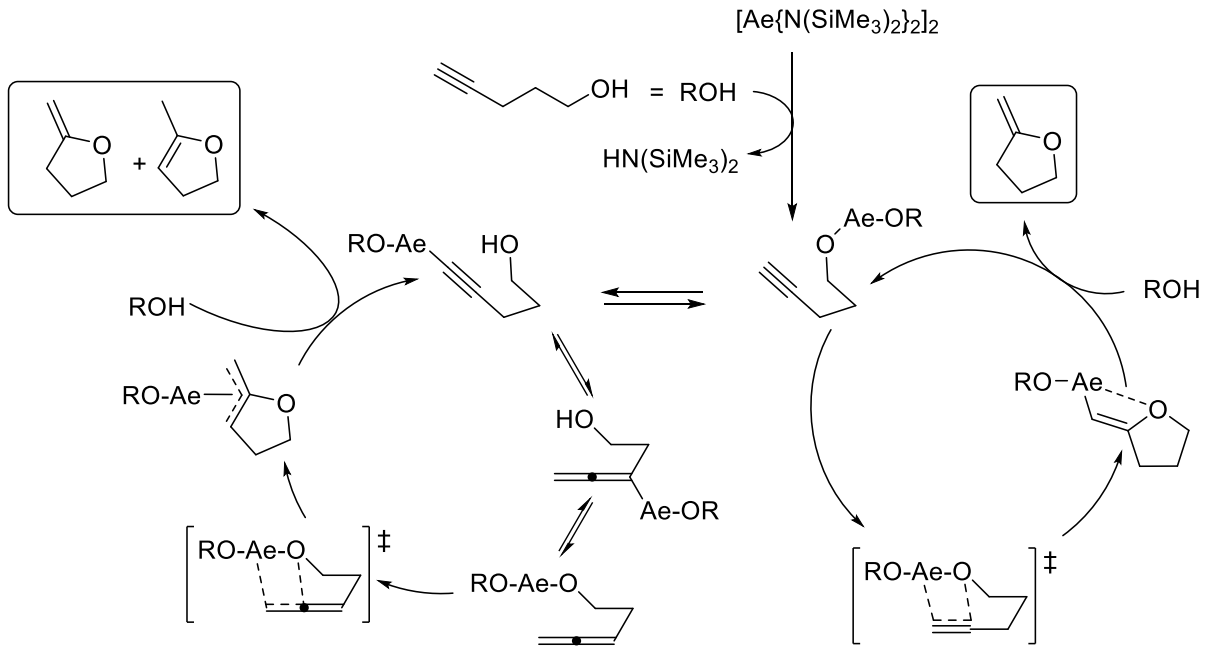

Figure 36. Proposed mechanism for the alkaline-earth catalyzed ring-closing intramolecular hydroalkoxylation of alkynylalcohols.

3.6 Hydroacetylenation of carbodiimides and related reactions

In 2008, Hill and co-workers utilized the heteroleptic β-diketiminato calcium precatalyst **1** to catalyze the hydroacetylenation of carbodiimides, using phenylacetylene and 1,3-diisopropylcarbodiimide as the benchmark substrates to produce the corresponding propargylamidine. In what was the first example of Ae-mediated C-C bond formation,[115] catalysis took place with 5 mol% catalyst at 80 °C for 14 h, but afford only moderate substrate conversion (isolated yield 59%). However, the supporting β-diketiminate ligand was found to be protonolyzed with the relatively acidic phenylacetylene, making comprehension of the catalyst speciation very difficult. A following study showed that $[Ca\{N(SiMe_3)_2\}_2\cdot(thf)_2]$ and even more so $[Sr\{N(SiMe_3)_2\}_2\cdot(thf)_2]$ were more competent precatalysts. The strontium derivative in particular converted a broad range of acetylenic substrates to substituted propargylamidines under overall relatively forcing conditions (2.5-10 mol%, 12-48 h, 60-100 °C; Figure 37).[116] Reactions rates slowed as steric demands on both the carbodiimide and acetylene derivatives increased.

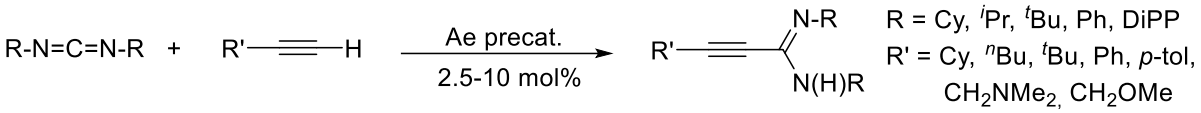

Figure 37. Alkaline-earth catalyzed hydroacetylenation of carbodiimides.

In very elegant studies, the Hill group used its experience in alkaline-earth catalyzed heterofunctionalizations to generate highly functionalized cyclic molecules. Using commercially available terminal alkynes and heterocumulenes, they assembled a suite of sophisticated imidazolidin-2-ones, imidazolidin-2-thiones, N,N'-[(5-benzylidene-imidazoldin-2,4-ylidene)diamines and 1,3-thiazolidin-2-thiones through a succession of 100% atom-efficient steps.[117,118] The reactions first involve the formation of propargylamidines, which once formed enter cyclisation reactions through addition of the isocyanate and isothiocyanate. This reactivity was rationalized to occur through a well-defined sequence of heterocumulene hydroacetylenation and alkyne hydroamidation. The simple $[Ae\{N(SiMe_3)_2\}_2\cdot(thf)_2]$ performed smoothly (loading 0.5-5.0 mol%), but required vastly different reactions conditions depending upon substrate selection. The rate and regioselectivity of the cyclisation reactions were found to be heavily dependent upon the nature of the metal. As an illustration, the one-pot sequential synthesis of imidazolidin-2-ones starting from arylacetylenes, isocyanates and carbodiimides could be deconvoluted into four consecutive Ae-promoted heterofunctionalization steps: (i) hydroacetylenation of carbodiimides, (ii) intermolecular isocyanate hydroamination, (iii) ring-closing intramolecular hydroamination of the resulting alkynylurea giving mixture of *E* and *Z* isomers for the exocyclic C=C double bond, and (iv) tautomerization into the thermodynamically more stable product (Figure 38).

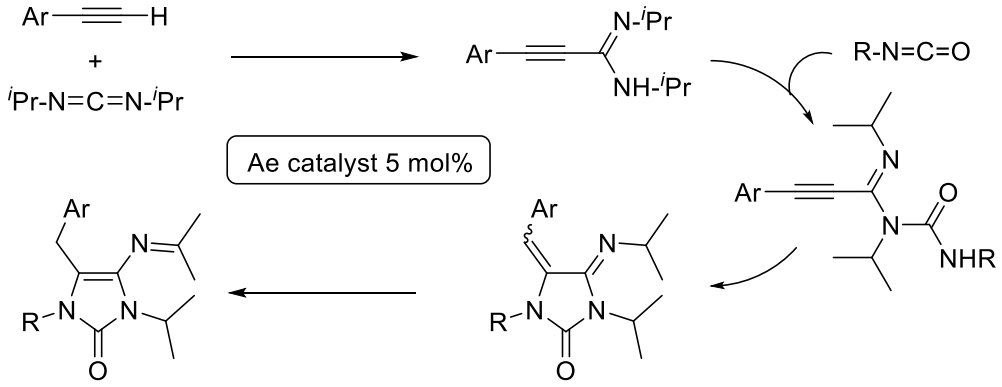

Figure 38. Sequential alkaline-earth catalyzed formation of substituted imidazolidin-2-ones.

3.7 Hydroboration catalysis

Unlike magnesium which has proved fairly competent in the catalysis of hydroboration reactions,[119] the large alkaline earths have seldom been used for hydroboration catalysis. A possible justification may be that in a first report of hydroboration of 1,1-diphenylethylene (DPE) with catecholborane (HBCat), the dimeric calcium hydride $[\{BDI^{DiPP}\}CaH\cdot(thf)]_2$ (**45**), $[Ca[2\text{-}\ Me_2N\text{-}\alpha\ Me_3Si\text{-benzyl})_2\cdot(thf)_2]$ (**46**) and $[\{BDI^{DiPP}\}Ca(9\text{-BBN})\cdot(thf)]$ (**47**) were all found to decompose HBCat into B_2H_6 and B_2Cat_3.[120] In this so-called Trojan Horse process, the product that formed was not the expected Ph_2CHCH_2Bcat ensuing from Ca-catalyzed hydroboration of DPE, but $(Ph_2CHCH_2)_3B$ coming from the reaction of B_2H_6.

Ketone hydroboration has met with mitigated success. The four calcium amidinates [{^{tBu}Am^{DIPP}}CaI·(thf)$_2$]$_2$ (**48**), [{^{tBu}Am^{DIPP}}Ca·(C$_6$H$_6$)]$^+$[B(C$_6$F$_5$)$_4$]$^-$ (**49**), [{^{tBu}Am^{DIPP}}CaN(SiMe$_3$)$_2$·(Et$_2$O)] (**50**) and [{^{tBu}Am^{DIPP}}Ca(μ-H)]$_2$ (**51**) were found to catalyze the addition of ketones and aldehydes with HBPin.[121] The catalytic activity (typical precatalyst loading 0.5-3.0 mol%, 10-300 min at 25 °C; TOF ca. 10-600 mol$_{subst}$ mol$_{Ca}^{-1}$ h^{-1}) was heavily dependent upon the identity of the anion, and increased in the order I$^-$ < B(C$_6$F$_5$)$_4^-$ < N(SiMe$_3$)$_2^-$ < H$^-$. Calcium hydrides were supposed to be operating in the case of the best systems **50** and **51**, assumed to ensue via a classical insertive pathway (Figure 39). No enantioselectivity was mentioned in the case of prochiral substrates. Catalyst loading could be decreased to as low as 0.05 mol% for the hydroboration of cyclohexanone.

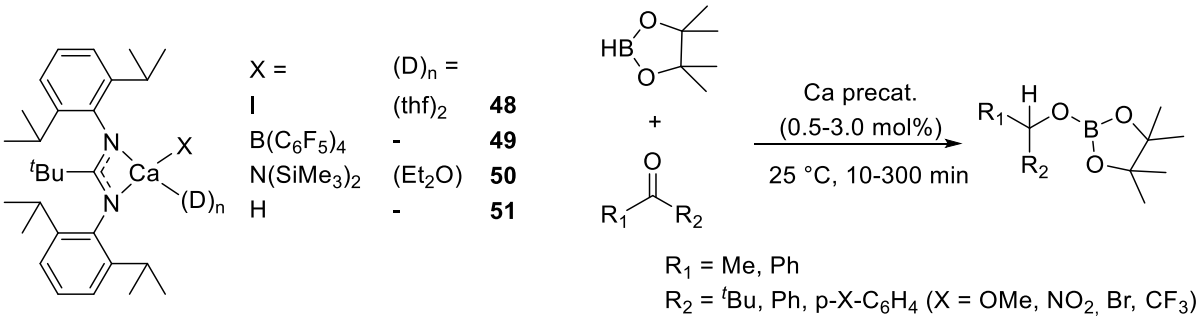

Figure 39. Alkaline-earth catalyzed hydroboration of ketones and aldehydes.

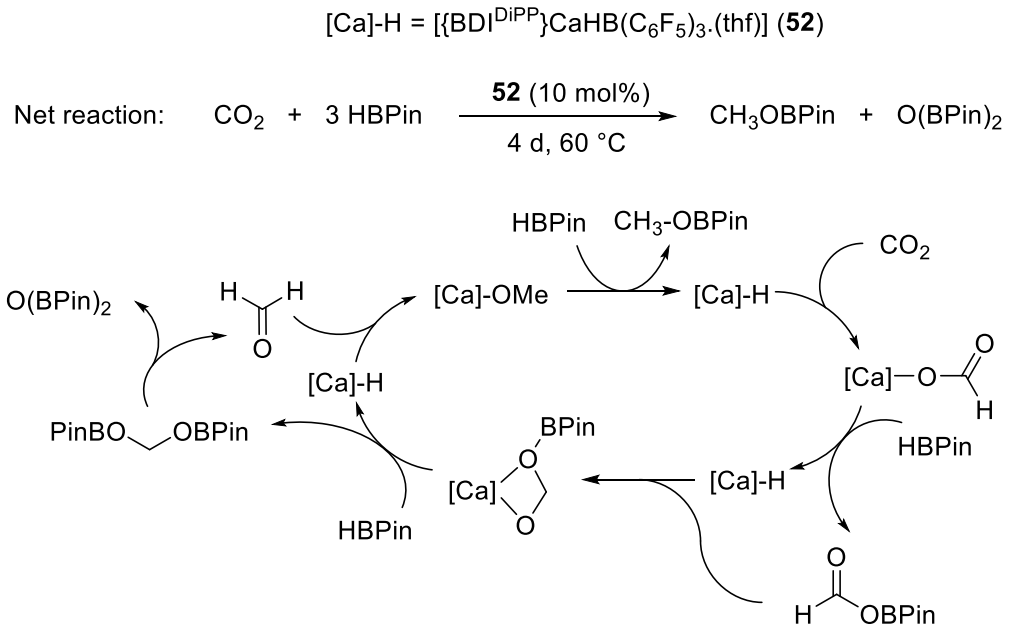

Figure 40. Proposed mechanistic pathway for the Ca-catalyzed reductive hydroboration of CO$_2$.

Finally, it was shown the structurally characterized tris(pentafluorophenyl)hydroborate [{BDI^{DiPP}}CaHB(C$_6$F$_5$)$_3$·(thf)] (**52**) could catalyze the reductive hydroboration of CO$_2$ to generate the methanol equivalent CH$_3$OBPin, along with the by-product O(BPin)$_2$.[122] However, the reactions were extremely slow, required 10 mol% of precatalyst and 4 days at 60 °C in thf to achieve full conversion. A multi-step mechanistic pathway was formulated (Figure 40), and was supported by the isolation of several intermediates, notably a boryl formate HC(=O)OBPin and the bis(boryl)acetal CH$_2$(OBPin)$_2$.

3.8 Hydrosilylation catalysis

A number of examples of alkaline-earth catalyzed hydrosilylation reactions, for the addition of hydrosilanes across C-C, C-O and C-N unsaturated bonds, have been described. Like hydroborations, Ae-mediated hydrosilylation reactions rely on polarized $^{\delta+}$Ae-H$^{\delta-}$ hydridic species that will often evolve through a σ-insertive pathway.

3.8.1 Hydrosilylation of alkenes

The group of Harder provided in 2006 the first example of calcium- and strontium-catalyzed hydrosilylation of alkenes, using diphenylethylene (a non-polymerizable substrate) and $PhSiH_2R$ (R = H, Me, Ph) hydrosilanes as the benchmark substrates (Figure 41). The reactions were catalyzed by the Ae-benzyls [Ae(DMAT)$_2$·(thf)$_2$] under mild conditions (0.5-2.5 mol% precatalyst, 25-50 °C) and afforded quantitative conversions and excellent regioselectivity (Ae = Ca, **53**; Sr, **54**; DMAT = 2-dimethylamino-2-trimethylsilylbenzyl).[123] In apolar solvents such as benzene, the branched Markovnikov product was formed with strict selectively (a regioselectivity that transition metals rarely enable), whereas in thf only the linear *anti*-Markovnikov product was generated. The strontium precatalyst proved an order of magnitude more efficient that its calcium congener **53**. Beyond diphenylethylene, conversion of α-methyl-styrene and styrene also returned the branched products. Notably, the hydrosilylation of styrene was extremely facile, proceeding at 25 °C with 0.5 mol% of precatalyst, without detectable formation of polystyrene. The monosilylation of cyclohexa-1,3-diene could be achieved selectively. The catalytically active species was deduced to be a series of hydride-rich clusters. The changing regioselectivity of the reaction with the nature of the solvent made it difficult to propose a mechanistic pathway with good confidence. Subsequent studies showed that the molecular hydride [{BDI^{DiPP}}CaH·(thf)]$_2$ (**45**) was an equally competent hydrosilylation precatalyst, yielding exclusively the Markovnikov product regardless of the solvent upon hydrosilylation of DPE with $PhSiH_3$,[124] while the calcium complexes **53** or [Ca{N(SiMe$_3$)$_2$}$_2$·(thf)$_2$] could be grafted onto dehydroxylated silica to generate heterogeneous catalysts that displayed the same selectivity as **53**.[125]

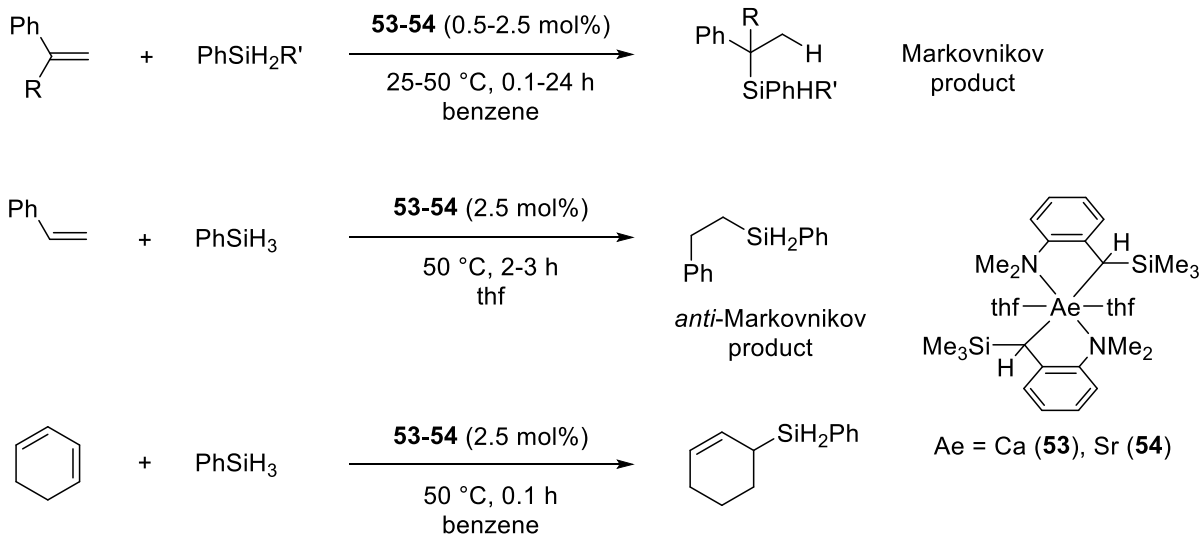

Figure 41. Alkaline-earth catalyzed hydrosilylation of C=C bonds.

The group of Okuda also reported on some pertinent alkene hydrosilylation catalysts. In 2012, they revealed that the cationic hydrido cluster of composition [{Me_3TACD}$_3$$Ca_3$($\mu^3$-H)$_2$][$Ph_3SiH_2$] (**55**), where {$Me_3$TACD}$^-$ is a macrocyclic ligand derived from the polyamine 1,4,7-trimethyl-1,4,7,10-tetraazacyclododecane (aka {Me_3TACD}H), effectively catalyzed the addition of Ph_2SiH_2 onto diphenylethylene at 25 °C (18 h, 5 mol% precatalyst).[126] Only the formation of the *anti*-Markovnikov addition product could be detected. Several years later, the Okuda group improved on their original results when they showed that the dinuclear hydrido dication [(Me_4TACD)$_2$$Ca_2$(μ-H)$_2$(thf)][B($C_6H_3$-3,5-$Me_2$)$_4$]$_2$ (**56**) was a highly versatile and efficacious catalyst.[127] It allowed for the functionalization of vinylarene and, remarkably, ethylene and non-activated α-olefins (Figure 42). The overall suitability of the system was established in the hydrosilylation of ethylene (1 bar) with a variety of hydrosilanes, which proceeded under mild conditions (2.5 mol% precatalyst, 70 °C, 15-60 min in thf-d_8. The selectivity was poor with arylhydrosilanes due to a kinetically competitive process of aryl exchange, but in contrast, the selectivity was excellent with alkylhydrosilanes. Higher α-olefins such as 1-octene and 1-hexene were hydrosilylated at 70 °C in 24 h at 70 °C, to give the *anti*-Markovnikov products with good regioselectivity; depending on the stoichiometry and the hydrosilane, secondary or tertiary silanes were obtained, but no reaction occurred with the tertiary products or Et_3SiH. Hydrosilylation did not occur for internal alkenes. The hydrosilylation of vinylarenes (styrene, α-methyl-styrene, diphenylethylene, *cis*- and *trans*-stilbene) also took place at 70 °C (0.5-48 h) and returned the Markovnikov addition products; reactions were faster with arylsilanes than with alkylsilanes, but selectivity was in this case again limited by aryl scrambling. Overall, using ^{n}OctSiH$_3$ as the benchmark hydrosilane, the following order of reactivity was evidenced: ethylene > styrene > 1-octene. The mechanism was not fully ascertained. Yet, the gathered experimental data was consistent with a scenario where the cation [CaH]$^+$ produced an alkyl calcium complex as the result of hydrometallation of the olefin, followed by σ-bond metathesis with the incoming hydrosilane to yield the hydrosilylated product and regenerate the catalytically active cation [CaH]$^+$. The nuclearity of the species responsible for catalytic turnovers was not determined.

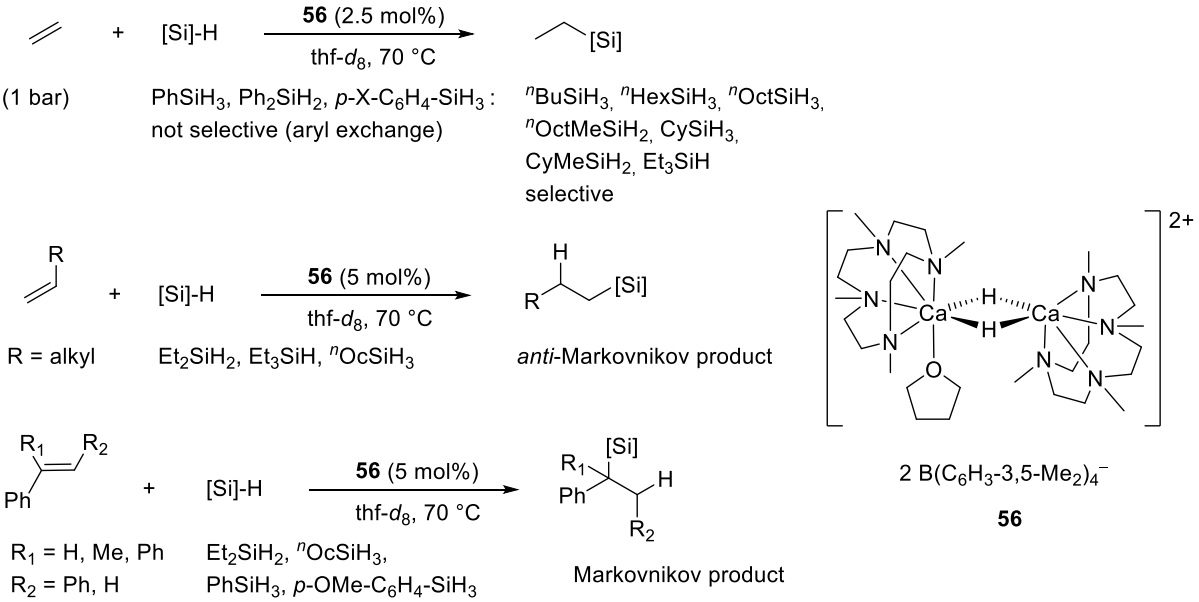

Figure 42. Hydrosilylation of alkenes catalyzed by the calcium cationic complex [(Me_4TACD)$_2$$Ca_2$(μ-H)$_2$(thf)][B($C_6H_3$-3,5-$Me_2$)$_4$]$_2$ (**56**).

The calcium bis(silanide) $[Ca(SiPh_3)_2{\cdot}(thf)_4]$ (**57**; 2.5 mol%) was also shown to catalyze the *anti*-Markovnikov addition of arylsilanes onto diphenylethylene and α-methyl-styrene.[128] Reactions occurred slowly at 60-100 °C in thf-d_8 (2-62 h), with a rate dependence followed the trend $PhSiH_3$ > Ph_2SiH_2 > Ph_3SiH. Under the same experimental conditions, styrene was found to be polymerized while 1-octene did not react.

A number or mechanistic proposals have been made to account for the varying regioselectivity of the alkaline-earth catalyzed hydrosilylation of olefins. They consider solvent effects, with polar solvent likely to encourage the formation of ionic species and allow for the switch of regioselectivity observed with **53** in thf or benzene. The fact that cationic hydrides (**56**) and silanides (**57**) mediate the formation of opposite regioisomers in the hydrosilylation of α-substituted styrenes is an element in these proposals. However, the debate is still open, and the exact nature of the prevailing mechanisms remains unclear. The input of DFT calculations would undeniably be helpful in this ongoing discussion.

3.8.2 Hydrosilylation of ketones

The calcium-catalyzed hydrosilylation of ketones was reported in 2008. The Ca-hydride **45** and the dibenzyl **53** were shown to enable the addition of $PhSiH_3$ onto benzophenone and enolizable ketones, e.g. acetone, acetophenone, cyclohexanone, dibenzylketone and 2-adamantone.[129] Catalysis took place at 50 °C in benzene, with 1.25 mol% precatalyst. Regardless of the ratio between substrates, the reactions consistently yielded the disiloxanes $PhSiH(OR)_2$ as the result of the activation of two Si-H bonds, indicating that the intermediate $PhSiH_2(OR)$, i.e. the product of monocoupling, was more reactive than the initial substrate $PhSiH_3$. In contrast, the formation of the tricoupled product $PhSi(OR)_3$ could barely be detected. Stoichiometric reactions between **45** and ketones were not selective towards the formation of a Ca-alkoxide, as α-deprotonation also systematically led to the formation of sizeable quantities of Ca-enolates. Yet, enolization hardly occurred under catalytic conditions.

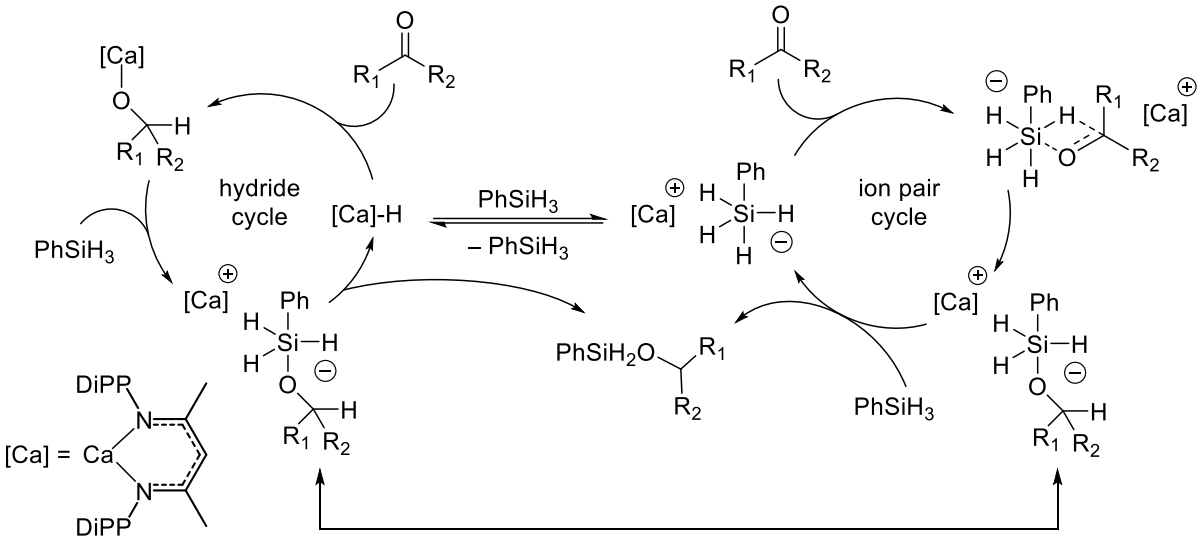

Figure 43. Potential mechanisms for the calcium-catalyzed hydrosilylation of ketones.

Although a Ca-mediated hydrosilylation "hydride" reaction manifold involving the addition of calcium hydride to the ketone could not be ruled out (Figure 43), the overall excellent alkoxy/enolate ratio in

the hydrosilylation products suggested a different route. Consistent with experimental observations and stoichiometric reactivity, an 'ion pair" mechanism was proposed instead. It implicates a hypervalent five-coordinate silicon intermediate, and a concerted step where the hydride atom is transferred from the silicon atom to the ketone (Figure 43). The two rival mechanisms could potentially be intertwined, and possibly competing, through the occurrence of a hypervalent alkoxysilicate intermediate.

3.8.3 Hydrosilylation of imines

The Harder group reported the first example of alkaline-earth catalysis for the hydrosilylation of imines in 2019.[130] The benzyl complexes **53** and **54** and the Ae-amides $[Ae\{N(SiMe_3)_2\}_2]_2$ (Ae = Ca, Sr, Ba) were found to catalyze the addition of $PhSiH_3$ onto eight different aldimines $R_1C(H)=N-R_2$ and one ketimine $R_1R_2C=N-R_3$ (1-5 mol% precatalyst, C_6D_6, 25-60 °C, 5 min to 24 h depending on substrate). The amides were less active than the benzyl complexes, and the activity increased with metal size according to Ca < Sr < Ba. The best system, utilizing precatalyst **54** (2.5 mol%), gave quantitative conversion within 5 minutes at room temperature. The fastest rates were measured for imines with *N*-alkyl and *C*-aryl substituents, as in $PhC(H)=N^tBu$. Variation of substituents (H, Me, Cl, MeO) in the *para* position of the Ph ring indicated adequate functional group tolerance. Kinetic rates with $^tBuC(H)=N^tBu$ or PhC(H)=NPh were much lower. An insertive mechanism involving a catalytically active metal hydride was proposed (Figure 44). The proposed mechanism was supported by stoichiometric reactions and by the successful isolation of reaction intermediates. It was corroborated by DFT computations based of the simple CaH_2 model, which indicated a rate-limiting conversion of calcium-amide intermediate into the catalytically active hydride. In this scenario, a *N*-aryl group stabilizes the intermediate Ca-amide through resonance and reduces its nucleophilicity, thereby decreasing reaction rates.

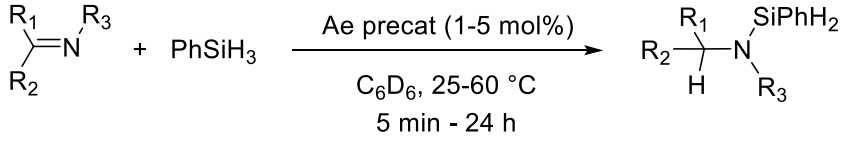

R_1 = H R_2 = Ph, *p*-X-C_6H_4 (X = Me, OMe, Cl), ^{t}Bu, ^{n}Pr R_3 = ^{t}Bu, Bn, Ph
R_1 = Ph, R_2 = Ph, R_3 = Ph

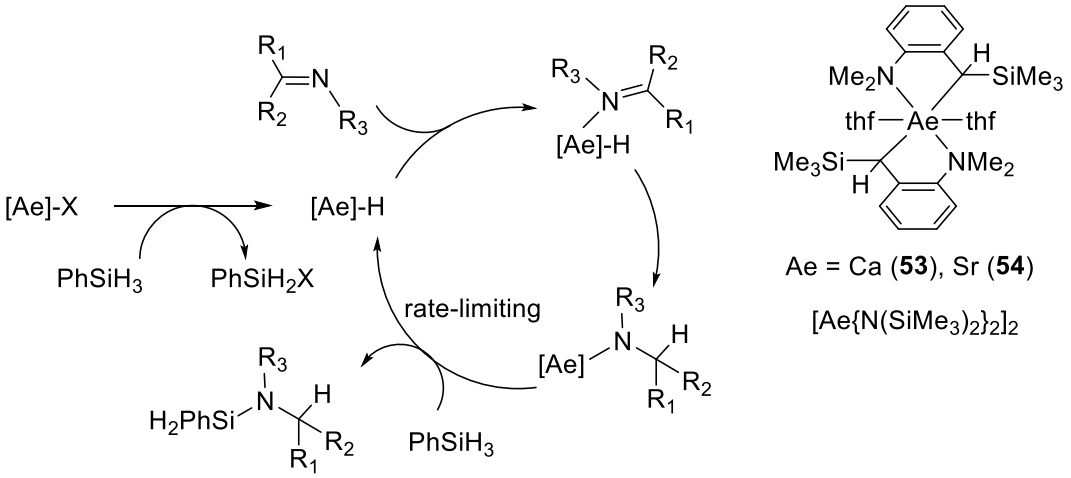

Figure 44. Alkaline-earth catalyzed hydrosilylation of imines.

The hydrosilylation of pyridine, quinoline and isoquinoline is catalyzed but the calcium hydride **45** and by [Ca{N(SiMe$_3$)$_2$}$_2$·(thf)$_2$].[131] High and selective conversion to the 1,2-dihydropyridine and 1,2-dihydroquinoline silanes was observed under mild conditions (5 mol% precatalyst, 25-60 °C, 24 h in C_6D_6). Catalysis was possible due to the fact that the dearomatized product resulting from hydride reduction of pyridine through 1,2-insertion into the Ca-H bond of **45** was stable. Remarkably, the product of 1,4-reduction could not be detected. An insertive mechanism involving a Ca-hydride active species and a pentavalent hydrosilicate intermediate was invoked (Figure 45).

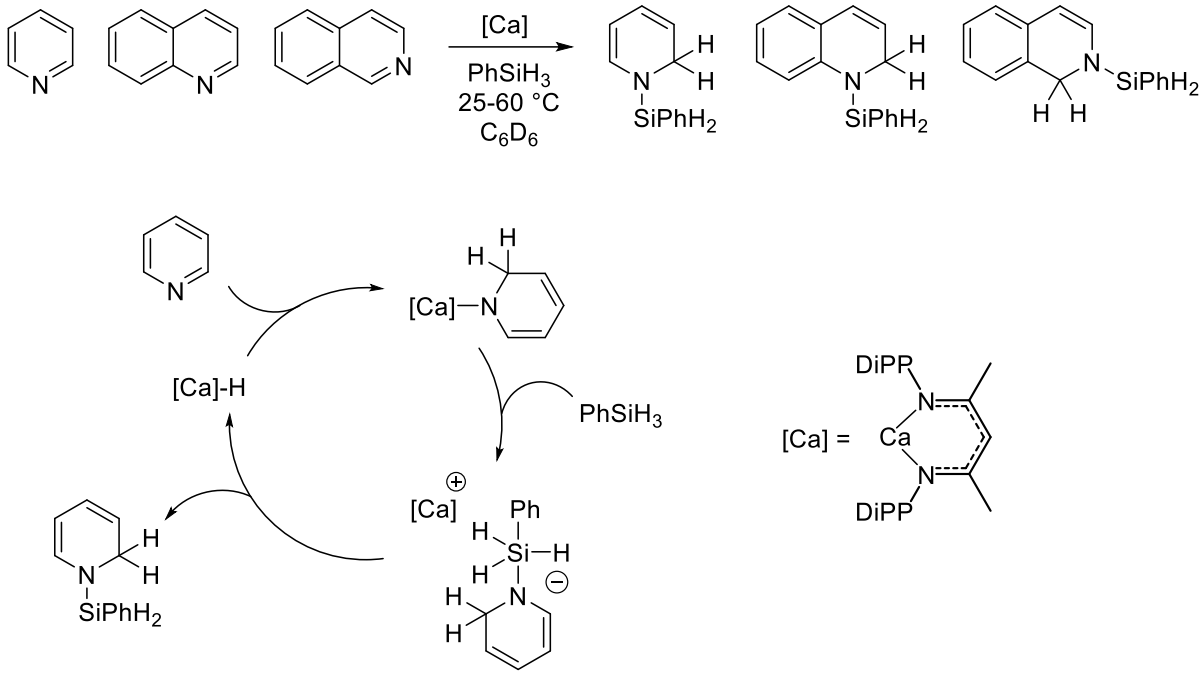

Figure 45. Calcium-catalyzed 1,2-selective hydrosilylation of pyridine and quinolines.

4 Hydrogenation catalysis

Despite traditionally being dominated by heterogeneous catalytic systems, homogeneous hydrogenation catalysis has evolved significantly over the past 60 years. Early work was centered on transition metal (TM) catalysts, such as Wilkinson's catalyst [RhCl(PPh$_3$)$_3$], Schrock-type catalysts such as [Rh{nbd}(PPh$_3$)][PF$_6$], and Crabtree's [Ir{cod}(PCy$_3$)(py)][PF$_6$].[132-134] The desire for catalytic hydrogenation without expensive transition metals initiated the development of a range of frustrated Lewis pairs and hydrogenation catalysts using earth-abundant metals. Although alkene hydrogenation based on TM catalysts indicated that d→π* back-bonding was essential for alkene activation, the development s-block metal hydrogenation catalysts has shown that this is not a strict requirement.

4.1 Hydrogenation of alkenes

4.1.1 Hydrogenation of activated alkenes

The first use of an alkaline-earth catalyst for the hydrogenation catalysis was that of Slaugh in 1967, who reported the partial hydrogenation of 1,3-pentadiene using [MgH$_2$] in a heterogeneous system

at high temperature and pressure (186 °C, 900-1500 psi).[135] Following up on the isolation of the soluble calcium-hydride [{BDI^{DiPP}}CaH·(thf)] (**45**),[19] the first mention of homogeneous alkene hydrogenation catalysis with large alkaline earths was reported in 2008, using activated alkenes as substrates.[136] Complexes **45**, [Ca(DMAT)$_2$·(thf)$_2$] (**53**) and [Sr(DMAT)$_2$·(thf)$_2$] (**54**) mediated the hydrogenation of styrene to ethylbenzene or DPE to diphenylethane at 20-60 °C (Figure 46).

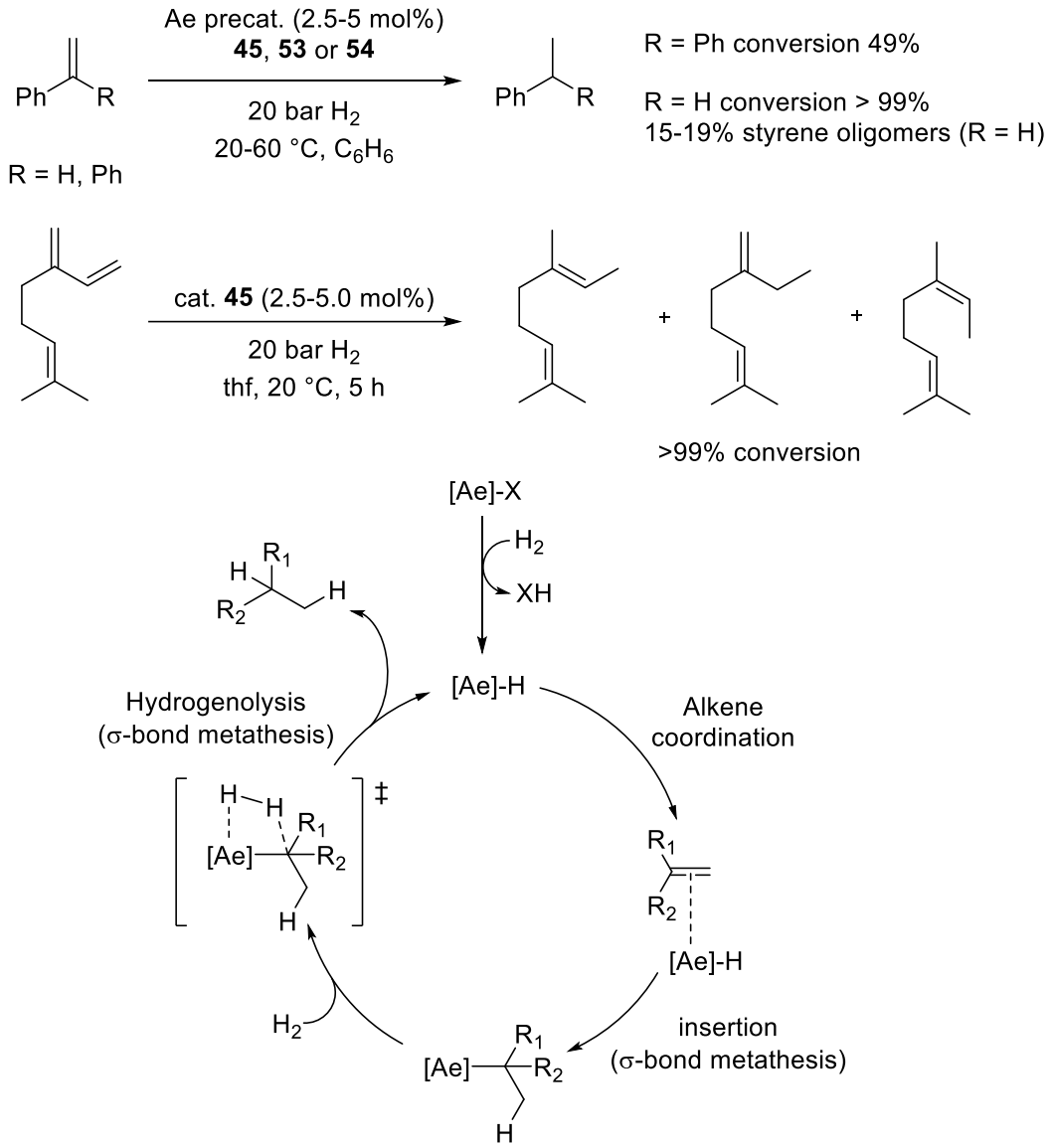

Figure 46. Hydrogenation of DPE, styrene and myrcene catalyzed by [{BDI^{DiPP}}CaH·(thf)] (**45**), [Ca(DMAT)$_2$·(thf)$_2$] (**53**) and [Sr(DMAT)$_2$·(thf)$_2$] (**54**), with the proposed catalytic cycle.

Although full conversions of styrene were achieved using either **45** or **53** after 15 h, up to 19% styrene oligomers were also formed, indicating that styrene polymerization was competitive with hydrogenation. A catalytic cycle involving Ae-hydrides active species was formulated; it was supported by characterization of the intermediates. In the case of **53** and **54**, an off-cycle initiation step generates the hydride. It followed by a regiospecific σ-bond metathesis generating the branched insertion product; hydride transfer occurs exclusively to the terminal carbon, due to the low stability of the alternatively generated primary alkyl species. The secondary alkyl intermediate then undergoes another σ-bond-metathesis, giving the hydrogenated product and regenerating the hydride catalyst.

In the case of styrene, higher H_2 pressures accelerated the reaction, resulting in a lower percentage of oligomers from the competing styrene polymerization. The hydrogenation of myrcene catalyzed by **45** gave a mixture of three partially hydrogenated isomers. Only the conjugated double bonds were hydrogenated, indicating that the catalytic system was limited to activated alkenes.

4.1.2 Hydrogenation of unactivated alkenes

More than ten years after the first isolation of **45**, the thf-free calcium hydride complex, [{BDI^{DiPP}}Ca(μ-H)]$_2$ (**58**) was unveiled.[18] This complex was shown to be a significantly stronger Lewis acid than **45**, capable of undergoing σ-insertion with 1-hexene or ethylene to generate the corresponding alkyl-bridged dimers.[137] Complex **58** is also able to catalyze the hydrogenation of unactivated alkenes with good conversions (Figure 47). However, reaction conditions, and in particular temperature and solvent identity, had to be carefully controlled, due to the propensity for ligand-redistribution to the catalytically inactive bis-ligated species [{BDI^{DiPP}}$_2$Ca] and nucleophilic attack of the reaction solvent at higher temperatures. Under such mild conditions (10 mol% catalyst, C_6D_6, 25 °C, 2 bar H_2, 7-21 d), long reaction times and slow turnovers only were observed.

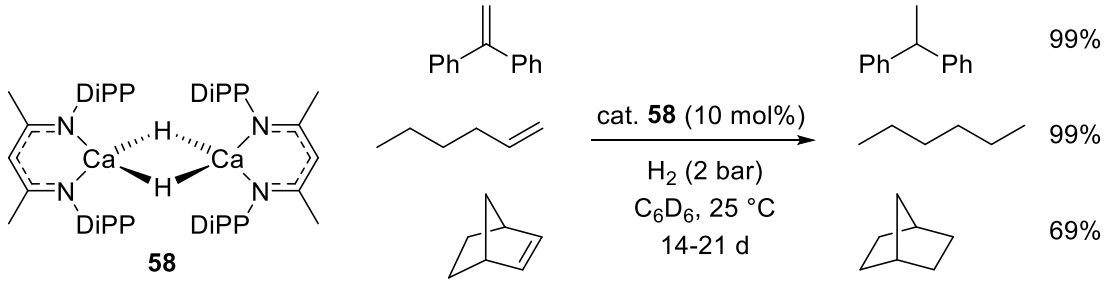

Figure 47. Hydrogenation of alkenes catalyzed by [{BDI^{DiPP}}Ca(μ-H)]$_2$ (**58**).

Okuda's calcium hydrides [{Me$_3$TACD}$_3$Ca$_3$(μ^3-H)$_2$][Ph$_3$SiH$_2$] (**55**), [(Me$_4$TACD)$_2$Ca$_2$(μ-H)$_3$][SiPh$_3$] (**59**) and [(Me$_4$TACD)$_2$Ca$_2$(μ-H)$_2$][B(C$_6$H$_4$-4-^{t}Bu)$_4$]$_2$ (**60**) were utilized for the hydrogenation of alkenes.[126,138,139] Although complex **55** was capable of hydrogenating DPE under very mild conditions (60 °C, 1 bar), the reaction was slow, taking 13 days to reach full conversion with high precatalyst loading (19 mol%, Figure 48). Complex **61**, generated from 1 equivalent of **59** with DPE, was significantly faster in the hydrogenation of DPE, fully converting the substrate within 24 h at 60 °C under a 1 bar pressure of H_2, although the catalyst loading was not reported.[138] The dicationic complex **60** was an even better catalyst, fully converting DPE to the corresponding alkane at 25 °C within 6 hours (1 bar H_2).[139] The difference in activity between Me$_x$TACD-supported complexes was attributed to their solubility, with the compounds bearing the neutral (Me$_4$TACD) ligand (**60** and **61**) dissolving fully in thf, whereas **55**, bearing the monoanionic (Me$_3$TACD)$^-$ was only partly soluble. Crucially, complex **60** also showed good catalytic behavior towards unactivated alkenes, fully or partially hydrogenating 4-vinylcyclohex-1-ene, hexa-1,5-diene and trimethyl(vinyl)silane, although these substrates required slightly forcing conditions (5 mol% precatalyst, 60 °C). It was assumed that the dipositive charge on the metal in **60** was key for the activation of the olefins, as the less electro-deficient calcium center in **61** led to poorer catalytic activity. As the nucleophilicity of the hydrides is lower in the dications, it feels legitimate to consider that electrophilic alkene activation prevails over hydride nucleophilicity in catalysis promoted by these systems.

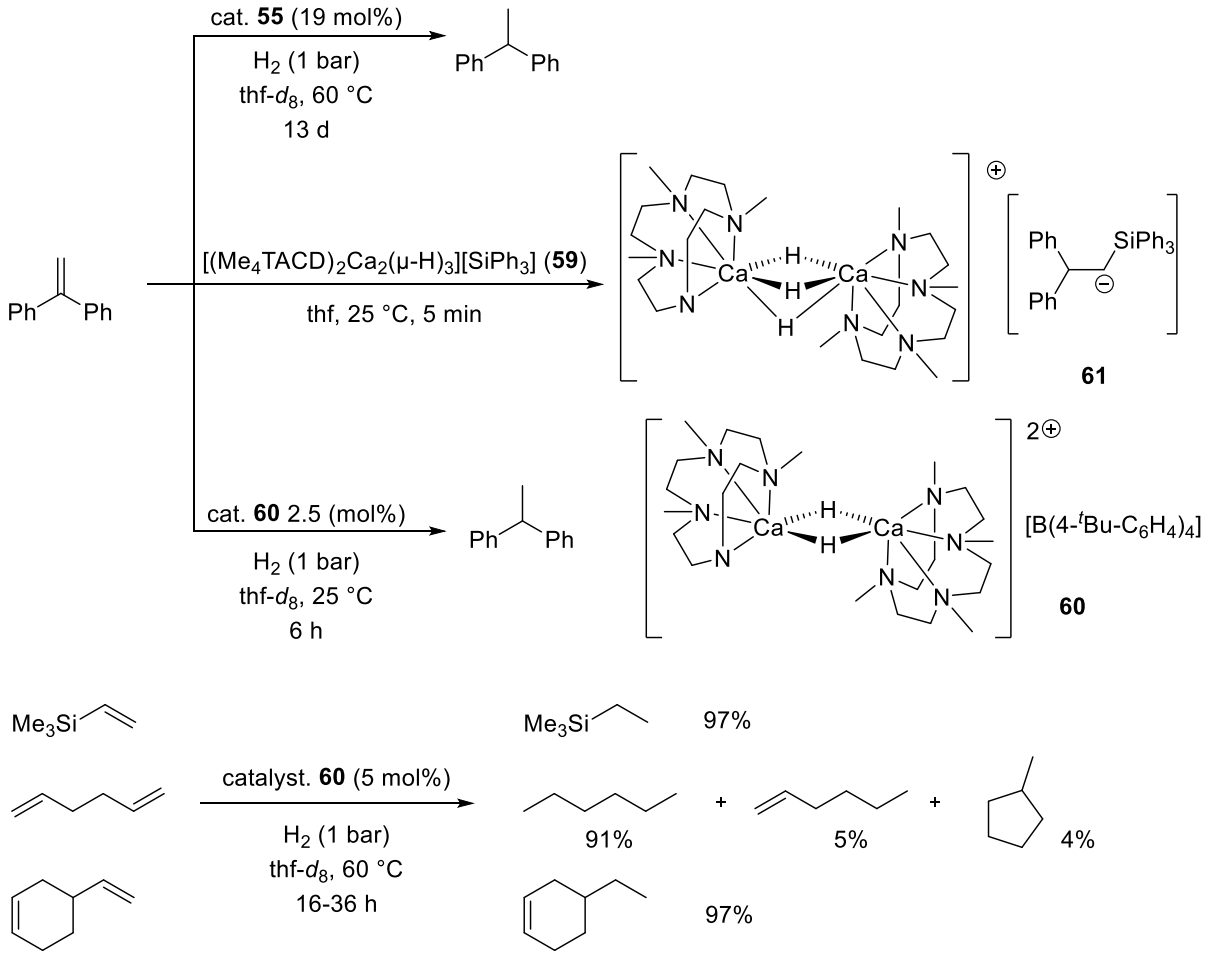

Figure 48. Hydrogenation of alkenes catalyzed by (Me_xTACD)-supported calcium hydrides.

Hydrides of the heavier alkaline earths have also been used in hydrogenation catalysis. The first isolated heteroleptic barium hydride complex [{$Tp^{Ad,iPr}$}Ba(μ-H)]$_2$ (**62**), reported by Cheng in 2017, catalyzed the hydrogenation of DPE under moderate conditions (2.5-5.0 mol% cat., 12 hours, 6 bar H_2) (Figure 49).[140,141] Changing the reaction solvent from benzene to thf increased the rate of the reaction, but also generated small amounts of 1,1,3,3-tetraphenylbutane, a product presumably formed upon insertion of a second equivalent of DPE occurs prior to the σ-bond metathesis with H_2 that regenerates the hydride catalytic species.

In 2020, Cheng and co-workers also reported the hydrogenation of a range of activated and unactivated alkenes using a calcium precatalyst supported by the same heteroscorpionate ligand, [($Tp^{Ad,iPr}$)Ca(*p*-$CH_2C_6H_4Me$)·(thp)] (**63**).[142] This complex fully converted a range of activated and unactivated alkenes under moderate temperature and pressure (40 °C, 10 atm H_2), including DPE, 1,2-diphenylethylene, $Me_3SiCH{=}CH_2$, 1-hexene, pent-4-en-1-ylbenzene, and even cyclohexene and norbornene with longer reaction times. The precatalyst also hydrogenated reluctant substrates such as internal alkenes, achieving 90% conversion of 2-octene to octane after 72 hours (Figure 49).[142] The heteroleptic Ae-hydrido complexes [(Cp^{Ar})Ae(μ-H)·(S)]$_2$ bearing a sterically demanding cyclopentadienyl ligand (Ae = Ca, **64**; Sr, **65**; Ba, **66**; {Cp^{Ar}}$^-$ = {(3,5-^{i}PrC_6H_3)$_5C_5$}$^-$; S = thf or dabco) have also been used to catalyze the hydrogenation of DPE with H_2 under mild conditions (Figure 49).[143] Hydrogenation rates were found to increase with metal size (Ca < Sr < Ba). The barium catalyst **66** could fully hydrogenate 1,1,2-triphenylethylene under mild conditions with a 5 mol% catalyst loading,

and could even partially hydrogenate 1,1,2,2-tetraphenylethylene after 24 h.[143] 1-Hexene was fully converted to hexane within 10 hours by both **65** and **66**.

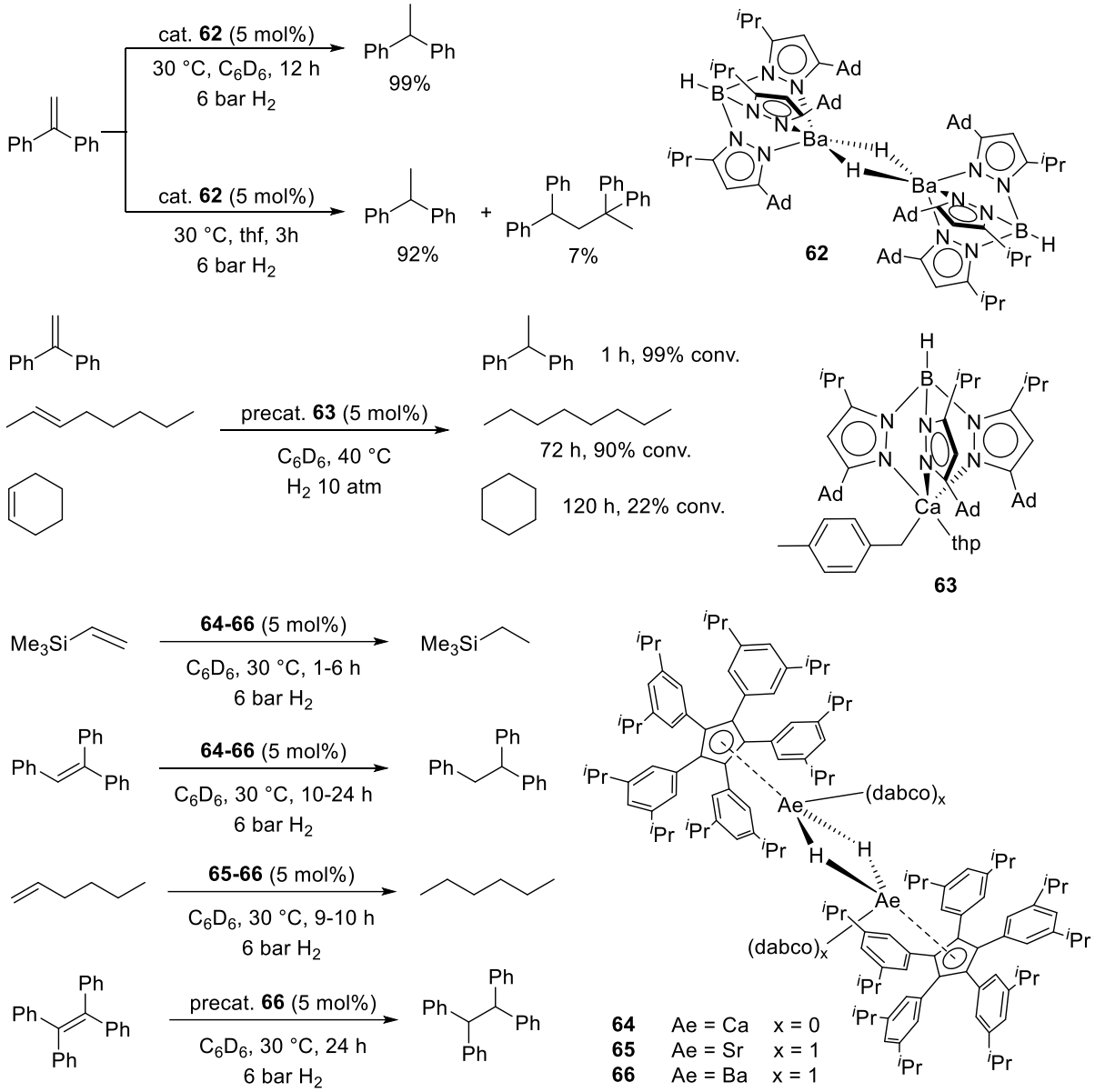

Figure 49. Selected data for alkene hydrogenation with Cheng's heteroleptic calcium, strontium and barium hydrido catalysts.

The extreme steric bulk of the ancillary ligands in complexes **62** and **66** highlight the amount of kinetic stabilization required to suppress ligand redistribution of barium complexes in solution. To alleviate the issue of ligand scrambling, Harder and co-workers reported in 2018 the efficient hydrogenation of a range of substrates using the simple amides $[Ae\{N(SiMe_3)_2\}_2]_2$ as precatalysts.[144] Activity increased with metal size, although all of the catalysts converted activated alkenes within 30 minutes at 120 °C (H_2 = 6 bar). Interestingly, if thf was added to the reaction medium, catalytic activity ceased, regardless of the precatalyst used. This contrasts with heteroleptic precatalysts such as **62** and **65** and alkyl precatalysts such as **53** and **54**, which displayed faster conversion when thf was used instead of benzene as the reaction solvent. Another positive feature of the $[Ae\{N(SiMe_3)_2\}_2]_2$ catalytic

systems was that in the case of styrene, competing polymerization of the substrate was not observed at all, indicating that the rate of σ-bond metathesis between H_2 and the Ae-alkyl species generated during the catalytic cycle was significantly faster than the competing insertion of another molecule of styrene (see Figure 46). Hydrogenolysis of the metal amide precursor was presumed to produce the Ae-hydrido catalytically active species, with a mechanistic pathway implicating a σ-insertion of the coordinated olefin into the Ae-to-H bond. Although hydrogenolysis of the resulting Ae-alkyl intermediate regenerates in one step the active species, the suggestion was made that the Ae-alkyl species could be protonated by the stoichiometric equivalent of Brønsted acidic $HN(SiMe_3)_2$ (pK_a = 25.8, pK_a of H_2 ≈ 49) liberated in the reaction medium during catalyst initiation.[145,146] This protonation regenerates the precatalyst $[Ae\{N(SiMe_3)_2\}_2]$, which can then undergo another hydrogenolysis with H_2 to re-enter the catalytic manifold (Figure 50).

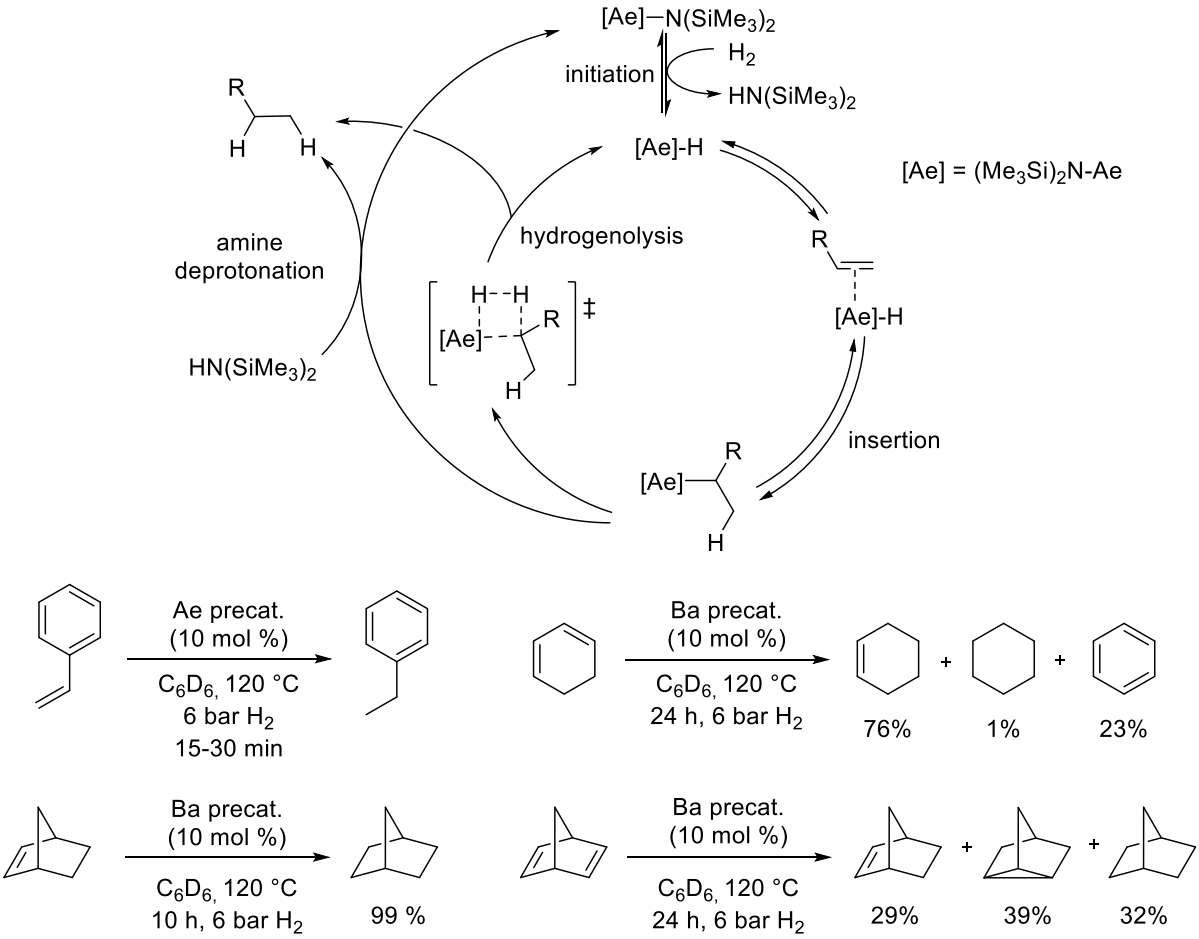

Figure 50. Alkene hydrogenation catalyzed by $[Ae\{N(SiMe_3)_2\}_2]_2$ complexes.

When excess amine was added to the reaction medium, conversion was slowed significantly. This was rationalized as the consequence of shifting the equilibrium back towards the homoleptic complex $[Ae\{N(SiMe_3)_2\}_2]$, thus decreasing the amount of the presumed catalytic species, thought to be an aggregated $[\{N(SiMe_3)_2\}Ae(H)]_n$ species, in solution. Several such multimetallic species have been isolated.[147] The most active precatalyst, $[Ba\{N(SiMe_3)_2\}_2]_2$ was capable of fully converting a range of vinylarenes within an hour (6 bar H_2, 120 °C) including *para*-methoxy-styrene, DPE, α-methyl-styrene and 1,2-diphenylethylene. 1,1,2-Triphenylethylene and tetraphenylethylene were not used as

substrates, so direct comparison cannot be made with the heteroleptic Ba-hydrides **62** and **66**. Unlike **60** and **63**, $[Ba\{N(SiMe_3)_2\}_2]_2$ could only partially hydrogenate 1-hexene, due to competing isomerization to 2-hexene, which itself could not be hydrogenated. However, $[Ba\{N(SiMe_3)_2\}_2]_2$ could hydrogenate other relatively unactivated alkenes such as $Me_3SiCH{=}CH_2$ (30 minutes), norbornene (10 hours), and norbornadiene (24 hours, although a distribution of three products was obtained). These results considered collectively demonstrate that there is no universal best hydrogenation catalyst, and that different catalysts may be suitable for different substrates.

The Harder group further elaborated on alkene hydrogenation by using the bulkier ligand systems $[Ae\{N(Si^iPr_3)_2\}_2]$ (**67**-**69**) and $[Ae\{N(Si^iPr_3)(DiPP)\}_2]$ (**70**-**72**).[148,149] The catalytic activity increased from Ca to Ba, while the $[Ae\{N(Si^iPr_3)_2\}_2]$ precatalysts outperformed their $[Ae\{N(Si^iPr_3)(DiPP)\}_2]$ relatives. Notably, complexes **67**-**69** were capable of partially hydrogenating aromatic ring systems such as anthracene, naphthalene and even benzene (Figure 51). Complexes **67**-**69** all hydrogenated 1-hexene under moderate conditions (6 bar H_2, 120 °C), with no observable isomerization to 2-hexene. In contrast, precatalysts **70**-**72** gave mixtures of hexane and 2-hexene. Dimerization of $SiMe_3CH{=}CH_2$ and α-methylstyrene when using the most active catalyst, **69**, was an issue. The authors suggested dimerization resulted from the significantly slower rate of amine deprotonation in the reaction manifold, as $HN(TRIP)_2$ is less acidic than $HN(SiMe_3)_2$ (see Figure 50), making a second insertion more rate competitive. Dimerization could be avoided by lowering the reaction temperature, but this also entailed longer reaction times to reach full conversions. A range of internal alkenes including cyclohexene, 4-vinylcyclohex-1-ene and 3-hexene were all fully hydrogenated by **69** (Figure 51).

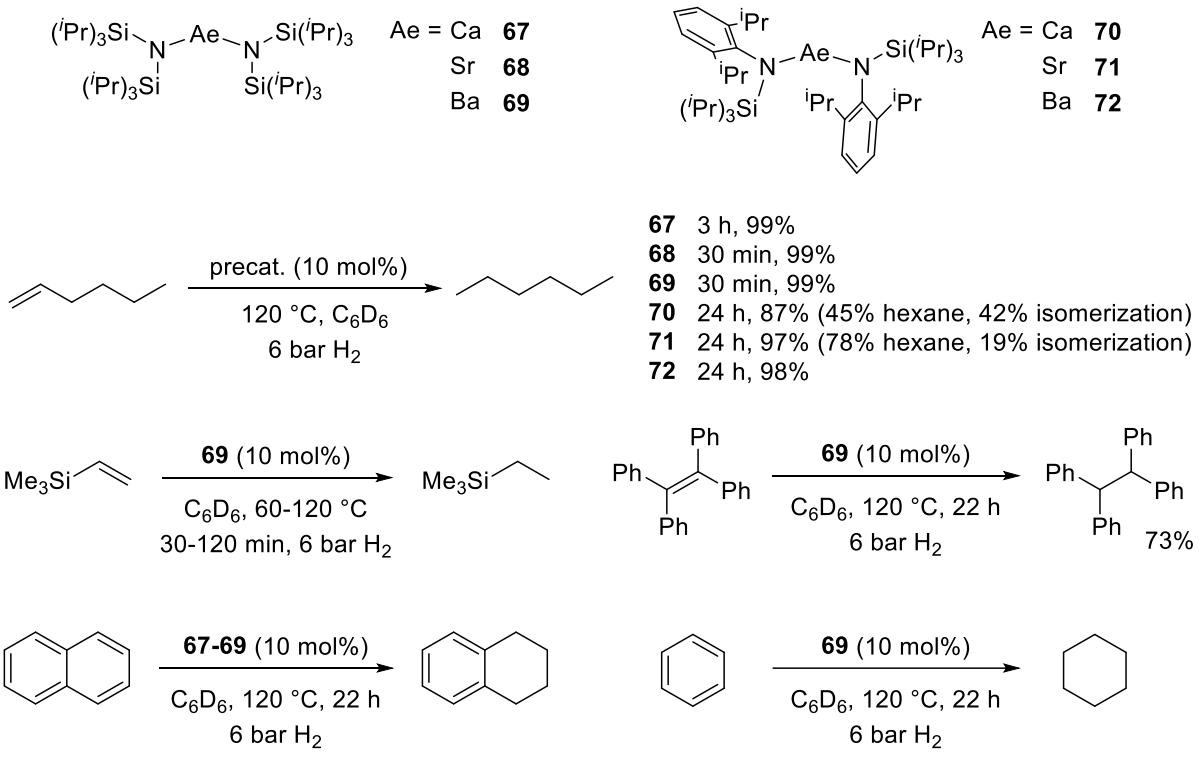

Figure 51. Selected data for the hydrogenation of alkenes catalyzed by **67**-**72**.

In 2021, Harder reported the hydrogenation of both activated and unactivated alkenes using 'activated' metallic barium (i.e Ba^0) deposited as a thin film under high vacuum.[150] The thin-film vapor deposition was deemed to be an essential part of the catalyst synthesis, as various other attempts to

activate metallic barium, such as dissolution in liquid ammonia, the use of freshly cut barium under an inert atmosphere, or the direct use of $[BaH_2]_n$ dried under high vacuum (200 °C, 1×10^{-2} mbar) all resulted in species that were completely inactive in alkene hydrogenation. Two different catalytic cycles were for the hydrogenation with Ba^0 were proposed. The first, based on a metal hydride system, uses BaH_2 as the catalytic species, formed from the oxidative addition of Ba^0 with H_2 (Figure 52, A). Alkene insertion into the Ba-H bond followed by hydrogenolysis regenerates the catalyst. The second, based on a Ba^0 catalytic species, implicates oxidative addition with the substrate, followed by sequential σ-bond metathesis steps and reductive elimination to regenerate Ba^0 (Figure 52, B). The reductive elimination of H_2 from $[BaH_2]$ starts occurring at 330 °C. However, it has been shown that a decrease of particle size decreases this onset temperature, which has been reported down to 100 °C.[151-153] Mercury poisoning experiments provided some evidence that a heterogeneous reaction mechanism was in play. It was also suggested that the true catalytic system could be a composite of these two mechanisms, i.e a system where alkenes are activated by Ba^0 to allow σ-bond metathesis with a $[BaH_2]$ catalyst. The catalytic pathway was probed by DFT calculations, which hinted at a catalytic manifold where Ba^0 activates the substrate (benzene) into a boat conformation with partial Ba^{2+}-1,3-cyclohexadiene^{2-} character. Although the computations were only indicative of a possible catalytic pathway due to the difficulties associated with heterogenous reaction mechanisms, the data suggested a clear accelerating effect for hydrogenation with Ba^0 compared to hydrogenation with $[BaH_2]$ as the sole species.

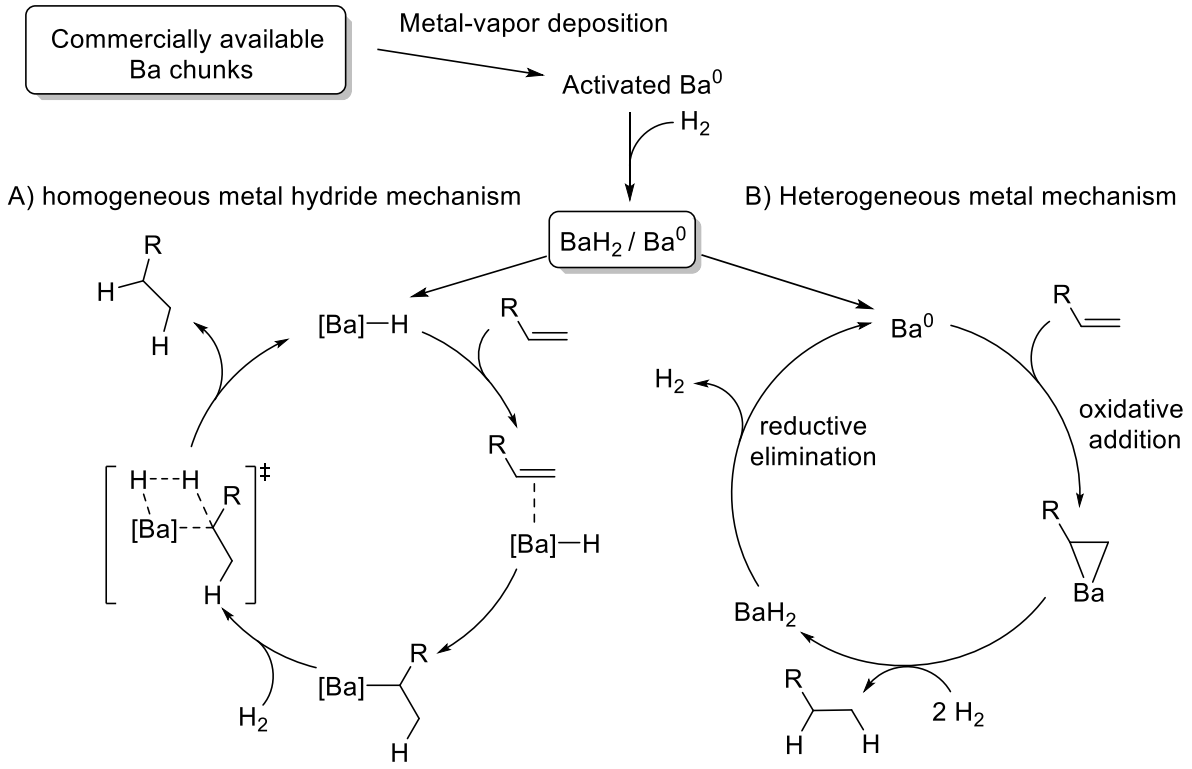

Figure 52. Possible catalytic pathways for the hydrogenation of alkenes using activated Ba^0.

A broad range of substrates were investigated, including acetylenes, unactivated internal alkenes such as 3-hexene, 4-vinylcyclohex-1-ene and 1,1,2,2-tetraphenylethylene. All were fully hydrogenated using moderate conditions (12 bar H_2, 120 °C, 10 mol% catalyst) (Figure 53). Under more forcing

conditions (50 bar H_2, 140-150 °C) a range of aromatic substrates including benzene, pyridine and isoquinoline could be hydrogenated within 96 hours. The ability of the Ba^0 system to hydrogenate heteroatom-containing substrates contrasts with the aforementioned [Ba{N(Si^{i}Pr$_3$)$_2$}$_2$] (**69**) which failed to hydrogenate them, likely due to deleterious coordination of the substrates onto the Lewis-acidic metal center that inhibited catalytic turnover.

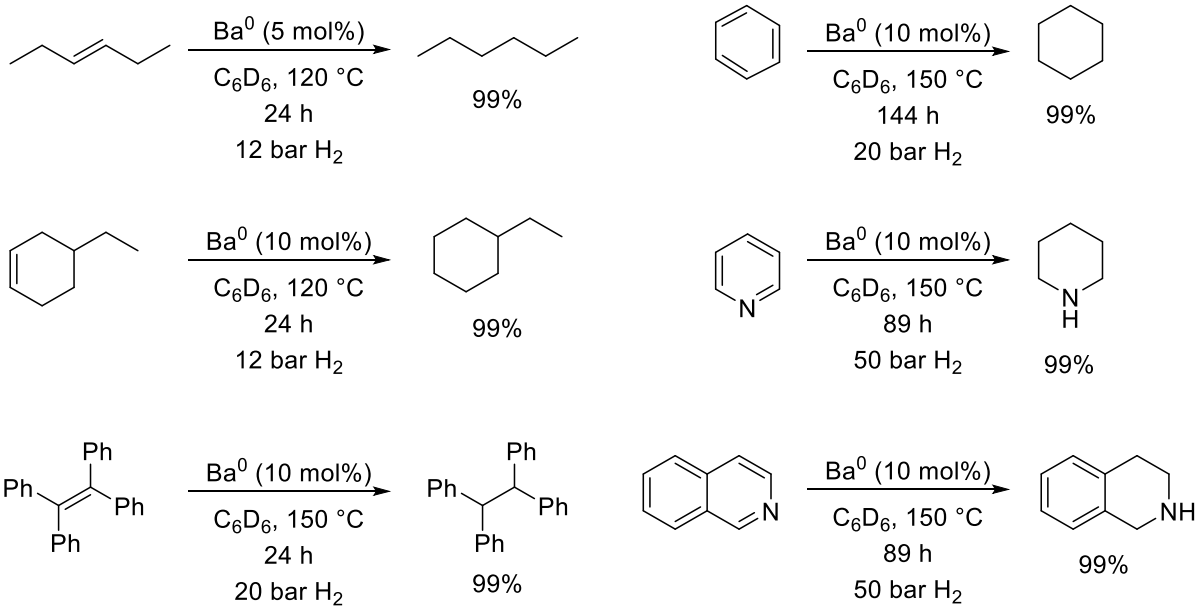

Figure 53. Selected results for the Ba^0-catalyzed hydrogenation of unactivated alkenes.

Although the activation of H_2 is the common hydride source in most alkaline-earth mediated hydrogenation reactions, it is not the only available source. Transfer hydrogenation of alkenes using 1,4-cyclohexadiene (1,4-CHD) as the H source has also been reported (Figure 54).[154] Although transfer-hydrogenation is not as atom efficient as conventional H_2 hydrogenation due to the formation of a tandem coproduct, the ability to avoid high-pressure gas setups can be desirable both for safety reasons and for some sensitive substrates, where harsher reaction conditions may lead to undesirable reaction pathways. The alkene transfer hydrogenation was reliant on catalyst choice. Hence, the Ae amides [Ae{N(SiMe$_3$)$_2$}$_2$]$_2$ successfully hydrogenated a range of vinylarenes under mild conditions, whereas the calcium alkyl [Ca(DMAT)$_2$·(thf)$_2$] (**53**) generated only polystyrene, and the heteroleptic precatalyst [{BDI^{DiPP}}CaN(SiMe$_3$)$_2$] (**73**) gave a mixture of the two products The best catalysts for the transfer hydrogenation were therefore found to be [Ae{N(SiMe$_3$)$_2$}$_2$], for which activity increased with metal size. A range of activated vinylarenes were hydrogenated, including DPE, 1,2-DPE, Me$_3$SiCH=CH$_2$ and 2,3,4,5-tetrahydro-1,1'-biphenyl. Poorly activated alkenes such as cyclohexene and 4-vinylcyclohex-1-ene were only partially hydrogenated under moderate conditions (120 °C, 24 h, 5 equivalents of CHD) with the most active system, [Ba{N(SiMe$_3$)$_2$}$_2$]. The catalytic pathway for the hydrogenation of styrene with [Ca{N(SiMe$_3$)$_2$}$_2$]$_2$ was investigated by DFT. The result indicated initial deprotonation of CHD by the amide precatalyst, generating what the authors described as a labile hydride Meisenheimer complex. Hydride transfer to the metal in this Meisenheimer intermediate generates a heteroleptic calcium hydride, that then undergoes an insertion reaction with styrene to generate a metal-alkyl species (Figure 54). In the final step, protonolysis with the fleeting amine HN(SiMe$_3$)$_2$ reconstructs the homoleptic amido precursor. The energy barrier for the polymerization

of styrene was calculated to be 4.3 kcal mol^{-1} higher than the protonolysis with $HN(SiMe_3)_2$, indicating that polymerization may only take place when $HN(SiMe_3)$ is not present in solution.

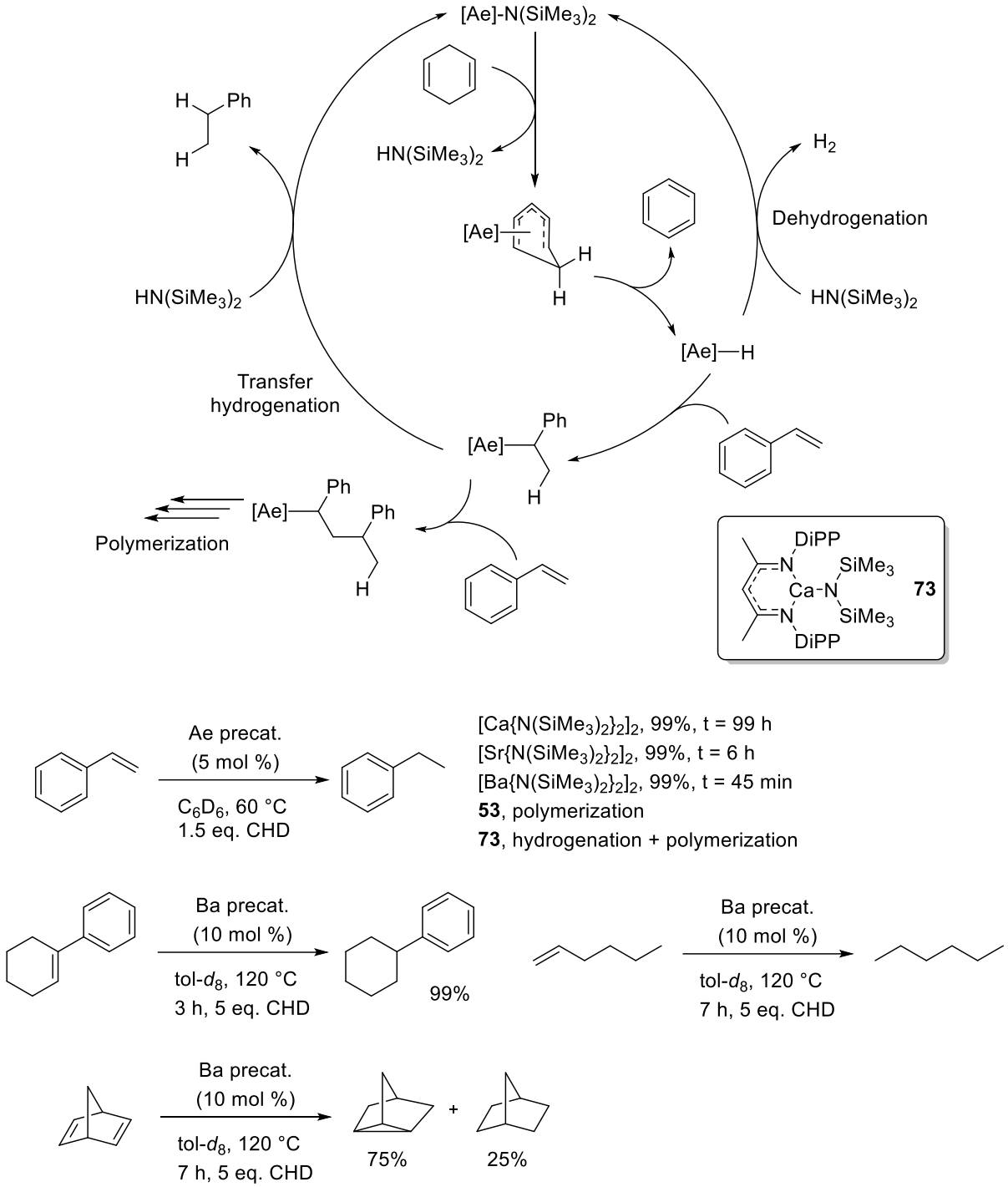

Figure 54. Alkaline-earth catalyzed transfer hydrogenation of activated and unactivated alkenes.

4.2 Hydrogenation of imines

The hydrogenation of imines using the heteroleptic alkaline-earth precatalysts $[Ae\{N(SiMe_3)_2\}_2]_2$ was demonstrated in 2018.[155] The results were said to be unexpected, as in the proposed catalytic cycle (Figure 55), the final σ-bond metathesis step between the product of imine insertion and H_2 was

deemed to be very unfavorable. This was due to the metal-amide intermediate being a significantly weaker Brønsted base relative to the metal-alkyl species seen in olefin hydrogenation. As such, it is conceivable to envisage a catalytic cycle where similarly to the aforementioned hydrogenation of alkenes using $[Ae\{N(SiMe_3)_2\}_2]_2$, the small amount of protonated $HN(SiMe_3)_2$ present in the reaction mixture is deprotonated by the metal-amide insertion product. However, against this hypothesis, when the precatalyst was changed from $[Ae\{N(SiMe_3)_2\}_2]_2$ to the alkyl complex $[Ca(DMAT)_2{\cdot}(thf)_2]$ (**53**) which generates the poorly acidic alkane {DMAT}-H after initial protonolysis, catalytic imine hydrogenation was fast and quantitative conversions were observed. The reaction rates of the precatalysts increased with metal size (Ca < Sr < Ba). Unexpectedly, the bis-thf adduct $[Ba\{N(SiMe_3)_2\}_2{\cdot}(thf)_2]$ showed greater activity than its unsolvated congener $[Ba\{N(SiMe_3)_2\}_2]_2$. Nonetheless, when the reaction solvent was changed from benzene to thf, conversion was inhibited, most likely because of saturation of the coordination sphere by thf molecules. Substrate scope was limited to aldimines; however, a range of various alkyl and aryl substitutions were possible. DFT calculations on imine hydrogenation were also completed, in which three different catalytic pathways were investigated: a classical Ae-hydride catalytic cycle, a route involving a bifunctional catalyst, and a last scenario which avoided the formation of a high energy metal-hydride intermediate. It emerged from the theoretical study that the conventional Ae-hydride mechanism was the likely prevailing mechanism. The turnover-limiting step was identified as the deprotonation of H_2 (Figure 55).

In 2020, the hydrogenation of imines using alkaline-earth alanates was described.[156] The homoleptic alkaline-earth complexes $[Ca\{AlH_4\}_2{\cdot}(thf)_4]_2$ (**74**), $[Sr\{AlH_4\}_2{\cdot}(thf)_5]$ (**75**) and the heteroleptic complexes $[\{BDI^{DiPP}\}Ca(AlH_4){\cdot}(thf)_2]$ (**76**) were all characterized in solution and in the solid-state by single-crystal X-ray diffraction. They displayed either H_3Al-(μ-H)-Ae or/and H_2Al-$(\mu\text{-H})_2$-Ae bridging motifs in the solid state (Figure 56). The complexes were all competent catalysts in the hydrogenation of imines. As per the earlier hydrogenation of imines, the activity of the catalyst increased with metal size. The heteroleptic complex **76** seemed to display improved activity compared to **74** and **75**. Only a limited range of substrates were investigated. However, these did include a ketimine, signifying an improvement of scope on the earlier reported imine hydrogenation catalysed by $[Ae\{N(SiMe_3)_2\}_2]_2$.[155] The number of catalytic turnovers increased with temperature. The pressure of dihydrogen only slightly effected the catalysis, as lowering it to 1 bar only resulted in a slight loss of conversion. In a subsequent extension of the scope of alkaline-earth catalyzed imine hydrogenation, the aforementioned Ba^0 catalytic system (see Figure 52) also proved excellent for imine (and pyridine) hydrogenation,[150] fully converting aldimines and ketimines to the corresponding amines with molar loadings up to 10% under moderate conditions (12 bar H_2, 120 °C; Figure 56).

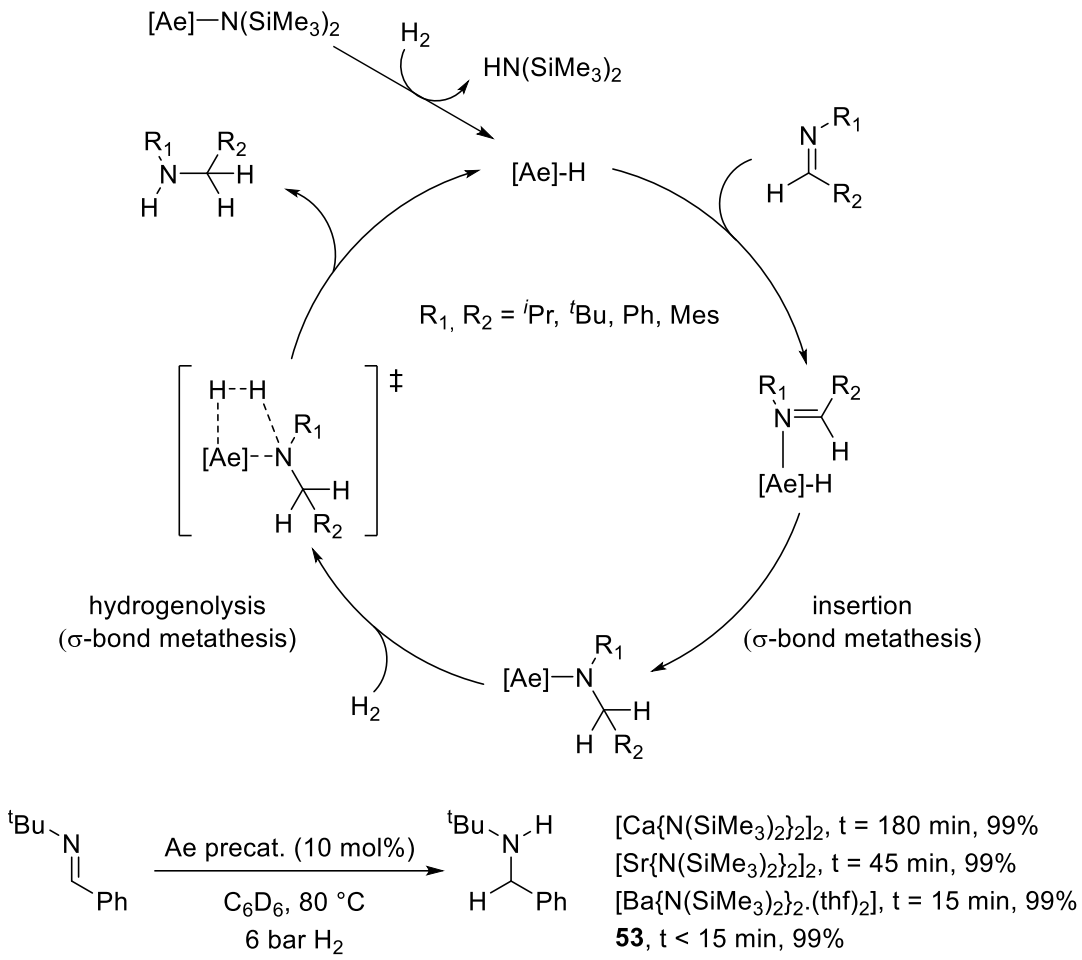

Figure 55. Proposed catalytic cycle for the alkaline-earth catalyzed hydrogenation of imines.

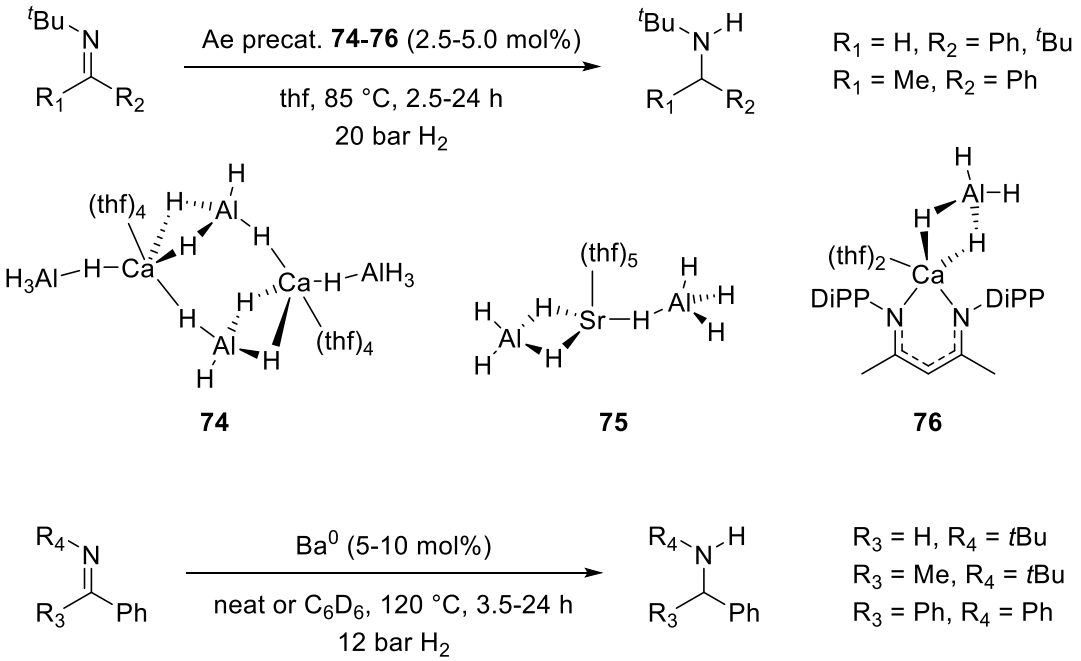

Figure 56. Imine hydrogenation catalyzed by alkaline-earth alanates and by the Ba^0 catalytic system.

5 Dehydrocoupling catalysis

Catalyzed dehydrocoupling reactions allows for the formation of E-E' bonds between two main group elements from E-H and E'-H substrates. The reactions are clean, and proceed through the loss of dihydrogen which makes them entropically favorable. Homodehydrocouplings are these reactions which enable the formation of apolar E-E bonds, i.e. E = E' such as in the coupling of silanes or stannanes. The more diverse and widespread heterodehydrocouplings build a polarized E-E' bond between two different elements, and have attracted considerable attention in recent years. The coupling of ditopic substrates that contain two E-H/E'-H bonds is particularly attractive, as it allows for the construction of polymers through dehydropolymerisations. The polarization of $^{\delta+}$E-H$^{\delta-}$ and $^{\delta-}$E'-H$^{\delta+}$ bonds (hydridic and protic substrates, respectively) is often critical in catalyzed heterodehydrocoupling reactions, as it heavily weighs on the nature of the mechanisms at work in the pertaining catalytic cycles leading to the creation of $^{\delta+}$E-E$^{\delta-}$ bonds. The feasibility of a specific coupling also relies on the specific thermodynamics of the reaction, as the net energy gain upon creation of E-E' and H-H bonds must outweigh the energy required to break the E-H and E'-H bonds. It can be anticipated using bond dissociation energies (BDE), with the formation of H_2 already releasing a substantial 104 kcal mol^{-1}. Alkaline-earth complexes have not been used to mediate homodehydrocoupling reactions. On the other hand, they have proved particularly competent precatalysts for the controlled formation of N-B, N-Si and Si-O bonds (Figure 57).

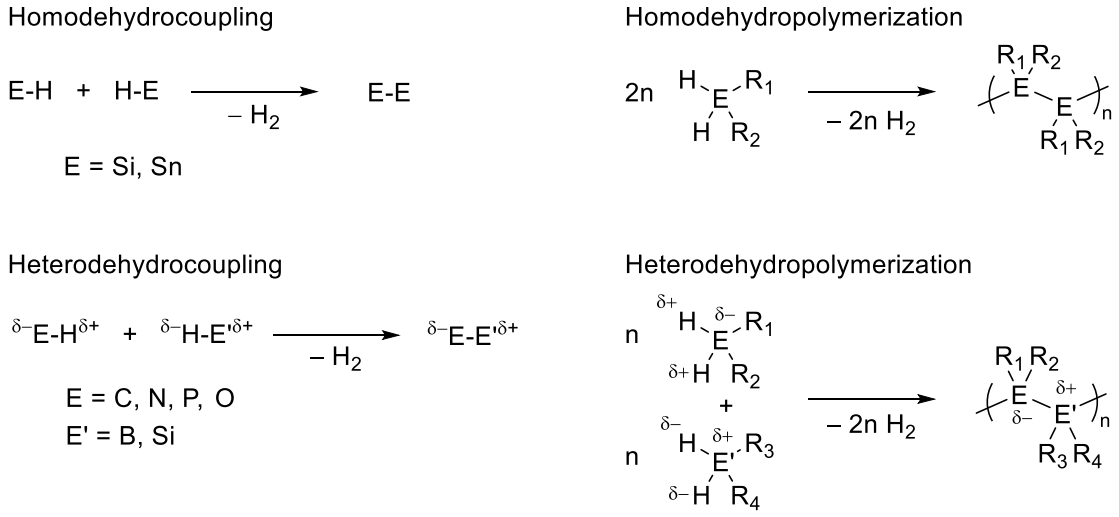

Figure 57. Generic representation of homo- and heterodehydrocoupling reactions.

5.1 Dehydrocoupling of amines and boranes

The coupling of amines and boranes that generates dimeric aminoboranes and borazines (respective BDE: N-H, 81 kcal mol^{-1}; B-H: 83 kcal mol^{-1}; B-N, 90 kcal mol^{-1}) has attracted substantial attention, triggered by the fact that ammonia borane H_3N-BH_3 (19.6 wt% H-content) is a potential material for the storage of dihydrogen.[157] With group 2 metals, catalysis for the dehydrocoupling of amines and boranes has essentially focused on magnesium and calcium; surprisingly, strontium and barium have seldom been looked at. The Harder group investigated in 2008 the decomposition of the calcium

amidoborane [{BDI^{DiPP}}CaNH$_2$BH$_3$·(thf)$_2$] as a preliminary step towards the development of hydrogen-storage materials (Figure 58).[158] This initial studies was followed by other stoichiometric and subcatalytic reactions.[159,160] On the whole, the complexes [{BDI^{DiPP}}CaN(H)RBH$_3$·(thf)$_n$] (n = 1-2; R = H, **77**; Me, **78**; ^{i}Pr, **79**) thermally decomposed to afford B-N coupling and concomitant loss of H$_2$. This process yielded the dinuclear complexes into the dinuclear [({BDI^{DiPP}}Ca·(thf))$_2${RN-BH-NR-BH$_3$}] bridged by the dianion {RN-BH-NR-BH$_3$}$^{2-}$. Thermal decomposition required increasing temperature as the steric bulk around the nitrogen atom became greater. Using the sterically demanding [{BDI^{DiPP}}CaN(H)DiPPBH$_3$·(thf)] (**80**), the monomeric borylamide [{BDI^{DiPP}}Ca{NDiPP=BH$_2$}·(thf)] incorporating the monoanionic fragment {H$_2$B=NDiPP}$^-$ was isolated.

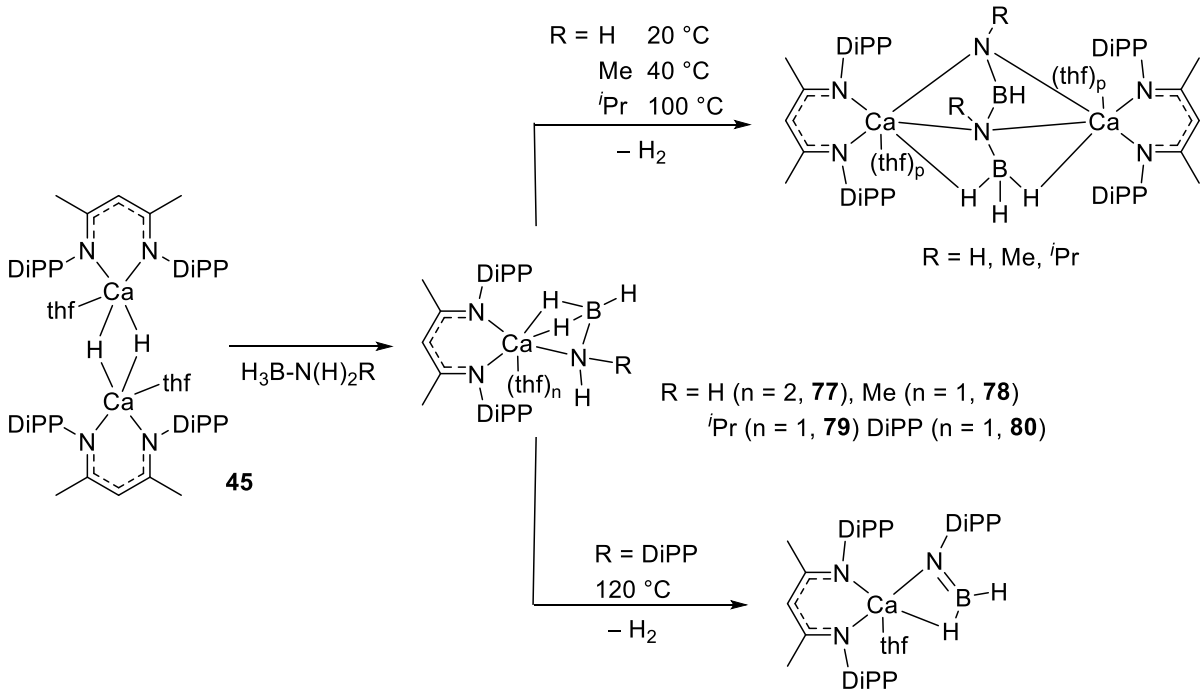

Figure 58. Synthesis and thermal decomposition of calcium amidoboranes.

5.1.1 Synthesis of asymmetrical diaminoboranes

The calcium bis(amide) [Ca{N(SiMe$_3$)$_2$}$_2$]$_2$ (2.5 mol%) was shown to catalyze the formation of asymmetrical diaminoboranes by selective heterodehydrocoupling of amines HNR$_1$R$_2$ and amine-boranes H$_3$B-N(H)R$_3$R$_4$ (Figure 59).[161] The reaction was generally selective and ensued via successive couplings. The chemoselectivity was governed by the relative difference of Lewis basicity between the two amines. Asymmetrical diaminoboranes were obtained when one of the amines was clearly more basic than the other, as otherwise mixtures of symmetrical and asymmetrical products were generated as a result of an off-cycle equilibrium between HNR$_1$R$_2$ + H$_3$B-N(H)R$_3$R$_4$ and HNR$_3$R$_4$ + H$_3$B-N(H)R$_1$R$_2$. A multi-step catalytic manifold relying on a calcium-hydride active species was proposed. Postulating that the Lewis basicity of HNR$_1$R$_2$ is lower than that of HNR$_3$R$_4$, the Ca-hydride first reacts with the amine-borane H$_3$B-N(H)R$_3$R$_4$ through aminolysis to generate a metallated amido borane. This transient species then expulses the intermediate aminoborane H$_2$B=NR$_3$R$_4$ through a β-hydride elimination, a process which also regenerates the hydrido active species. At this stage, the metal-hydride enters a second cycle where it reacts in a protonolysis reaction with the more (Lewis) acidic amine HNR$_1$R$_2$ to yield the amido Ca-NR$_1$R$_2$. This intermediate then intercepts the floating H$_2$B=NR$_3$R$_4$

to produce a metal-bound diamidoborate, which releases the final diaminoboranes through β-hydride elimination.

5.1.2 Dehydrocoupling of dimethylamine-borane and tert-butylamine-borane

The catalyzed dehydrocoupling of dimethylamine-borane Me_2NH-BH_3 has been attracting attention both as a dihydrogen storage material and as a field of debated mechanistic investigations. A number of metal-based systems are known to mediate the formation of the cyclic dimer *c*-$(Me_2NBH_2)_2$ with minimal formation of the bis(dimethylamino)borane by-product, $(Me_2N)_2BH$.

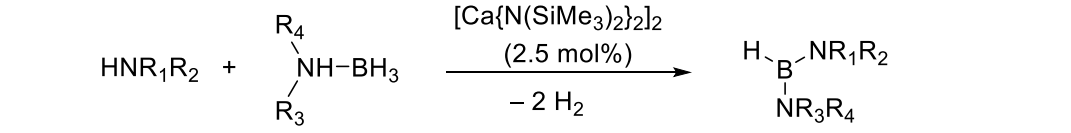

HNR_1R_2 = $HNMe_2$, $HN(CH_2)_4$, H_2N^tBu HNR_3R_4 = $HN(CH_2)_4$, HN^iPr_2, H_2N^tBu, $HNPh_2$

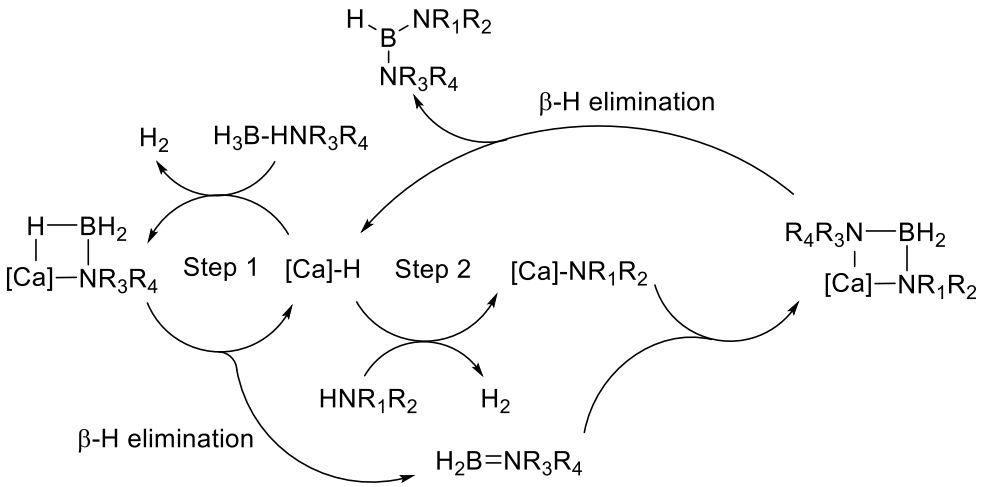

Figure 59. Calcium-earth catalyzed synthesis of diaminoboranes and proposed reaction manifold.

In a contribution focusing mostly on the related magnesium chemistry, Hill reported that treatment of the calcium complex **1** with Me_2NH-BH_3 afforded [{BDI^{DiPP}}Ca{NMe_2BH_3}·(thf)] (**81**). This thermally stable complex was characterized by X-ray diffraction analysis and NMR spectroscopy in C_6D_6.[162] Heating a solution of **81** for 4 h at 80 °C in C_6D_6 led to the formation of small quantities of the unsaturated $Me_2N{=}BH_2$ along with the calcium hydride **45**. The authors suggested that **81** was prone to a thermally induced β-hydride elimination/intramolecular σ-bond metathesis process. Following this discovery, it was found that both **1** and [$Ca\{CH(SiMe_3)_2\}_2$·$(thf)_2$] reacted with Me_2NH-BH_3 to afford the dimer *c*-$(Me_2NBH_2)_2$ under catalytic conditions. The experimental observations (in particular spectroscopic detection of $H_2B{=}NMe_2$) and distribution of products were reminiscent of those made for related magnesium catalysts. Both systems were postulated to follow a similar mechanistic pathway involving successive β- and δ-hydride elimination and insertion steps (Figure 60); the magnesium system was more active than its thermally-triggered calcium counterpart.

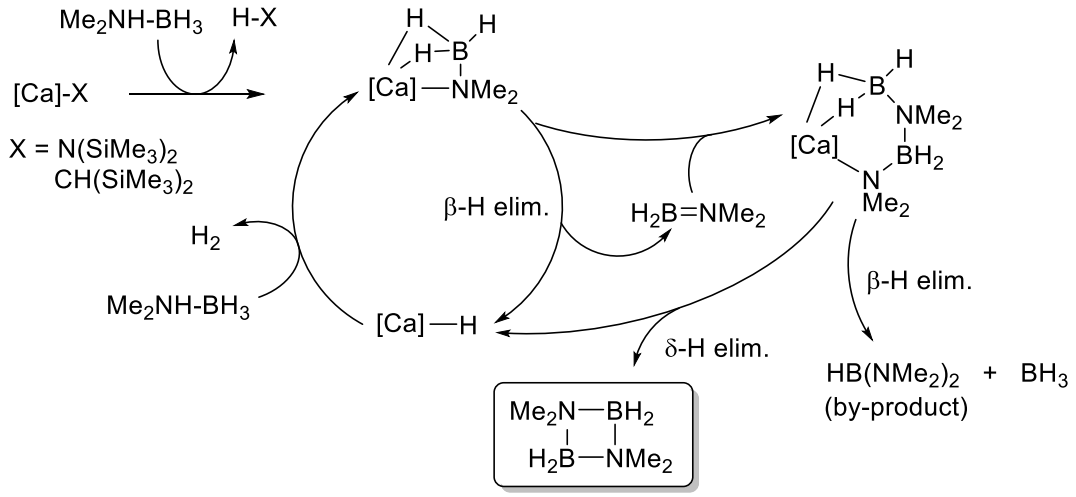

Figure 60. Initial mechanistic proposal for the calcium-catalyzed dehydrocoupling of $Me_2NH\text{-}BH_3$.

A DFT investigation of the coupling of dimethylamine-borane by **81** suggested instead that due to the large size of the Ca^{2+} cation (in contrast with magnesium), the relative instability of the calcium-hydride intermediate precluded the thermally-induced δ-hydride elimination.[163] The authors proposed instead an alternative concerted proton-assisted pathway, where an incoming dimethylamine-borane molecule enables the formation of the cyclic product without recourse to a putative calcium-hydride. In this mechanism, the additional $Me_2NH\text{-}BH_3$ molecule displaces thf from **81** (a mandatory step as thf was found to inhibit catalytic turnovers), and intermolecular elimination of H_2 occurs by interaction of the N-H proton of the dimethylamine-borane molecule and a β-hydride of the ligated amidoborane. This results in the release of the aminoborane $Me_2N{=}BH_2$ while the thf-free amidoborane catalyst is regenerated. Coordination of another molecule of dimethylamine-borane restarts the catalytic cycle. Hill and co-workers then re-explored their original mechanism, and showed that the reaction of **81** with $Me_2NH\text{-}BH_3$ led to the formation of [({BDI^{DiPP}}Ca{$Me_2N\text{-}BH_2\text{-}NMe_2\text{-}BH_3$}] through loss of dihydrogen.[164] The same reaction with deuterated $Me_2ND\text{-}BH_3$ and $Me_2NH\text{-}BD_3$ indicated that the formation of this complex proceeded in both cases with a non-negligible KIE (1.4 and 1.6, respectively). Consistent with these findings, Hill proposed a refined dimethylamine-borane assisted mechanism involving solely **81** and [{BDI^{DiPP}}Ca{$Me_2N\text{-}BH_2\text{-}NMe_2\text{-}BH_3$}] as the metallated catalyst and intermediate, respectively (Figure 61). The β- and δ-elimination steps inducing the formation of the cyclic dimer *c*-$(Me_2NBH_2)_2$ were both suggested to take place through N*H*-assisted release of H_2 and without participation of any Ca-hydride or aminoborane $Me_2N{=}BH_2$ species.

In a separate investigation, the Hill group also reported on the stoichiometric and catalytic reactivity of the calcium amide **1** with *tert*-butylamine-borane, $^tBuNH_2\text{-}BH_3$.[165] Catalysis towards the formation of the trisubstituted borazine occurred very slowly (20 % conversion after 138 h at 60 °C in toluene, 5 mol% precatalyst), and was accompanied by significant catalyst decomposition resulting in the formation of the catalytically inactive $[Ca(BH_4)_2]_n$. Product distribution was poorly controlled, as the formation of by-products in substantial amounts was detected (Figure 62). The formation of borazine was assumed to be the outcome of ring-expansion from the spectroscopically detected dimer *c*-$(^tBuN(H)BH_2)_2$. Although some of the experimental observations were similar to those for the coupling of dimethylamine-borane, a clear mechanistic pathway accounting for the formation of the borazine and the different by-products could not be formulated.

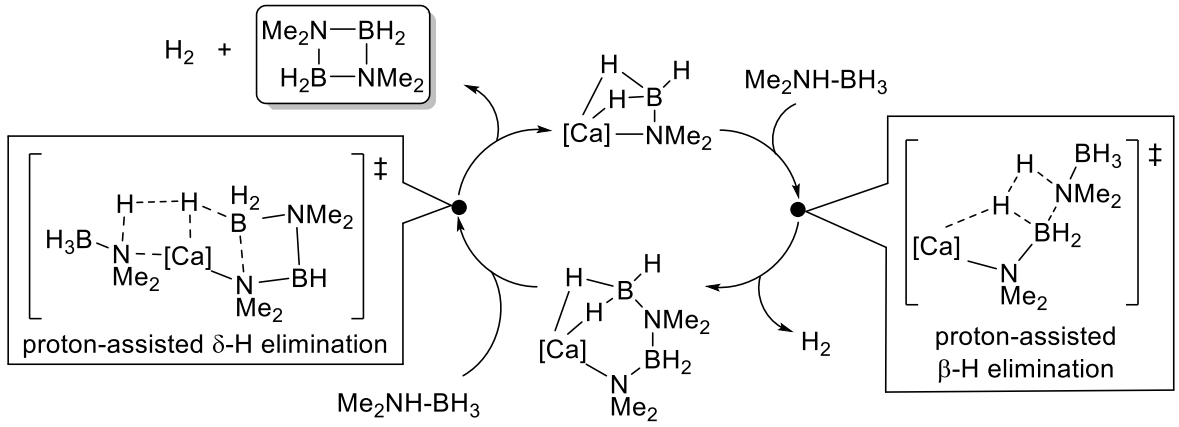

Figure 61. Proton-assisted mechanism for the calcium-catalyzed dehydrocoupling of dimethylamine-borane and formation of *c*-$(Me_2NBH_2)_2$.

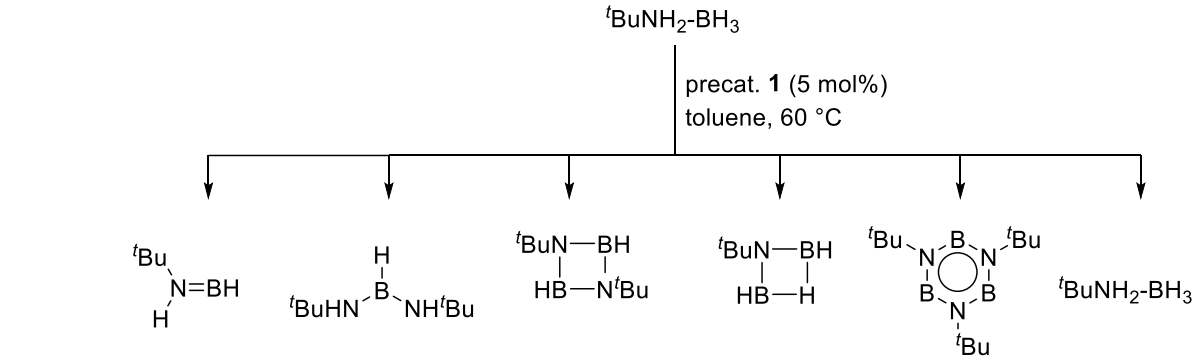

after 24 h	1%	13%	5%	7%	-	68%
after 138 h	-	13%	45%	< 3%	20%	14%

Figure 62. Calcium-catalyzed dehydrocoupling of $BuNH_2$-BH_3.

5.1.3 Dehydrocoupling of amines and boranes

Early work by Hill and co-workers showed that the calcium amide [{BDI^{DiPP}}$CaNPh_2$·(thf)] (**82**) reacted stoichiometrically with the 9-BBN dimer in toluene at 25 °C to give cleanly the isolated calcium borohydride **83** along with formation of an aminoborane (Figure 63).[166] The same group exploited this knowledge to investigate the alkaline-earth catalyzed coupling of amines and monohydroboranes.[167] A range of primary/secondary amines and anilines along with 9-BBN and pinacolborane were selected as typical substrates (Figure 63), and **1** was used as the precatalyst (10 mol%). Conversion to the corresponding aminoboranes and aminodi(borane)s took place under mild conditions (25-60 °C in C_6D_6). The weaker Lewis acid HBPin was found to give noticeably higher reaction rates (generally less than 1 h) than 9-BBN (ca. 12-144 h). With primary amines R'NH_2, monocoupling to R_2B-NHR' was selectively achieved during equimolar reactions with both 9-BBN and HBPin. However, with a twofold excess of the borane, catalytic production of the aminodi(borane)s R'$N(BR_2)_2$ could only be achieved for aliphatic amines and with HBPin, and required extended reaction times (ca. 24 h). For these catalyzed dehydrocoupling reactions, the calcium precatalyst **1** proved inferior to its magnesium congener, and the ensuing detailed study focused solely on the smaller metal. The mechanism of the

calcium-promoted catalysis was not ascertained, and there is no evidence that the convincing mechanistic scenario established for magnesium could be confidently extrapolated to calcium.

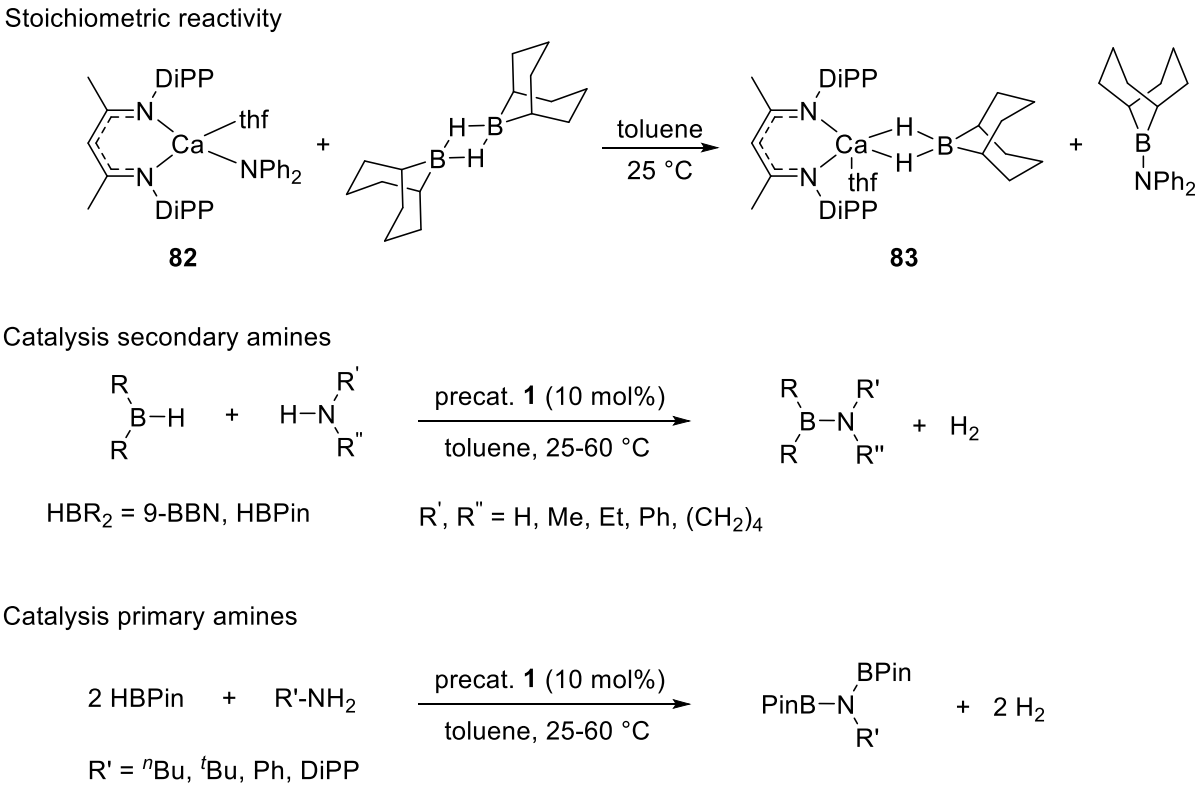

Figure 63. Calcium catalyzed dehydrocoupling of amines and boranes.

5.2 Heterodehydrocoupling of amines and silanes

The construction of N–Si bonds through the atom-efficient catalyzed dehydrocoupling of primary or secondary amines with hydrosilanes yields silazanes. These compounds are routinely employed as ligands in in coordination chemistry,[168] as bases,[169] silylating agents[170] or protecting groups for amines, indoles and anilines, making their clean synthesis a desirable synthetic aim.[171] In addition, oligo- and polysilazanes are used as precursors to Si_3N_4 ceramics.[172] Alkaline-earth catalysis has proved particularly effective in the selective dehydrocouplings of hydrosilanes with amines, hydrazines or ammonia. In the past decade, a detailed exploration of substrate scope and operating mechanism in the formation of mono- or disilazanes has paved the way for more ambitious applications in the area of polymer synthesis.

5.2.1 Catalyzed NH/HSi heterodehydrocouplings for the formation of mono- and disilazanes

A small number of well-defined alkaline-earth precatalysts have been utilized to mediate the dehydrocoupling of amines with silanes, leading to a range of products with high reaction rates and selectivity. The reaction outcome is heavily influenced by steric and electronic factors, but can be orientated favorably with the choice of an adequate precatalyst (Figure 64). Chemoselectivity, i.e. the ability to direct and control the number of created N-Si bonds starting with substrates containing more than one Si-H or one N-H, was a key factor in the efforts paid to extend substrate scope.

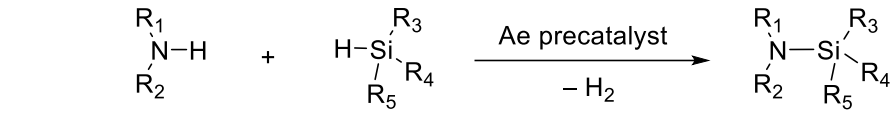

Possible distribution of products for $R_1 = R_3 = R_4 = H$, $R_2 = {}^{i}Pr$, $R_5 = Ph$

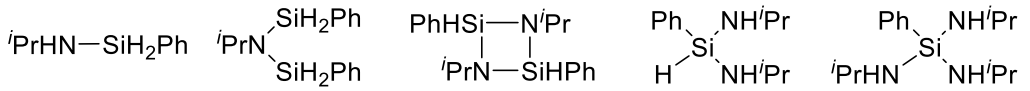

Figure 64. Alkaline-earth catalyzed NH/HSi heterodehydrocoupling.

5.2.1.1 Catalyst selection and substrate scope

Harder first mentioned in 2007 that the calcium dibenzyl **53** and the solvated azametallacyclopropane [Ca(η^2-Ph_2CNPh)(hmpa)] (**84**) could be used as competent precatalysts for the coupling of primary and secondary amines with the tertiary silane Ph_3SiH.[173] The reactions proceeded smoothly at 20 °C in thf, with 3-10 mol% of precatalyst. Although substrate scope was limited, it appeared that alkylamines were more reactive than anilines, even if the introduction of cumbersome tertiary alkyl substituents led to a decrease of reaction rates. A small selection of Ca, Sr and Ba precatalysts that included the amido and alkyl complexes [Ae{E($SiMe_3$)$_2$}$_2$·(thf)$_2$] (E = N, CH), and [Ae{N($SiMe_3$)$_2$}$_2$]$_2$ as well as the Ae-iminoanilides **7**-**9** and **10**-**12** were subsequently reported by the groups of Hill[174] and Sarazin[175,176] to successfully allow for the coupling of a broad suite of substrates. Although the benchmark substrates for the evaluation of catalyst performance were pyrrolidine and triphenylsilane, substrate scope was extended to a very large selection of amines and hydrosilanes (Figure 65). Catalysis generally occurred in the temperature range 25-60 °C in C_6D_6, and quantitative conversions were observed typically within 1-2 h using 5 mol% precatalyst. Simple silanes like $PhSiH_3$, Ph_2SiH_2 and $PhSiH_3$ were found to be very easily coupled with primary and secondary amines, e.g. $EtNH_2$, $HNCy_2$, $BnNH_2$, pyrrolidine, piperidine, $^{t}BuNH_2$ and $DiPPNH_2$. The couplings of α,ω-dihydrosilanes or α,ω-diamines was also shown to be possible. Importantly, the chemoselectivity of the reactions was excellent in the cases of primary amines and primary or secondary silanes, that is, the number of N-Si bonds created during the catalytic process could be adjusted and controlled by appropriate choice of the ratio between the two substrates. The reactions were fast and the catalysts were highly active; in these cases where chemoselectivity was sought, judicious choice of the precatalyst to favor selectivity over reaction rates was a key factor, e.g. by preferring the Ba-amide **9** over the more active Ba-alkyl **12**.

Several main conclusions emerged from catalyst and substrate screening by Hill and Sarazin.[174-176] Regarding the substrates, reactions rates were reduced with increasing substitution of the amine or the silane; in particular, Ph_3SiH was significantly less reactive than Ph_2SiH_2 and $PhSiH_3$. The reaction kinetics were found to increase for more nucleophilic amines (alkylamines > anilines), whereas the reactions were faster when the silane was more electrophilic. Several trends for catalyst selection were also reported. Regardless of the identity of the supporting ligands in a homologous series of Ae precatalysts, the catalytic activity increases in the order Ca < Sr < Ba; the Ba precatalysts afforded unmatched TOF values that could be in excess of 3600 mol_{subst} mol_{Ba}^{-1} h^{-1}. The bis-amido complexes [Ae{E($SiMe_3$)$_2$}$_2$·(thf)$_2$] (E = N, CH) and [Ae{N($SiMe_3$)$_2$}$_2$]$_2$ were more effective than their heteroleptic counterparts **9** and **12**. Uncharacteristically, the presence of coordinated thf molecules in the bis-amido precatalysts [Ae{N($SiMe_3$)$_2$}$_2$·(thf)$_2$] did not influence the overall catalytic efficiency,

as they were found to be equally competent as their unsolvated congeners $[Ae\{N(SiMe_3]_2\}_2]_2$. Moreover, the alkyl complexes were tangibly more efficient than their amido analogues, an observation rationalized by the fact that the formation of the catalytically active species by aminolysis is irreversible with the former while it is an equilibrium for the latter. It resulted from this screening that the barium alkyl $[Ba\{CH(SiMe_3]_2\}_2\cdot(thf)_2]$, a compound reasonably easy to synthesize under crystalline form,[177] was the precatalyst of choice for the heterodehydrocoupling of amines and silanes.

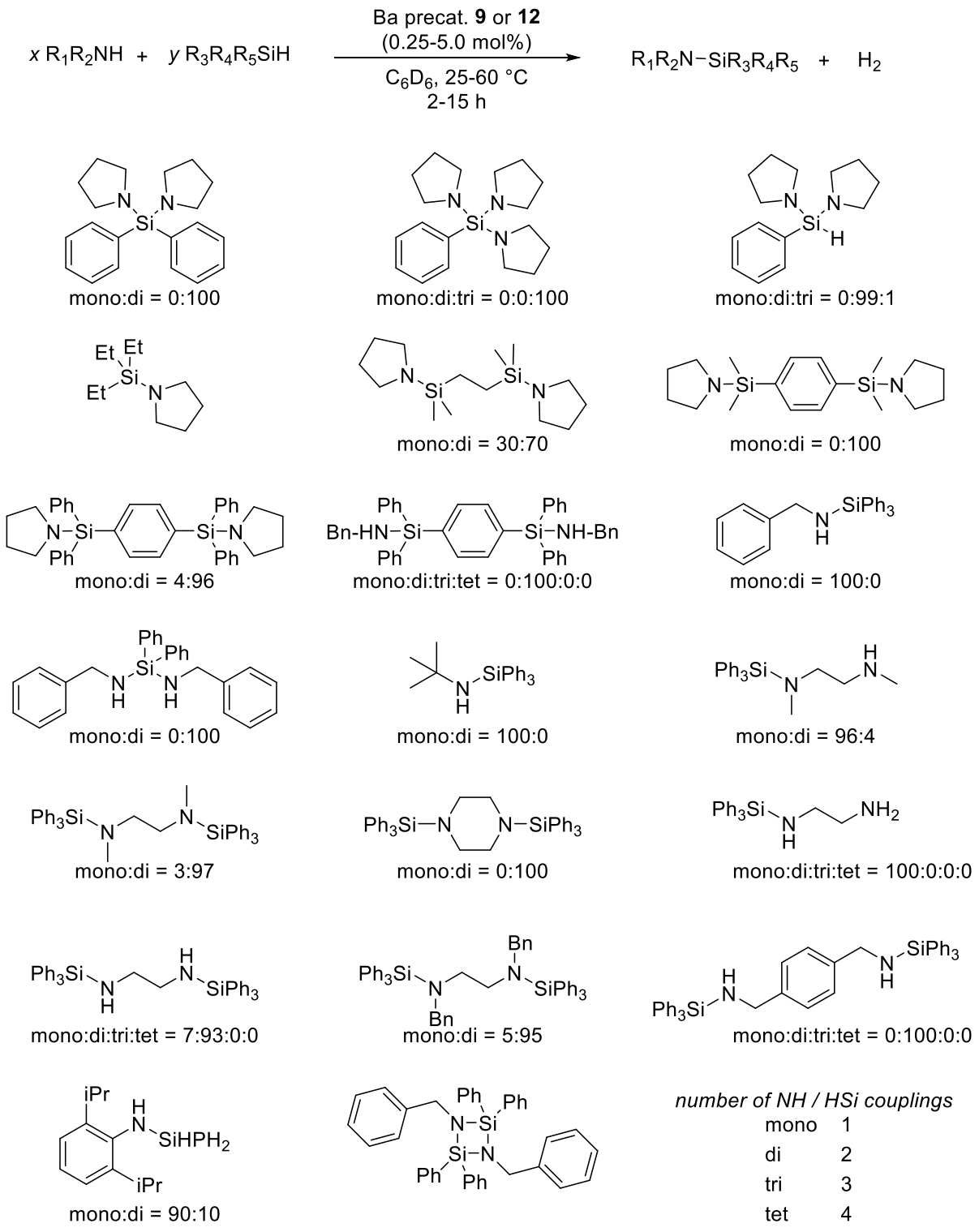

Figure 65. Selected data for the barium-catalyzed heterodehydrocoupling of amines with silanes.

The NHC-supported calcium bis(alkyl) complex $[Ca\{CH(SiMe_3)_2\}_2]_2\cdot(I^iPr_2Me_2)_2]$ (**85**), where $I^iPr_2Me_2$ is the N-heterocyclic carbene 1,3-diisopropyl-4,5-dimethylimidazol-2-ylidene, displayed high activity and excellent chemoselectivity in the catalyzed coupling reactions of hindered amines and silanes, including with $^tBuNH_2$ and $DiPPNH_2$, which were earlier found to be among the least reactive substrates.[178] The authors also achieved the moderately enantioselective coupling of $(Naph)(Ph)SiH_2$ and $BnNH_2$ (*ee* up to 26%) by combining a chiral NHC ligand and the calcium bis(alkyl) precursor. These results further highlighted the close relationship between metal size and catalytic performance in Ae-promoted dehydrocoupling reactions. Taken collectively,[174-177] the experimental observations suggested that the overall efficiency (both in terms of reaction rates and selectivity) was a composite of two key factors: accessibility of the metal center, and reactivity (often linked to the strength) of the pertaining polarized Ae-to-heteroelement bonds.

5.2.1.2 Mechanistic insight

The mechanism of Ae-mediated amine-silane dehydrocoupling was probed by kinetic and computational analyses. Hill showed that the kinetic rate laws given in equations (4) and (5) for the coupling of Et_2NH and Ph_2SiH_2 catalyzed by the solvent-free $[Ae\{N(SiMe_3)_2\}_2]_2$ (Ae = Ca or Sr) unexpectedly depended on the identity of the metal.[174]

$$\text{Rate} = k_{Ca}\,[Ca]^1\,[Et_2NH]^1\,[Ph_2SiH_2]^0 \qquad (4)$$

$$\text{Rate} = k_{Sr}\,[Sr]^2\,[Et_2NH]^1\,[Ph_2SiH_2]^1 \qquad (5)$$

The partial kinetic order of 1 in [catalyst] suggested a monometallic active species in the turnover-limiting step, while for strontium, the partial order of 2 was seen as the expression of a dinuclear active species. Dimerization for strontium was rationalized as being the outcome of its greater size and resulting affinity for higher coordination numbers, often with bridging ligands. Unexpectedly in the light of other comprehensive data,[175,176,179,180] the strontium precursor was less active than its calcium analogue, which was hypothesized to be the outcome of this dimerization process. The zero-order dependence in $[Ph_2SiH_2]$ agreed with a rate-determining aminolysis step in the case of calcium. With strontium, the first-order dependence in both $[Et_2NH]$ and $[Ph_2SiH_2]$ was said to be consistent with a concerted, proton-assisted β-hydride transfer.

The mechanisms of the dehydrocoupling of pyrrolidine and Ph_3SiH catalyzed by **9** was probed in detail by Sarazin and co-workers by combination of synthetic, kinetic and computational investigations.[175,176] The substrates and precatalyst were selected to enable convenient monitoring of kinetics by NMR spectroscopy. The catalytically active species was inferred to consist of an iminoanilide-supported Ae-pyrrolide. This working hypothesis agreed with the fact the bis(silanide) precursors $[Ae(SiPh_3)_2\cdot(thf)_3]$ were found to be inactive, whereas the performances of pre-isolated Sr-iminoanilide $[\{N\hat{}N\}Sr\{N(CH_2)_4\}\cdot(NH(CH_2)_4)]$ ($\{N\hat{}N\}^-$ =$\{DiPPN(o\text{-}C_6H_4)C(H)=NDiPP\}^-$) matched those of **8**. Kinetic analysis allowed for the determination of the kinetic rate law given in equation (6):

$$\text{Rate} = k\,[\mathbf{9}]^1\,[\text{pyrrolidine}]^0\,[Ph_3SiH]^1 \qquad (6)$$

By contrast with analysis for other systems, the kinetic rate law with **9** is independent from the concentration in amine. Hammett analysis was performed on the coupling of pyrrolidine with *para*-substituted triarylsilanes $Ph_2(p\text{-}X\text{-}C_6H_4)SiH$ substrates, with X chosen amongst Me, OMe, F and CF_3. Electron-withdrawing *p*-substituents were found to increase substantially the reaction rate (ρ = 2.0), suggesting they helped stabilize an incipient negative charge in the transition state. Kinetic measurements with *Si*-deuterated silane and *N*-deuterated pyrrolidine indicated a maximal kinetic isotopic effect with the silane (k_{SiH}/k_{SiD} = 4.7), whereas none was found for the amine (k_{NH}/k_{ND} = 1.0). Both the kinetic rate law and KIE pointed at a rate-limiting step involving Si-H bond breaking and without direct participation of pyrrolidine. The activation parameters $\Delta H^{‡}$ = 15.6(23) kcal mol^{-1} and $\Delta S^{‡}$ = –13.3(7.5) cal mol^{-1} K^{-1} ($\Delta G^{‡}$ = 19.6(1) kcal mol^{-1} at 298 K) were estimated by Eyring analysis. The negative value of ΔS‡, diagnostic of an associative mechanism, was much smaller than those mentioned for the bis(amido) Ca and Sr precatalysts.[174] This was thought to be the consequence of the larger radius of the Ba^{2+} cation, leading a less constrained arrangement about the metal in the turnover-limiting step. A detailed computational analysis for the cross-dehydrocoupling of pyrrolidine and Ph_3SiH catalyzed by **9** was performed to determine the prevailing mechanistic pathway (Figure 66). A σ-bond breaking metathesis route was found to be energetically non-competitive. Instead, the DFT analysis provided compelling evidence that the coupling progressed via a stepwise mechanism involving first N–Si bond forming through nucleophilic attack of the catalytically competent Ba-pyrrolide onto the incoming silane, followed by rate-limiting β-hydride elimination liberating the silazane. The Ba-hydride intermediate formed then further reacts with pyrrolidine to regenerate the Ba-pyrrolide upon dehydrogenative aminolysis. The proposed catalytic manifold was fully consistent with the experimental observations and with the kinetic analysis. The potential involvement of a Ba-silanide was shown to be energetically prohibited, consistent with the observation that [Ae]–$SiPh_3$ precursors did not show any catalytic ability. The experimentally-determined reactivity trend Ca < Sr< Ba was rationalized by DFT calculations as the outcome of the greater accessibility of the metal center and decreasing Ae-$N_{pyrrolide}$ bond strength upon descending group 2.

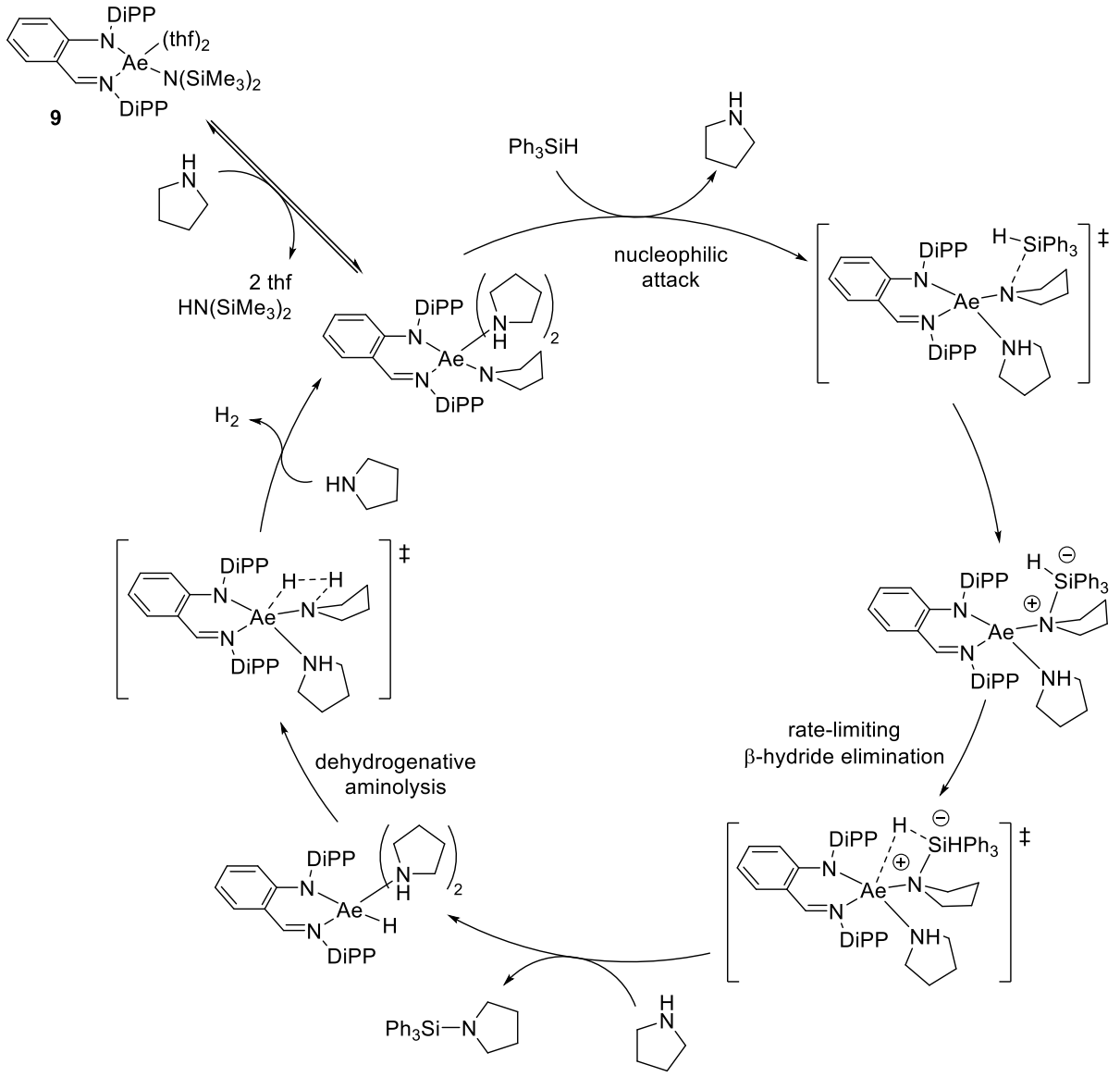

Figure 66. Prevailing mechanistic pathway for the alkaline-earth catalyzed dehydrocoupling of amines and silanes, with [{N^N}AeN(CH$_2$)$_4$] (Ae = Ca, Sr, Ba) as the catalytically active species and triphenylsilane and pyrrolidine substrates; {N^N}$^-$ = {DiPPN(*o*-C$_6$H$_4$)C(H)=NDiPP}$^-$.

5.2.2 Formation of cyclic disilazanes

The chemoselectivity observed in the alkaline-earth catalyzed formation of regular silazanes allowed for the multi-step synthesis of tailor-made disilazanes and cyclic disilazanes through iterative dehydrocoupling steps (Figure 67).[179] Starting from Ph$_3$SiH, the barium precatalyst [Ba{CH(SiMe$_3$)$_2$}$_2$·(thf)$_2$] was used to produce Ph$_3$SiN(Bn)SiPh$_2$NHBn by a smooth succession of quantitative and fully chemoselective NH/HSi dehydrocouplings between BnNH$_2$ and Ph$_3$SiH or Ph$_2$SiH$_2$ (20-60 °C, 0.25-1.0 mol% precatalyst, 1-2 h). Substrate scope was extended to other silanes, e.g. Ph$_2$(*p*-CF$_3$-C$_6$H$_4$)SiH, and to different amines, notably 2,4,6-Me$_3$-C$_6$H$_2$-CH$_2$NH$_2$ and 1,4-(CH$_2$NH$_2$)$_2$C$_6$H$_4$. Further attempts at chain extension by dehydrocoupling of Ph$_2$SiH$_2$ with Ph$_3$SiN(Bn)SiPh$_2$NHBn failed. It afforded instead the cyclic disilazane *c*-(Ph$_2$Si-NBn)$_2$ following a very unusual cyclisation process and concomitant elimination of C$_6$H$_6$; the gradual and quantitative formation of benzene could be

visualized by NMR spectroscopy. Identification of *c*-(Ph_2Si-$NBn)_2$ was confirmed by X-ray diffraction analysis (all synthetic intermediates were also analyzed by XRD and by NMR spectroscopy) and by independent barium-catalyzed dehydrocoupling of Ph_2SiH_2 with the diaminosilane $Ph_2Si(NHBn)_2$. The selective elimination of trifluoromethylbenzene was favored over that of benzene when Ph_2(*p*-CF_3-C_6H_4)SiH was used as the starting material hinted at a mechanism involving a silicate intermediate, where the negative charge was stabilized by the electron-withdrawing group in *para* position of the aromatic ring.

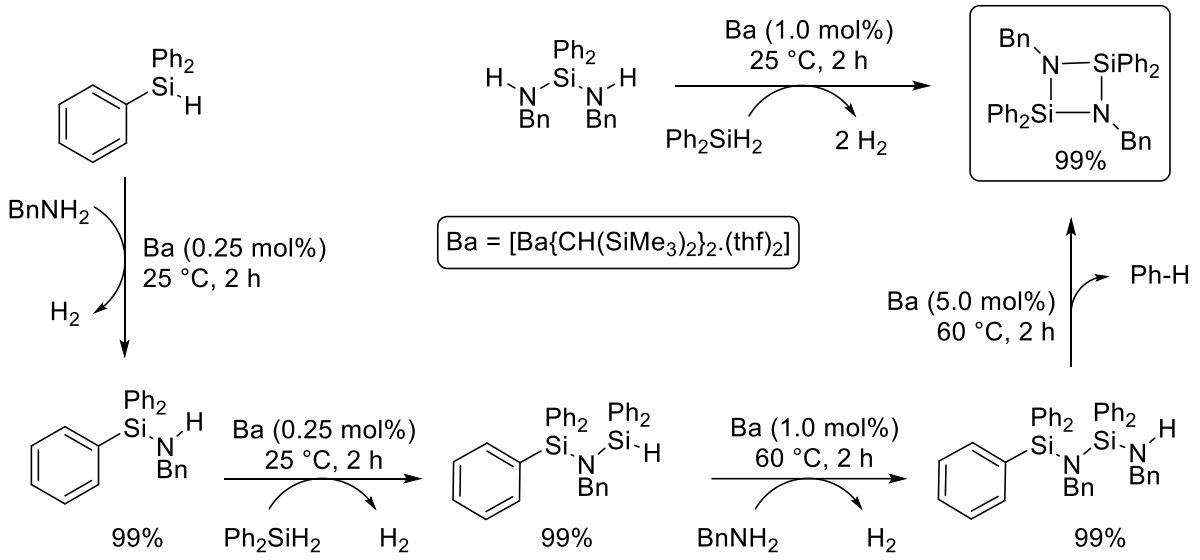

Figure 67. Barium-catalyzed synthesis of the cyclodisilazane *c*-(Ph_2Si-$NBn)_2$.

The pertaining mechanism for the cyclisation of $Ph_3SiN(Bn)SiPh_2NHBn$ under catalytic conditions was delineated by a comprehensive combination of experimental and DFT investigations. Stoichiometric treatment of $[Ba\{CH(SiMe_3)_2\}_2\cdot(thf)_2]$ with $Ph_3SiN(Bn)SiPh_2NHBn$ afforded the reactive $[Ba\{N(Bn)SiPh_2N(Bn)SiPh_3\}_2]$, which was authenticated by NMR in C_6D_6. From this point, in a stepwise process, intramolecular nucleophilic attack of the metal-bound *N*-amide atom onto the terminal silicon atom was proposed to generate a five-coordinate silicate (Figure 68). This step is followed by a rate-determining C_6H_5-transfer to barium, which assembles the cyclic product *c*-(Ph_2Si-$NBn)_2$ and produces a [Ba]–Ph intermediate. The catalytic manifold is completed by aminolysis of the transient barium to regenerate $[Ba]–N(Bn)SiPh_2N(Bn)SiPh_3$. DFT computations revealed that the irreversible production of *c*-(Ph_2Si-$NBn)_2$ through this stepwise pathway, traversing a pentavalent silicate transition state, was much more kinetically affordable ($\Delta G^{‡}$ = 26.2 kcal mol^{-1}) than an alternative, kinetically prohibited σ-metathesis pathway ($\Delta G^{‡}$ = 48.2 kcal mol^{-1}).

5.2.3 Catalyzed NH/HSi dehydropolymerizations

The well-understood barium dehydrocoupling precatalyst $[Ba\{CH(SiMe_3)_2\}_2\cdot(thf)_2]$ also proved very effective for the controlled production of polycarbosilazanes from difunctional amines and silanes.[180] The rapid and controlled syntheses of either linear or cyclic polymers by dehydropolymerization of *p*-xylylenediamine (1,4-$(CH_2NH_2)_2$-C_6H_4) and Ph_2SiH_2 were achieved within 10-60 min at 25-60 °C with 1 mol% precatalyst (Figure 69). The estimated molecular weights of the resulting polycarbosilazanes ranged between 1,000 and 10,000 g mol^{-1}, depending on the initial NH/HSi feed ratio. The

experimental number-average degree of polymerization agreed with its theoretical value calculated using Carothers' equation.[181] Analysis of these polymers by ^{1}H, ^{29}Si and ^{13}C NMR spectroscopy showed that exclusive formation of cyclic polymers was achieved during reactions performed with equimolar amounts of Ph_2SiH_2 and *p*-xylylenediamine, whereas linear materials were selectively obtained with excellent control of the chain-end when one of the comonomers was used in excess. The mechanism of the iterated catalytic event leading to the creation of multiple N-SI bonds along the macromolecules was inferred to be similar to that described for the coupling of amines with silanes (see Figure 66). However, it was not specified whether monomer diffusion and potentially impeded access to the metal center impacted the overall polymerization kinetics.

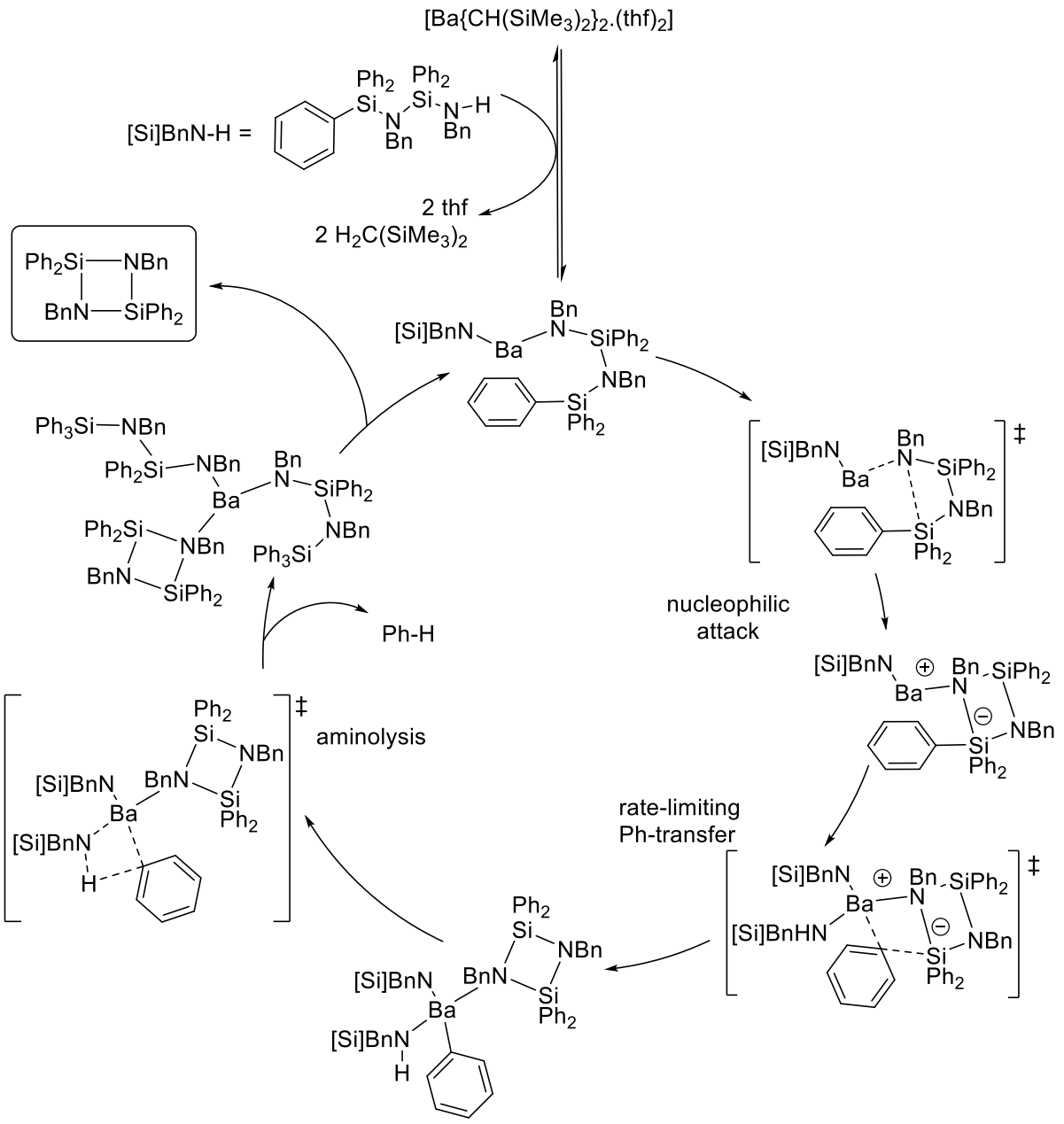

Figure 68. Proposed mechanism for the barium-catalyzed ring-closure of $Ph_3SiN(Bn)SiPh_2NHBn$.

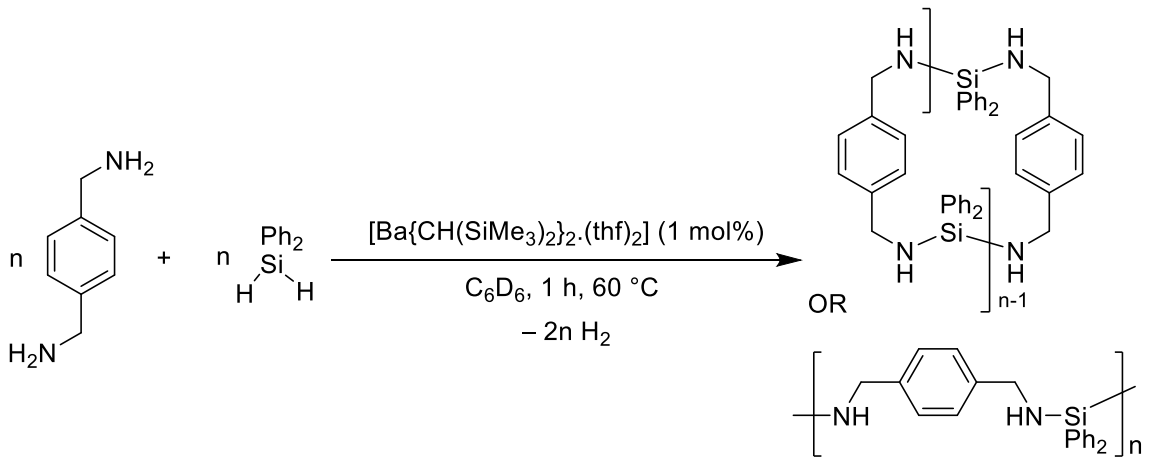

Figure 69. Barium-catalyzed dehydropolymerization of 1,4-$(CH_2NH_2)_2C_6H_4$ and Ph_2SiH_2, yielding cyclic or linear polycarbosilazanes.

In a further development, Hill and Manners used $[Ba\{N(SiMe_3)_2\}_2\cdot(thf)_2]$ to catalyze the synthesis of ferrocene-containing polycarbosilazanes.[182] The barium precursor catalyzed the coupling of the hydrosilane $[CpFe(CpSiPhH_2)]$ with 1,4-$(CH_2NH_2)_2C_6H_4$ to give polycarbosilazanes with dangling ferrocene groups (Figure 70). Well-defined polycarbosilazanes with ferrocene contained within the polymer backbone were prepared by dehydrocoupling of $[Fe(Cp(SiPhH_2))_2]$ and $[Fe(Cp(SiMe_2H))_2]$ with 1,4-$(H(Me)\text{-}NCH_2)_2C_6H_4$ and 1,4-$(CH_2NH_2)_2C_6H_4$, respectively. The materials were subjected to electrochemical studies and proved to be promising precursors to magnetic iron-containing ceramics. This dehydrocoupling strategy could also be applied to the synthesis of monomeric Fe-containing silanes with by mono- and decoupling $BnNH_2$, e.g. for the preparation of $[CpFe\{CpSiPhN(H)Bn\}_2]$ and related compounds.

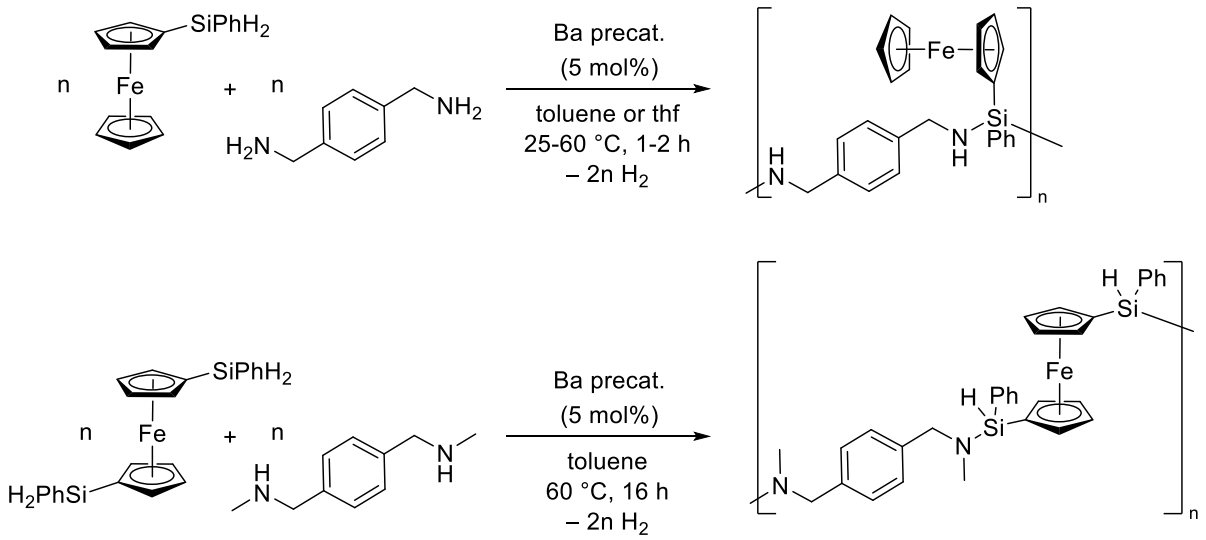

Figure 70. Barium-catalyzed syntheses of selected ferrocene-containing polycarbosilazanes by dehydrocoupling of amines and silanes.

5.3 Other alkaline-earth catalyzed heterodehydrocouplings

Beyond the dehydrocouplings of amine-boranes and amines with silanes, the two sets of reactions which have attracted the lion's share of the attention, alkaline-earth complexes have demonstrated their ability to catalyze several other heterodehydrocoupling reactions, displaying a unique combination of high selectivity and rates. The atom-efficient creation of Si-O bonds has been particularly scrutinized, as polysiloxanes are main materials, with the extremely robust Si-O-Si unit resulting in excellent thermal and chemical stability.

5.3.1 Dehydrocouplings of silanes and alcohols

The compounds [Ae{N(SiMe$_3$)$_2$}$_2$·(thf)$_2$] and [Ae{CH(SiMe$_3$)$_2$}$_2$·(thf)$_2$] (Ae=Ca, Sr, Ba) were found to be convenient precatalysts for the dehydrocoupling of silanes and alcohols (HexOH, ^{n}BuOH, ^{i}PrOH, ^{t}BuOH, DiPPOH, Ph$_3$COH; Figure 71).[183] Primary, secondary, and tertiary alcohols were efficiently coupled to PhSiH$_3$ or Ph$_2$SiH$_2$. The catalyzed reactions were typically performed in C$_6$D$_6$, using 0.5-5.0 mol% precatalyst in the temperature range 25-60 °C.

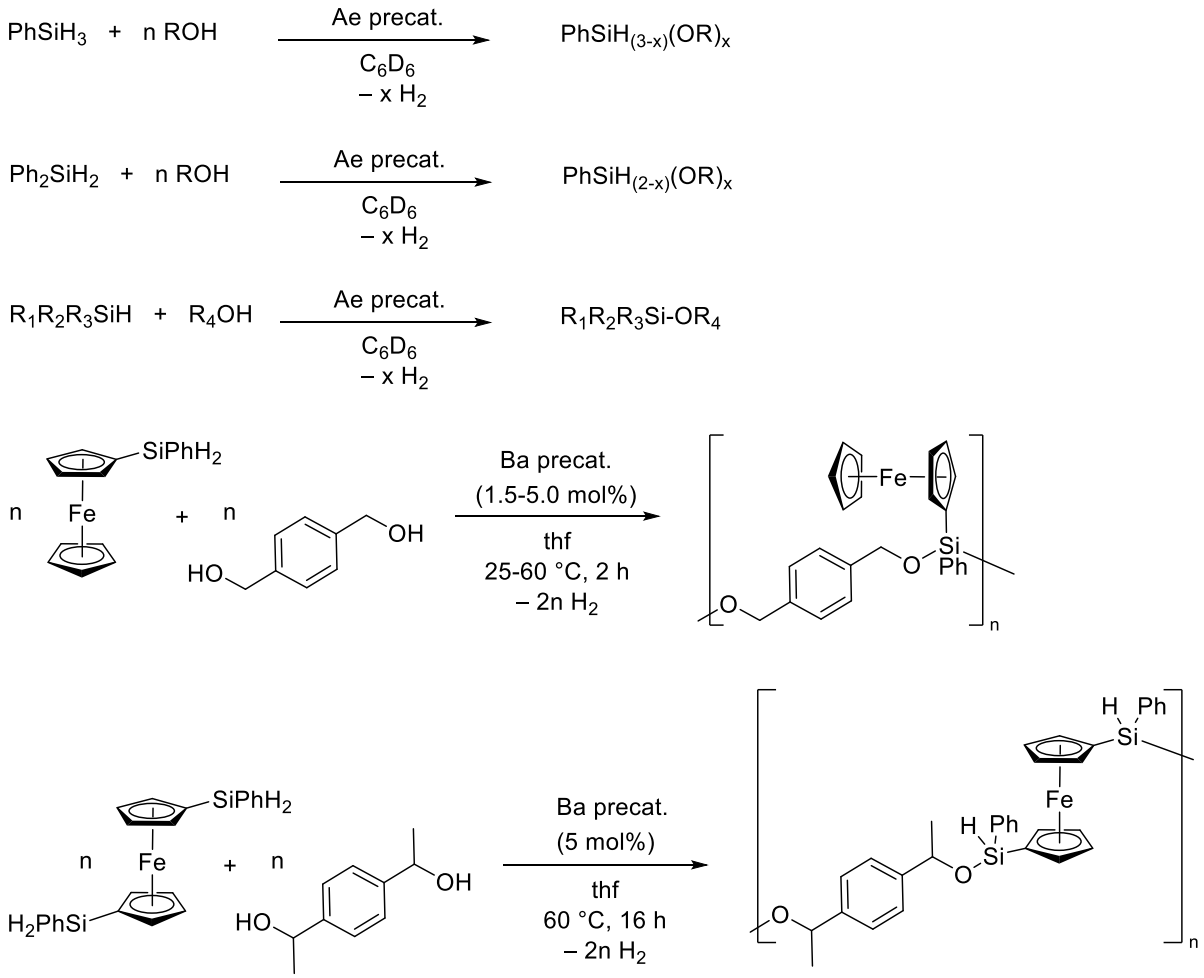

Figure 71. Alkaline-earth catalyzed dehydrocoupling of silanes and alcohols towards the synthesis of ferrocene-containing polysilylethers.

As commonly encountered for the coupling of amines and silanes,[175,176] turnover frequencies increased very substantially with metal size (Ca < Sr < Ba). Chemoselectivity enabled the construction of mono-, di- or tri-substituted silylethers, depending on reaction conditions. Tertiary silanes were less reactive, requiring barium precatalysts. The ferrocenylsilylether [CpFe($C_5H_4SiPh(OBn)_2$] was obtained upon coupling of ferrocenylsilane [CpFe($C_5H_4SiPhH_2$)] with benzyl alcohol. Stoichiometric experiments were consistent with the participation of Ae-alkoxide and Ae-hydride species to the reaction manifold. Mechanistic experiments suggested a complex manifold with dimeric or possibly polynuclear active species. Kinetics depended on the identities and concentrations of the precatalyst and of each substrate. In the coupling of ^{t}BuOH and $PhSiH_2$, [Ba{$N(SiMe_3)_2$}$_2$·$(thf)_2$] was found by kinetic analysis to display an apparent first-order dependence in both [silane] and [alcohol]. In a way recalling the syntheses of ferrocene-containing polycarbosilazanes,[182] barium catalysis allowed for the synthesis of poly- and oligosilylethers that contained ferrocenes either as dangling groups or within the main chain. The molecular weight of the macromolecules reached over 20,000 g mol^{-1}. Cyclic voltammetry investigations showed the iron centers displayed reversible redox behavior. Thermal analysis indicated these materials constituted viable precursors to magnetic ceramic materials.

5.3.2 Dehydrocouplings of silanes and borinic acids

The alkaline-earth boryloxides [Ae$(OBR_2)_2$·$(thf)_x$] and [Ae$N(SiMe_3)_2(OBR_2)$·$(thf)_x$] can be conveniently synthesized for Ae = Ca, Sr, Ba upon reaction of [Ae{$N(SiMe_3)_2$}$_2$·$(thf)_2$] and [Ae{$CH(SiMe_3)_2$}$_2$·$(thf)_2$] with borinic acids R_2BOH with appropriate adjustment of the stoichiometry.[184] The syntheses were limited to using boronic acids with sterically demanding substituents on the boron atom (e.g. R = $CH(SiMe_3)_3$, 2,4,6-$^{i}Pr_3$-C_6H_2, 2,4,6-$(CF_3)_3$-C_6H_2), presumably so that the metal center in these low coordinate Ae complexes is sufficiently shielded. The coupling of the hindered borinic acid {$(Me_3Si)_2CH$}$_2$BOH and silanes was competently catalyzed by the amides [Ae{$N(SiMe_3)_2$}$_2$·$(thf)_x$] (Ae = Ca, Sr, Ba; x = 0 or 2), or by the barium boryloxides [Ba$(OB\{CH(SiMe_3)_2\}_2)_2$·$(thf)_x$] with x = 0 (**86**, a two-coordinate monomer with loose intra- and intermolecular Ba···H-C interactions in the solid-state) or 2 (**87**), and by [Ba{μ-$N(SiMe_3)_2$}$(OB\{CH(SiMe_3)_2\}_2)]_2$ (**88**).[185,186] Catalysis occurred smoothly at 60 °C in C_6D_6, with 1-2 mol% precatalyst (Figure 72). For a homologous suite of precursors, reaction rates increased with metal size, Ca < Sr < Ba. Substrate scope could be extended to *para*-substituted phenylsilane, butylsilane and tris(isopropoxy)silane. However, no turnover occurred with Ph_2SiH_2 or with less encumbered borinic acids, thus limiting somewhat the scope of the reaction. The coupling of {2,4,6-$(CF_3)_3$-C_6H_2}$_2$BOH and (2,4,6-$^{i}Pr_3$-C_6H_2)$_2$BOH with $PhSiH_3$ using the most active barium precatalysts required more forcing conditions ($[SiH]_0/[BOH]_0/[Ba]_0$=10:10:1, 24 h, 60 °C), and only reached moderate conversions. Regardless of precatalyst selection, reaction conditions and initial borinic acid-to-silane ratio, excellent chemoselectivity towards the production of the secondary products $PhSi(H)_2OB\{CH(SiMe_3)_2\}_2$, $PhSi(H)_2OB$(2,4,6-$^{i}Pr_3$-C_6H_2)$_2$ and $PhSi(H)_2OB$\{2,4,6-$(CF_3)_3$-C_6H_2\}$_2$ was achieved, without detectable formation of tertiary or quaternary silanes. No conclusive explanation was provided to account for the greater reactivity of {$(Me_3Si)_2CH$}$_2$BOH with respect to (2,4,6-$^{i}Pr_3$-C_6H_2)$_2$BOH and {2,4,6-$(CF_3)_3$-C_6H_2}$_2$BOH. It was tentatively proposed to reflect greater nucleophilicity of the O atoms in {$(Me_3Si)_2CH$}$_2$BOH / {$(Me_3Si)_2CH$}$_2BO^-$ than in the aromatic substrates. Another possibility was that the boryloxides (2,4,6-$^{i}Pr_3$-C_6H_2)$_2BO^-$ and {2,4,6-$(CF_3)_3$-C_6H_2}$_2BO^-$ that were shown to induce multiple stabilizing Ba···F-C and Ba···C(π) secondary interactions in the molecular solid-state,[184] entailed the formation of barium species of limited reactivity in the reaction manifold.

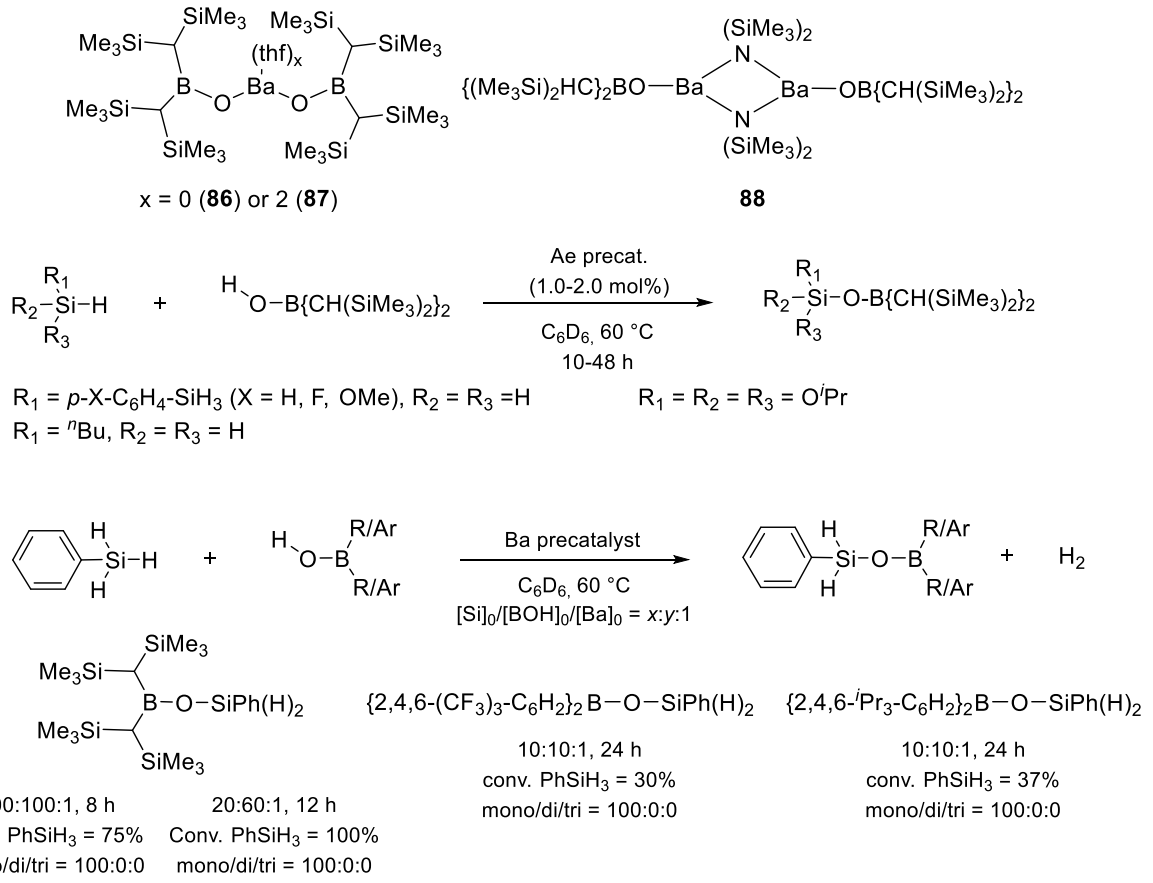

Figure 72. Alkaline-earth catalyzed dehydrocoupling of $PhSiH_3$ and borinic acids.

The barium-catalyzed coupling of $PhSiH_3$ with $\{(Me_3Si)_2CH\}_2BOH$ was kinetically investigated. The apparent rate constants measured in C_6D_6 for $[Ba\{N(SiMe_3)_2\}_2\cdot(thf)_2]$ **86**-**87** were commensurate, suggesting that a bis(boryloxide) was the likely active species in the catalytic cycle. Kinetic analysis for $[Ba\{N(SiMe_3)_2\}_2\cdot(thf)_2]$ and **88** provided the rate laws given in equations (7) and (8), respectively, showing zero-order dependence in [borinic acid] and first-order dependence in $[PhSiH_3]$.

$$\text{Rate} = k\,[Ba\{N(SiMe_3]_2\}_2\cdot(thf)_2]^2\,[\text{borinic acid}]^0\,[PhSiH_3]^1 \qquad (7)$$

$$\text{Rate} = k'\,[\mathbf{88}]^1\,[\text{borinic acid}]^0\,[PhSiH_3]^1 \qquad (8)$$

The unusual second-order in [precatalyst] for the monomeric $[Ba\{N(SiMe_3)_2\}_2\cdot(thf)_2]$ implicated dimerization of a metallic species to produce a bimetallic transition state in the rate-limiting step. This working hypothesis was corroborated by first-order dependence in [**88**], a precatalyst that exists as an amide-bridged dimer. It was also supported by an initial DFT study which showed that any Ba-amide or Ba-boryloxide precatalyst was very likely to eventually dimerize as $[Ba(OB\{CH(SiMe_3)_2\}_2)_2]_2$ (**86₂**) in the presence of excess borinic acid. Eyring analysis showed the reaction is kinetically facile, i.e. $\Delta G^{\ddagger}$ = 16.4(5) kcal mol^{-1} at 25 °C with the precatalyst $[Ba\{N(SiMe_3)_2\}_2\cdot(thf)_2]$. Hammett analysis showed the inclusion of electron-withdrawing groups in *para*-substituted arylsilanes *p*-X-C_6H_4-SiH_3 in the coupling with $\{(Me_3Si)_2CH\}_2BOH$ catalyzed by $[Ba\{N(SiMe_3)_2\}_2\cdot(thf)_x]$ was beneficial to reaction rates (ρ = 2.03(9)), consistent with a mechanism involving the accumulation of a negative charge on the silicon atom in the turnover-limiting step. The prevailing mechanism for barium catalysis was determined by

DFT calculations. Complex **86₂** was referred to as the zero-point energy for the mechanistic pathway depicted in Figure 73. The proposed catalytic cycle starts with the nucleophilic attack of one of the oxygen atoms of on $PhSiH_3$. The resulting intermediate presents a negatively charged pentasilicate and evolves readily to a more stable intermediate through replacement of the bridging oxygen with the Si-H moiety. This step is required to facilitate the following H-transfer affording a bridged Ba-hydride with release of $PhSi(H)_2OB\{CH(SiMe_3)_2\}_2$. Protonolysis of the Ba-hydride intermediate with an additional $\{(Me_3Si)_2CH\}_2BOH$ that coordinates to barium promotes the release of H_2 and regenerates the dimeric catalyst. Overall, the proposed dominant stepwise pathway was found to be kinetically ruled by the initial nucleophilic attack of barium boryloxide onto the incoming silane, and was in full agreement with all experimental observations.

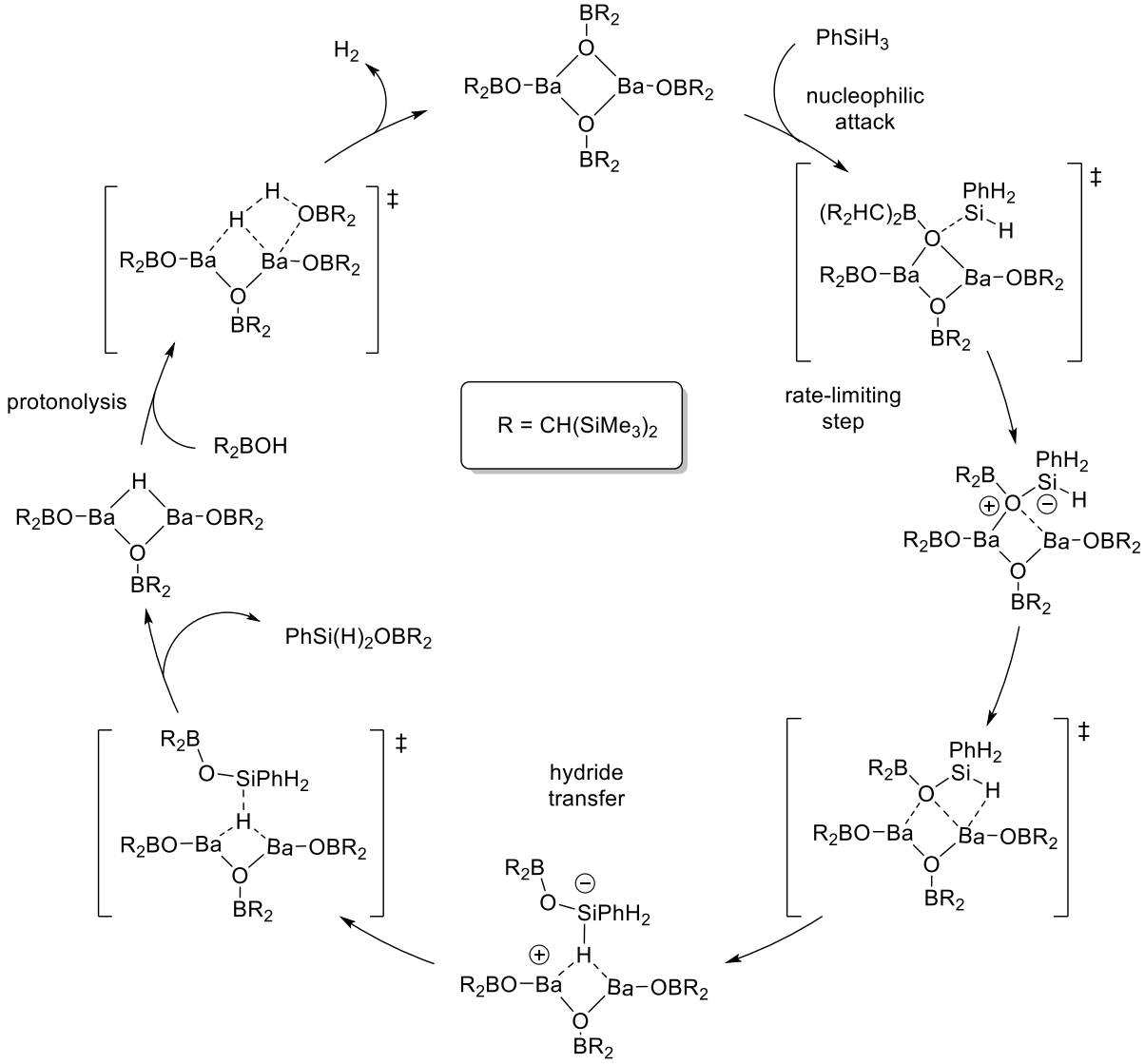

Figure 73. Mechanistic pathway for the barium-catalyzed coupling of $\{(Me_3Si)_2CH\}_2BOH$ with $PhSiH_3$.

5.3.3 Dehydrocouplings of silanes and silanols

Metal-based catalysts, and *a fortiori* alkaline-earth ones, have seldom been implemented in the controlled production of siloxanes, despite the commercial importance of oligo- and polysiloxanes.

Asymmetric R_3Si-O-SiR'_3 siloxanes can be prepared by conventional condensations involving a silanol (with a base) or a metal silanolate and a halosilane R_3SiX, but these protocols have low atom efficiency, often generating large amounts of by-products. The homoleptic barium amide $[Ba\{N(SiMe_3)_2\}_2]_2$ and the well-defined dimeric siloxides $[Ba_2\{\mu\text{-}OSi(SiMe_3)_3\}_3\{OSi(SiMe_3)_3\}]$ (**89**) and $[Ba\{\mu\text{-}OSi(SiMe_3)_3\}\{N(SiMe_3)_2\}]_2$ (**90**) were shown to promote the formation of asymmetric siloxanes R_3Si-O-SiR'_3 through the first reported case of main group metal-mediated, atom-efficient dehydrocoupling of silanols and hydrosilanes (Figure 74).[187] The formation of $Ph_2(H)SiOSi(SiMe_3)$ upon coupling of Ph_2SiH_2 with $(Me_3Si)_3SiOH$ took place within 4 h with 2 mol% precatalyst in C_6D_6, generally at 30 °C. $PhSiH_3$ was dehydrocoupled with similar efficacy to $^tBu_3SiOH$ to return $PhSi(H)_2OSitBu_3$. The coupling of (p-X-C_6H_4)SiH_3 (X = MeO, Me, H, F) with $(Me_3Si)_3SiOH$ was quantitative and chemoselective; traces of (p-X-C_6H_4)$H_{3-n}Si\{OSi(SiMe_3)_3\}_n$ (n = 2 or 3) could not be detected. In addition, when using $PhSiH_3$, the mono-coupled $Ph(H)_2SiOSi(SiMe_3)_3$ was still the only product regardless of reaction conditions and substrate ratio. The reactivity of the hydrosilanes overall decreased with increasing substitution: $ArSiH_3 > Ar_2SiH_2 > {}^nBuSiH_3 >> Ar_3SiH$, Et_2SiH_2, Et_3SiH. Couplings with Ph_3SiOH were more sluggish and less selective than those starting from $(Me_3Si)_3SiOH$ and $^tBu_3SiOH$.

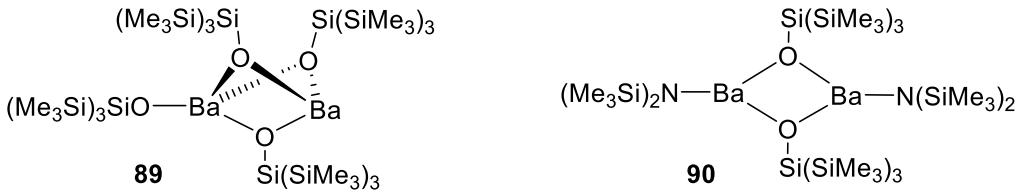

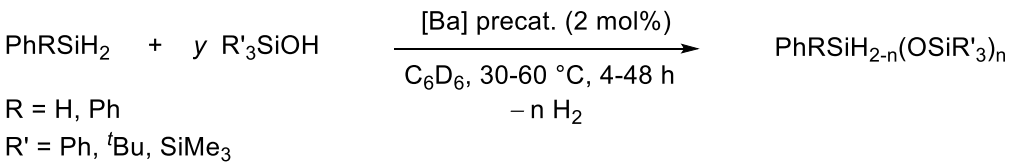

Figure 74. Barium-catalyzed dehydrocoupling of silanols and silane towards the formation of asymmetric siloxanes.

All homoleptic Ae-amides $[Ae\{N(SiMe_3)_2\}_2]_2$ were found to catalyze the benchmark coupling of Ph_2SiH_2 and $(Me_3Si)_3SiOH$, and kinetic analysis indicated that the rates increased when descending group 2, Ca < Sr < Ba. The reaction kinetics were zero-order in $[(Me_3Si)_3SiOH]$ and first-order in $[Ph_2SiH_2]$ The dependence in [catalyst] could not be ascertained, likely due to catalyst inhibition by the silanol. Hammett analysis showed that the rates increased with electron-withdrawing groups in *para* position of the aryl-substituted (p-X-C_6H_4)SiH_3 (X = MeO < Me < H < F). The available kinetic data agreed with a mechanism involving nucleophilic attack of the Ba-bound *O*-siloxide atom onto the hydrosilane in a scenario recalling that seen in the barium-catalyzed formation of silazanes[175,176] and borasiloxanes,[185,186] but no reaction manifold was conjectured in the absence of supporting computational analysis.

5.3.4 Dehydrogenative silylation of activated C-H bonds

Alkynylsilanes can be synthesized by stoichiometric reactions between metal alkynides and chlorosilanes. However, an atom-efficient halogen-free and metal-poor route is more desirable. The

Harder group showed the dehydrogenative silylation of 1-hexyne with Ph_3SiH was catalyzed by the azametallacyclopropane [Ca(η²-Ph_2CNPh)(hmpa)] (**84**).[173] The product ^{n}Bu-C≡C-$SiPh_3$ could be isolated in yields over 80% after 17 h (thf, 20 °C). However, despite quantitative conversions, the coupling with secondary silane $PhMeSiH_2$ systematically returned a mixture of mono- and dialkynated silanes, that is, ^{n}Bu-C≡C-Si(H)PhMe and (^{n}Bu-C≡C)$_2$SiPhMe, respectively.

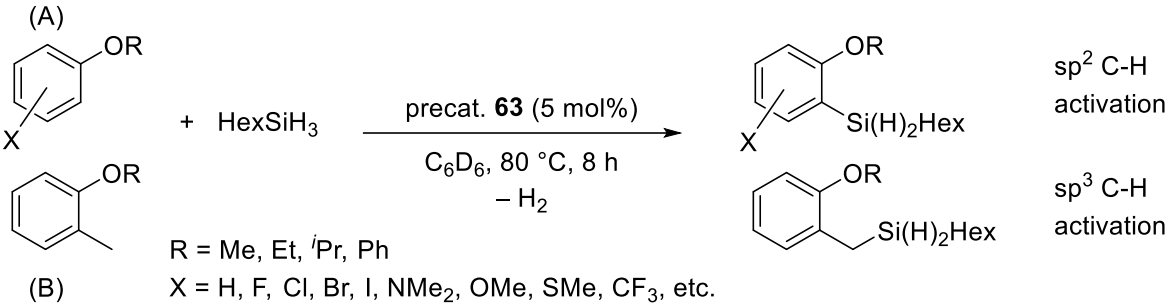

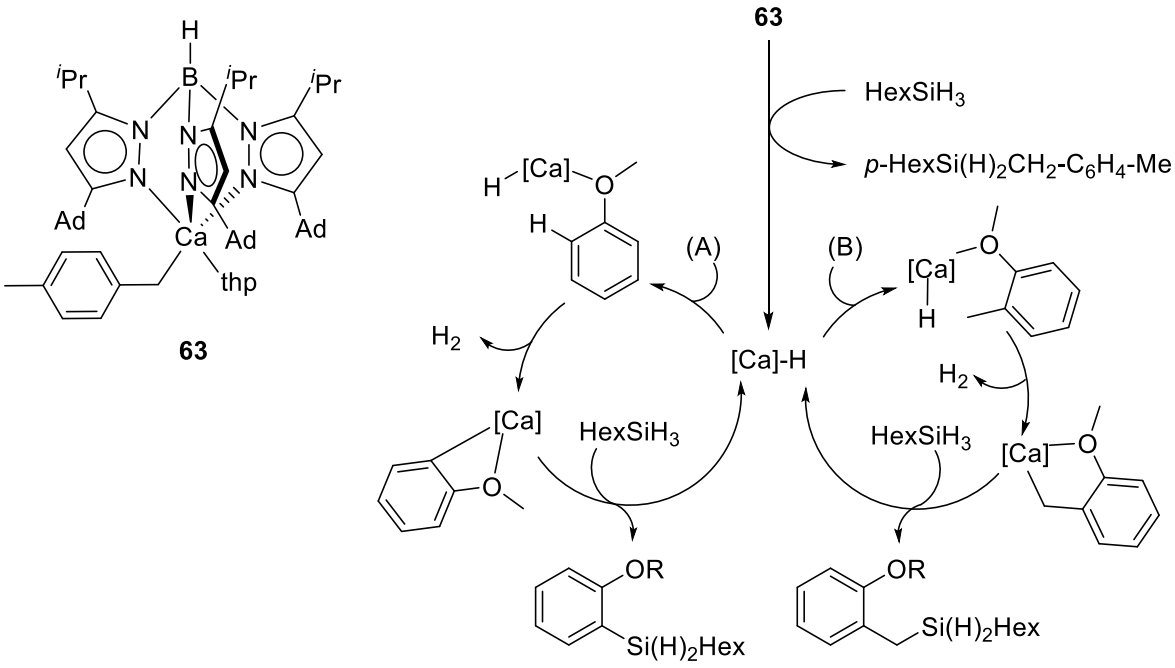

Figure 75. Calcium-catalyzed dehydrogenative C−H silylation of substituted anisoles.

Cheng and co-workers have confirmed the calcium-catalyzed regioselective C−H silylation of a wide range of alkoxy-substituted benzene derivatives (e.g. anisoles, Figure 75) with primary hydrosilanes.[188] This dehydrogenative, atom-efficient process affords silyl-substituted aromatic ethers without recourse of a hydrogen acceptor. The reactions were mediated by the calcium benzyl [($Tp^{Ad,iPr}$)Ca(*p*-$CH_2C_6H_4Me$)·(thp)] (**63**; $Tp^{Ad,iPr}$ = hydrotris(3-adamantyl-5-isopropylpyrazolyl)borate). Good functional group tolerance was evidenced through detailed examination of the substrate scope. The silylation of anisole derivatives without *ortho*-substituent exclusively occurred at the *ortho*-sp² C-H bond, yielding the pertaining *ortho*-silylated anisoles. With 2-methylanisole, silylation occurred solely on one of the benzylic sp³ C-H bonds. The products of di- or tricoupling at silicon were not detected. Complexes such as the isolated and structurally characterized [($Tp^{Ad,iPr}$)Ca(*o*-MeO-*m*-Br-C_6H_3)] and [($Tp^{Ad,iPr}$)Ca(*o*-Me-$OCH_2C_6H_4$)] were proposed as likely intermediates in the catalytic

manifold. The catalytic silylation of *o*-deuterated 4-methyl-anisole with $HexSiH_3$ indicated a strong kinetic isotope effect (k_H/k_D = 2.45), suggesting C-H bond breaking occurred in the rate-limiting step. A path involving pre-coordination of the anisole onto the known calcium hydride [($Tp^{Ad,iPr}$)CaH·(thp)] was hypothesized, but it was not supported by further experimental of theoretical data.

6 Miscellaneous Ae-catalyzed reactions with reactive [Ae]-X (pre)catalysts

A number of pertinent alkaline-earth catalyzed reactions that are mechanistically different from those described in the preceding sections have been reported. These are collated here and discussed in the light of the available mechanistic information, where possible in link with related Ae-mediated catalyzed elementary steps or more complex processes.

6.1 Dimerization of aldehydes – Tishchenko reaction

Hill and co-workers reported in 2007 on the alkaline-earth catalyzed Tishchenko reaction, i.e. the dimerization of aromatic and aliphatic aldehydes into the corresponding carboxylic esters (Figure 76).[189] Catalyst activity decreased with increasing metal size in the series $[Ae\{N(SiMe_3)_2\}_2]_2$ (Ba < Sr < Ca), with calcium providing the highest turnovers (1-5 mol% precatalyst, C_6D_6, 20 °C). The catalyzed process involved hydride transfer between two molecules of the substrate. The quenching of the dimerization with benzaldehyde in its early stage indicated the formation of a calcium-alkoxide intermediate, assumed to be generated through Meerwein-Ponndorf-Verley reduction of the aldehyde along with concomitant release of a stochiometric equivalent of benzamide. Once formed, the Ae-alkoxide was thought to react with a second aldehyde via insertion into the Ae-O bond, thus generating a metallated acetal derivative. This intermediate further reacted with an additional molecule of aldehyde in six-center concerted step to produce the final ester product and regenerate the Ae-alkoxide active species.

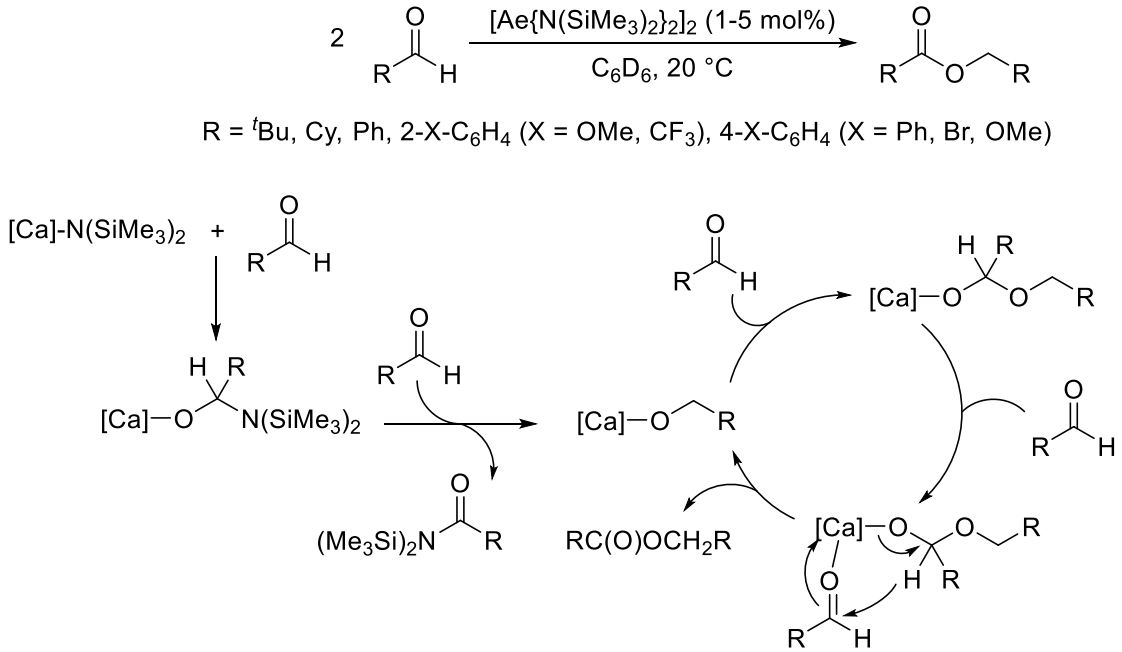

Figure 76. Alkaline-earth catalyzed Tishchenko dimerization of aldehydes, with proposed mechanism.

6.2 Trimerization of isocyanates

The Harder group demonstrated that the congested calcium methanediide **91** catalyzed the cyclotrimerization of isocyanates to isocyanurates (Figure 77).[190] The conversion of phenyl isocyanate was facile (1 mol% precatalyst, 3 h at 20 °C in thf-d_8) although the reaction was very sluggish for cyclohexyl isocyanate (5 mol% precatalyst, 50 °C, one week). The poor reactivity of the latter substrate allowed for the isolation of the double insertion product **92**, which was not stable in solution. It instead decomposed to give the mono insertion product and release an equivalent of cyclohexyl isocyanate, which was then found to trimerize to the isocyanurate.

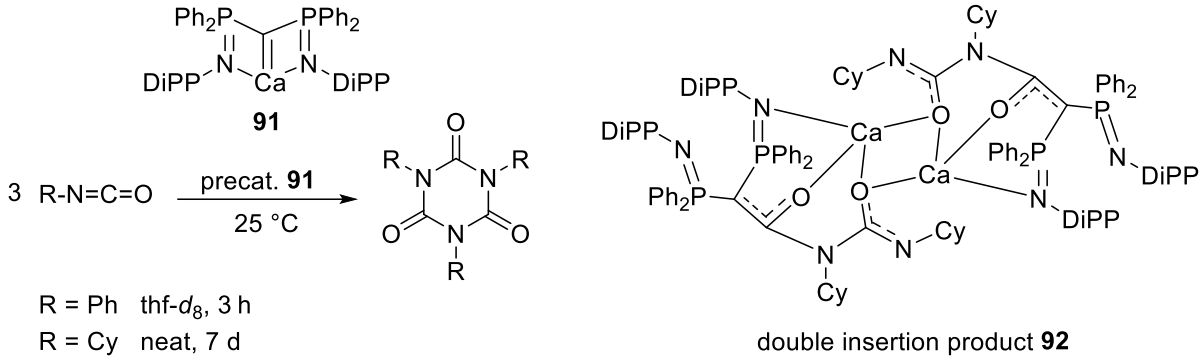

Figure 77. Calcium-catalyzed trimerization of isocyanates.

6.3 Alkylation reactions

6.3.1 *Dimerization of terminal alkynes*

Further elaborating on their initial observation that a side-on (π-type) electrostatic interaction in asymmetric β-diketiminato calcium-acetylide dimers allowed for an effective dissipation of negative charge over both acetylide carbon centers,[191] Hill revealed that the precursors [Ae{E(SiMe$_3$)$_2$}$_2$·(thf)$_2$] (Ae = Ca, Sr; E = N, CH) and complexes **1** and **3** mediated the head-to-head dimerization of ether-functionalized terminal alkynes.[192,193] Reactions were limited to a single turnover with the homoleptic complexes, but the heteroleptic **1** and **3** enabled for catalytic dimerization (5 mol% precatalyst in toluene/thf mixtures, 48-72 h at 100 °C). Propargyl ethers and amines were dimerized to a mixture of *E* and *Z* isomers of 2,3,4-hexatriene (Figure 78). By contrast, for aryl- and silyl-substituted acetylenes, mixtures of the thermodynamically favored (*E*) and (*Z*)-enynes were obtained, although the reactions required more drastic conditions. For ether- or amine-functionalized acetylenes, the selectivity towards the hexatrienes was imputed to the presence of the donor group. Coordination of the heteroatom to the metal center reduced repulsion between the two α-carbanions, and encouraged an intramolecular proton transfer from the propargylic carbon atom to the hexatriene with concomitant intermolecular deprotonation of two O-coordinated acetylenic substrates. This concerted process was corroborated by experiments run with deuterated acetylenes, where deuterium transfer to the terminal methylene unit in the product was detected (Figure 78).

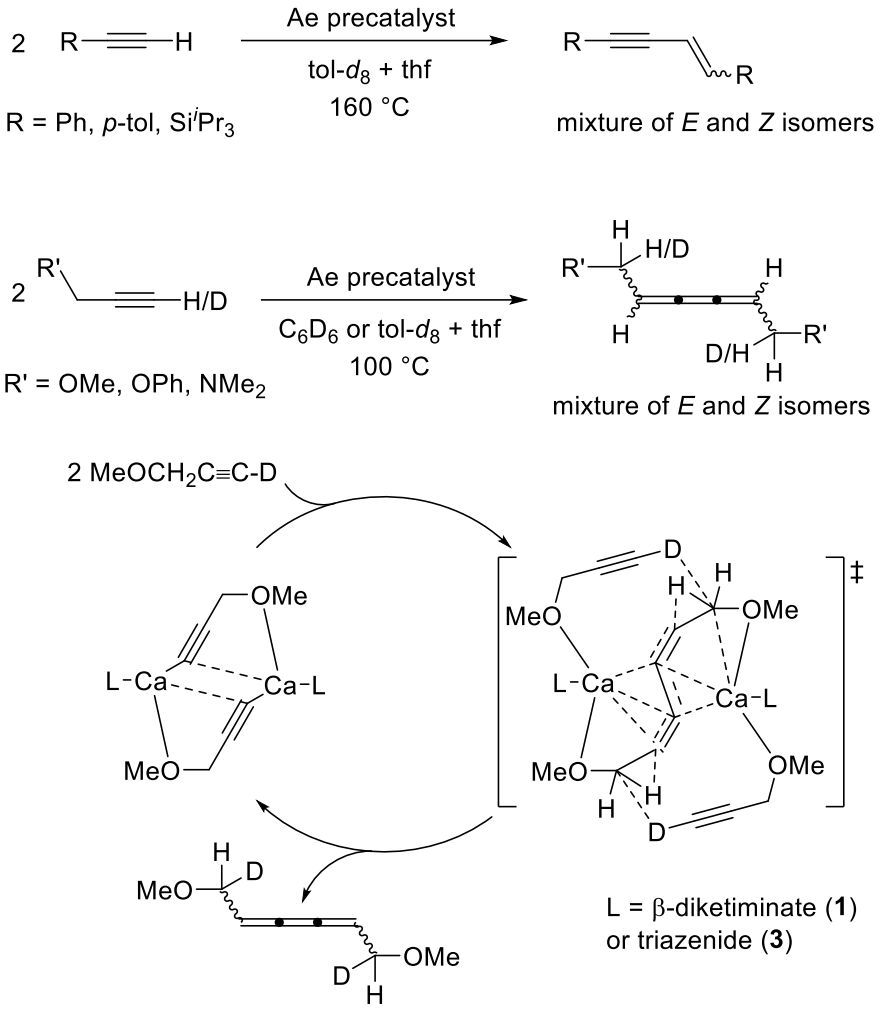

Figure 78. Alkaline-earth catalyzed dimerization of donor-functionalized terminal alkynes.

6.3.2 *Alkylation of aromatic rings*

In a groundbreaking contribution, the Hill group demonstrated that the unsolvated dimeric calcium-hydride [{BDI^{DiPP}}Ca(μ-H)]$_2$ (**58**) reacted at 25 °C with n-alkenes to generate well-defined calcium alkyls.[18] These complexes further reacted quantitatively at 60 °C with protio or deuterio benzene through nucleophilic substitution of an aromatic C–D/H bond to give the n-alkyl benzenes (e.g. ethyl-, ^{n}butyl- and ^{n}hexylbenzene) and return a calcium deuteride dimer (Figure 79). A single alkylation of the aromatic ring was observed, while a second alkylation step giving di(n-alkyl) benzene derivatives was not mentioned. Alkylation of n-alkyl benzene is almost certainly kinetically prohibited with respect to benzene, due to the presence of the n-alkyl substituent that will disfavor nucleophilic substitution through destabilization of the corresponding Meisenheimer intermediate. Density functional theory calculations highlighted a Meisenheimer complex in the C–H activation transition state. Although the process was essentially stoichiometric, regeneration of the starting **58** upon release of the n-alkyl benzenes suggested that it held the potential to be transformed into a catalytic reaction in the presence of excess n-alkenes. In a further development, Harder later showed that the same reactivity could be extended to the solvent-free strontium hydride [{BDI^{DiPeP}}Sr(μ-H)]$_2$ (**93**), using the highly congested β-diketiminato ligand {BDI^{DiPeP}}, where DiPeP is the particularly bulky 2,6-diisopentylphenyl substituent.[194]

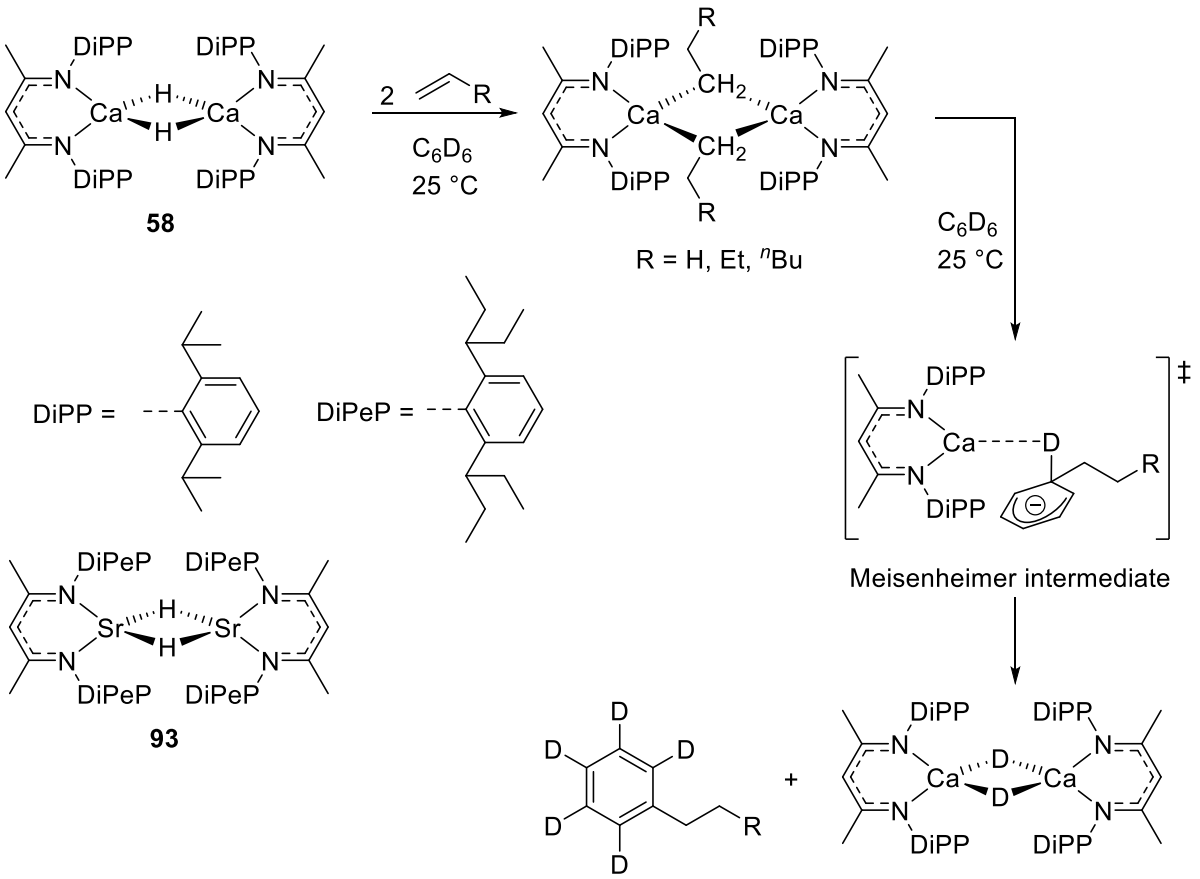

Figure 79. Formation of n-alkyl benzenes by reaction of a calcium/strontium n-alkyls and benzene. The product is formed by nucleophilic substitution traversing a Meisenheimer intermediate.

6.3.3 *Alkylation of alkylpyridines*

The dinuclear calcium hydride **45** was shown to react with 2,6-lutidine in thf to yield the calcium alkyl **94** through selective dehydrogenative C-H activation (Figure 80).[195] The observed stoichiometric benzylic C-H activation was elaborated into a catalytic functionalization of 2,6-lutidine and other 2,6-disubstituted pyridine derivatives. Coupling with vinylarenes, conjugated dienes and non-activated alkenes (including internal ones, e.g. norbornene) catalyzed by **45** took place to create C-C bonds and afford alkylated pyridines. Although the reactions required forcing conditions (5 mol% precatalyst **4**, 120 °C in toluene, 12-72 h), good selectivity was observed, and the products of double benzylic alkylation were not detected. Reaction with ethyl-substituted pyridines showed that alkylation selectively occurred once in α position. Hammett analysis confirmed that reaction rates increased significantly with electron-withdrawing groups in *para* position of substituted styrene (ρ = 4.53). Complex **94** displayed the same overall catalytic performance as **45**, showing that it was a likely intermediate in the corresponding catalytic cycle. A strong kinetic isotope effect was observed when 2,6-$(CD_3)_2$-pyridine was employed (k_H/k_D = 4.96), hinting that C-H bond activation was a key component in the rate-determining step. A mechanism was proposed, where insertion of the C=C unsaturation into the Ca−C bond of **94** was thought to assemble into a metallacycle. This intermediate is protonolyzed with another 2,6-lutidine molecule to form the alkylation product and regenerate the catalyst. For aromatic olefins, 2,1-insertion was assumed to stabilize of the calcium center through

favorable Ca···C(π) interactions, affording the linear *anti*-Markovnikov alkylation product. Conversely, 1,2-insertion forming the branched Markovnikov products was said to be preferred for aliphatic olefins in order to minimize steric repulsion with the metal.

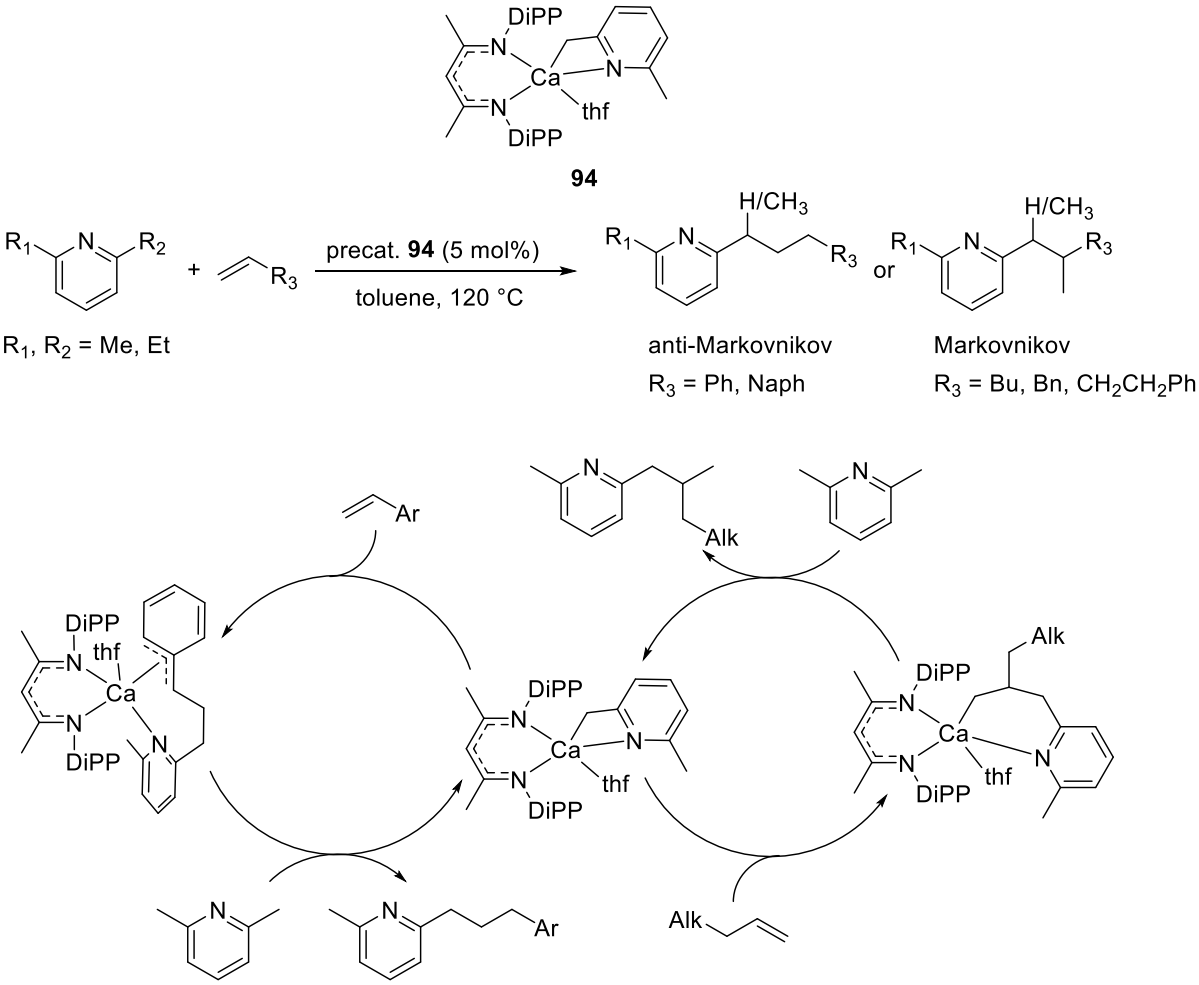

Figure 80. Calcium-catalyzed alkylation of 2,6-lutidine with alkenes, with the proposed mechanism.

6.4 Catalyzed H/D exchange

Deuterium or tritium-labeled compounds find widespread use throughout many scientific disciplines, though are primarily used for NMR spectroscopy, kinetic studies and as molecular markers in chemistry, biology and physics.[196,197] The development of high-performance mass-spectrometry (MS) and liquid chromatography-mass spectrometry (LC-MS) techniques has further increased demand for deuterated molecules. The introduction of deuterium into organic molecules is generally achieved in two ways. The first, classical synthesis from commercially available deuterated compounds can be synthetically challenging, as well as time- and resource-consuming. The second, hydrogen-deuterium exchange/hydrogen-isotope exchange (HIE), is normally carried out directly on the non-deuterated target molecule, potentially saving considerable time and effort from a synthetic standpoint, as well as significantly increasing atom efficiency. Traditional catalytic approaches to HIE have required transition metal catalysts, often based on precious metals, and require harsh reaction conditions that often give poor selectivity.[198] Recently, a range of direct HIE reactions using alkaline-earth hydrides have been reported for the aryl and alkyl substrates.

In 2017, the HIE between the calcium hydride $[(Me_4TACD)_2Ca_2(\mu\text{-}H)_2][B(C_6H_4\text{-}4\text{-}^tBu)_4]_2$ (**60**) and D_2 was described, catalytically generating HD from an equal molar mixture of H_2 and D_2.[139] The reaction reached the equilibrium point within 5 minutes at 25 °C with a 5% molar loading of **60**. Alternatively, when **60** was treated with pure HD under the same conditions, statistical amounts of H_2 and D_2 were observable by NMR spectroscopy. The HIE of the strontium hydride $[(Me_3TACD)_3Sr_3H_2][SiPh_3]$ (**95**) with D_2 was also reported.[199] Treatment of **95** with D_2 generated the deuterated derivative **95**-D_2. The HIE was proposed to proceed via a multi-step mechanism involving a hypervalent silicate (Figure 81), in which the cation initially reacts with D_2 to generate an unstable neutral strontium hydride/deuteride and $DSiPh_3$. The unstable intermediate subsequently rearranges via hydride/deuteride transfer to generate another cationic hydride cluster with a hypervalent silicate counterion. This species is also unstable, and undergoes reductive elimination to either generate a benzene species PhH_XD_{1-X} or hydrogen species H_XD_{2-X} and the corresponding cationic Sr cluster. This process continues, to generate the cation $[(Me_3TACD)_3SrD_2]^+$ and various phenylsilanide anions. The proposed mechanism was supported by attached DFT calculations.

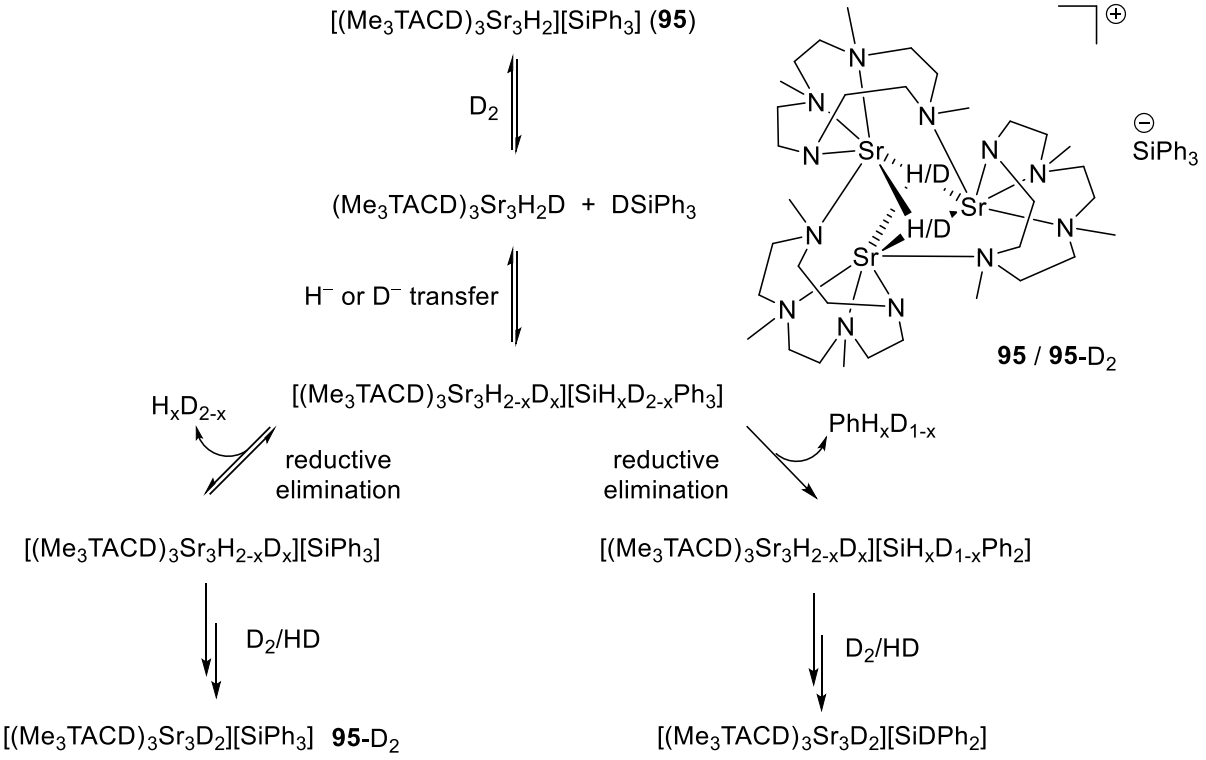

Figure 81. Proposed mechanism for deuteration and anion degradation of $[(Me_3TACD)_3Sr_3H_2][SiPh_3]$ in the presence of H_2/D_2.

HIE between the strontium hydride complex $[\{BDI^{DiPeP}\}Sr(\mu\text{-}H)]_2$ (**93**) and deuterated benzene upon heating to 60 °C was also demonstrated (Figure 82).[194] When the same complex was exposed to D_2 (1.5 bar), the deuterated compound **93**-D_2 and HD were generated within 2 hours at 20 °C, with no evidence of complex decomposition. Indeed, when **93** was used catalytically (5 mol%, 60 °C, 1.5 bar D_2) in benzene, benzene was converted to C_6H_5D with a 12% yield after 5 days. This assumed only mono-deuteration took place, a hypothesis made as distinguishing C_6H_5D from other deuterated benzenes by ^2H NMR spectroscopy proved difficult. The mechanism for the exchange was suggested

to occur via nucleophilic aromatic substitution between an activated benzene molecule and the hydride complex, generating a Meisenheimer-type cyclohexadienyl anion (Figure 82).

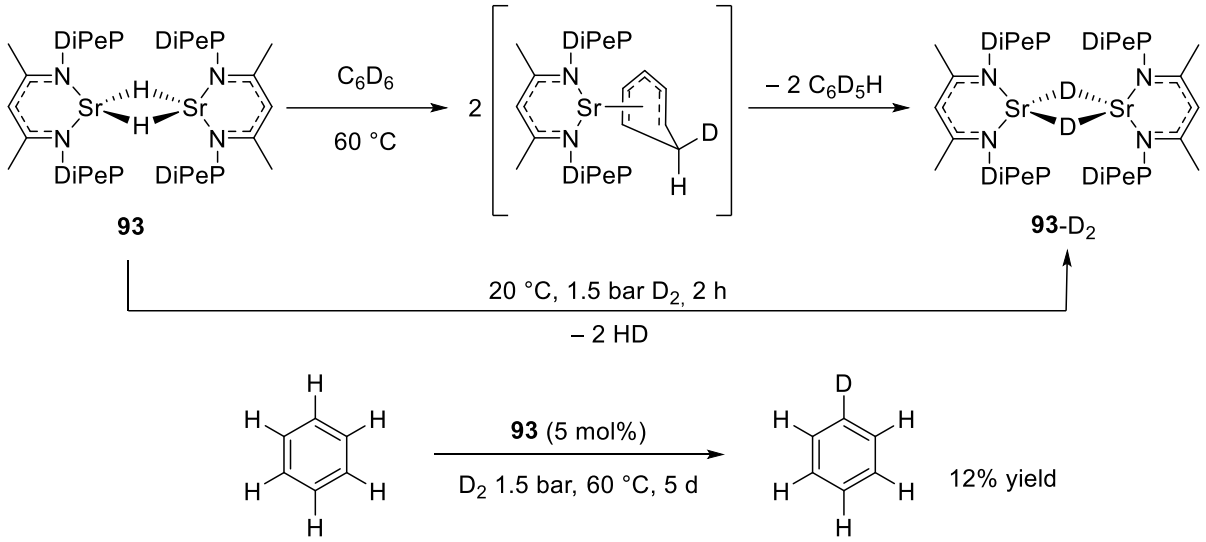

Figure 82. Hydrogen-isotope exchange reactions with the strontium hydride [{BDI^{DiPeP}}Sr(μ-H)]$_2$ (**93**). DiPeP = 2,6-diisopentylphenyl.

Harder extended this work in 2020, reporting the catalytic HIE of a range of aromatic complexes using the homoleptic alkaline earth amide complexes [Ae{N(SiMe$_3$)$_2$}$_2$]$_2$, [Ae{N(Si^{i}Pr$_3$)$_2$}$_2$] (**67**-**69**) and [Ae{N(Si^{i}Pr$_3$)(DiPP)}$_2$] (**70**-**72**) as (pre)catalysts (Figure 83).[200] reaction rates increased according to Ca < Sr < Ba, an observation rationalized by the greater ionic character and weaker Ae-N bonding in the heavier Ae complexes. The catalytic activity of [Ba{N(Si^{i}Pr$_3$)$_2$}$_2$] (**69**) was also superior to that of [Ba{N(Si^{i}Pr$_3$)(DiPP)}$_2$] (**72**) and [Ba{N(SiMe$_3$)$_2$}$_2$]$_2$, which was ascribed to the increased steric bulk of the {N(Si^{i}Pr$_3$)$_2$}$^-$ ligand, thus generating smaller and more active aggregates of the presumed true catalytic species [{Si^{i}Pr$_3$)$_2$N}Ba(H)]. The chosen deuterium source for the catalysis was C$_6$D$_6$, to allow for *in situ* reaction monitoring. The conditions for the HIE were found to be extremely important, as under more harsh conditions (140 °C, 50 bar H$_2$), the most active (pre)catalyst, **69**, would hydrogenate the solvent to cyclohexane.

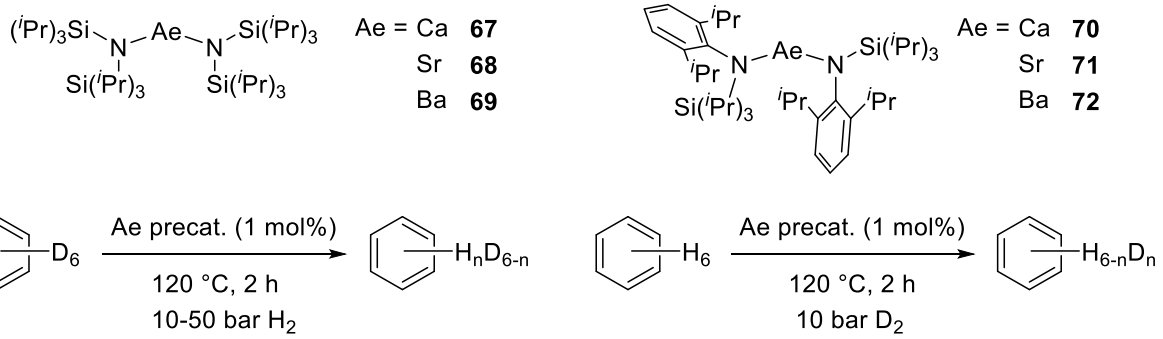

Figure 83. Hydrogen-isotope exchange between protio or deuterio benzene with H$_2$ or D$_2$ using alkaline-earth amide precatalysts

The reverse reaction, where D$_2$ is used as the deuterium source and benzene as the reaction solvent, occurs 1.5-2 times faster, due to the kinetic isotope effect. The extent of deuterium incorporation was

investigated for a range of substituted arenes. Alkyl substituted benzene gave moderate substitutions for hydrogens on the α-carbon (up to 42% for ethylbenzene), but no substitution of β-hydrogens. Interestingly, under longer reaction times, the initially high α-D content in alkylbenzenes decreases, while the overall percentage of deuteration of the molecule increases. Precatalyst **69** could not facilitate the HIE with unactivated (sp^3)-C-H bonds, however it could achieve the HIE of a range of (sp^3)-Si-H bonds with D_2. DFT calculations indicated a nucleophilic aromatic substitution mechanism via a Meisenheimer anion was favorable over a deprotonation/protonation mechanism. This analysis was substantiated by experimental evidence, in particular as a deprotonation/protonation mechanism would be expected to generate HD; yet, this gaseous co-product that was not detected when deuterated benzene was used as the deuterium source in reactions without H_2.

A similar HIE exchange was reported with the solvent-free calcium hydride [{BDI^{DiPP}}Ca(μ-H)]$_2$ (**58**).[201] In an attempt to replicate the HIE reaction reported in Figure 82, a solution of **58** in C_6D_6 was heated to 60 °C for 12 hours (Figure 84). ^{1}H NMR analysis of the resulting suspension only had identifiable [Ca{BDI^{DiPP}}$_2$] resonances, indicating kinetic ligand redistribution. Instead, after keeping a solution of **58** for 21 days at room temperature, a new unresolved set of {BDI^{DiPP}}$^-$ resonances grew in at the expense of the starting material, while the hydride signal broadened into an unresolved 1:2:1 triplet. This was attributed to deuterium incorporation generating the previously reported **58**-D_1.[18] The observed reactivity was not elaborated into a given catalytic process.

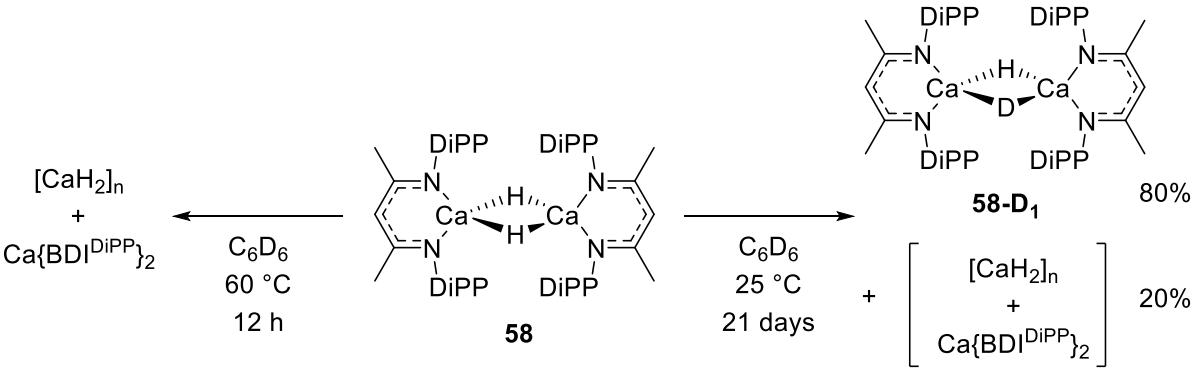

Figure 84. Decomposition and deuteration reactions for [{BDI^{DiPP}}Ca(μ-H)]$_2$ (**58**).

6.5 Polymerization of ethylene

Like most main group elements, Ziegler-Natta polymerization of α-olefins is certainly a field where alkaline-earth metals have not (yet?) been efficient. Alkaline-earth complexes have been found to catalyze the polymerization of styrenes, as hinted at elsewhere in this chapter. However, with α-olefins, they do not display equal proficiency as other oxophilic metals such as lanthanides and group 4 transition metals, and also do not compete with the more functional group-tolerant late transition metals (e.g. Ni, Pd). Yet, A note of optimism came from recent results by the Harder and Hill groups.

As discussed in Section 6.3.2, the heteroleptic strontium hydride [{BDI^{DiPeP}}Sr(μ-H)]$_2$ (**93**) reacts with alkenes to generate strontium alkyls that lead to the nucleophilic alkylation of benzene.[194] The Sr-ethyl complex [{BDI^{DiPeP}}Sr(μ-CH_2CH_3)]$_2$ (**96**) was obtained within minutes by treatment of **93** with ethylene in C_6D_6 at 20 °C and 1 bar pressure. Complex **96** further reacted by ethylene through iterative σ-insertions to give Sr-butyl, Sr-hexyl and higher oligomers. However, chain growth in this process akin to the well-known aluminum-mediated Aufbau reaction was hampered by the propensity of strontium-alkyl species derived from **93** to react with C_6D_6 and yield n-alkylated benzene derivatives.

Nonetheless, the isolation of small quantities of insoluble, higher molecular weight material was detected; GC-MS analysis indicated the formation of linear alkanes and low molecular weight oligomers $(C_2H_4)_nH_2$ with n = 5-15. Of note, the calcium analogue $[\{BDI^{DiPP}\}Ca(\mu\text{-}CH_2CH_3)]_2$ did not polymerize ethylene,[18] suggesting that the higher polarity of the metal-to-carbon in **96** was key to the ability to catalyze the polymerization of apolar ethylene. Although these results are only preliminary, they suggest that strongly polarized alkaline-earth alkyls offer the prospect to be elaborated into more effective α-olefin polymerization catalysts. The choice of comparatively more polarized higher α-olefinic substrates, and the utilization of toluene as a non-reactive, non-coordinating solvent, appear to be reasonable options in this direction.

6.6 Reduction of carbon-oxygen unsaturated compounds

Alkaline-earth complexes have met limited success in catalysis towards the reduction of unsaturated C-O bonds. In a remarkable synthetic contribution, the highly Lewis acidic *ansa*-arene dicationic strontium complex $[(DXE)Sr\cdot(1,2\text{-}F_2\text{-}C_6H_4)_2][Al\{OC(CF_3)_3\}_4]_2$ (**97**; DXE = dixylylethylene) was reported to catalyze the reduction of CO_2 into CH_4, using triethylsilane as the hydrogen source (Figure 85).[202] The reaction with a 0.6 mol% catalyst loading was slow, requiring 14 days to reach 24% conversion of the silane. A scenario involving sequential reaction with Et_3SiH and release of hexaethyldisiloxane was tentatively proposed, but further mechanistic studies were not conducted.

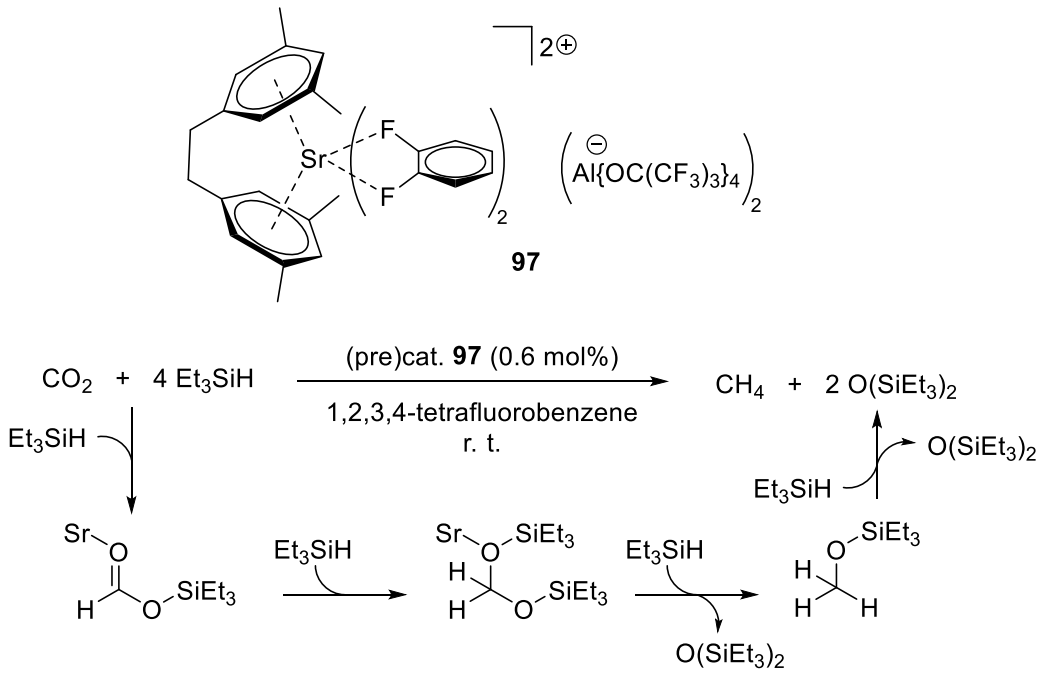

Figure 85. Postulated pathway for the reductive hydrosilylation of CO_2 into CH_4 catalyzed by **97**.

The ability of the calcium hydride $[\{BDI^{DiPP}\}CaH\cdot(thf)]_2$ (**45**) to catalyze the reduction of carbon monoxide with phenylsilane was examined.[203] Like its lighter magnesium derivative,[204] complex **45** was found to react with CO (1 atm) at room temperature to generate a *cis*-ethenediolate dianion **98** (Figure 86), although the C-C bond formation was not a catalytic process. Yet, the reaction of CO and $PhSiH_3$ catalyzed by **45** at room temperature in toluene-d_8 gave the methylene silyl ether $PhH_2SiOCH_2SiPhH_2$ within 60 min. Unlike the corresponding reaction with the magnesium catalyst, the formation of the fully reduced silane $PhSiMeH_2$ could not be enforced with **45**. Based on thorough DFT

calculations and experimental data, the reactions were proposed to involve the formation of a Ca-formyl intermediates (Figure 86).

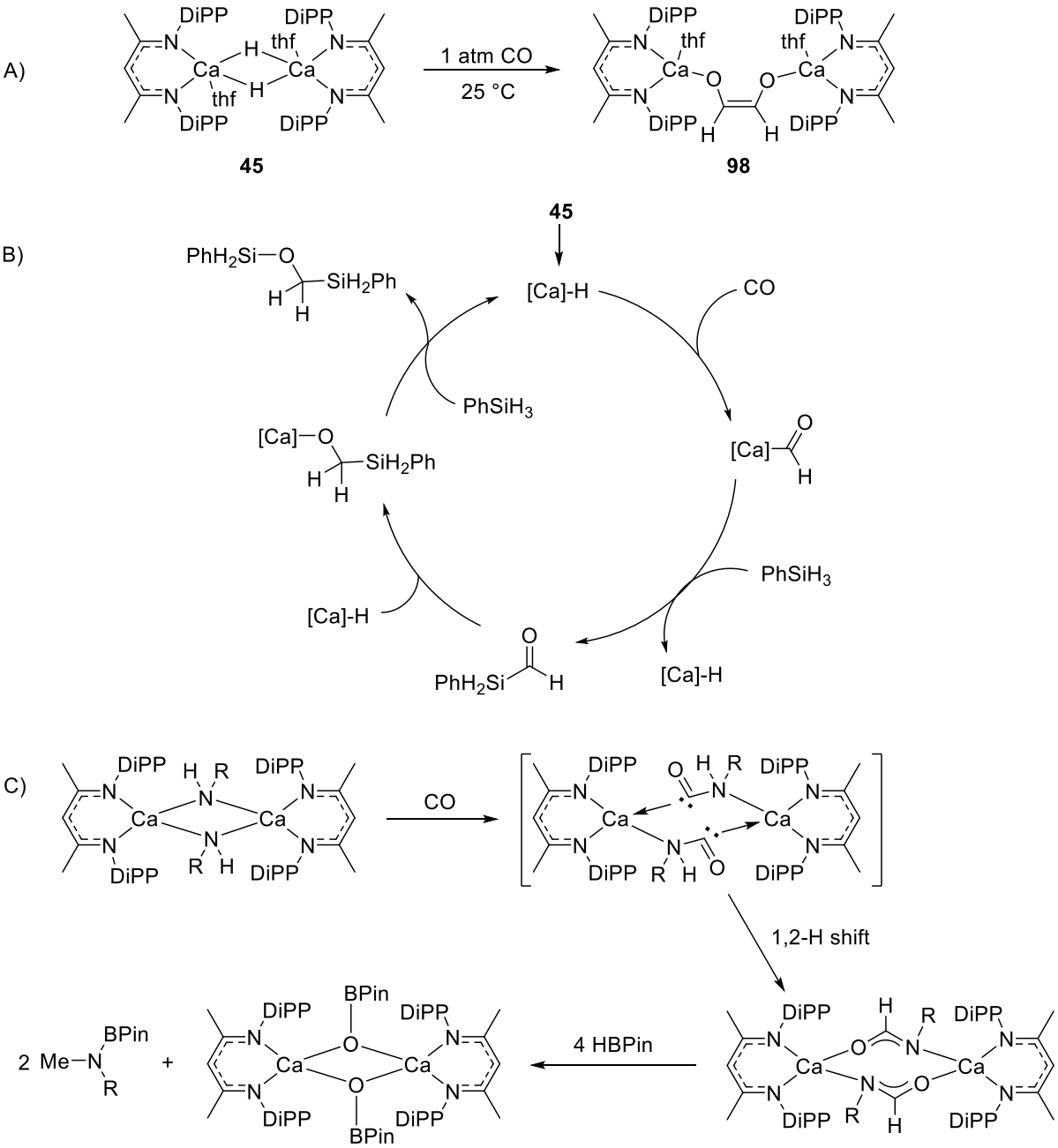

Figure 86. Calcium-catalyzed reduction of carbon monoxide: A) Stoichiometric formation of dianionic ethenediolate from the hydride **45**; B) Proposed mechanism for the reduction with phenylsilane catalyzed by **45**; C) Reaction with calcium-amides and pinacolborane forming methylamines.

When reacted with primary calcium-amides, insertion of CO in the Ca-N bond with concomitant migration of hydrogen from nitrogen to carbon was observed, giving well defined di- or trinuclear calcium formamidates (Figure 86). In stoichiometric studies, further reduction of these intermediates with pinacolborane led to the formation of the resultant N-borylated methylamines. The proposed multi-stem mechanism, starting with the generation of amidatohydridoborate, was

reminiscent of that established for the deoxygenative hydroboration of isocyanates catalyzed by a magnesium hydride precatalyst.[205] The attempts to elaborate this stoichiometric reactivity into a more complex catalytic manifold for the utilization of CO as a C_1 synthon towards the production of methylamines were hampered by competitive calcium-catalyzed dehydrocoupling of the amines with pinacolborane, and by the limited solubility of CO under the chosen experimental conditions (1 atm).

6.7 Redistribution and cross-coupling of arylsilanes

Owing to the main importance of hydrosilanes in many facets of synthetic chemistry, it is not surprising that catalysts have been developed to enable the controlled redistribution of hydrosilanes in order to diversify the range of potentially usable compounds. The asymmetric β-diketiminato calcium alkyl complex **99**, which reacted cleanly with an equivalent amount of $PhSiH_3$ to form the dimeric hydrido compound **100**, was shown to catalyze the selective redistribution of $ArSiH_3$ or $Ar(alkyl)SiH_2$ to Ar_3SiH and SiH_4 or $Ar_2(alkyl)SiH$ and $alkylSiH_3$, respectively (Figure 87).[206] It also allowed for the controlled cross-coupling between the electron-withdrawing substituted $Ar(alkyl)SiH_2$ and the electron-donating substituted $Ar'(alkyl)SiH_2$, producing $ArAr'(alkyl)SiH$ in good yields. The reactions took place within 20-180 min in C_6D_6, using 0.5-2.0 mol% precatalyst in the temperature range 37-50 °C. A broad range of aryl-functionalized substrates were utilized, and the redistributions remained highly selective. Cross-coupling reactions proved challenging, as the heterocoupled products were contaminated by the presence of variable amounts of homocoupled redistribution by-products. Experimental and theoretical studies (DFT) indicated that the catalytically active species was a calcium-hydride complex, e.g. **100** or a related compound. The inferred reaction manifold for the redistribution of $PhSiMeH_2$ (Figure 88) was found to be kinetically very affordable. It is initiated by the formation of the calcium-hydride upon reaction of the alkyl precatalyst with $PhMeSiH_2$. The concerted formation of a transient Ca-phenyl intermediate through a four-membered transition state with H/Ph exchange then ensues. A second, rate-limiting σ-bond metathesis between this intermediate with a second $PhSiMeH_2$ equivalent regenerates the Ca-hydride while also releasing the final product of redistribution, Ph_2SiMeH. A similar study revealed that the tris(pyrazolyl)hydroborate barium benzyl $[\{Tp^{Ad,iPr}\}Ba(CH_2C_6H_4\text{-}o\text{-}NMe_2)]$[207] derived from the hydrido parent **62** also competently catalyzed the homo- and cross-coupling of aryl and benzyl primary silanes to secondary silanes.[208] High conversions and generally excellent selectivity towards the secondary silanes were achieved, both for homo- and cross-couplings, under mild conditions (precatalyst loading 5 mol% in C_6D_6, 25 °C).

The ability to catalyze the controlled formation of new suites of arylsilanes is certainly an exciting result as it broadens the scope of potential substrates for the many reactions relying on the participations of hydrosilanes. However, it may be possible that this reactivity also sometimes proves troublesome in alkaline-earth catalyzed reactions involving the transformation of arylsilanes. One notable such reaction is the heterodehydrocoupling of amines and silanes (see Section 5.2). In such cases, it is important that the catalyst and reaction conditions are chosen appropriately so that arylsilane redistribution does not become kinetically competitive with the targeted catalyzed reaction.

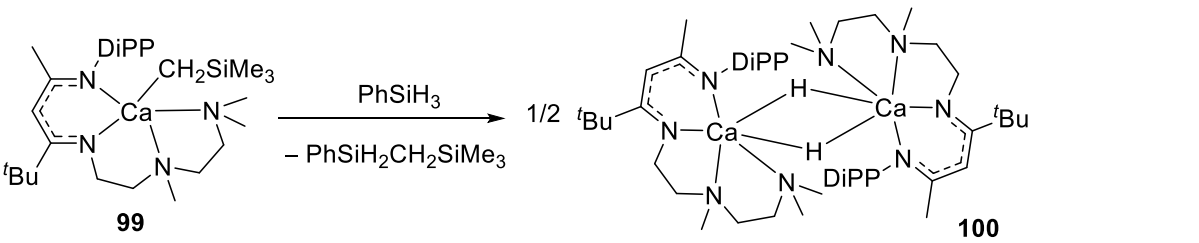

A) Redistribution R = Me, Et

X = H, *p*-Ph, *p*-F, *p*-Cl, *p*-CF_3, *p*-Me, *p*-OMe, *p*-NMe_2, *m*-Me, *m*-Cl, *o*-Me, *o*-OMe

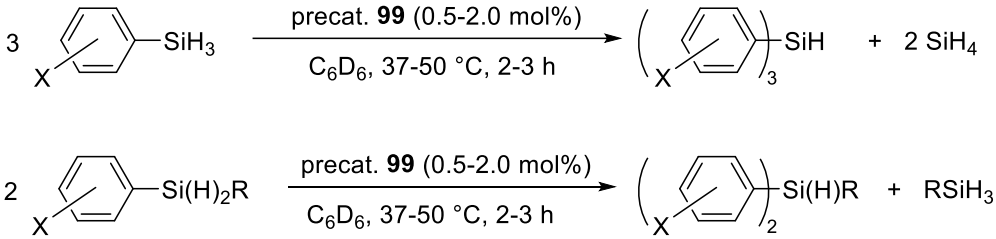

B) Cross-coupling

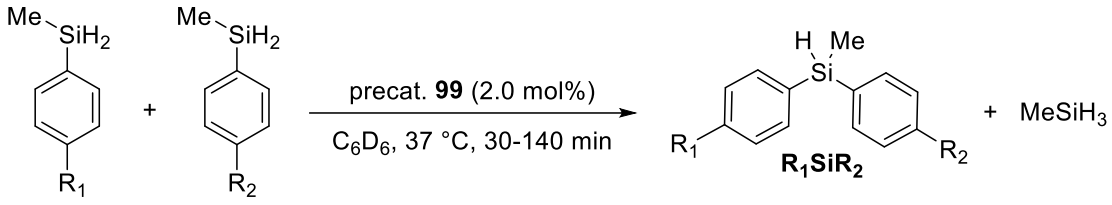

R_1 = F, Cl, CF_3 R_2 = H, Me, OMe, NMe_2

Figure 87. Calcium-catalyzed redistribution (A) and cross-coupling (B) of arylsilanes.

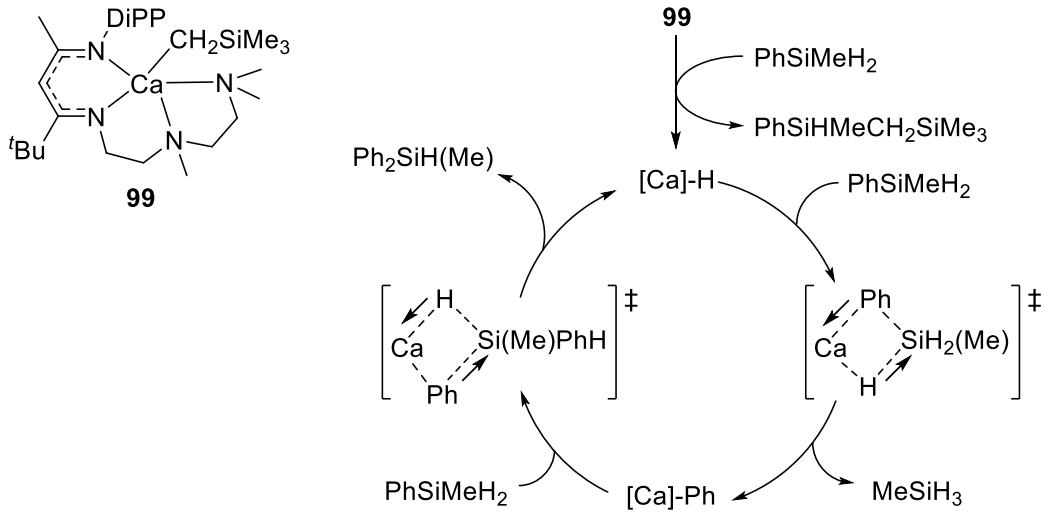

Figure 88. Proposed mechanism for the calcium-catalyzed redistribution of arylsilanes.

6.8 Reactions other than hydrofunctionalizations and dehydrocouplings

6.8.1 *Disilacoupling of silaboranes and amines*

The fragility of the B-Si bond (BDE = 76 kcal mol^{-1}) was exploited by the Hill group. They reported on the desilacoupling of the commercially available silaborane PinB-$SiMe_2Ph$ with a variety of primary and secondary amines catalyzed by [Ae{$N(SiMe_3)_2$·$(thf)_2$, with formation of the corresponding aminoboranes through creation of a B-N bond (BDE bond: 90 kcal mol^{-1}) accompanied by $PhMe_2SiH$ as the sole coproduct (Figure 89).[209] In C_6D_6, these reactions were complete within 24 h at room temperature with 5 mol% precatalyst. Secondary amines were overall more reactive than primary ones; while both aliphatic and aromatic amines could be used as coupling partners. The reaction rate increased with metal size (Mg < Ca < Sr). This catalyzed procedure provided the first example for the coupling of two heteroelements E and E' that was not dependent of the concomitant production of dihydrogen.

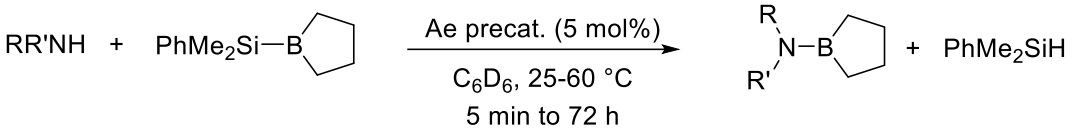

R = Bn, ^{t}Bu, Ph, DiPP, Et R' = H, Me, Et, Ph R, R' = $(CH_2)_4$

Figure 89. Alkaline-earth catalyzed coupling of silaboranes and primary/secondary amines.

6.8.2 *Cyanosilylation of carbonyls*

The addition of Me_3SiCN onto pre-polarized aromatic aldehydes and ketones ArC(=O)R giving cyanohydrin derivatives was proved to be catalyzed by the amidinato calcium iodide **101** (Figure 90).[210] These cyanosilylation reactions afforded high substrate conversion at room temperature in toluene within 30 min, using a 2 mol% metal loading, and without the need for any additional co-catalyst.[211] A very broad range of carbonyl substrates was used, demonstrating excellent tolerance towards functional groups. Based on experimental and theoretical investigations, the authors concluded that the mechanism at work did not obey a classical σ-insertive pathway, because neither the substrates nor the precatalyst possess any reactive Ca-H or E-H site. Instead, they proposed a more unusual outer-sphere scenario where polarization of the Si-CN bond by coordination onto the Lewis acidic metal facilitated the nucleophilic attack by the carbonyl.

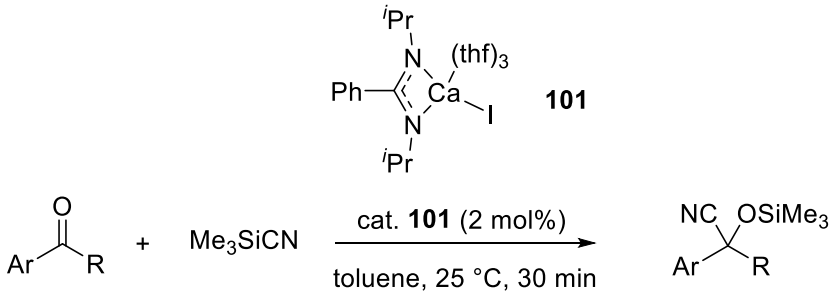

R = H, aryl, alkyl

Figure 90. Calcium-catalyzed cyanosilylation of carbonyls with Me_3SiCN.

6.8.3 *Alumination of C_{sp2}-H bonds*

Simple, selective and efficient C-H bond activation has long been one of the most desirable goals in both organic and inorganic chemistry. The ability to directly activate and functionalize C-H bonds allows unnecessary functionalization and derivatization steps to be avoided, increasing stepwise, atom and (potentially) energy efficiency.[212] Although a vast number of metal and organic complexes and materials have been reported to catalyze various C-H bond activations, there has only been one select example of Ae-mediated C-H bond activation, that of an arene C-H bond activation with an Al(I) complex reported in 2019.[213] The catalysis was discovered serendipitously. In an attempt to generate a Ca-Al bond, two equivalents of the aluminum(I) complex [{BDI^{DiPP}}Al] (**102**) were reacted with [{BDI^{DiPP}}Ca(μ-H)]$_2$ (**58**) in benzene (Figure 91). However, instead of generating the desired heterobimetallic complex, the oxidative addition product, [{BDI^{DiPP}}Al(H)(Ph)], was generated within 1 hour at room temperature via cleavage of a C_{sp2}-H bond. Subsequent investigations showed the process was catalytic, and that the reaction could proceed to full conversion at room temperature using down to a 5% molar loading of **58**. If the reaction solvent was changed to toluene, activation of the *ortho* and *meta* hydrogen atoms was achieved in a 1:9 ratio. *p*-Xylene could also be activated; however, the reaction was slightly slower, only reaching 73% conversion after 8 hours. The observed stoichiometric reactivity (in terms of reagents) catalyzed by **58** could not be upgraded in a "true" catalytic reaction, i.e. with multiple calcium-mediated turnovers.

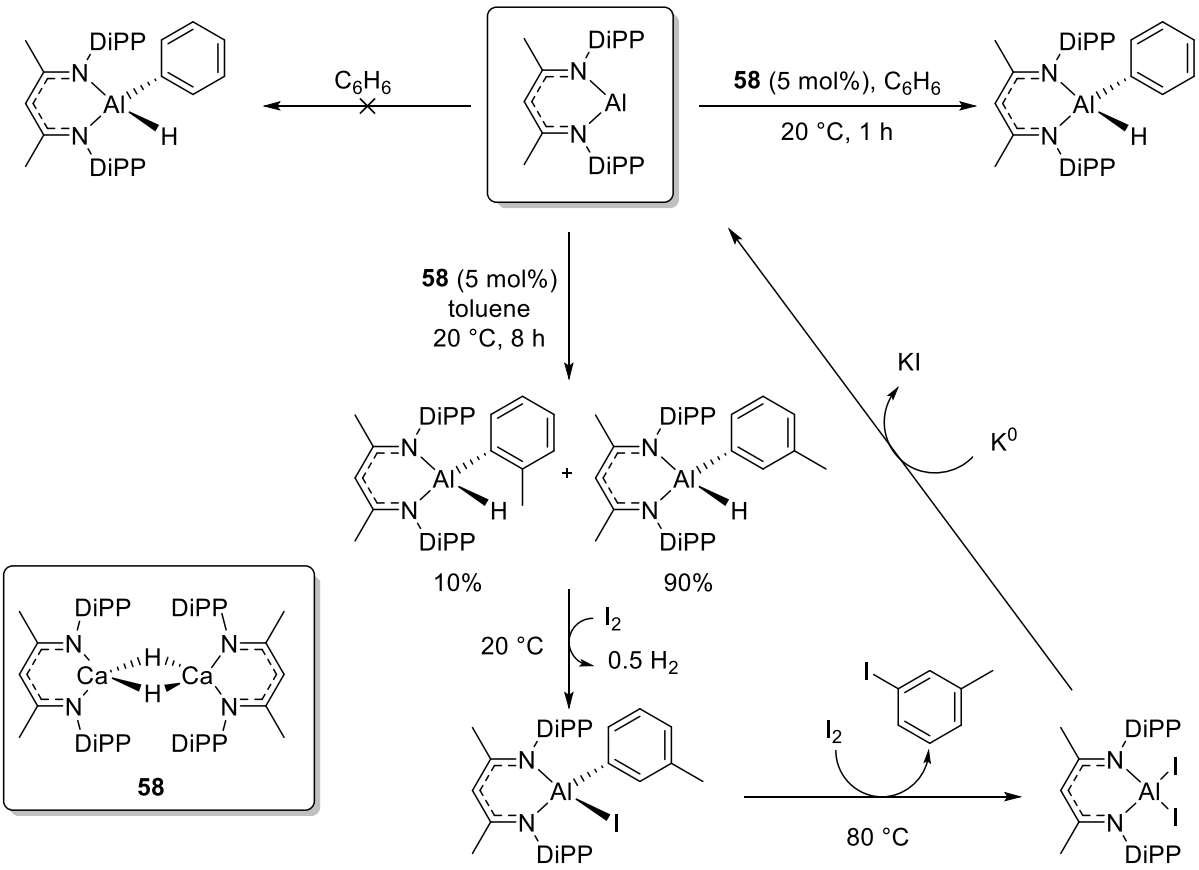

Figure 91. Reactions of the aluminum(I) complex [{BDI^{DiPP}}Al] (**102**) with benzene and toluene catalyzed by the calcium hydride [{BDI^{DiPP}}Ca(μ-H)]$_2$ (**58**).

When the catalyst **58** was replaced by the amido complex [{BDI^{DiPP}}CaN(SiMe$_3$)$_2$] (**73**), no oxidative addition was observed, even when the solution was heated to 60 °C, indicating the hydride functionality plays a vital role in the reaction. Regeneration of the [{BDI^{DiPP}}Al] starting material could be achieved using stoichiometric equivalents of iodine followed by reduction with potassium (Figure 91). DFT calculations suggested that the most likely reaction pathway proceeded via direct oxidative addition, initiated by the formation of a the weakly bound Ca-Al complex [{BDI^{DiPP}}Al(H)-Ca{BDI^{DiPP}}] in equilibrium with the bridged [{BDI^{DiPP}}Al(μ-H)Ca{BDI^{DiPP}}]. Yet, the computations could not entirely rule out other competitive mechanisms based on Meisenheimer or anti-aromatic $C_6H_6^{2-}$ intermediates. Attempts to establish which of the catalyst **58** or the aromatic substrate was the source of hydride in the product by D-labeling experiments proved inconclusive.

7 Alkaline-earth mediated Lewis-acid catalysis

A number of pertinent alkaline-earth catalyzed reactions that are mechanistically different from those described in the preceding sections have been reported. These are collated here and discussed in the light of the available mechanistic information, where possible in link with related Ae-mediated catalyzed elementary steps or more complex processes. The section encompasses a range of C-C, C-N and C-O bond forming reactions catalyzed by compounds based on calcium, strontium and barium via Lewis-acid catalysis. Although it attempts to give a detailed overview on some of the most recent chemistry from this growing field, the reader is also directed to a range of other publications and monographs specializing on this growing field.[214-218]

7.1 Introduction

7.1.1 Lewis acidity of the group 2 metal cations

Broadly defined, a Lewis acid is any compound that possesses an empty orbital capable of accepting electron density (a lone pair from another atom) from a donor molecule, the Lewis base. There are six main recognized types of Lewis acid (Figure 92).

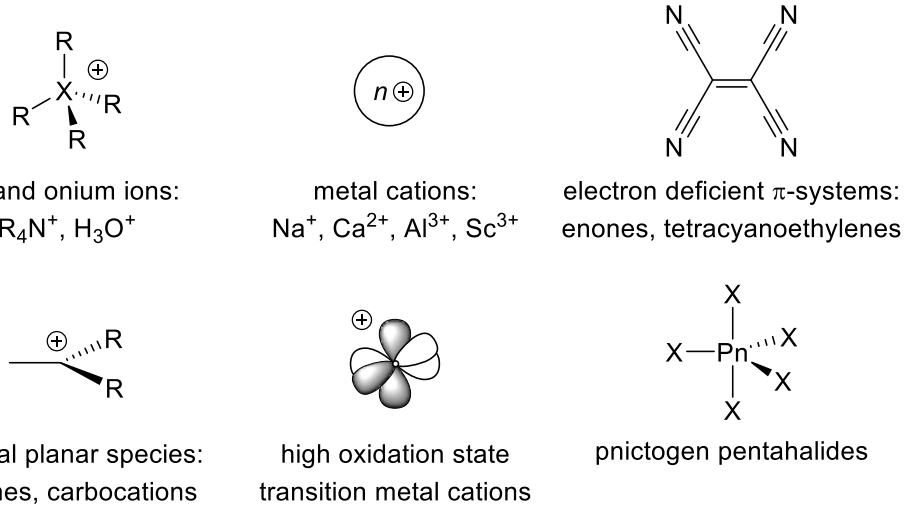

Figure 92. The six different types of Lewis acids often discussed.

The redox chemistry of group 2 Lewis acids is quite simple in comparison to their transition-metal (TM) counterparts. Their lack of valence *d* electrons results in an almost exclusive +2 oxidation state (OS), meaning that the alkaline-earth metals do not undergo any of the catalytic redox reactivity seen with transition metals. In this +2 oxidation state, their shell-like LUMO is made up of superimposed *s* orbitals that are not easily accessible and cannot accept or donate electron density from the Lewis base. By contrast, although TM Lewis-acid/Lewis base interactions are primarily σ-donor interactions from the base to the metal, the ability of the metal to accept of donate electron density through its *d*-orbitals heavily influences the nature and subsequent reactivity of the Lewis adduct. The relative strength of the σ interaction between the Lewis base and the alkaline-earth Lewis acid is dictated by two chief factors: the charge, and the ionic radius of the metal cation. Although the oxidation state of the alkaline-earth metal cations is consistent down the periodic table, the decreasing electronegativity and increasing ionic radii of the dications result in a decreasing charge density from Mg to Ba, with the consequence that for most purposes, group 2 Lewis acid catalysis is dominated by Mg^{2+} and Ca^{2+} compounds.

7.1.2 Measuring Lewis acidity

By the definition of Lewis acidity given above, one could believe that quantifying Lewis acidity is a simple task. However, differences with the steric and electronic nature of the complementary Lewis base can create difficulties. As such, several classification methods have been developed to assist the prediction of Lewis acidity. There are four commonly employed procedures for the quantification of Lewis acidity:

1) The Gutmann-Beckett method, which correlates Gutmann's Acceptor Number (AN) with a change in the ^{31}P NMR chemical shift of $Et_3P{=}O$ upon adduct formation.[219,220]

2) The Childs protocol uses a crotonaldehyde to form a complex in a similar method to the Gutmann-Beckett.[221] The change in chemical shift of the hydrogen atom in γ position is used as a gauge to measure relative Lewis acidity.

3) The Fluoride ion affinity (FIA), a computational method based on ab initio calculations originally at the MP2/PDZ level of theory.[222]

4) The global electrophilicity index (GEI) is a quantitative and base-independent metric of Lewis acidity and is a measure of the ability of a molecule to take up electrons, based on chemical potential and chemical hardness, where hardness is defined as the resistance to deformation or change.[223,224] It is relatively easy to calculate, requiring only the optimized HOMO and LUMO molecular orbitals of the Lewis acid in question.

7.2 Lewis acid catalyzed transformations: C-C bond forming reactions

7.2.1 Mannich reactions

Alkaline-earth amides and alkoxides have been used in stereoselective Mannich-type addition reactions between sulfonylimidates and secondary Boc-protected aldimines (1:1.5 ratio), exhibiting good stereocontrol based on reaction solvent (Figure 93).[225] The magnesium alkoxide $[Mg\{O^tBu\}_2]$ had the best activity for *anti*-addition, with yields up to 99% and moderate stereoselectivity, giving up to a 4:96 *syn/anti* product ratio when reactions were carried out in DMF. When the reaction solvent was

changed to thf, the catalyst $[Sr\{N(SiMe_3)_2\}_2]_2$ in conjunction with a Schiff-type ligand gave yields of up to 99% and moderate stereoselectivity for *syn*-addition, with up to a 93:7 *syn/anti* product ratio. In a similar system, high enantioselectivity was achieved using $[Sr\{O^iPr\}_2]_n$ and a bis(sulfonamide) chiral ligand with a diphenylethylenediamine backbone.[226] Similar Mannich-type reactions have also been described, including the highly diastereoselective addition of *N*-Boc-amides to *N*-diphenylphosphinoyl imines, followed by a Boc migration in the presence of a $[Ba\{O^tBu\}_2]$/[2'-methoxybiphenyl-2-ol] catalytic system.[227,228]

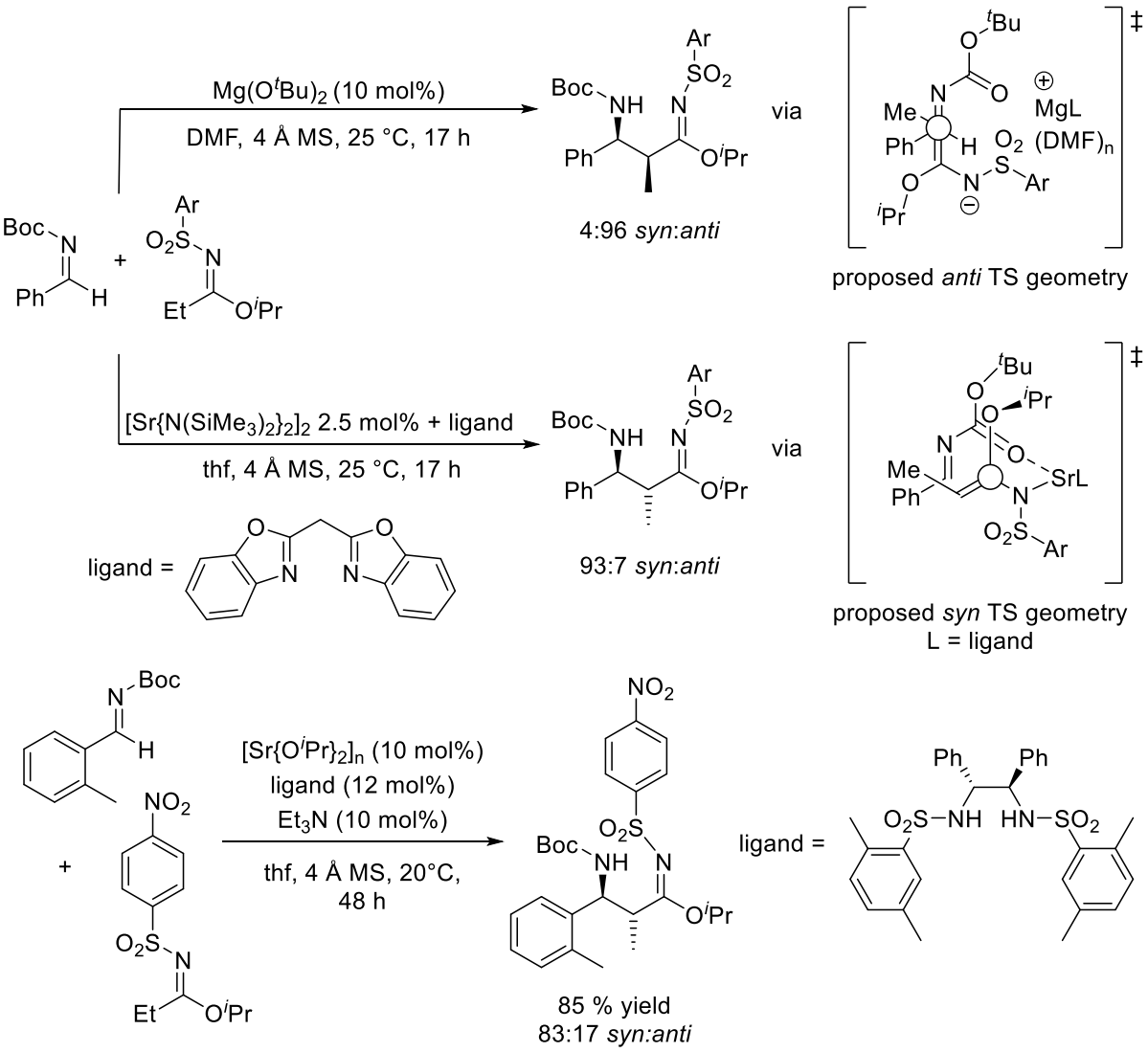

Figure 93. Alkaline-earth catalyzed Mannich-type addition reactions of sulfonylimidates.

Chiral Schiff-base ligands have also been used in alkaline-earth catalyzed Mannich-type addition reactions of a methyl-α-isothiocyanato ester (Figure 94).[229] The use of $[Mg\{^nBu\}_2]$ as a catalyst favored the *syn* addition with 80-95% ee and 90:10-93:7 dr (*syn/anti*), while $[Sr\{O^iPr\}_2]_n$ was found to favor *anti* addition with 84-97% ee and 17:83-4:96 dr (*syn/anti*). A range of substrates were investigated, primarily aryl or heteroaryl methyl ketimines, with both diasteromers being accessible by switching the metal source.

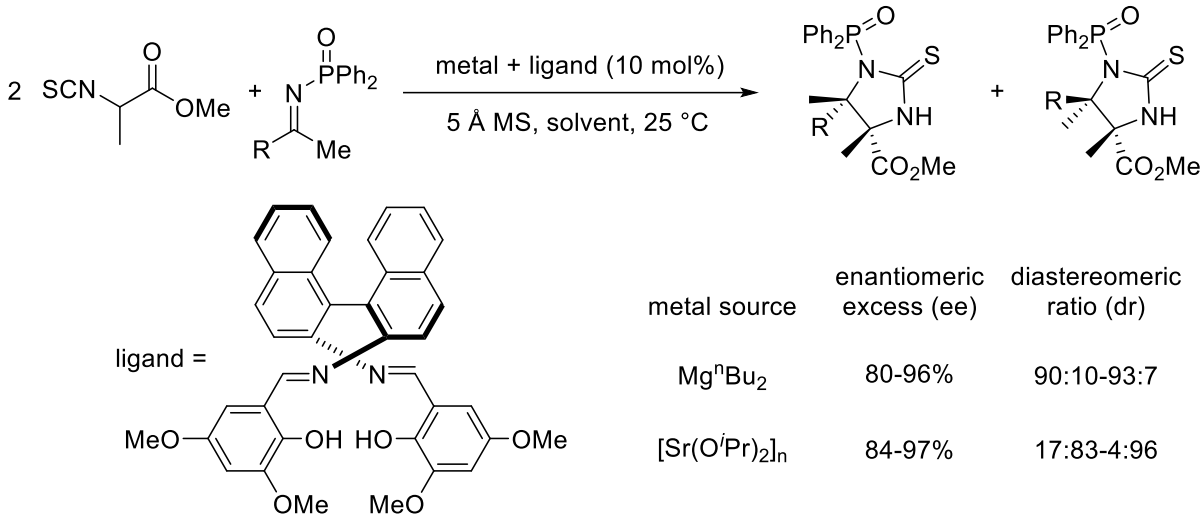

Figure 94. Asymmetric alkaline-earth catalyzed Mannich-type addition reactions with methyl-α-isothiocyanato esters.

Asymmetric Mannich-type reactions between *N*-Boc imines and 1,3-dicarbonyl substrates have be investigated using complexes bearing a chiral phosphate ligand based on a BINOL backbone (Figure 95).[230,231] The catalytic system was especially efficient for 1,3-dicarbonyl compounds with poorly acidic α-protons, such as β-ketoesters and thiomalonates. This work was extended to include pyrone and 1,3- diketones as carbonyl sources (Figure 96).[232] The most active catalytic species was observed to be the Ca-BINOL phenolate complex with tris-2,4,6-triisopropyl-phenyl groups as the R moiety at the 3 and 3' positions of the aryl backbone.

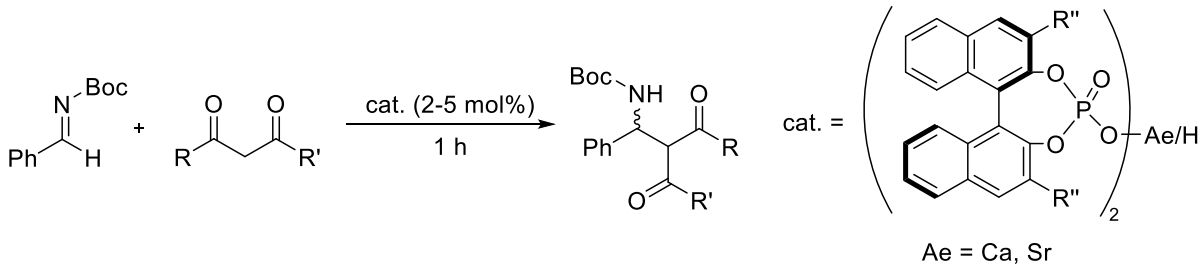

Figure 95. Chiral Ae-phosphate catalyzed asymmetric Mannich reactions.

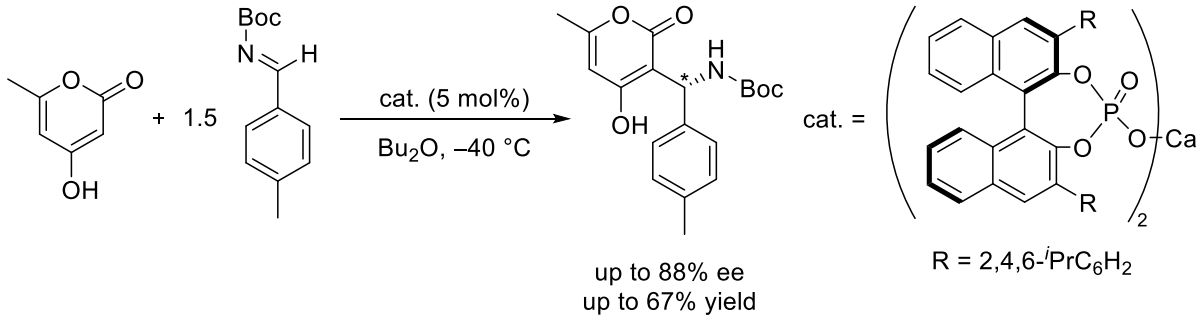

Figure 96. Chiral Ca-phosphate catalyzed asymmetric Mannich reactions of substituted pyrones.

Chiral barium catalysts, bearing optically pure (*S*)-BINOL or another optically pure (*S*)-aryldiol (shown in Figure 97) have been shown to catalyze the Mannich-type reaction between β,γ-unsaturated esters and *N*-diphenylphosphinoyl imines.[233] The assumed catalytic species, the Ba phenolate, is generated *in situ* from $[Ba\{O^iPr\}_2]_n$ and the appropriate optically pure diol. The reaction had good enantioselectivity, generating the α,β-unsaturated ester with ees of up to 88%. As per all of the previously mentioned Mannich-type reactions, the catalysis proceeds via a σ-bond metathesis step between the precatalyst (in this case a barium phenolate) and the carbonyl of the substrate, followed by insertion of the imine and formation of the carbon-carbon bond.

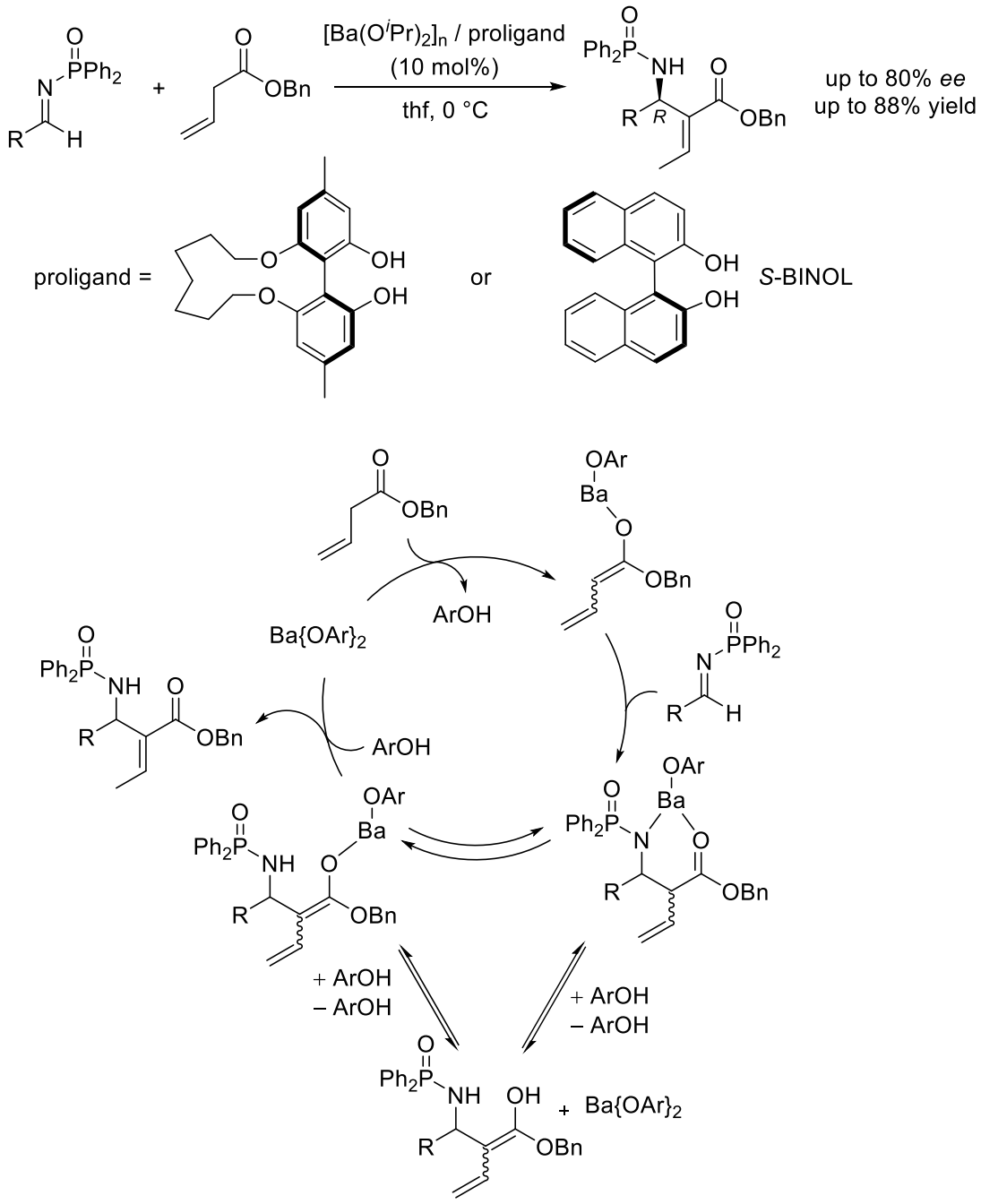

Figure 97. Chiral barium-aryloxide-catalyzed Mannich reactions of β,γ-unsaturated esters with imines, with the postulated catalytic cycle.

7.2.2 Cycloaddition reactions

Cycloadditions have long been a favorite topic of investigations for synthetic chemists. They allow for the convenient synthesis of highly functionalized, complex ring systems, with good stereochemical control over the product formation. A number of alkaline-earth catalytic systems have displayed good efficacy in these processes.[234]

7.2.2.1 [3+2] Cycloadditions

Kobayashi and co-workers investigated alkaline-earth catalyzed [3+2] cycloadditions of Schiff bases derived from glycine with β-substituted α, β-unsaturated esters such as methyl crotonate.[235] These reactions were catalyzed by a chiral $[Ca(O^iPr)_2]_n$/bis(oxazoline) system and generated chiral pyrrolidine derivatives in high yields with excellent enantioselectivity (Figure 98).[236,237] When aldimines were used opposed to a secondary arylketimine, the substrates were less stable, possibly due to tautomerization leading to the formation of enamines. Moreover, the secondary arylketimine likely forms a more stable carbocation, thus moving the equilibrium to favor the formation of cyclic adducts and also inducing better enantioselectivity. A range of substrates derived from other α-amino acids including alanine, methionine, leucine, and serine derivatives were also used.

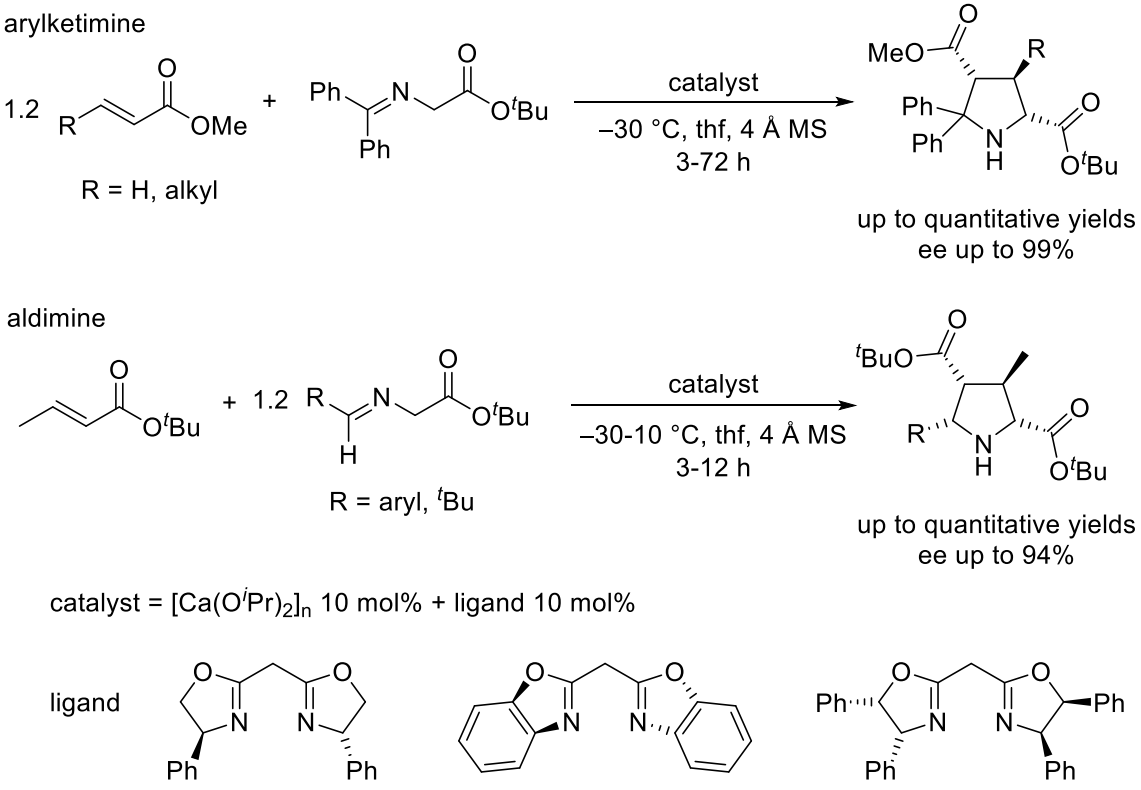

Figure 98. [3+2] cycloaddition reactions catalyzed by $[Ca(O^iPr)_2]_n$/bis(oxazoline) systems.

In these systems, an heteroleptic alkoxo catalyst bearing a chelating bis(oxazolinato) ligand is produced *in situ* via deprotonation of the proligand by $[Ca\{O^iPr\}_2]_n$. In the proposed catalytic cycle (Figure 99), the substrate derived from an amino-acid is deprotonated. The resulting enolate acts as a nucleophile in the nucleophilic attack onto the α,β-unsaturated carbonyl substrate, which itself has

had its electrophilicity increased through coordination to the metal. Cyclization followed by pronation generates the pyrrolidine product, with the stereochemistry being induced by the chirality of the Ca-coordinated ancillary ligand.

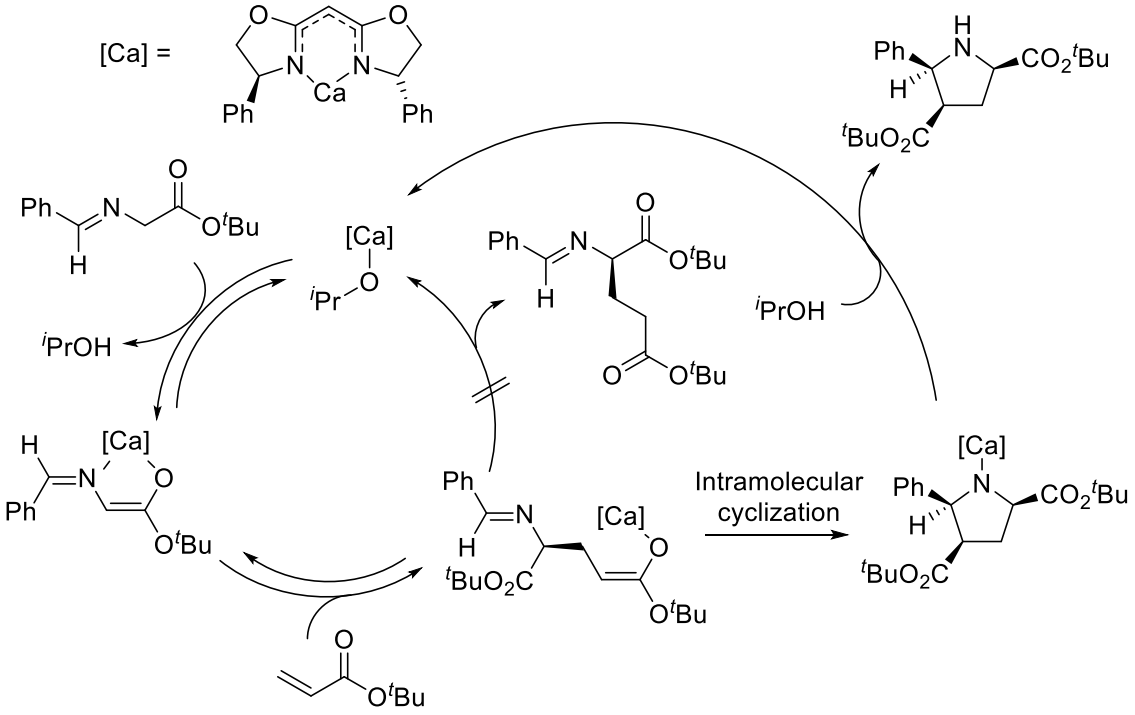

Figure 99. Proposed catalytic cycle for the [3+2] cycloaddition between an α-amino ester aldimine and *tert*-butyl-acrylate catalyzed by the system $[Ca(O^iPr)_2]_n$/bis(oxazoline).

Further investigations showed that using a stronger Brønsted base such as the calcium hexamethyldisilazide $[Ca\{N(SiMe_3)_2\}_2]_2$ as a precatalyst could also be successful in these types of reactions. The bulky silazide group offers the added advantage of increased solubility in many organic solvents, overall making the corresponding complexes better suited to organic synthesis.[234,237,238]

7.2.2.2 [4 + 2] Cycloadditions

Lewis-acid catalyzed Diels-Alder reactions have been frequently reviewed.[239] Chiral calcium phosphate complexes catalyzed the [4+2] cycloaddition between 3-siloxydiene and an activated alkene, giving the desired cyclic product in moderate yields and enantioselectivity (ee up to 55%) (Figure 100).[240] Similar reactions between heteroatom-containing α-ketoesters and siloxydienes gave the desired 6-membered heteroatom rings in high yields with excellent ees up to 99%.[241] Oxo-Diels-Alder reactions between heterodienes and vinyl ethers have also been reported, generating chiral dihydropyran-fused indole molecules in good yields with excellent enantioselectivity (up to 99% ee). In these reactions, both oxygen atoms on the carbonyl of the Boc group and in the vinyl ether chelate with the calcium of the chiral phosphate catalyst to form a 6-coordinate transition-state that heavily favors *endo* selectivity for the hetero-Diels-Alder product.[242] An enantioselective Diels-Alder reaction has also been reported with a chiral Ba catalyst (Figure 100).[243] The catalyst, proposed to be a trimeric cluster in solution, was generated *in situ* from a chiral diol and $[Ba\{O^iPr\}_2]_n$.

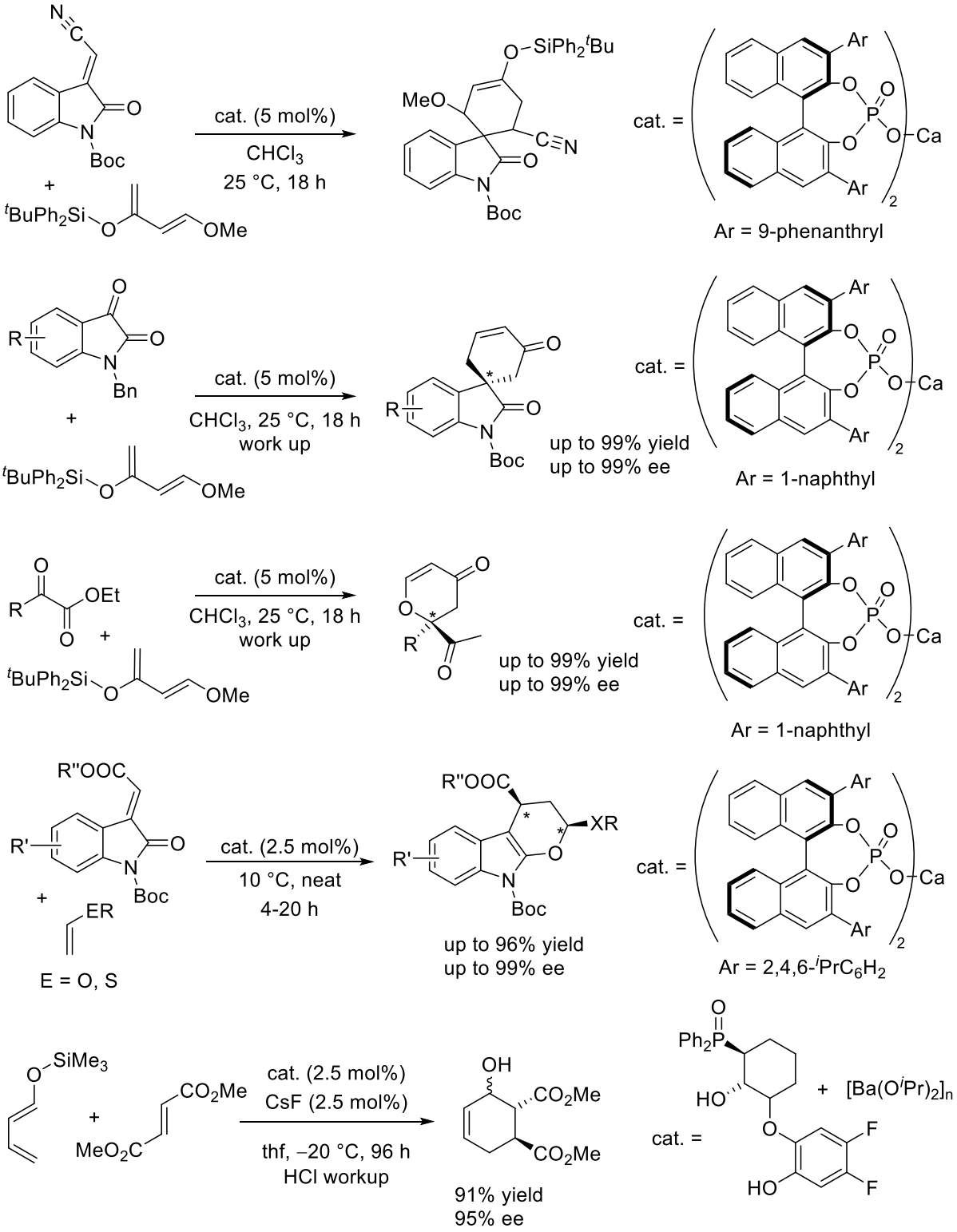

Figure 100. [4+2] cycloadditions catalyzed by chiral calcium-phosphate and barium-alkoxide catalysts.

The one-pot synthesis of dihydropyrrolo[1,2-*a*]quinolines has been reported using calcium trifluoromethanesulfonimide [Ca{NTf_2}$_2$] as the catalyst. The proposed mechanism for the cascade reaction starts with a [4+2] cycloaddition (Figure 101).[244] The solely *syn* products are generated from an inverse electron demand [4+2] aza-Diels−Alder cycloaddition, followed by a further [3+2] cyclization with a suitable activated alkyne. The difference in regioselectivity between benzo[*b*]furan

and 2,3-dihydrofuran was ascribed to the different identity of the most nucleophilic carbon between the two substrates. Tricyclic azepines have also been synthesized from ynones and amidines using a [4+2] cycloaddition strategy, catalyzed by calcium triflate, while a [5+2] cycloaddition strategy using this same catalyst has been used to synthesize cyclohepta[*b*]indole derivatives from alkylidene β-ketoesters and olefins.[245,246]

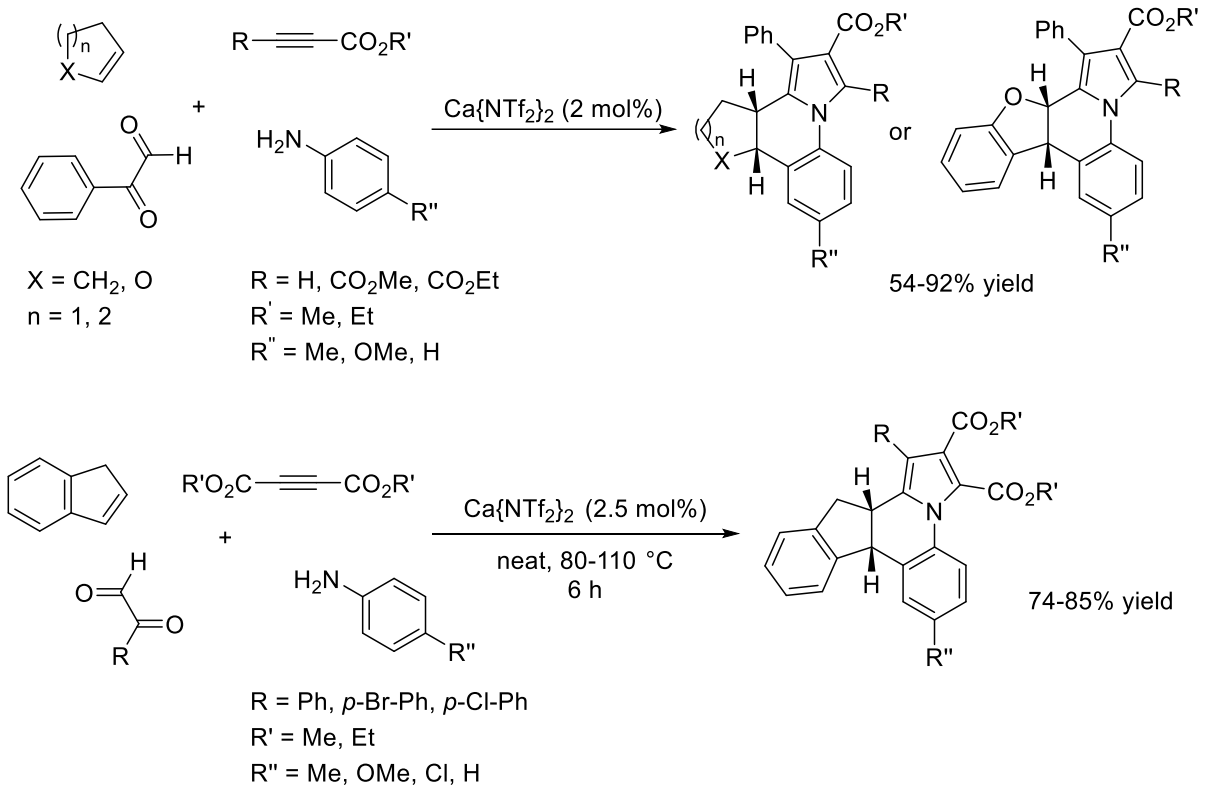

Figure 101. One-pot synthesis of dihydropyrrolo[1,2-*a*]quinolines mediated by [Ca{NTf_2}$_2$].

7.2.3 Chiral 1,4-addition reactions

The heavy alkaline-earth metals have been used as Lewis-acid catalysts in a plethora of enantioselective 1,4-addition reactions. Early examples of enantioselective calcium-catalyzed 1,4-addition reactions include the reaction between malonates and β-ketoesters with α,β-unsaturated carbonyl compounds.[245-249]

The Kobayashi group reported the enantioselective 1,4-addition reaction between Schiff bases of an α-aminoether with α,β-unsaturated carbonyl compounds, using the aforementioned [Ca{^{i}OPr}$_2$]$_n$/bis(oxazoline) system (see Section 7.2.2.1).[235,236] The system generated the desired 1,4-addition products in quantitative yields with excellent enantioselectivity, up to 99% (Figure 102). The same system was used to extend the substrate scope to β-substituted α,β-unsaturated carbonyl compounds, while a range of neutral pyridine-based bi(oxazolinato) ligands (PyBox) were used in asymmetric Michael reactions between dimethyl malonate and α,β-unsaturated carbonyl compounds (Figure 102).[250-252]

In 2009 Kobayashi *et al.* used a chiral calcium-PyBox aryloxide system for the enantioselective 1,4-addition of malonates with nitroalkenes, obtaining quantitative yields and ees up to 96% (Figure 102).[253] It was also found that the same PyBox ligand could be used with $CaCl_2$ and triethylamine in a

system for the 1,4-addition of malonates by nitroalkenes (Figure 102).[254,255] This study described the first example of a calcium chloride being used in Lewis-acid catalyzed enantioselective additions; the reactions could be carried out in heterogeneous conditions in a continuous flow reactor, leading to turn over numbers up to 25-fold greater than the earlier reported homogeneous chiral calcium-PyBox aryloxide system.[255] Due to the relative abundancy, stability and non-toxic nature of $CaCl_2$, its use with a chiral ligand in continuous flow processes is currently a research area of great interest, as has been shown by its use in the synthesis of (*R*)-Rolipram.[256]

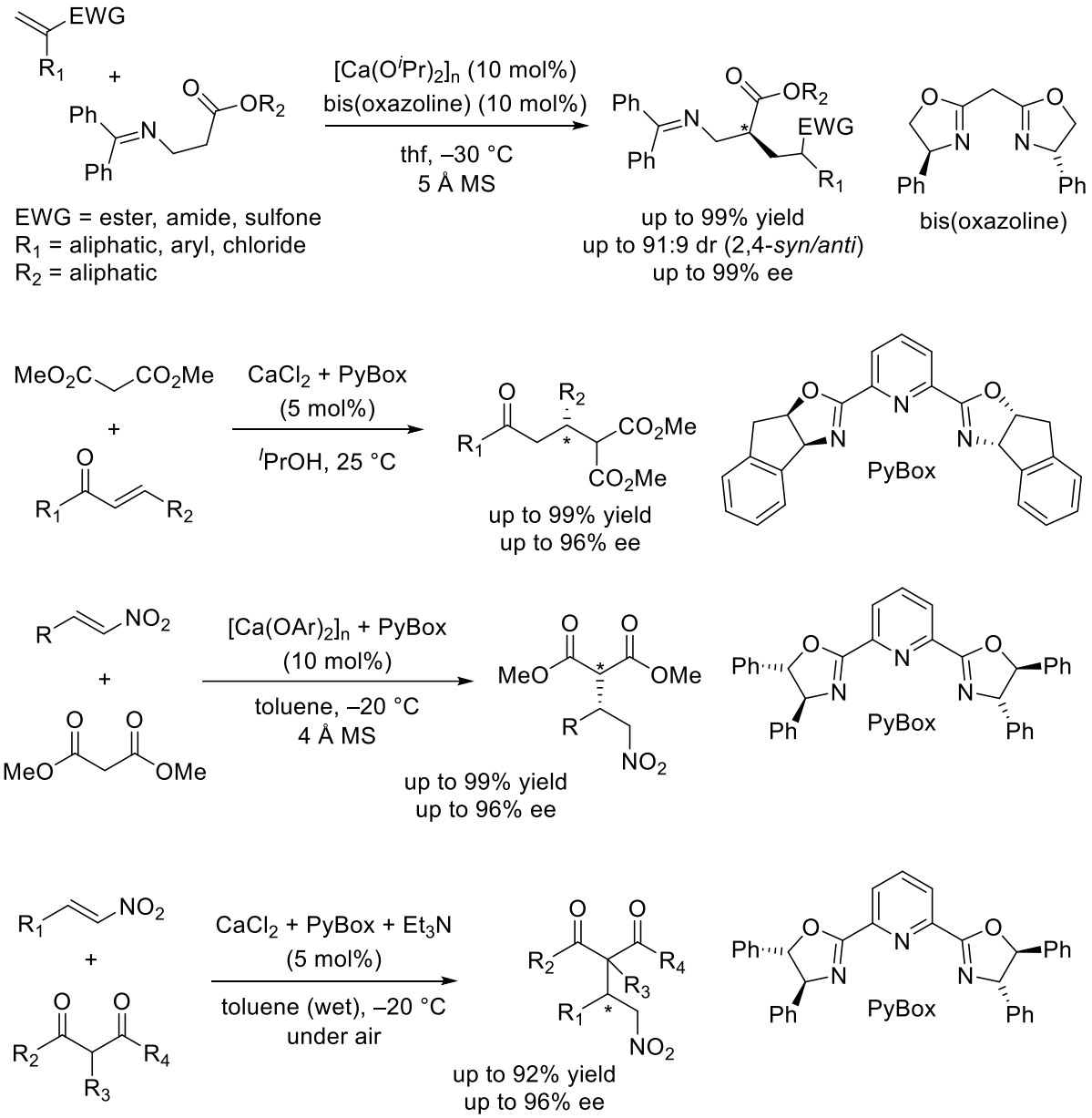

Figure 102. Enantioselective 1,4-addition reactions with calcium-based catalytic systems.

Chiral strontium and barium catalysts have also been used as catalysts in 1,4-addition reactions. A chiral strontium bis(amide), generated from $[Sr\{O^iPr\}_2]_n$ and the parent chiral diamine, gave good yields and excellent enantioselectivity for the reaction of aromatic enones (chalcones) with malonates (Figure 103).[257] When a catalytic species synthesized from $[Sr\{N(SiMe_3\}_2\}_2]_2$ and the same proligand was subjected to identical reaction conditions, turnovers were improved from the

isopropoxide catalyst.[258] A chiral barium catalyst, synthesized from $[Ba\{N(SiMe_3\}_2\}_2]_2$ and a silyl-functionalized BINOL derivative, was used for the 1,4-addition of chalcones with indoles (Figure 103).[259] The desired functionalized indole was obtained in near quantitative yields with excellent enantioselectivity, giving with the (*S*) enantiomer quasi exclusively. Interestingly, if the metal source was switched to $[Ca\{N(SiMe_3\}_2\}_2]_2$ and conventional BINOL was used as the proligand, the opposite enantiomer (*R*) of the indole was obtained, though with only a low ee of 33%.

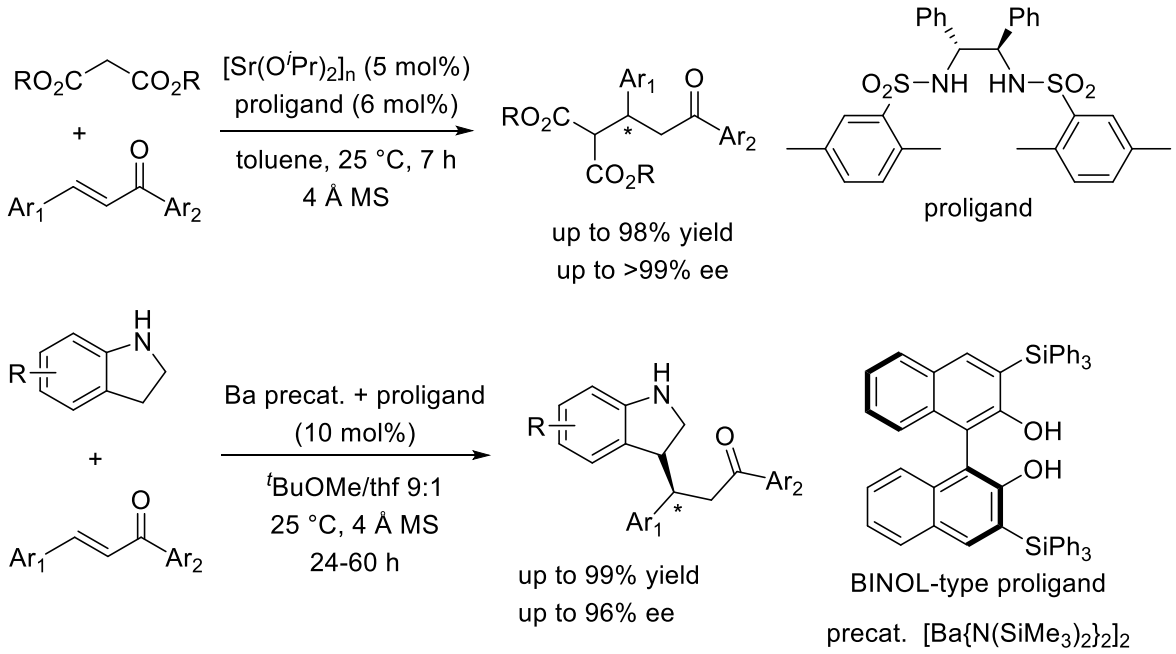

Figure 103. 1,4-Addition-reactions catalyzed by strontium and barium catalytic systems.

Enantioselective α-protonations have also been reported using chiral calcium catalysts. These reactions occur via enolate formation followed by nucleophilic attack on a α,β-unsaturated carbonyl compound. Assuming either the enolate or α,β-unsaturated carbonyl substrate are substituted at an α position, a chiral center can be created.[260-263] A calcium-PyBox system has been used to catalyze the reaction between dibenzyl malonate and an α,β-unsaturated amide with an α aryl or alkyl group, giving high yields and high ees up to 96% (Figure 104).[260] Alternatively, the reaction between α-aryl functionalized indoles and a methyl-vinyl ketone has been catalyzed by a chiral calcium-phosphate complex with high yields and ees (Figure 104).[261] Similar reactions for azalactones and indoles are also known.[262,263] The addition reaction between basic primary amines and maleimides catalyzed by a chiral calcium-phosphate complex was also reported (Figure 104).[264] Although these reactions do not proceed via enolate formation, they nicely exemplify asymmetric conjugate additions where a Lewis-base acts as a nucleophile in the presence of a relatively strong Lewis acid.

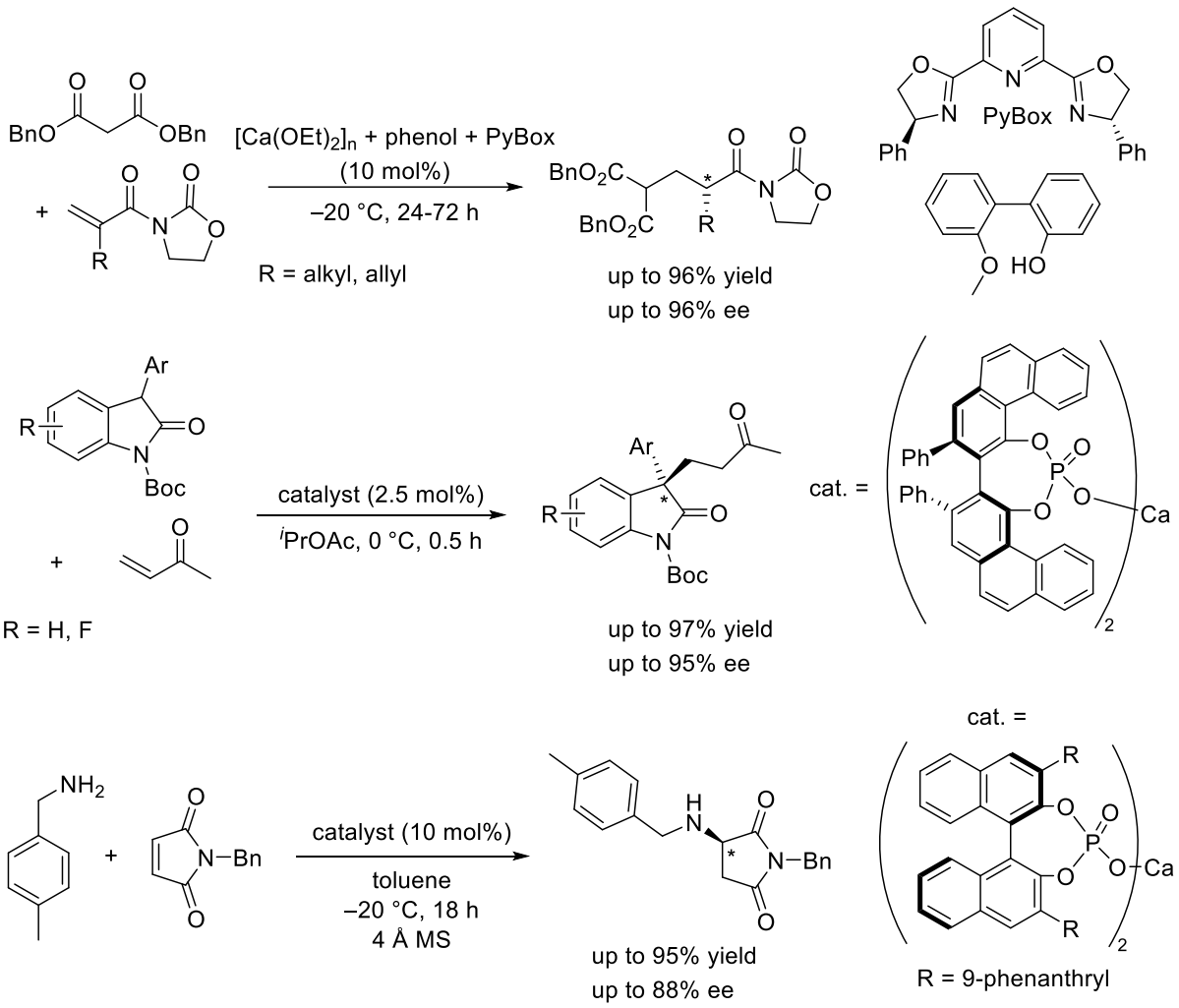

Figure 104. α-Protonations catalyzed by calcium Pybox and BINOL-based phosphate systems.

7.2.4 Hydroarylation of alkenes

The functionalization of olefins catalyzed by alkaline-earth Lewis-acid is considered a difficult reaction, primarily due to the lack of an electronegative heteroatom with a free electron pair that can interact with the electropositive Ae-metal center. However, a smattering of examples of alkaline-earth promoted olefin functionalization exist. The calcium-catalyzed hydroarylation of alkenes using a $[Ca\{NTf_2\}_2]/[Bu_4N][PF_6]$ binary system was reported in 2010.[265] Although triflimide (Tf_2NH) is a weaker Brønsted acid than triflic acid (TfOH), metal triflimidates are stronger Lewis-acids than metal triflates, due to the greater delocalization of the negative charge and the larger volume.[266,267] The system was limited to the addition electron-rich aromatic substrates across both activated and unactivated alkenes, including aliphatic alkenes (Figure 105). Notably, the reaction exclusively generates the Markovnikov addition product, which contrasts to other alkaline-earth catalyzed hydroelementation reactions. The reaction had good functional group tolerance, proceeding smoothly under mild conditions (2.5 mol% catalyst) in the presence of halides, furans and thiophenes. No mechanism for the reaction was proposed, but it was noted that both $[Bu_4N][PF_6]$ and trace water were needed for the catalysis to occur. It was hence suggested that the reaction ensues via a carbinol intermediate, though such species could not be detected. Related work has found that $[Ca\{NTf_2\}_2]/[Bu_4N][PF_6]$ catalytic system can functionalize electron-rich arenes with a variety of alcohols, including secondary

and tertiary benzylic alcohols, as well as propargylic and allylic alcohols.[268] In these reactions, it was presumed that the system forms a more reactive charge-separated $[Ca\{NTf_2\}][PF_6]$ salt for which some spectroscopic evidence has been provided. The substrate scope of hydroarylation of alkenes was extended for the same $[Ca\{NTf_2\}_2]/[Bu_4N][PF_6]$ catalytic system by using hexafluoroisopropanol (hfip) as a solvent (Figure 105).[269] Styrenes with strongly election withdrawing substituents were utilized as electrophiles, including various fluorinated as well as SF_5- and CN-containing vinylarenes. Halobenzenes, *m*-xylene, benzene or naphthalene were used as nucleophiles. The Markovnikov products of addition were obtained exclusively.

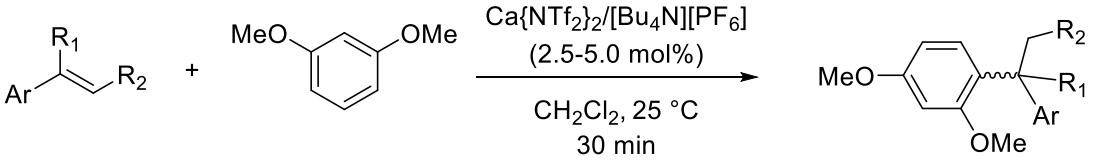

Ar = Ph, *m*-F-Ph, *p*-Cl-Ph, *o*-OH-*p*-OMe-C_6H_3 up to 95% yield
R_1 = H, Me, Ph; R_2 = H, Me
$R_1 = R_2 = (CH_2)_4$

With hexafluoroisopropanol (hfip):

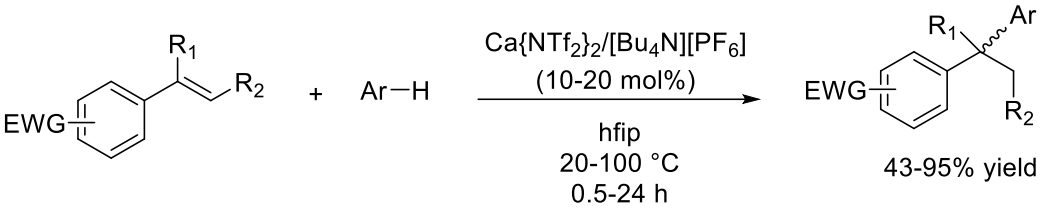

EWG = *o*-CF_3, *m*-CF_3, *p*-CF_3, *p*-NO_2, (*m*-CF_3)$_2$, *p*-SF_5, *p*-CN, *p*-CO_2Me
R_1, R_2 = H, Me
ArH = C_6H_6, *m*-xylene, PhF, PhBr, anisole, naphthalene

Figure 105. Hydroarylation of alkenes with the $[Ca\{NTf_2\}_2]/[Bu_4N][PF_6]$ binary catalytic system.

The mechanism of the hydroarylation in hfip was probed by DFT calculations. The data suggested that the initial step is a proton transfer from an hfip molecule activated by the Lewis acid $[Ca\{NTf_2\}]^+$ to the vinylarene molecule, hence producing a carbocation and a calcium-hexafluoroisopropoxide. The nucleophilic arene then undergoes addition on the carbocation to generate a Wheland intermediate. This intermediate is then deprotonated by NTf_2^- ligand, a step that releases the final Markovnikov addition product. Finally, deprotonation of the Tf_2NH ligand by the calcium-hexafluoroisopropoxide regenerates the catalyst.

Anilines have also been alkylated in the *ortho* position using highly deactivated alkenes and vinylarenes, using the same $[Ca\{NTf_2\}_2]/[Bu_4N][PF_6]$/hfip catalytic system (Figure 106).[270] The Lewis-acid $[Ca\{NTf_2\}_2]$ was not pivotal in the catalytic process; the use of other Lewis-acids including $[Ba\{OTf\}_2]$ and $HNTf_2$ also worked well, though the $[Ca\{NTf_2\}_2]/[Bu_4N][PF_6]$/hfip system gave the best outcome. Only the Markovnikov products were obtained. The alkylation of a large number of anilines with electron-poor alkenes (for instance *p*-CN-styrene) was investigated, with *ortho*-alkylation occurring preferentially. Exceptions included carbazole (*ortho*/*para* alkylation ratio of 67:33) and triarylamines, which gave the *para*-alkylated products, which the authors ascribed to the difference

of pK_a of their conjugate acids (pK_a Ph_3NH^+= −3.9, $Ph_2NH_2^+$ = 0.8, $PhNH_3^+$ = 4.6).[271] The *para*-substituted products presumably formed via protonation of the alkene by Ph_3NH^+, leading to an electrophilic aromatic substitution reaction. When electron-rich alkenes were used, e.g. 1,1-diphenylethylene, α- and β-methyl-styrenes, 4-methoxystyrene, 4-aminostyrene, (*E*)-1-phenyl-1,3-butadiene or acenaphthylene, *para*-alkylation of the aniline was obtained exclusively, in moderate to high yields (68-93%). The reaction pathway was probed by DFT calculations, using [Ca{NTf_2}][PF_6] salt as the likely metal species formed in the reaction medium. A reaction mechanism where two hfip molecules were acting in tandem with one [Ca{NTf_2}$^+$] cation as the catalytic species, and traversing a Wheland intermediate, was suggested (Figure 106).

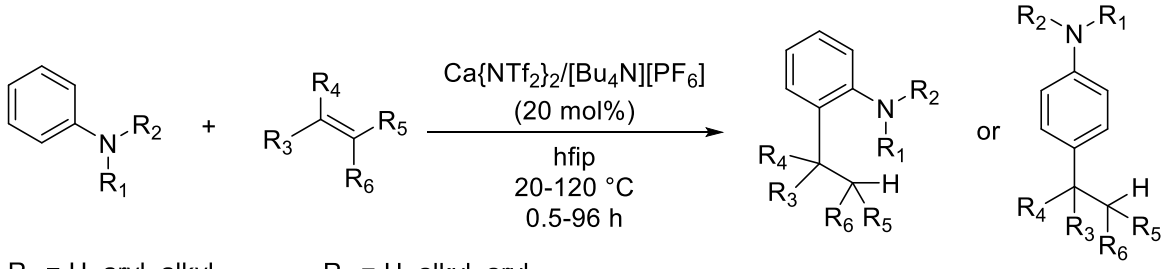

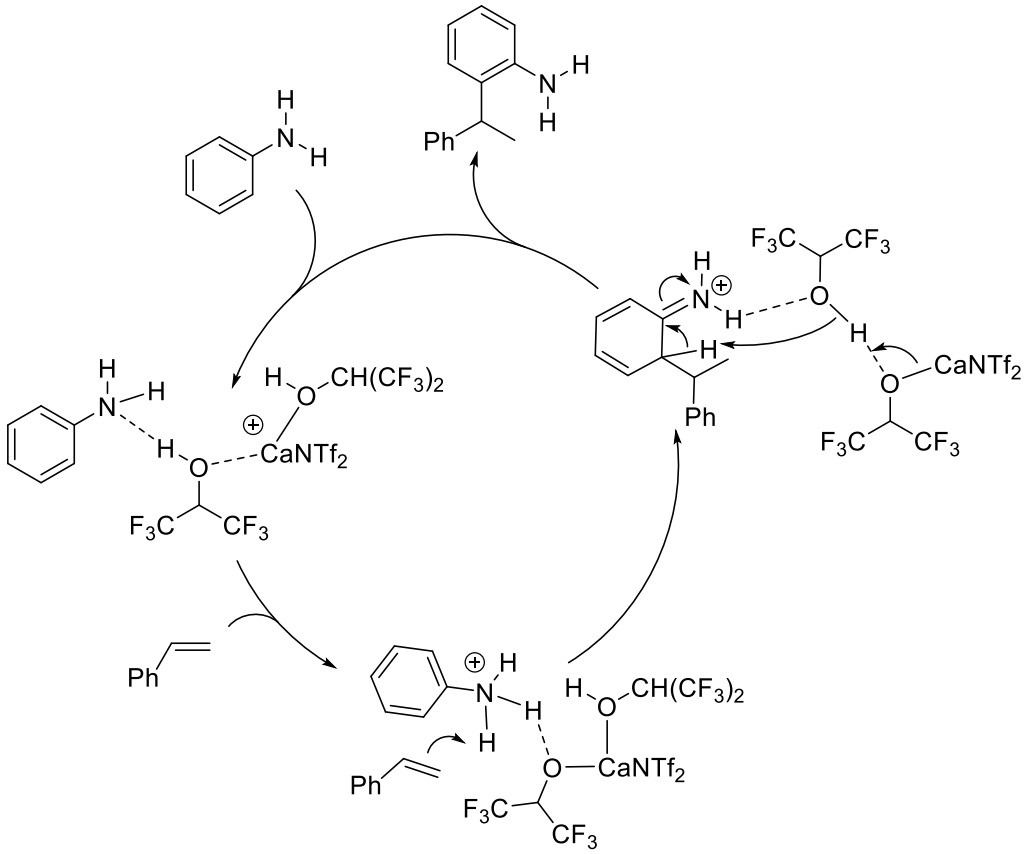

Figure 106. *Ortho*-alkylation of anilines by the [Ca{NTf_2}$_2$]/[Bu_4N][PF_6]/hfip catalytic system, with the proposed catalytic cycle.

7.2.5 Heterofunctionalization of alkenes

Other related Ca^{2+}-mediated heterofunctionalizations of alkenes, such as hydroalkoxylation, hydroamidation or hydroacyloxylation have also reported.[272-274] The hydroalkoxylation reaction, a ring-closing intramolecular process catalyzed by $[Ca\{NTf_2\}_2]/[Bu_4N][PF_6]$, exclusively generated the Markovnikov product, and occurred at room temperature (Figure 107). Formation of the pyran or furan was shown to be governed by angle of compression effects induced by the substituents in the α-position from the alcohol functional group. A wide range of aryl of alkyl substrates were investigated and with overall excellent yields. The intramolecular hydroamidation of unactivated alkenes using the three-component $[Ca\{NTf_2\}_2]/[Bu_4N][PF_6]$/hfip catalytic system also proceeded exclusively to generate the Markovnikov products (Figure 107). DFT calculations showed the $[\{NTf_2\}Ca(hfip)_n]^+$ moiety, generated *in situ* in the reaction medium, could activate the amide at a basic site of the $\{NTf_2\}^-$ ligand and the alkene with one acidic hfip proton.[273] A wide range of substrates were investigated, with the formation of the Markovnikov pyridinyl or pyrrolidinyl products occurring in excellent yields. The same study also reported the intermolecular hydroamidation of electronically deactivated styrenes using *p*-toluenesulfonamide. The cyclizing intramolecular hydroacyloxylation of unactivated alkenes has also been reported using the same catalytic system (Figure 107).[274]

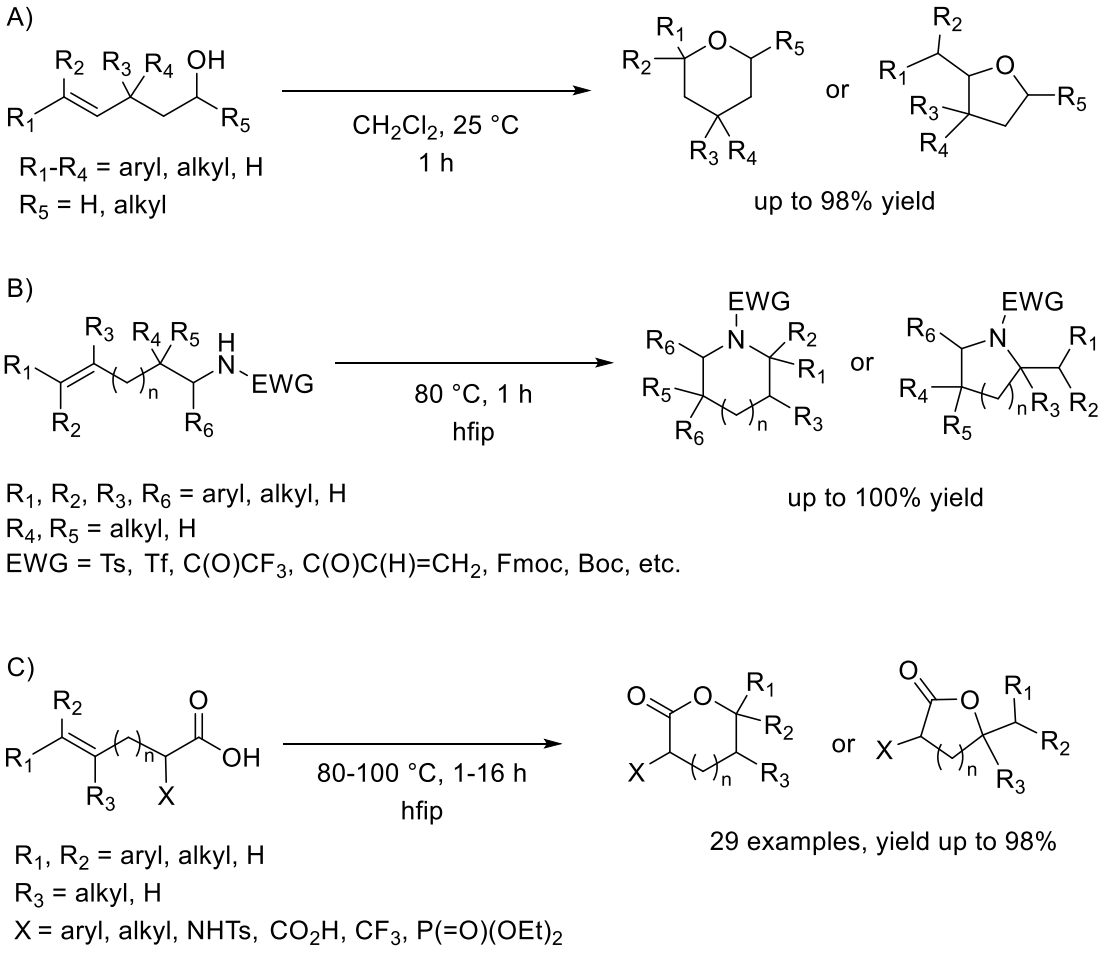

Figure 107. $[Ca\{NTf_2\}_2]/[Bu_4N][PF_6]$ catalytic system (loading 5 mol%) for the ring-closing hydroalkoxylation (A) hydroamidation (with hfip; B) and hydroacyloxylation (with hfip; C) of alkenes.

7.2.6 Cyclic rearrangements

7.2.6.1 Nazarov cyclisation

In 2014, the calcium-catalyzed Nazarov electrocyclization using the [Ca{NTf_2}$_2$]/[Bu_4N][PF_6] catalytic system was described.[275] This 4π conrotatory ring closure is used to generate cyclopentanone compounds.[276-278] A range of substrates were investigated, which included electron rich and electron poor aryl and alkyl substituted species (Figure 108). The cyclizations gave generally good yields (74-99%). The reactions showed good selectivity, favoring formation of the *trans* product with diastereomeric ratios in the range 92:8 to 98:2. The beneficial role in this cyclisation of the counter-ion PF_6^-, thought to exacerbate the Lewis acidity of the metal cation for instance by comparison with BF_4^- or I^-, was specifically highlighted.

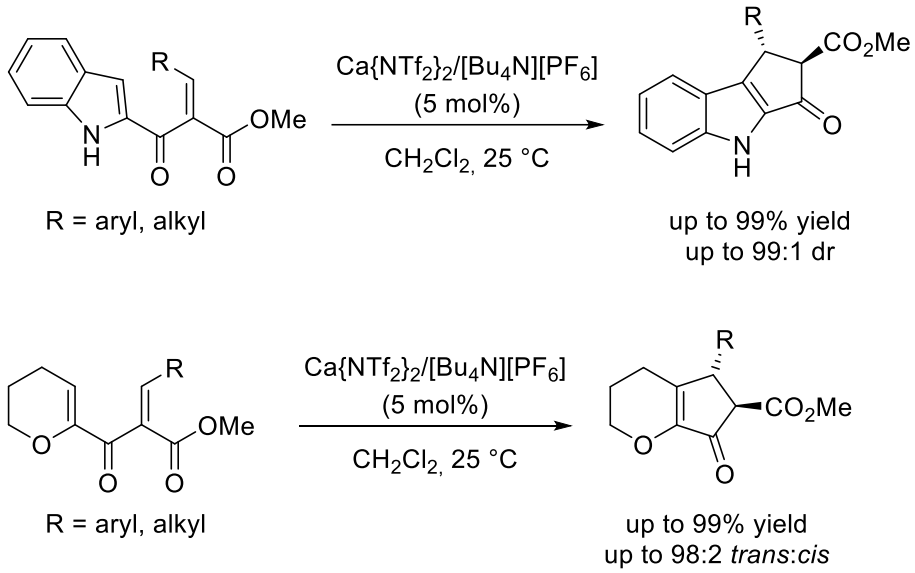

Figure 108. Calcium-catalyzed intramolecular Nazarov cyclization.

7.2.6.2 Aza-Piancatelli cyclization

The Aza-Piancatelli cyclization has also been reported to be catalyzed by the three-component [Ca{NTf_2}$_2$]/[Bu_4N][PF_6]/hfip system.[279-281] This reaction consists of the transformation of 2-furylcarbinols into 4-aminocyclopentenones when anilines are employed as nucleophiles. The reaction is a development from the Piancatelli rearrangement, which is mostly used for the synthesis of prostaglandin derivatives or other natural products.[214,221,282,283] The Aza-Piancatelli cyclization proceeds via Lewis-acid catalyzed formation of an oxonium ion, which undergoes nucleophilic addition with the aniline, followed by a 4π-conrotatory electrocyclization (Figure 109, A). The process has been implemented both for regular Aza-Piancatelli reactions[280,281] and successive sequences of Aza-Piancatelli and Michael addition.[279] Early work on this reaction used the catalytic calcium Lewis-acid system [Ca{NTf_2}$_2$]/[Bu_4N][PF_6] in nitromethane (Figure 109, B).[280] The reaction was later developed using hfip as a solvent, which both increased the reactivity and allowed for a widening of the substrate scope (Figure 109, C).[281] As per the other systems using the [Ca{NTf_2}$_2$]/[Bu_4N][PF_6]/hfip catalytic system, the primary reactivity is derived from the Lewis-acidity of hfip, which is enhanced by *in situ* generated [Ca{NTf_2}][PF_6]. This was highlighted by the fact that some of the Aza-Piancatelli reactions

could proceed only in the presence of hfip with catalytic $HNTf_2$, although higher yields were obtained with the $[Ca\{NTf_2\}_2]/[Bu_4N][PF_6]$/hfip system. More recently, the reaction has been used to synthesize natural products (Figure 109, D).[279] Finally, in another sequential process, the Aza-Piancatelli reaction of propargylic amines, extended by a copper(II)-catalyzed hydroamination reaction, was used to generate substituted cyclopenta[*b*]pyrroles in a one-pot protocol (not shown).[283-285]

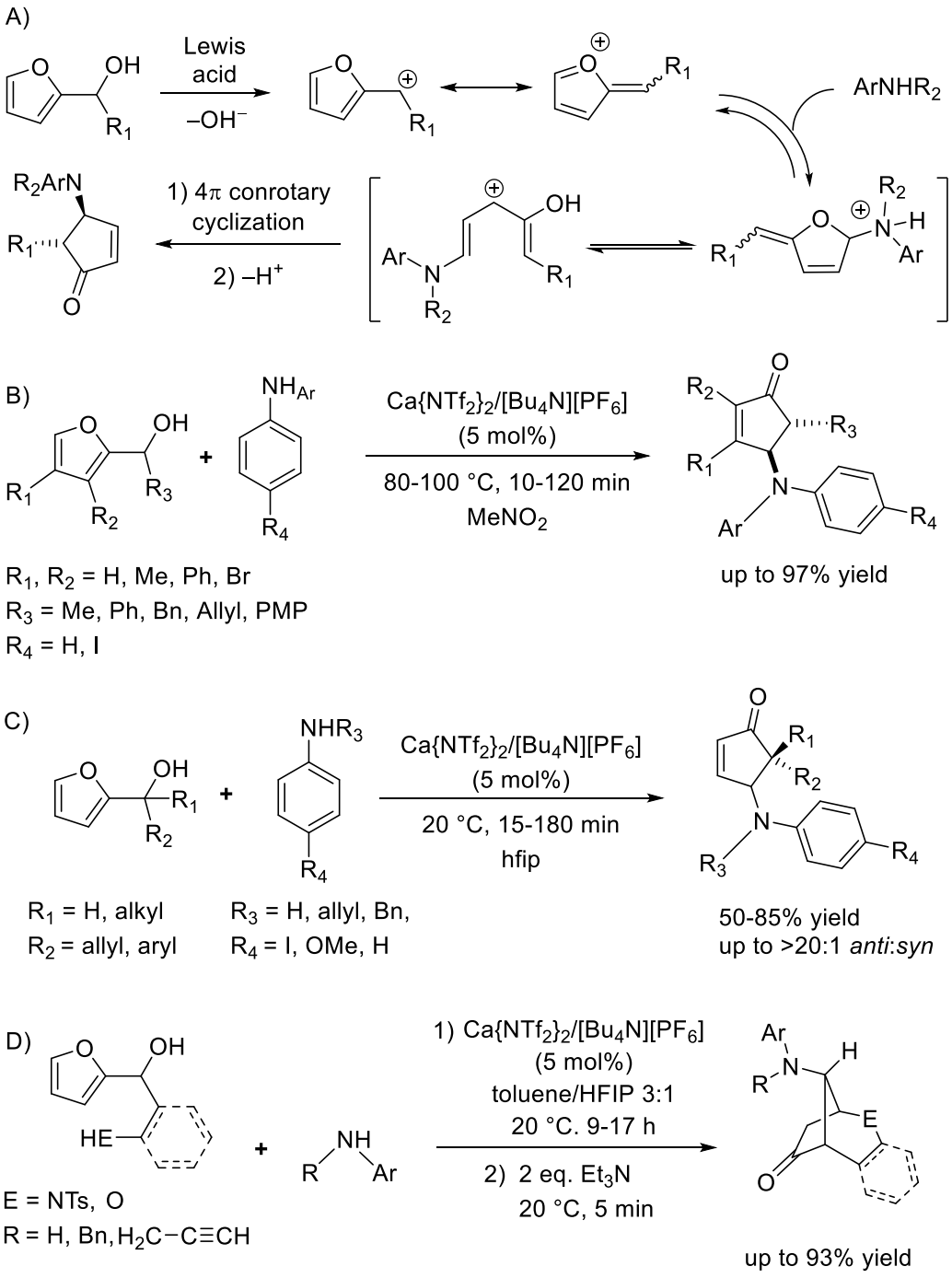

Figure 109. Calcium-catalyzed Aza-Piancatelli reaction: A) Simplified reaction pathway; B) Reactions in nitromethane; C) Reaction in hfip; D) Aza-Piancatelli reaction - Michael addition sequence.

7.2.7 Ca^{2+}-catalyzed dehydroxylation reactions

Alcohols are among the most common groups of organic chemistry. As such, reactions that allow direct functionalization of alcohol-containing substrates are highly desirable, especially if these reactions also have good chemoselectivity and stereoselectivity. However, due to the poor nature of the OH^- anion as a leaving group, hydroxyls often have to be substituted or transformed into halides, carboxylates or carbonates prior to subsequent derivatization.[214] Perhaps surprisingly, Ca^{2+} in almost unparalleled in its high proficiency for dihydroxylation of alcohols at room temperature. A general reaction manifold is sketched in Figure 110. The initial reactivity between a L_2Ca species and an alcohol results in a σ-bond metathesis step induced by the polarization of the Ca^{2+} cation; a second alcohol moiety may assist in the stabilization of the transition state. The resulting L^-R^+ moiety reacts with a nucleophile to generate the desired Nu-R compound and a protonated ligand species, which reacts slowly with the poorly soluble heteroleptic calcium hydroxide species to regenerate the catalyst L_2Ca. The ligand L^- used in these reactions is usually $\{NTf_2\}^-$ which is capable of readily stabilizing the negative charge through extensive delocalization. As a carbocation R^+ plays a role in the proposed mechanism, the regular constraints of carbocation formation dictate the substrate scope available for the reaction.

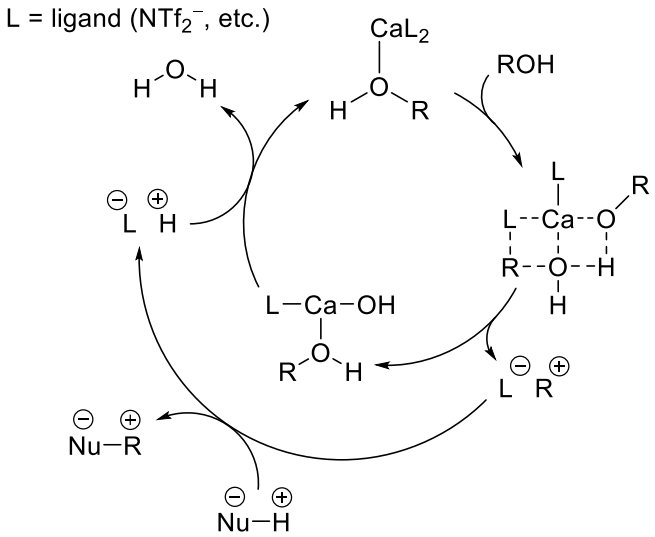

Figure 110. Proposed mechanistic pathway for the calcium-catalyzed dehydroxylation of alcohols.

Several reactions making use of the binary $[Ca\{NTf_2\}_2]/[Bu_4N][PF_6]$ catalytic system were described. The seminal work of calcium Lewis acid catalyzed dehydroxylation of electron-rich arenes with alcohols was reported by Niggemann in 2010 to give the corresponding substituted aryl products (Figure 111, A).[268] The substrate scope of the reaction was later extended to include anilines, carbamates, sulfonamides and propargyl alcohols tethered to β-ketoesters, before a microwave-assisted nitrile variation of the Ritter reaction was also developed (Figure 111, B).[286,287] The dehydroxylation strategy using has also been used with an oxime to generate amides via a Beckmann rearrangement.[288] Alkylation has also been achieved using unsaturated silicon and boron compounds as sources of nucleophilic carbon (Figure 111, C).[289,290] The diastereoselective formation of highly substituted indanes and tetralines, from diastereomeric mixtures of alcohols, has been reported through a strategy that exploits a Wagner-Meerwein hydride shift (Figure 111, D).[291] In a somewhat

similar reaction, a vinyl cation tethered to an olefin has been used to generate diastereoselective bicyclic amines via a dynamic multicomponent reaction;[292] the process relied on the high Lewis-acidity of the Ca^{2+} cation for the generation of the most thermodynamically stable amine product.

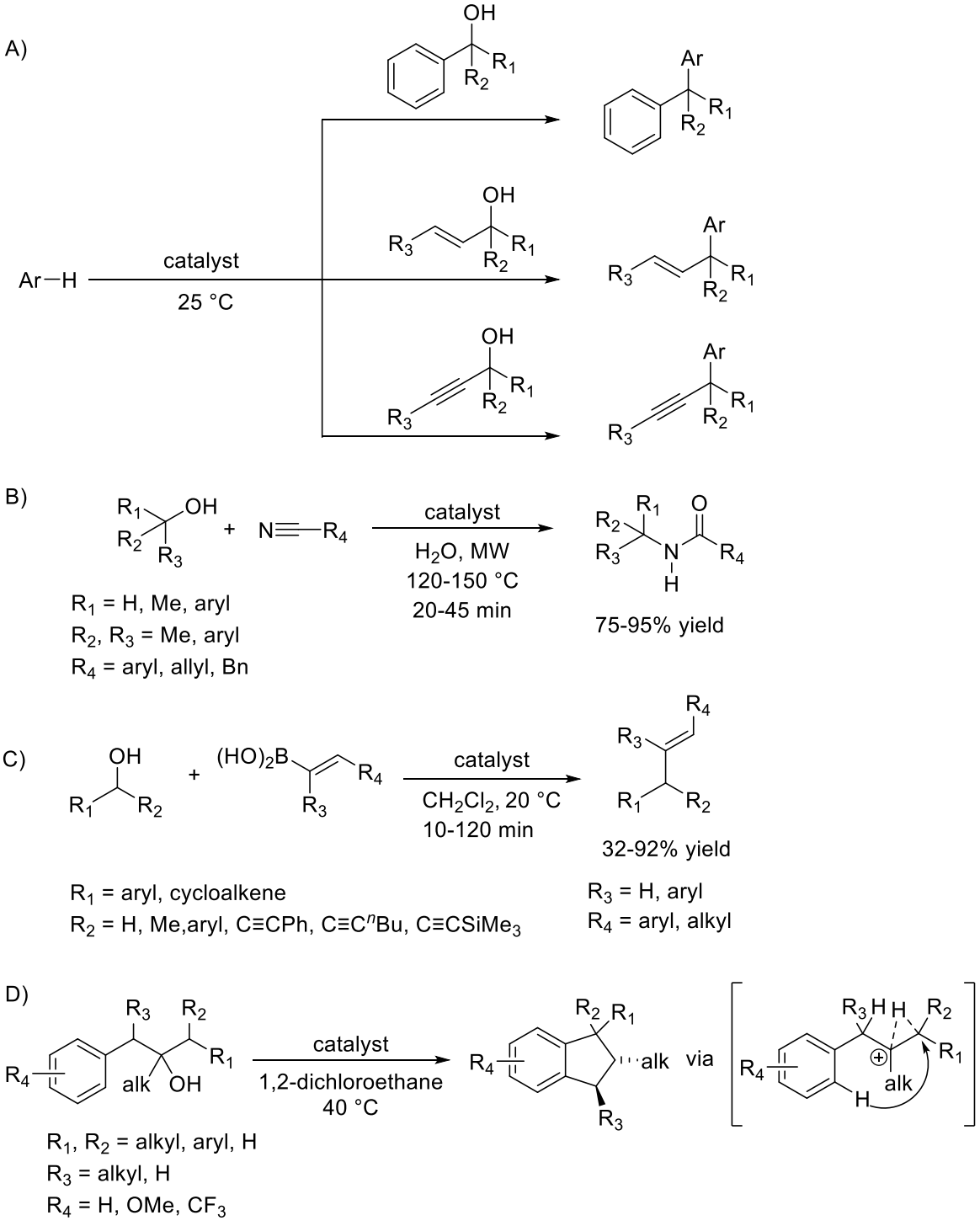

Figure 111. Selected dehydroxylation reactions catalyzed by the binary $[Ca\{NTf_2\}_2]/[Bu_4N][PF_6]$ system (5 mol% of each component). A) Arylation of alcohols. B) Microwave-assisted Ritter reaction. C) Alkenylation of allyl alcohols D) Stereo-redistributing diastereoselective synthesis of indanes.

In another multicomponent reaction catalyzed by [Ca{OTf}$_2$]/[Bu$_4$N][PF$_6$], a sequence starting with enolization of a cyclic diketone followed by addition to a dehydroxylated propargylic alcohol and concluding with a Michael cyclization was used to generate highly substituted furans (Figure 112).[293] A similar dihydroxylation-addition-cyclization process has also been used for the synthesis of other substituted furans and pyrans.[294,295]

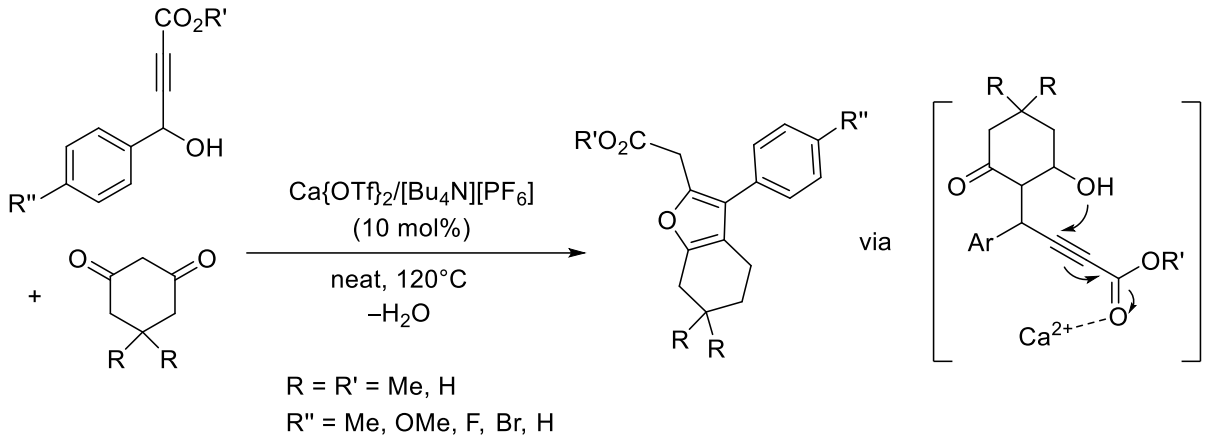

Figure 112. Multistep synthesis of functionalized furans catalyzed by [Ca{OTf}$_2$]/[Bu$_4$N][PF$_6$].

Allenyl cations accessed as a mesomeric form of propargylic carbocations have also been used in cycloisomerizations. These reactions mimic the chemistry coinage metals for the construction of a range of valuable products.[296] The seminal work was the cycloisomerization of an enynol to generate substituted cyclopropanes using [Ca{NTf$_2$}$_2$]/[Bu$_4$N][X] as the catalytic system, where X$^-$ was the PF$_6^-$ or SbF$_6^-$ anion (Figure 113).[297] The proposed mechanism, which was supported with DFT calculations, suggested an initial dehydroxylation step followed by a cascading range of C-C bond forming steps and a cyclization. Other Ca-catalyzed allenyl-cyclopropyl rearrangements have also have also been studied.[298]

8 In lieu of a conclusion

The past 20 years have taught us that far from being simple and intricate derivatives of magnesium, unable to compete with other systems for metal-promoted homogeneous catalysis, the large alkaline-earth metals calcium, strontium and barium can be used to assemble competent catalysts and precatalysts for a growing array of organic transformations. Beyond the simple derivatization of the behavior observed with their lanthanoid cousins, the large alkaline earths have been used to catalyze new, original reactions. Along the way, several paradigms have been broken. The efforts paid to elucidate mechanistic pathways by combining experimental and theoretical (DFT) studies have shown that the initially conceptualized reaction pathways, such as those depicted in Figures 6 and 7, are often over-simplistic, if not plainly wrong. In short, the three heavy alkaline earths display a reactivity of their own, and this is a very positive omen indeed. Far from being a mature field, Ae-mediated catalysis is on a fast-rising curve. We can expect it to grow much beyond the initial hydrofunctionalization and dehydrocoupling catalysis that were abundantly investigated in the early years. Quite the contrary, the story is still very fresh, many exciting catalyzed reactions lie ahead, and the scope of alkaline earth catalysis now appears to be limited only by the imagination of the synthetic chemists astute enough to tackle this field. It is undeniable that some inspiration may be gained from the much more

developed chemistry of magnesium and that of the lanthanides. But beyond this, exciting discoveries disclosed in recent years, such as the calcium-catalyzed non-dehydrogenative desilacoupling of silaboranes and amines,[209] or the alkylation of aromatic rings[18,194] show that boundaries need not be set. The field does face ongoing challenges; catalyst loadings required for many catalytic systems are often significantly higher than the for similar transition metal or organo- catalyzed transformations, hampering the commercial development of industrial processes based on this chemistry. Asymmetric alkaline-earth catalysis is another area where major improvements are required. However, the impressive molecular reactivity exhibited by unusual alkaline-earth complexes will likely lead to further development in the future. Many potential milestones still lie ahead, and the very first Ca(I)-Ca(I) complex is certainly one of many valid entry points in this respect.[299] Barium is a metal that is certainly difficult to tame and therefore it has perhaps been less investigated than its lighter congeners, but recent experience has shown that the efforts are often highly rewarding.[28] These countless challenges and opportunities are now well recognized by the community of organometallic chemists, and the growing number of groups across the world that design and implement alkaline-earth complexes for organic synthesis is a very positive sign of the vitality of the field. May it continue!

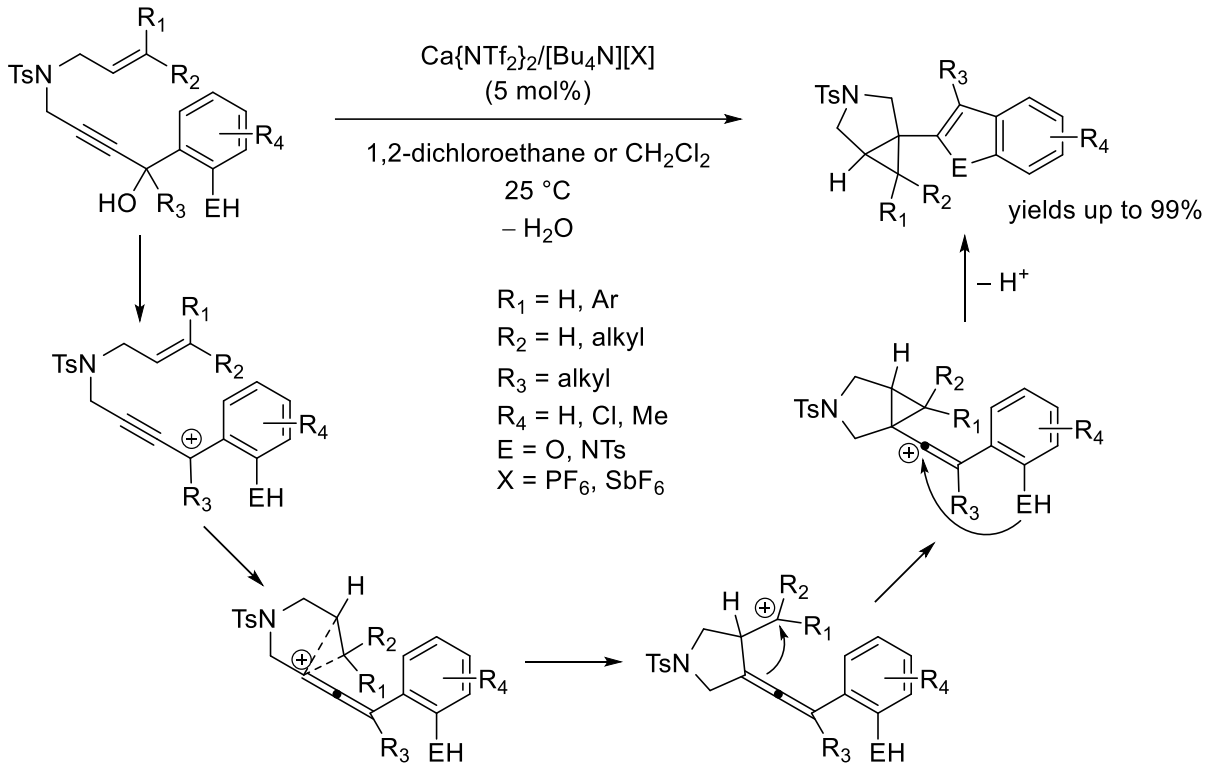

Figure 113. Cycloisomerization of an enynol and formation cyclopropanes using [Ca{NTf_2}$_2$]/[Bu_4N][X].

Acknowledgements

Y. S. thanks the *Centre National de la recherche Scientifique* (CNRS) for support.

Reference List

1 Dagorne, S.; Bellemin-Laponnaz, S. Group 13 metal-Mediated Organic Reactions. In *The Group 13 Metals Aluminium, Gallium and Thallium: Chemical Patterns and Peculiarities*; Aldridge, S.; Downs, J. D., Eds.; John Wiley and Sons, Ltd., Chichester, 2011; pp. 654–700.

2 Otera, J.; Biesemans, M.; Pinoie, V.; Poelmans, K.; Willem, R. Green Organotin Catalysts. In *tin Chemistry: Fundamentals, Frontiers and Applications*; Davies, A. G.; Gielen, M.; Panel, K. H.; Tiekink, E. R. T., Eds; John Wiley and Sons, Ltd., Chichester, 2008; pp. 667–680.

3 Blank, W. J.; Hessell, E. T. Organotin Catalysts for Isocyanate Reactions. In *tin Chemistry: Fundamentals, Frontiers and Applications*; Davies, A. G.; Gielen, M.; Panel, K. H.; Tiekink, E. R. T., Eds; John Wiley and Sons, Chichester, 2008; pp. 681–700.

4 Fouquet, E. Synthetic Applications of Organic Germanium, Tin and Lead Compounds. In *The Chemistry of Organic Germanium, Tin and Lead Compounds*. Rappoport, Z., Ed.; John Wiley and Sons, Chichester, 2002; Vol. 2, pp. 1333–1400.

5 *Early Main Group Metal Catalysis.* Harder, S., Ed.; Wiley-VCH, Weinheim, 2020.

6 Harder, S. *Chem. Rev.* **2010**, *110*, 3852–3876.

7 Barrett, A. G. M.; Crimmin, M. R.; Hill, M. S.; Procopiou, P. A. *Proc. R. Soc. A*, **2010**, *466*, 927–963.

8 Carpentier, J.-F.; Sarazin, Y. *Top. Organomet. Chem.* **2013**, *45*, 141–189.

9 Crimmin, M. R.; Hill, M. S. *Top. Organomet. Chem.* **2013**, *45*, 191–241.

10 Arrowsmith, M.; Hill; M. S.; Alkaline-Earth Chemistry: Applications in Catalysis. In *Comprehensive Inorganic Chemistry II*. Reedijk, J.; Poeppelmeier, K. Eds; Elsevier, 2013; Vol. 1, pp. 1189–1216.

11 Bhoelan, B. S.; Stevering, C. H.; Bogg, V. D.; Heyden, V. D. *Clin. Toxicol.* **2014**, *52*, 584–593.

12 McNeill, I. R.; Isoardi, K. Z. *Toxicol. Commun.* **2019**, *3*, 88–90.

13 Shannon, R. *Acta Cryst. Sect. A*, **1976**, *32*, 751–767.

14 Krieck, S.; Görls, H.; Yu, L.; Reiher, M.; Westerhausen, M. *J. Am. Chem. Soc.* **2009**, *131*, 2977–2985.

15 Rösch, B.; Gentner, T. X.; Langer, J.; Färber, C.; Eyselein, J.; Zhao, L.; Ding, C.; Frenking, G.; Harder, S. *Science* **2021**, *371*, 1125–1128.

16 Hill, M. S.; Liptrot, D. J.; Weetman, C. *Chem. Soc. Rev.* **2016**, *45*, 972–988.

17 Schlenk, W.; Schlenk, W., Jr. *Chem. Ber.* **1929**, *62*, 920–924.

18 Wilson, A. S. S.; Hill, M. S.; Mahon, M. F.; Dinoi, C.; Maron, L. *Science* **2017**, *358*, 1168–1171.

19 Harder, S.; Brettar, J. *Angew. Chem. Int. Ed.* **2006**, *45*, 3474–3478.

20 Ruspic, C.; Nembenna, S.; Hofmeister, A.; Magull, J.; Harder, S.; Roesky, H. W. *J. Am. Chem. Soc.* **2006**, *128*, 15000–15004.

21 Nembenna, S.; Roesky, H. W.; Nagendran, S.; Hofmeister, A.; Magull, J.; Wilbrandt, P-J.; Hahn, M. *Angew. Chem. Int. Ed.* **2007**, *46*, 2512–2514.

22 Avent, A. G.; Crimmin, M. R.; Hill, M. S.; Hitchcock, P. B. *Dalton Trans.* **2005**, 278–284.

23 Gentner, T. X.; Rösch, B.; Thum, K.; Langer, J.; Ballmann, G.; Pahl, J.; Donaubauer, W. A.; Hampel, F.; Harder, S. *Organometallics* **2019**, *38*, 2485–2493.

24 Ballmann, G.; Rösch, B.; Harder, S. *Eur. J. Inorg. Chem.* **2019**, 3683–3689.

25 Chapple, P. M.; Kahlal, S.; Cartron, J.; Roisnel, T.; Dorcet, V.; Cordier, M.; Saillard, J.-Y.; Carpentier, J.-F.; Sarazin, Y. *Angew. Chem. Int. Ed.* **2020**, *59*, 9120–9126.

26 Chapple, P. M.; Cordier, M.; Dorcet, V.; Roisnel, T.; Carpentier, J.-F.; Sarazin, Y. *Dalton Trans.* **2020**, *49*, 11878–11889.

27 Liu, B.; Roisnel, T.; Carpentier, J.-F.; Sarazin. Y. *Angew. Chem. Int. Ed.* **2012**, *51*, 4943–4946.

28 Chapple, P. M.; Sarazin, Y. *Eur. J. Inorg. Chem.* **2020**, 3321–3346.

29 Buchanan, W. D.; Allis, D. G.; Ruhlandt-Senge, K. *Chem. Commun.* **2010**, *46*, 4449–4465.

30 Sarazin, Y.; Roşca, D.; Poirier, V.; Roisnel, T.; Silvestru, A.; Maron, L.; Carpentier, J.-F. *Organometallics* **2010**, *29*, 6569–6577.

31 Mukherjee, D.; Shirase, S.; Beckerle, K.; Spaniol, T. P.; Mashima, K.; Okuda, J. *Dalton Trans.* **2017**, *46*, 8451–8457.

32 Roşca, S.-C.; Roisnel, T.; Dorcet, V.; Carpentier, J.-F.; Sarazin, Y. *Organometallics* **2014**, *33*, 5630−5642.

33 Roueindeji, H.; Ratsifitahina, A.; Roisnel, T.; Dorcet, V.; Kahlal, S.; Saillard, J.-Y.; Carpentier, J.-F.; Sarazin, Y. *Chem. Eur. J.* **2019**, *25*, 8854–8864.

34 Fischer, C. A.; Rösch, A.; Elsen, H.; Ballmann, G.; Wiesinger, M.; Langer, J.; Färber, C.; Harder, S. *Dalton Trans.* **2019**, *48*, 6757–6766.

35 Hauber, S. O.; Lissner, F.; Deacon, G. B.; Niemeyer, M. *Angew. Chem. Int. Ed.* **2005**, *44*, 5871–5875.

36 Roşca, S.-C.; Dinoi, C.; Caytan, E.; Dorcet, V.; Etienne, M.; Carpentier, J.-F. ; Sarazin, Y. *Chem. Eur. J.* **2016**, *22*, 6505–6509.

37 Westerhausen, M. *Inorg. Chem.* **1991**, *30*, 96–101.

38 Vaartstra, B. A.; Huffman, J. C.; Streib, W. E.; Caulton, K. G. *Inorg. Chem.* **1991**, *30*, 121–125.

39 Cloke, F. G. N.; Hitchcock, P. B.; Lappert, M. F.; Lawless, G. A.; Royo, B. *J. Chem. Soc. Chem. Commun.* **1991**, 724–726.

40 Hanusa, T. P. *Chem. Rev.* **1993**, *93*, 1023–1036.

41 Westerhausen, M. *Coord. Chem. Rev.* **1998**, *176*, 157–210.

42 Hanusa, T. P. *Coord. Chem. Rev.* **2000**, *210*, 329–367.

43 Alexander, J. S.; Ruhlandt-Senge, K. *Eur. J. Inorg. Chem.* **2002**, 2761–2774.

44 Hanusa, T. P. *Organometallics* **2002**, *21*, 2559-2571.

45 Chisholm, M. H.; Gallucci, J.; Phomphrai, K. *Chem. Commun.* **2003**, 48–49.

46 Chisholm, M. H.; Gallucci, J.; Phomphrai, K. *Inorg. Chem.* **2004**, *43*, 6717–6725.

47 Crimmin, M. R.; Casely, I. J.; Hill, M. S. *J. Am. Chem. Soc.* **2005**, *127*, 2042–2043.

48 Hill, M. S. Miscellaneous Reactions. In *Early Main Group Metal Catalysis*. Harder, S., Ed.; Wiley-VCH, Weinheim, 2020, pp. 347–372.

49 Waterman, R.; *Organometallics* **2013**, *32*, 7249–7263.

50 Crimmin, M. R.; Arrowsmith, M.; Barrett, A. G. M.; Casely, I. J.; Hill, M. S.; Procopiou, P. A. *J. Am. Chem. Soc.* **2009**, *131*, 9670–9685.

51 Avent, A. G.; Crimmin, M. R.; Hill, M. S.; Hitchcock, P. B. *Dalton Trans.* **2004**, 3166–3168.

52 Barrett, A. G. M.; Crimmin, M. R.; Hill, M. S.; Kociok-Köhn, G.; Lachs, J. R.; Procopiou, P. A. *Dalton Trans.* **2008**, 1292–1294.

53 Barrett, A. G. M.; Casely, I. J.; Crimmin, M. R.; Hill, M. S.; Lachs, J. R.; Mahon, M. F.; Procopiou, P. A. *Inorg. Chem.* **2009**, *48*, 4445–4453.

54 Arrowsmith, M.; Crimmin, M. R.; Barrett, A. G. M.; Hill, M. S.; Kociok-Köhn, G.; Procopiou, P. A. *Organometallics* **2011**, *30*, 1493–1506.

55 Hong, S.; Marks, T. J. *Acc. Chem. Res.* **2004**, *37*, 673–686.

56 Dunne, J. F.; Fulton, D. B.; Ellern, A.; Sadow, A. D. *J. Am. Chem. Soc.* **2010**, *132*, 17680–17683.

57 Tobisch, S. *Chem. Eur. J.* **2011**, *17*, 14974–14986.

58 Barrett, A. G. M.; Crimmin, M. R.; Hill, M. S.; Hitchcock, P. B.; Kociok-Köhn, G.; Procopiou, P. A. *Inorg. Chem.* **2008**, *47*, 7366–7376.

59 Datta, S.; Roesky, P. W.; Blechert, S. *Organometallics* **2007**, *26*, 4392–4394.

60 Datta, S.; Gamer, M. T.; Roesky, P. W. *Organometallics* **2008**, *27*, 1207–1213.

61 Liu, B.; Roisnel, T.; Carpentier, J.-F.; Sarazin, Y. *Chem. Eur. J.* **2013**, *19*, 2784–2802.

62 Liu, B.; Roisnel, T.; Carpentier, J.-F.; Sarazin, Y. *Chem. Eur. J.* **2013**, *19*, 13445–13462.

63 Jenter, J.; Köppe, R.; Roesky, P. W. *Organometallics* **2011**, *30*, 1404–1413.

64 Arrowsmith, M.; Hill, M. S.; Kociok-Köhn, G. *Organometallics* **2011**, *30*, 1291–1294.

65 Arrowsmith, M.; Hill, M. S.; Kociok-Köhn, G. *Organometallics* **2009**, *28*, 1730–1738.

66 Tobisch, S. *Chem. Eur. J.* **2015**, *21*, 6765–6779.

67 Zhang, X.; Emge, T. J.; Hultzsch, K. C. *Angew. Chem. Int. Ed.* **2012**, *51*, 394–398.

68 Zhang, X.; Tobisch, S.; Hultzsch, K. C. *Chem. Eur. J.* **2015**, *21*, 7841–7857.

69 Buch, F.; Harder, S. *Z. Naturforsch.* **2008**, *63b*, 169–177.

70 Wixey, J. S.; Ward, B. D. *Chem. Commun.* **2011**, *47*, 5449–5451.

71 Wixey, J. S.; Ward, B. D. *Dalton Trans.*, **2011**, *40*, 7693–7696.

72 Nixon, T. D.; Ward, B. D. *Chem. Commun.* **2012**, *48*, 11790–11792.

73 Neal, S. R.; Ellern, A.; Sadow, A. D. *J. Organomet. Chem.* **2011**, *696*, 228–234.

74 Stegner, P. C.; Eyselein, J.; Ballmann, G. M.; Langer, J.; Schmidt, J.; Harder, S. *Dalton Trans.* **2021**, *50*, 3178-3185.

75 Barrett, A. G. M.; Brinkmann, C.; Crimmin, M. R.; Hill, M. S.; Hunt, P.; Procopiou, P. A. *J. Am. Chem. Soc.* **2009**, *131*, 12906–12907.

76 Brinkmann, C.; Barrett, A. G. M.; Hill, M. S.; Procopiou, P. A. *J. Am. Chem. Soc.* **2012**, *134*, 2193–2207.

77 Tobisch, S. *Chem. Eur. J.* **2014**, *20*, 8988–9001.

78 Lachs, J.; Barrett, A. G. M.; Crimmin, M. R.; Kociok-Köhn, G.; Hill, M. S.; Mahon, M. F.; Procopiou, P. A. *Eur. J. Inorg. Chem.* **2008**, 4173–4179.

79 Barrett, A. G. M.; Boorman, T. C.; Crimmin, M. R.; Hill, M. S.; Kociok-Köhn, G.; Procopiou, P. A. *Chem. Commun.* **2008**, 5206–5208.

80 Barrett, A. G. M.; Crimmin, M. R.; Hill, M. S.; Hitchcock, P. B.; Procopiou, P. A. *Dalton Trans.* **2008**, 4474–4481.

81 Glock, C.; Görls, H.; Westerhausen, M. *Chem. Commun.* **2012**, *48*, 7094–7096.

82 Glock, C.; Görls, H.; Westerhausen, M. *Dalton Trans.* **2011**, *40*, 8108–8113.

83 Younis, F. M.; Krieck, S.; Görls, H.; Westerhausen, M. *Dalton Trans.* **2016**, *45*, 6241–6250.

84 Ziemann, S.; Krieck, S.; Görls, H.; Westerhausen, M. *Organometallics* **2018**, *37*, 924–933.

85 Younis, F. M.; Krieck, S.; Görls, H.; Westerhausen, M. *Organometallics* **2015**, *34*, 3577–3585.

86 Glock, C.; Younis, F. M.; Ziemann, S.; Görls, H.; Imhof, W.; Krieck, S.; Westerhausen, M. *Organometallics* **2013**, *32*, 2649–2660.

87 Douglass, M. R.; Marks, T. J. *J. Am. Chem. Soc.* **2000**, *122*, 1824–1825.

88 Douglass, M. R.; Stern, C. L.; Marks, T. J. *J. Am. Chem. Soc.* **2001**, *123*, 10221–10238.

89 Takaki, K.; Koshoji, G.; Komeyama, K.; Takeda, M.; Shishido, T.; Kitani, A.; Takehira, K. *J. Org. Chem.* **2003**, *68*, 6554–6565.

90 Crimmin, M. R.; Barrett, A. G. M.; Hill, M. S.; Hitchcock, P. B.; Procopiou, P. A. *Organometallics* **2007**, *26*, 2953–2956.

91 Hu, H. ; Cui, C. *Organometallics* **2012**, *31*, 1208–1211.

92 Anga, S. ; Carpentier, J.-F. ; Panda, T. K. ; Roisnel, T. ; Sarazin, Y. *RSC Adv.* **2016**, *6*, 57835–57843.

93 Basalov, I. V., Yurova, O. S., Cherkasov, A. V., Fukin, G. K., Trifonov, A. A. *Inorg. Chem.* **2016**, *55*, 1236–1244.

94 Lapshin, I. V.; Yurova, O. S.; Basalov, I. V.; Yu. Rad'kov V.; Musina, E. I.; Cherkasov, A. V.; Fukin, G. K.; Karasik, A. A.; Trifonov, A. A. *Inorg. Chem.* **2018**, *57*, 2942–2952.

95 Tolpygin, A. O.; Cherkasov, A. V.; Fukin, G. K.; Kovylina, T. A.; Lyssenko, K. A.; Trifonov, A. A. *Eur. J. Inorg. Chem.* **2019**, 4289–4296.

96 Lapshin, I. V.; Basalov, I. V.; Lyssenko, K. A.; Cherkasov, A. V.; Trifonov, A. A. *Chem. Eur. J.* **2019**, *25*, 459–463.

97 Selikhov, A. N.; Plankin, G. S.; Cherkasov, A. V.; Shavyrin, A. S.; Louyriac, E.; Maron, L.; Trifonov, A. A. *Inorg. Chem.* **2019**, *58*, 5325–5334.

98 Basalov, I. V.; Liu, B.; Roisnel, T.; Cherkasov, A. V.; Fukin, G. K.; Carpentier, J.-F.; Sarazin, Y.; Trifonov, A. A. *Organometallics* **2016**, *35*, 3261–3271.

99 Roşca, S.-C.; Roisnel, T.; Dorcet, V.; Carpentier, J.-F.; Sarazin, Y. *Organometallics* **2014**, *33*, 5630–5642.

100 He, M.; Gamer, M. T.; Roesky, P. W. *Organometallics* **2016**, *35*, 2638–2644.

101 Ward, B. J.; Hunt, P. A. *ACS Catal.* **2017**, *7*, 459–468.

102 Ghebreab, M. B.; Bange, C. A.; Waterman, R., *J. Am. Chem. Soc.* **2014**, *136*, 9240–9243.

103 Geer, A. M.; Serrano, A. L.; de Bruin, B.; Ciriano, M. A.; Tejel, C. *Angew. Chem. Int. Ed.* **2015**, *54*, 472–475.

104 Bange, C. A.; Ghebreab, M. B.; Ficks, A.; Mucha, N. T.; Higham, L.; Waterman, R. *Dalton Trans.* **2016**, 45, 1863–1867.

105 Bange, C. A.; Conger, M. A.; Novas, B. T.; Young, E. R.; Liptak, M. D.; Waterman, R. *ACS Catal.* **2018**, *8*, 6230–6238.

106 Al-Shboul, T. M. A.; Görls, H.; Westerhausen, M. *Inorg. Chem. Commun*. **2008**, *11*, 1419**–**1421.

107 Al-Shboul, T. M. A.; Pálfi, V. K.; Yu, L.; Kretschmer, R.; Wimmer, K.; Fischer, R.; Görls, H.; Reiher, M.; Westerhausen, M. *J. Organomet. Chem.* **2011**, *696*, 216–227.

108 Crimmin, M. R.; Barrett, A. G. M.; Hill, M. S.; Hitchcock, P. B.; Procopiou, P. A. *Organometallics* **2008**, *27*, 497–499.

109 Al-Shboul, T. M. A.; Volland, G.; Görls, H.; Westerhausen, M. *Z. Anorg. Allg. Chem.* **2009**, *635*, 1568–1572.

110 Fener, B. E.; Scheler, P.; Ueberschaar, N.; Bellstedt, P.; Görls, H.; Krieck, S.; Westerhausen, M. *Chem. Eur. J.* **2020**, *26*, 7235–7243.

111 Al-Shboul, T. M. A.; Görls, H.; Krieck, S.; Westerhausen, M. *Eur. J. Inorg. Chem.* **2012**, 5451–5455.

112 Härling, S.; Greiser, J.; Al-Shboul, T. M. A.; Görls, H.; Krieck, S.; Westerhausen, M. *Aust. J. Chem.* **2013**, *66*, 1264–1273.

113 Liu, B. ; Carpentier, J.-F. ; Sarazin, Y., *Chem. Eur. J.* **2012**, *18*, 13259–13264.

114 Brinkmann, C.; Barrett, A. G. M.; Hill, M. S.; Procopiou, P. A.; Reid, S. *Organometallics* **2012**, *31*, 7287–7297.

115 Barrett, A. G. M.; Crimmin, M. R.; Hill, M. S.; Hitchcock, P. B.; Lomas, S. L.; Mahon, M. F.; Procopiou, P. A.; Suntharalingam, K. *Organometallics* **2008**, *27*, 6300–6306.

116 Arrowsmith, M.; Crimmin, M. R.; Hill, M. S.; Lomas, S. L.; Sae Heng, M.; Hitchcock, P. B.; Kociok-Köhn, G. *Dalton Trans.* **2014**, *43*, 14249–14256.

117 Arrowsmith, M.; Shepherd, W. M. S.; Hill, M. S.; Kociok-Köhn, G. *Chem. Commun.* **2014**, *50*, 12676–12679.

118 Arrowsmith, M.; Hill, M. S.; Kociok-Köhn, G. *Chem. Eur. J.* **2015**, *21*, 10548–10557.

119 Sadow, A. D. Alkali and Alkaline Earth Element-Catalyzed Hydroboration Reactions. In *Early Main Group Metal Catalysis*. Harder, S., Ed.; Wiley-VCH, Weinheim, 2020, pp. 201–224.

120 Harder, S.; Spielmann, J. *J. Organomet. Chem.* **2012**, *698*, 7–14.

121 Brand, S.; Causero, A.; Elsen, H.; Pahl, J.; Langer, J.; Harder, S. *Eur. J. Inorg. Chem.* **2020**, 1728–1735.

122 Anker, M. D.; Arrowsmith, M.; Bellham, P.; Hill, M. S.; Kociok-Köhn, G.; Liptrot, D. J.; Mahon, M. F.; Weetman, C. *Chem. Sci.* **2014**, *5*, 2826–2830.

123 Buch, F.; Brettar, H.; Harder, S. *Angew. Chem. Int. Ed.* **2006**, *45*, 2741–2745.

124 Ruspic, C.; Spielmann, J.; Harder, S. *Inorg. Chem.* **2007**, *46*, 5320–5326.

125 Gauvin, R. M.; Buch, F.; Delevoye, L.; Harder, S. *Chem. Eur. J.* **2009**, *15*, 4382–4393.

126 Jochmann, P.; Davin, J. P.; Spaniol, T. P.; Maron, L.; Okuda, J. *Angew. Chem. Int. Ed.* **2012**, *51*, 4452–4455.

127 Schuhknecht, D.; Spaniol, T. P.; Maron, L.; Okuda, J. *Angew. Chem. Int. Ed.* **2020**, *59*, 310–314.

128 Leich, V.; Spaniol, T. P.; Maron, L.; Okuda, J. *Chem. Commun.* **2014**, *50*, 2311–2314.

129 Spielmann, J.; Harder, S. *Eur. J. Inorg. Chem.* **2008**, 1480–1486.

130 Elsen, H.; Fischer, C.; Knüpfer, C.; Escalona, A.; Harder, S. *Chem. Eur. J.* **2019**, *25*, 16141–16147.

131 Intemann, J.; Bauer, H.; Pahl, J.; Maron, L.; Harder, S. *Chem. Eur. J.* **2015**, *21*, 11452–11461.

132 Osborn, J. A.; Jardine, F. H.; Young, J. F.; Wilkinson, G. *J. Chem. Soc. A*, **1966**, 1711–1732.

133 Schrock, R. R.; Osborn, J. A. *J. Am. Chem. Soc.* **1976**, *98*, 2134–2143.

134 Crabtree, R. H. *Acc. Chem. Res.* **1979**, *12*, 331–337.

135 Slaugh, L. H. *Tetrahedron*, **1966**, *22*, 1741–1746.

136 Spielmann, J.; Buch, F.; Harder, S. *Angew. Chem. Int. Ed.* **2008**, *47*, 9434–9438.

137 Wilson, A. S. S.; Dinoi, C.; Hill, M. S.; Mahon, M. F.; Maron, L. *Angew. Chem. Int. Ed.* **2018**, *57*, 15500–15504.

138 Leich, V.; Spaniol, T.P.; Maron, L.; Okuda, J. *Angew. Chem. Int. Ed.* **2016**, *55*, 4794–4797.

139 Schuhknecht, D.; Lhotsky, C.; Spaniol, T.P.; Maron, L.; Okuda, J. *Angew. Chem. Int. Ed.* **2017**, *56*, 12367–12371.

140 Shi, X.; Hou, C.; Zhou, C.; Song, Y. Cheng, J. *Angew. Chem. Int. Ed.* **2017**, *56*, 16650–16653.

141 Shi, X.; Cheng, J. *Dalton Trans.* **2019**, *48*, 8565–8568.

142 Shi, X.; Hou, C.; Zhao, L.; Deng, P.; Cheng, J. *Chem. Commun*. **2020**, *56*, 5162–5165.

143 Shi, X.; Qin, G.; Wang, Y.; Zhao, L.; Liu, Z.; Y. Cheng, J. *Angew. Chem. Int. Ed.* **2019**, *58*, 4356–4360.

144 Bauer, H.; Alonso, M.; Fischer, C.; Rösch, B.; Elsen, H.; Harder, S. *Angew. Chem. Int. Ed.* **2018**, *57*, 15177–15182.

145 Fraser, R. R.; Mansour, T. S.; Savard, S. *J. Org. Chem.* **1985**, *50*, 3232–3234.

146 Abdur-Raschid, K.; Fong, T. P.; Greaves, B.; Gusev, D. G.; Hinman, J. G.; Landau, S. E.; Lough, A. J.; Morris, R. H. *J. Am. Chem. Soc*. **2000**, *122*, 9155–9171.

147 Wiesinger, M.; Maitland, B.; Färber, C.; Ballmann, G.; Fischer, C.; Elsen, H.; Harder, S. *Angew. Chem. Int. Ed.* **2017**, *56*, 16654–16659.

148 Martin, J.; Knüpfer, C.; Eyselein, J.; Färber, C.; Grams, S.; Langer, J. Thum, K.; Wiesinger, M.; Harder, S. *Angew. Chem. Int. Ed.* **2020**, *59*, 9102–9112.

149 Leng, J.-D.; Goodwin, C. A. P.; Victorica-Yrezabal, I. J.; Mills, D. P.; *Chem. Commun.* **2018**, *47*, 12526–12533.

150 Stegner, P.; Färber, C.; Zenneck, U.; Knüpfer, C.; Eyselein, J.; Wiesinger, M.; Harder, S. *Angew. Chem. Int. Ed.* **2021**, *60*, 4252–4258.

151 Weller, S.; Wright, L. *J. Am. Chem. Soc.* **1954**, *76*, 5302–5305.

152 Wright, L.; Weller, S. *J. Am. Chem. Soc.* **1954**, *76*, 5305–5308.

153 Wagemans, W. P. W.; van Lenthe, J. H.; de Jongh, P. E.; Jos van Dillen, J.; de Jong, K. P. *J. Am. Chem. Soc.* **2005**, *127*, 16675–16680.

154 Bauer, H.; Thum, K.; Alonso, D.; Fischer, C.; Harder, S. *Angew. Chem. Int. Ed.* **2019**, *58*, 4248–4253.

155 Bauer, H.; Alonso, M.; Färber, C.; Elsen, H.; Pahl, J.; Causero, A.; Ballmann, G.; De Proft, D.; Harder, S. *Nat. Catal*. **2018**, *1*, 40–47.

156 Elsen, H; Langer, J.; Wiesinger, M.; Harder, S. *Organometallics*, **2020**, *39*, 4238–4246.

157 Staubitz, A.; Robertson, A. P. M.; Manners, I. *Chem. Rev.* **2010**, *110*, 4079–4124.

158 Spielmann, J.; Jansen, G.; Bandmann, H.; Harder, S. *Angew. Chem. Int. Ed.* **2008**, *47*, 6290–6295.

159 Spielmann, J. Harder, S. *J. Am. Chem. Soc.* **2009**, *131*, 5064–5065.

160 Harder, S.; Spielmann, J.; Tobey, B. *Chem. Eur. J.* **2012**, *18*, 1984–1991.

161 Bellham, P.; Hill, M. S.; Kociok-Köhn, G.; Liptrot, D. J. *Chem. Commun.* **2013**, *49*, 1960–1962.

162 Liptrot, D. J.; Hill, M. S.; Mahon, M. F.; MacDougall, D. J. *Chem. Eur. J.* **2010**, *16*, 8508–8515.

163 Butera, V.; Russo, N.; Sicilia, E. *Chem. Eur. J.* **2014**, *20*, 5967–5976.

164 Bellham, P.; Anker, M. D.; Hill, M. S.; Kociok-Köhn, G.; Mahon, M. F. *Dalton Trans.* **2016**, *45*, 13969–13978.

165 Bellham, P.; Hill, M. S.; Kociok-Köhn, G. *Organometallics* **2014**, *33*, 5716–5721.

166 Barrett, A. G. M.; Crimmin, M. R.; Hill, M. S.; Hitchcock, P. B.; Procopiou, P. A. *Organometallics* **2007**, *26*, 4076–4079.

167 Liptrot, D. J.; Hill, M. S.; Mahon, M. F.; Wilson, A. S. S. *Angew. Chem. Int. Ed.* **2015**, *54*, 13362–13365.

168 *Metal Amide Chemistry*. Lappert, M.; Power, P. P.; Protchenko, A.; Seeber, A., Eds; John Wiley & Sons, Ltd., Chichester, 2009.

169 *Reagents in Organic Chemistry*. Fieser, L. F.; Fieser, M., Eds; Wiley, New York, 1967.

170 Tanabe, Y.; Misaki, T.; Kurihara, M.; Iida, A.; Nishii, Y. *Chem. Commun.* **2002**, 1628–1629.

171 *Protecting Groups, 3rd edition*. Kocieński, P. J., Ed.; Thieme, Stuttgart, 2005, pp. 595–599.

172 Birot, M.; Pilot, J.-P.; Dunoguès, J. *Chem. Rev.* **1995**, *95*, 1443–1477.

173 Buch, F.; Harder, S. *Organometallics* **2007**, *26*, 5132–5135.

174 Hill, M. S.; Liptrot, D. J.; MacDougall, D. J.; Mahon, M. F.; Robinson, T. P. *Chem. Sci.* **2013**, *4*, 4212–4222.

175 Bellini, C.; Carpentier, J.-F.; Tobisch, S.; Sarazin, Y. *Angew. Chem. Int. Ed.* **2015**, *54*, 7679–7683.

176 Bellini, C.; Dorcet, V.; Carpentier, J.-F.; Tobisch, S.; Sarazin, Y. *Chem. Eur. J.* **2016**, *22*, 4564–4583.

177 Crimmin, M. R.; Barrett, A. G. M.; Hill, M. S.; MacDougall, D. J.; Mahon, M. F.; Procopiou, P. A. *Chem. Eur. J.* **2008**, *14*, 11292–11295.

178 Li, N.; Guan, B.-T. *Eur. J. Inorg. Chem.* **2019**, 2231–2235.

179 Bellini, C.; Roisnel, T.; Carpentier, J.-F.; Tobisch, S.; Sarazin, Y. *Chem. Eur. J.* **2016**, *22*, 15733–15743.

180 Bellini, C.; Orione, C.; Carpentier, J.-F.; Sarazin, Y. *Angew. Chem. Int. Ed.* **2016**, *55*, 3744–3748.

181 *Principles of Polymerization, 4th Edition*. G. Odian, Ed.; John Wiley & Sons, Hoboken, 2004, pp. 75–80.

182 Morris, L. J.; Whittell, G. R.; Eloi, J.-C.; Mahon, M. F.; Marken, F.; Manners, I.; Hill, M. S. *Organometallics* **2019**, *38*, 3629–3648.

183 Morris, L. J.; Hill, M. S.; Mahon, M. F.; Manners, I.; McMenamy, F. S.; Whittell, G. R. *Chem. Eur. J.* **2020**, *26*, 2954–2966.

184 Le Coz, E.; Hammoud, J.; Roisnel, T.; Cordier, M.; Dorcet, V.; Kahlal, S.; Carpentier, J.-F.; Saillard, J.-Y.; Sarazin, Y. *Chem. Eur. J.* in the press, DOI: 10.1002/chem.202101687.

185 Le Coz, E.; Dorcet, V.; Roisnel, T.; Tobisch, S.; Carpentier, J.-F.; Sarazin, Y. *Angew. Chem. Int. Ed.* **2018**, *57*, 11747–11751.

186 Le Coz, E.; Zhang, Z.; Roisnel, T.; Cavallo, L.; Falivene, L.; Carpentier, J.-F.; Sarazin, Y. *Chem. Eur. J.* **2020**, *26*, 3535–3544.

187 Le Coz, E.; Kahlal, S.; Saillard, J.-Y.; Roisnel, T.; Dorcet, V.; Carpentier, J.-F.; Sarazin, Y. *Chem. Eur. J.* **2019**, *25*, 13509–13513.

188 Zhao, L.; Shi, X.; Cheng, J. *ACS Catal.* **2021**, *11*, 2041–2046.

189 Crimmin, M. R.; Barrett, A. G. M.; Hill, M. S.; Procopiou, P. A. *Org. Lett.* **2007**, *9*, 331–333.

190 Orzechowski, L.; Harder, S. *Organometallics* **2007**, *26*, 2144–2148.

191 Avent, A. G.; Crimmin, M. R.; Hill, M. S.; Hitchcock, P. B. *Organometallics* **2005**, *24*, 1184–1188.

192 Barrett, A. G. M.; Crimmin, M. R.; Hill, M. S.; Hitchcock, P. B.; Lomas, S. L.; Procopiou, P. A.; Suntharalingam, K. *Chem. Commun.* **2009**, 2299–2301.

193 Arrowsmith, M.; Crimmin, M. R.; Hill, M. S.; Lomas, S. L.; MacDougall, D. J.; Mahon, M. F. *Organometallics* **2013**, *32*, 4961–4972.

194 Rösch, B.; Gentner, T. X.; Elsen, H.; Fischer, C. A.; Langer, J.; Wiesinger, M.; Harder, S. *Angew. Chem. Int. Ed.* **2019**, *58*, 5396–5401.

195 Zheng, X.; del Rosal, I.; Xu, X.; Yao, Y.; Maron, L.; Xu, X. *Inorg. Chem.* **2021**, *60*, 5114–5121.

196 Atzrodt, J.; Derdau, V.; Fey, T.; Zimmermann, J. *Angew. Chem. Int. Ed.* **2007**, *46*, 7744–7765.

197 Atzrodt, J.; Derdau, V.; Kerr, W. J.; Reid, M. C. *Angew. Chem. Int. Ed.* **2018**, *57*, 3022–3047.

198 Di Giuseppe, A.; Castarlenas, R.; Oro, L. A. *C. R. Chim*. **2015**, *18*, 713–741.

199 Mukherjee, D.; Höllerhage, T.; Leich, V.; Spaniol, T. P.; Englert, U.; Maron, L.; Okuda, J. *J. Am. Chem. Soc.* **2018**, *140*, 3403–3411.

200 Martin, J.; Eyselein, J.; Grams, S.; Harder, S. *ACS Catal.* **2020**, *10*, 7792–7799.

201 Wilson, A. S. S.; Dinoi, C.; Hill, M. S.; Mahon, M. F.; Maron, L.; Richards, E. *Angew. Chem. Int. Ed.* **2020**, *59*, 1232–1237.

202 Dabringhaus, P.; Schorpp, M.; Scherer, H.; Krossing, I. *Angew. Chem. Int. Ed.* **2020**, *59*, 22023–22027.

203 Anker, M. D.; Kefalidis, C. E.; Yang, Y.; Fang, J.; Hill, M. S.; Mahon, M. F.; Maron, L. *J. Am. Chem. Soc.* **2017**, *139*, 10036–10054.

204 Anker, M. D.; Hill, M. S.; Lowe, J. P.; Mahon, M. F. *Angew. Chem. Int. Ed.* **2015**, *54*, 10009–10011.

205 Yang, Y.; Anker, M. D.; Fang, J.; Mahon, M. F.; Maron, L.; Weetman, C.; Hill, M. S. *Chem. Sci.* **2017**, *8*, 3529–3537.

206 Li, T.; McCabe, K. N.; Maron, L.; Leng, X.; Chen, Y. *ACS Catal.* **2021**, *11*, 6348–6356.

207 Shi, X.; Liu Z.; Cheng, J. *Dalton Trans.* **2019**, *48*, 17919–17924.

208 Liu, Z.; Shi, X.; Cheng, J. *Dalton Trans.* **2020**, *49*, 8340–8346.

209 Liptrot, D. J.; Arrowsmith, M.; Colebatch, A. L.; Hadlington, T. J.; Hill, M. S.; Kociok-Köhn, G.; Mahon, M. F. *Angew. Chem. Int. Ed.* **2015**, *54*, 15280–15283.

210 Yadav, S.; Dixit, R.; Vanka, K.; Sen, S. S. *Chem. Eur. J.* **2018**, *24*, 1269–1273.

211 Alaaeddine, A.; Roisnel, T.; Thomas, C. M.; Carpentier, J.-F. *Adv. Synth. Catal.* **2008**, *350*, 731–740 and references therein.

212 Hartwig, J. F.; *J. Am. Chem. Soc.* **2016**, *138*, 2–24.

213 Brand, S.; Elsen, H.; Langer, J.; Grams, S.; Harder, S. *Angew. Chem. Int. Ed*. **2019**, *58*, 15496–15503.

214 Rauser, M.; Schröder, A.; Niggemann, M. Early Main Group Metal Lewis Acid Catalysis. In *Early Main Group Metal Catalysis*. Harder, S., Ed.; Wiley-VCH, Weinheim, 2020, pp. 279–310.

215 Pozhydaiev, V.; Power, M.; Gandon, V.; Moran, J.; Lebœuf, D. *Chem. Commun*. **2020**, *56*, 11548–11564.

216 Yamashita, Y,; Tsubogo, T.; Kobayashi, S. Enantioselective Group 2 metal Lewis Acid Catalysis. In *Early Main Group Metal Catalysis*. Harder, S., Ed.; Wiley-VCH, Weinheim, 2020, pp. 311–345.

217 Domżalska, A.; Ulikowski, A.; Furman, B. Alkaline-Earth Metal-Based Chiral Lewis Acids. In *Chiral Lewis Acids in Organic Synthesis*. Mlynarski, J., Ed.; Wiley-CH, Weinheim, 2017, pp. 1–25.

218 Begouin, J-M.; Niggemann, M. *Chem. Eur J.* **2013**, *19*, 8030–8041.

219 Mayer, U.; Gutmann, V.; Gerger, W. *Monatsh. Chem.* **1975**, 106, 1235–1257.

220 Beckett, M. A.; Strickland, G. C.; Holland, J. R.; Varma, K. S. *Polymer* **1996**, *37*, 4629–4631.

221 Childs, R. F.; Mulholland, D. L.; Nixon, A. *Can. J. Chem.* **1982**, *60*, 801–808.

222 Christe, K. O.; Dixon, D. A.; McLemore, D.; Wilson, W. W.; Sheehy, J. A.; Boatz, J. A. *J. Fluorine Chem.*, **2000**, 101, 151–153.

223 Jupp, A. R.; Johnstone, T. C.; Stephan, D. W. *Dalton Transactions* **2018**, *47*, 7029–7035.

224 Jupp, A. R.; Johnstone, T. C.; Stephan, D. W. *Inorg. Chem.* **2018**, *57*, 14764–14771.

225 Nguyen, H. V.; Matsubara, R.; Kobayashi, S. *Angew. Chem. Int. Ed.* **2009**, *48*, 5927–5929.

226 Matsubara, R.; Berthiol, F.; Nguyen, H. V.; Kobayashi, S. *Bull. Chem. Soc. Jpn.* **2009**, *82*, 1083–1102.

227 Lu, G.; Yoshino, T.; Morimoto, H.; Matsunaga, S.; Shibasaki, M. *Angew. Chem. Int. Ed.* **2011**, *50*, 4382–4385.

228 Saito, S.; Tsubogo, T.; Kobayashi, S. *Chem. Commun*. **2007**, 1236–1237.

229 Kobayashi, S.; Matsubara, R. *Chem. Eur. J*. **2009**, *15*, 10694–10700.

230 Hatano, M.; Moriyama, K.; Maki, T.; Ishihara, K. *Angew. Chem. Int. Ed.* **2010**, *49*, 3823–3826.

231 Hatano, M.; Ishihara, K. *Synthesis*, **2010**, 3785–3801.

232 Rueping, M.; Bootwicha, T.; Sugiono, E. *Synlett* **2011**, 323–326.

233 Yamaguchi, A.; Aoyama, N.; Matsunaga, S.; Shibasaki, M. *Org. Lett.* **2007**, *9*, 3387–3390.

234 Kobayashi, S.; Yamashita, Y. *Acc. Chem. Res.* **2011**, *44*, 58–71.

235 Saito, S.; Tsubogo, T.; Kobayashi, S. *J. Am. Chem. Soc.* **2007**, *129*, 5364–5365.

236 Tsubogo, T.; Saito, S.; Seki, K.; Yamashita, Y.; Kobayashi, S. *J. Am. Chem. Soc.* **2008**, *130*, 13321–13332.

237 Yamashita, Y.; Tsubogo, T.; Kobayashi, S. *Top. Organomet. Chem.* **2015**, *62*, 121–145.

238 Tsubogo, T.; Yamashita, Y.; Kobayashi, S. *Top. Organomet. Chem.* **2013**, *45*, 243–270.

239 Corey, E.J. *Angew. Chem. Int. Ed.* **2002**, 41, 1650–1667.

240 Li, G.; Liang, T.; Wojtas, L.; Antilla, J. C. *Angew. Chem. Int. Ed.* **2013**, *52*, 4628–4632.

241 Liang, T.; Li, G.; Wojtas, L.; Antilla, J. C. *Chem. Commun*. **2014**, *50*, 14187–14190.

242 Mao, Z.; Li, W.; Shi, Y.; Mao, H.; Lin, A.; Zhu, C.; Cheng, Y. *Chem. Eur. J.* **2013**, *19*, 9754–9759.

243 Yamatsugu, K.; Yin, L.; Kamijo, S.; Kimura, Y.; Kanai, M.; Shibasaki, M. *Angew. Chem. Int. Ed.* **2009**, *48*, 1070–1076.

244 Dada, R.; Sulthan, M.; Yaragorla, S*. Org. Lett.* **2020**, *22*, 279–283.

245 Reddy, T. P.; Gujral, J.; Roy, P.; Ramachary, D. B. *Org Lett.* **2020**, *22*, 9653–9657.

246 Parker, A. N.; Martin, M. C.; Shenje, R.; France, S. *Org Lett.* **2019**, *21*, 7268–7273.

247 Kumaraswamy, G.; Sastry, M.N.V.; Jena, N. *Tetrahedron Lett.* **2001**, *42*, 8515–8517.

248 Kumaraswamy, G.; Sastry, M.N.V.; Jena, N.; Kumar, K. R.; Vairamani, M. *Tetrahedron: Asymmetry* **2003**, *14*, 3797–3803.

249 Kumaraswamy, G.; Jena, N.; Sastry, M.N.V.; Padmaja, M.; Markondiaah, B. *Adv. Synth. Catal.* **2005**, *347*, 867–871.

250 Kobayashi, S.; Tsubogo, T.; Saito, S.; Yamashita, Y. *Org. Lett.* **2008**, *10*, 807–809.

251 Hut'ka, M.; Tsubogo, T.; Kobayashi, S. *Adv. Synth. Catal.* **2013**, *355*, 1561–1569.

252 Lippur, K.; Kaabel, S.; Järving, I.; Rissanen, K.; Kanger, T. *J. Org. Chem*. **2015**, *80*, 6336–6341.

253 Tsubogo, T.; Yamashita, Y.; Kobayashi, S. *Angew. Chem. Int. Ed.* **2009**, *48*, 9117–9120.

254 Tsubogo, T.; Yamashita, Y.; Kobayashi, S. *Chem. Eur. J*. **2012**, *18*, 13624–13628.

255 Tsubogo, T.; Yamashita, Y.; Kobayashi, S. *Top. Catal*. **2014**, *57*, 935–939.

256 Tsubogo, T.; Oyamada, H.; Kobayashi, S. *Nature* **2015**, *520*, 329–332.

257 Agostinho, M; Kobayashi, S. *J. Am. Chem. Soc.* **2008**, *130*, 2430–2431.

258 Kobayashi, S.; Yamaguchi, M.; Agostinho, M.; Schneider, U. *Chem. Lett.* **2009**, *38*, 299–300.

259 Tsubogo, T.; Kano, Y.; Yamashita, Y.; Kobayashi, S. *Chem. Asian. J.* **2010**, *5*, 1974–1977.

260 Poisson, T.; Yamashita, Y.; Kobayashi, S. *J. Am. Chem. Soc*. **2010**, *32*, 7890–7892.

261 Zheng, W.; Zhang, Z.; Kaplan, M.J.; Antilla, J. C*. J. Am. Chem. Soc.* **2011**, *133*, 3339–3341.

262 Tsubogo, T.; Kano, Y.; Ikemoto, K.; Yamashita, Y.; Kobayashi, S. *Tetrahedron: Asymmetry* **2010**, *21*, 1221–1225.

263 Yamashita, Y.; Tsubogo, T.; Kobayashi, S. *Chem. Sci.* **2012**, *3*, 967–975.

264 Uno, B.E.; Dicken, R.D.; Redfern, L.R.; Stern, C. M.; Krzywicki, G. G.; Scheidt, K. A. *Chem. Sci.* **2018**, *9*, 1634–1639.

265 Niggemann, M.; Bisek, N. *Chem. Eur. J.* **2010**, *16*, 11246–1249.

266 Foropoulos, J. Jr.; DesMarteau, D. D. *Inorg. Chem.* **1984**, *23*, 3720–3723.

267 Mathieu, B; Goshez, L. *Tetrahedron* **2002**, *58*, 8219–8226.

268 Niggemann, M.; Meel, M. J. *Angew. Chem. Int. Ed.* **2010**, *49*, 3684–3687.

269 Qi, C.; Gandon, V.; Lebœuf, D. *Angew. Chem. Int. Ed*. **2018**, *57*, 14245–14249.

270 Wang, S.; Force, G.; Guillot, R.; Carpentier, J.-F.; Sarazin, Y.; Bour, C.; Gandon, V.; Lebœuf, D. *ACS Catal*. **2020**, *10*, 10794–10802.

271 Kaljurand, I.; Lilleorg, R.; Murumaa, A.; Mishima, M.; Burk, P.; Koppel, I.; Koppel, I. A.; Leito, I. *J. Phys. Org. Chem.* **2013**, *26*, 171–181.

272 Diba, A. K.; Begouin, J.-M.; Niggemann, M. *Tetrahedron Lett*. **2012**, *53*, 6629–6632.

273 Qi, C.; Hasenmaile, F.; Gandon, V.; Lebœuf, D. *ACS Catal.* **2018**, *8*, 1734–1739.

274 Qi, C.; Yang, S.; Gandon, V.; Lebœuf, D. *Org. Lett.* **2019**, *21*, 7405–7409.

275 Davies, J.; Leonori, D. *Chem. Commun*. **2014**, *50*, 15171–15174.

276 Hutson, G. E.; Türkmen, Y. E.; Rawal, V. H. *J. Am. Chem. Soc.* **2013**, *135*, 4988–4991.

277 Janka, M.; He, W.; Frontier, A. J. *J. Am. Chem. Soc.* **2004**, *126*, 6864–6865.

278 Rueping, M.; Ieawsuwan, W.; Antonchick, A. P.; Nachtstein, B. J. *Angew. Chem. Int. Ed.* **2007**, *46*, 2097–2100.

279 Wang, S.; Guillot, R.; Carpentier, J.-F.; Sarazin, Y.; Bour, C.; Gandon, V.; Lebœuf, D. *Angew. Chem. Int. Ed*. **2020**, *59*, 1134–1138.

280 Lebœuf, D.; Schulz. E.; Gandon, V. *Org. Lett.* **2014**, *16*, 6464–6468.

281 Lebœuf, D.; Marin, L.; Michelet, B.; Perez-Luna, A.; Guillot, R.; Schulz, E.; Gandon, V. *Chem. Eur. J.* **2016**, *22*, 16165–16171.

282 Piancatelli, G.; Dauria, M.; Donofrio, F. *Synthesis* **1994**, 867–889.

283 Marin, L.; Force, G.; Gandon, V.; Schulz, E.; Lebœuf, D. *Eur. J. Org. Chem*. **2020**, 5323–5328.

284 Marin, L.; Gandon, V.; Schulz, E.; Lebœuf, D. *Adv. Synth. Catal.* **2017**, *359*, 1157–1163.

285 Marin, L.; Guillot, R.; Gandon, V.; Schulz, E.; Lebœuf, D. *Org. Chem. Front*. **2018**, *5*, 640–647.

286 Morcillo, S. P.; Lebœuf, D.; Bour, C.; Gandon, V. *Chem. Eur. J*. **2016**, *22*, 16974–16978.

287 Yaragorla, S.; Singh, G.; Lal Saini, P.; Reddy, M. K. *Tetrahedron Lett*. **2014**, *55*, 4657–4660.

288 Kiely-Collins, H. J.; Sechi, I.; Brennan, P. E.; McLaughlin, M. G. *Chem. Commun.* **2018**, *54*, 654–657.

289 Lebœuf, D.; Presset, M.; Michelet, B.; Bour, C.; A.; Bezzenine-Lafolée, S.; Gandon, V. *Chem. Eur. J.* **2015**, *21*, 11001–11005.

290 Qi, C.; Gandon, V.; Lebœuf, D. *Adv. Synth. Catal.* **2017**, *359*, 2671–2675.

291 Begouin, J.-M.; Capitta, F.; Wu, X.; Niggemann, M. *Org. Lett.* **2013**, *15*, 1370–1373.

292 Gao, S.; Stopka, T.; Niggemann, M. *Org. Lett.* **2015**, 17, 5080–5083.

293 Yaragorla, S.; Dada, R.; Pareek, A., Singh, G. *RSC Adv.* **2016**, *6*, 28865–28870.

294 Yaragorla, S.; Dada, R.; Singh, G.; Pareek, A.; Rana, M.; Sharma, A. K. *ChemistrySelect* **2016**, *1*, 6902–6906.

295 Yaragorla, S.; Pareek, A.; Dada, R. *Tetrahedron Lett.* **2017**, *58*, 4642–4647.

296 Fürstner, A. *Chem. Soc. Rev.* **2009***, 38*, 3208–3221.

297 Haven, T.; Kubik, G.; Haubenreisser, S.; Niggemann, M. *Angew. Chem. Int. Ed.* **2013**, *52*, 4016–4019.

298 Meyer, V.J.; Ascheberg, C.; Niggemann, M. *Chem. Eur. J.* **2015**, *21*, 6371–6374.

299 Rösch, B.; Gentner, T. X.; Langer, J.; Färber, C.; Eyselein, J.; Zhao, L.; Ding, C.; Frenking, G.; Harder, S. *Science* **2021**, *371*, 1125–1128.